An investigation into the influence of soil pattern on preferential flow and groundwater recharge in fractured bedrock and cover sand aquifers.

By

McLachlan Du Toit Stander

Thesis presented in partial fulfilment of the requirements for the degree Master of Agriculture at the University of Stellenbosch

Supervisor

Dr. Andrei Rozanov, Stellenbosch University

Co-supervisors

Dr. Nebo Jovanovic, CSIR
Dr. Freddie Ellis, Stellenbosch University

Faculty of Agrisciences
Department of Soil Science

December 2011

DECLARATION

By submitting this thesis/dissertation electronically, I declare that the entirety of the work contained therein is my own, original work, that I am the sole author thereof (save to the extent explicitly otherwise stated), that reproduction and publication thereof by Stellenbosch University will not infringe any third party rights and that I have not previously in its entirety or in part submitted it for obtaining any qualification.

December 2011

ABSTRACT

Increased pressure on groundwater sources due to increased population size and threats of climate change is driving research to better understand the process of aquifer recharge. Soil pattern is of interest as it serves to partition rainwater into different flowpaths destined for surface runoff, evapotranspiration and deep percolation. The challenges inherent to studying these flowpaths are almost universal as uncertainties concerning spatial and temporal heterogeneity in catchments make the upscaling of models complex.

This research addresses these challenges as it aims to improve the catchment scale hydrological models of two aquifer systems: One a fractured bedrock system at the Kogelberg Nature Reserve, Kleinmond, and the other a cover sand system in Riverlands Nature Reserve, Malmesbury. This study focussed on strengthening the link between what is known about a given soil form and the hydrological assumptions that can be drawn from that classification, and formulating the results so that they may ultimately be used to calibrate the recharge prediction models for the respective catchments.

The research was done in two parts: The first phase was to conduct soil surveys in both reserves during which soils were classified according to South African Soil Classification. Samples were collected at representative observation points which provided textural data for use in pedotransfer functions (PTFs). These PTFs were used to estimate plant available water (PAW) and hydraulic conductivity (K) for the observed profiles. Infiltration experiments were subsequently done to investigate the infiltration patterns of distinctly different soil forms at two sites from each reserve. The experiments included double ring and mini disc infiltration, volumetric water content determination and flow path visualisation using a staining dye.

A statistical comparison between the hydrological properties (K and PAW) of the different soil forms suggest that hydraulic properties differed between the deep sandy soil forms (Fernwood, Pinegrove and Witfontein in Kogelberg and Witfontein, Concordia and Lamotte in Riverlands) and the shallow rocky soil forms (Cartref and Glenrosa in Kogelberg). Thus grouping of hydrological similar units (HSUs) could be done on the basis of the soil forms present within the given catchments.

The infiltration study showed that shallow, rocky soils that grade into bedrock would have infiltration rates far greater than those estimated using PTFs in Kogelberg. This is due to the prevalence of continuous preferential flow (PF) of water between coarse fragments in

these profiles. Recharge estimates would thus be inaccurate in such soils and calibration using locally derived data is recommended.

On the contrary, PTFs produced accurate infiltration estimates relative to measured infiltration rates in deep sandy soils in Kogelberg and Riverlands. The Lamotte soil form is an example of such a soil form. It should however be noted that an increase in PF in these soils had subsequently higher K values than estimated, thus illustrating the link between PF and accelerated infiltration rates.

These results confirm that using soil survey information, in the form of a soil map, and calibrated hydrological properties, one can delineate HSUs that encompass a large degree of heterogeneity in a given catchment.

OPSOMMING

Verhoogde druk op grondwaterhulpbronne weens die groeiende bevolking en klimaatsverandering dryf tans navorsing om akwifeer hervulling beter te verstaan. Die grondlaag is van belang sienend dat dit reënwater verdeel in oppervlak afloop, evapotranspirasie en diep dreinering. Die uitdagings in hidrologiese navorsing is universeel as gevolg van onsekerhede oor ruimtelike en tydelike variasie wat lei tot komplekse grondwatermodelle.

Diè navorsing mik om die tekortkominge in akwifeer hervulling aan te vul deur groundwatermodelle van twee akwifeersisteme te verbeter: Die een is ‘n gebroke rots sisteem in die Kogelberg Natuur Reservaat, Kleinmond, en die ander is ‘n sand-bedekde sisteem in Riverlands Natuur Reservaat, Malmesbury. Die navorsing streef om die verhouding tussen ‘n spesifieke grondvorm en sy hidroliese vloeipaaie te bestudeer en om die gevolgtrekkings so te formuleer dat dit kan gebruik word om die onderskeie grondwatermodelle te kalibreer.

Die eerste fase van die navorsing was om ‘n grondopname van die onderskeie reservate te doen waartydens die gronde geklassifiseer was volgens die Suid Afrikaanse Grondklassifikasie Sisteem. Grondmonsters is by verteenwoordigende observasiepunte geneem en geanaliseer om tekstuurdata vir pedo-oordraagbare-funksies (PTFs) te kry. Die PTFs was gebruik om plant beskikbare water (PBW) en hidrouliese geleiding (K) te voorspel vir die verskeie observasiepunte. Infiltrasie eksperimente was daarna gedoen om die infiltrasie patroon van twee verskillende grondvorms van elke reservaat te bestudeer. Die eksperimente sluit dubbel- en minidisk-infiltrasie, volumetriese waterinhoud bepaling en vloeipad visualisering met die gebruik van ‘n kleurstof in.

Die statistiese vergelyking van die hidrouliese eienskappe (K en PBW) en grondvorm dui aan dat die hidrouliese eienskappe verskil tussen die diep, grondvorms met ‘n oorwegende sand tekstuur (Fernwood, Pinegrove en Witfontein in Kogelberg en Witfontein, Concordia en Lamotte in Riverlands) en die vlakker, klipperige grondvorms (Cartref en Glenrosa in Kogelberg). Groepering van hidrologies soortgelyke eenhede (HSE’s) kan dus op die basis van die teenwoordige grondvorms in ‘n opvangsgebied gedoen word.

Die infiltrasie studie het bewys dat vlak, klipperige gronde wat tot die rotsbodem gradueer ‘n baie hoër infiltratsie tempo sal hê as die PTF voorspelde waardes. Dit is as gevolg van

die voorkoms van aaneenlopende voorkeurvloei (VV) van water tussen die growwe materiaal in die profiele, veral die gebroke rots ondergorond. Voorspellings van akwifeer hervulling sal dus onakkuraat wees en kalibrasie met plaaslike data word dus aanbeveel.

In teendeel met die begenoemde, het die PTFs akkurate voorspellings gemaak relatief tot die gemete infiltrasie tempo's in die diep sanderige grondvorms in Kogelberg en Riverlands. Dit was duidelik met metings dat 'n toename in aaneenlopende VV hoër gemete K waardes getoon as die voorspelde waardes. Die verband tussen VV en verhoogde infiltrasie tempo word dus hiermee geillustreer.

Die resultate bevestig dus dat grondopname data, in die vorm van 'n grondkaart en gekalibreerde hidrouliese eienskappe gebruik kan word om hidrologies soortgelyke eenhede uiteen te sit wat die meerderheid van die variasie in 'n gegewe opvangsgebied insluit. Die HSE's kan gebruik word om grondwatermodelle meer akkuraat te laat funksioneer en dus beter voorspellings te genereer.

DEDICATION

Gal 6:4-5

"Each one should test his own actions. Then he can take pride in himself, without comparing himself to somebody else, for each one should carry his own load.

This MSc thesis is dedicated to The Almighty God, for it is He who gives us the strength to persevere.

ACKNOWLEDGEMENTS

- To my **father and mother** for supporting me for the last 24 years of my life. I know I will never stop learning from you.
- My promoter, **Dr Rozanov**, for your invaluable support for the last two years. You maintained a perfect balance between giving me enough space to follow my intuition yet stayed close enough to keep me from bumping my head.
- My co-promoter, **Dr Ellis**, for your insightful suggestions and even more so the way you impart knowledge in a loving and uplifting manner, never failing to leave a smile on the face and a thought in my mind.
- The CSIR, specifically my co-promoter **Dr Jovanovic**, for initiating this exciting project and for their financial support the last two years, without which none of this would be possible.
- To **Mary Lynne** who has gone through good times and bad times with me in the last five years as my friend, girlfriend and fiancée. I look forward to our next challenges.
- To all my **fellow students** from the 2010, 2011 and 2012 Soil Science MSc groups. I will always remember the friends I made here; the late nights, early mornings, coffee breaks, funny and inspiring emails, social opportunities, frustrations and laughs. Thank you!
- To the lecturers, **Dr De Clercq, Oom Jan, Dr Hardie and Dr Hoffman**, for all the extra inputs that added to my education here in the Lombardi Building.
- To the rest of the department; those who never had the responsibility of educating me as part of my degree, yet most often made the largest contribution to my all-round university education through their welcoming, affectionate, understanding and loyal support. Thank you **Nigel, Tannie Annetjie, Aunt Delphine, Herschel, Esme and Uncle Matt**.
- To the management and staff at both Riverlands, **Johnny**, and Kogelberg, **Mark**, for your friendly welcome.
- To **Garth** and **Adriaan** at Dept. Geology for always helping me with tedious tasks.
- Finally to **friends** and **family** who put up with my fascination and often overzealous excitement over SOIL.

TABLE OF CONTENTS

LIST OF FIGURES

LIST OF TABLES

LIST OF APPENDICES

LIST OF ABBREVIATIONS

BD_{est}	Estimated Bulk Density (Saxton & Rawls, 2006)
BD_{meas}	Measured Bulk Density
BDT	Binary Decision Tree
CSIR	Council for Scientific and Industrial Research
EC	Electrical Conductivity
EMV	Expected Moisture Value
FC_{est}	Estimated Field Capacity (Saxton & Rawls, 2006)
GIS	Geographic Information System
GPS	Global Positioning System
GWC	Gravimetric Water Content
HEP	Hydrologically Effective Porosity
HSU	Hydrologically Similar Unit
K	Hydraulic Conductivity
OC	Organic Carbon
OM	Organic Material
PAW	Plant Available Water
PF	Preferential Flow
PFP	Preferential Flow Path
PFV	Preferential Flow Visualisation
PGW	Perennial Groundwater
PTF	Pedo Transfer Function
REV	Representative Elementary Volume
RG	Reference Group
RS	Remote Sensing
SPAW	Soil Plant Air Water computer software (Saxton & Rawls, 2006)
TGW	Transient Groundwater
USDA	United States Department of Agriculture
USGS	United States Geological Survey
VWC_{est}	Volumetric Water Content calculated using estimated bulk density
VWC_{meas}	Volumetric Water Content calculated using measured bulk density
WRC	Water Research Commission
WT	Water Table

CHAPTER ONE

1.1. General Introduction

Growing populations, industry and agriculture is increasing pressure on Southern Africa's water resources. Thus the demand for improved resource management is increasing accordingly. Groundwater is a major source of water for the Western Cape Province and there are numerous types of aquifer systems. Predicting the sustainability of tapping these aquifers is a crucial, yet very difficult task. The threat of climate change is further complicating these prediction models.

Two factors contribute to the sustainability of an aquifer: The rate of water extraction and the rate of water recharge. Understanding the process of groundwater recharge from rainwater is the key to making accurate recharge estimations. There are however many factors that contribute to groundwater dynamics.

A drive to improve the accuracy of process based groundwater recharge estimations has recently been launched by the Council for Scientific and Industrial Research (CSIR). This project, funded by the Water Research Commission (WRC), will aim to derive an improved model which can be used to predict process based leaching and contaminant transport dynamics in large catchments. This model will also take into account the environmental effects such as temperature and evapotranspiration on groundwater dynamics allowing the model to predict changes in recharge in a climate change scenario.

The challenges inherent to this form of hydrological research are almost universal. Spatial and temporal heterogeneity in catchments make the upscaling of models very difficult. An increase in size or local relief of a catchment will increase the degree of variation and so too decrease the accuracy of predictions.

Meticulous monitoring of a large catchment is possible, yet not always a viable option due to limited funds. Such large scale projects require advanced computer hardware and software in order to process and present the acquired data in a logical manner. These limitations present the opportunity for researchers to advance existing or develop new alternative hydrological monitoring techniques that are less labour and resource intensive.

This dissertation is a building block of the project run by the CSIR and WRC. This segment of the research will address the mapping of soils in a given catchment and aim to

strengthen the link between what is known about a given soil form and the hydrological assumptions that can be drawn from that classification.

The two sites that will be investigated in this study are very different in terms of catchment size, topography, location, complexity of soil cover and geomorphology. This grants the opportunity to experiment with different and innovative mapping techniques. Transect and grid surveys will be conducted in the homogenous cover sand catchment, set in Riverlands Nature Reserve south-west of Malmesbury, Western Cape. Due to the unsophisticated soil pattern distribution in Riverlands, interpolated soil mapping can be used to compile a soil map of the unsurveyed areas using aerial photographs, topographic maps and field survey information. The mountainous fractured rock aquifer system in the Kogelberg Nature Reserve near Kleinmond in the Western Cape, is however more heterogeneous in terms of soil pattern and a reference group based approach using remote sensing (RS) and GIS will be used when conducting a more detailed survey. In both cases digital soil mapping was enforced due to the strict conservation policies of the respective nature reserves which limited the allowance of excavation of soil profile pits.

Subsequent infiltration experiments will be performed to investigate the infiltration patterns of distinctly different soil forms. These studies will be done to advance the knowledge of the effects that preferential flow has on the rate of infiltration and groundwater recharge; possibly reaching a level of understanding where the estimation model can be calibrated for a specific soil pattern to compensate for the different infiltration patterns expressed.

Combining the outcomes of the infiltration tests with the soil maps from the surveys can aid in accurately calibrating and upscaling hydrological models. This desired outcome is based on a hydropedological standpoint as the soils that form in the catchment, as indicated by the soil map, are related to the general hydrological regime. It is this relationship between soil type and hydrology that needs to be more accurately modelled to perform accurate upscaling.

As previously mentioned, the low degree of heterogeneity in Riverlands will make interpolated mapping possible, based on the field soil survey and terrain morphology. Whereas interpolation in Kogelberg will be done using a binary decision tree (BDT) to allocate field survey data to unsampled observation points. This decision tree will be part of an innovative method to upscale models in very heterogeneous terrain based on soil maps and hydrological data.

This research project will aim to improve hydrological estimation models by incorporating soil pattern as a spatial distinctive factor, through using innovative hydropedological methods to simplify the mapping and upscaling processes.

1.2. Literature Review

1.2.1. Flow modelling in soils on fractured bedrock and cover sands

The partitioning of rainfall into surface runoff and groundwater flow is greatly influenced by the physical properties of the soil surface and the first few centimetres of the topsoil (Joel & Messing, 2001; Weiler & Naef, 2002). Infiltration in sloping land is strongly influenced by rainfall intensity, vegetation density, soil macropore configuration, soil bulk density and stratification, surface hydrophobicity, and surface roughness and topography (Joel & Messing, 2001). Infiltrated water will then flow in the soil by either uniform or non-uniform flow, or both.

Uniform flow occurs as a more or less horizontal wetting front, usually parallel to the soil surface. Non-uniform flow, referred to as preferential flow (PF), occurs as an irregular wetting front in which water or solutes will move faster in certain areas of the soil than in others (Hendrickx & Flurry, 2001). PF was found to increase the rate of aquifer recharge (Sililo & Tellman, 2000), but to what extent is not yet clear.

This section of the literature review will investigate the different preferential flow paths (PFPs) in soil. It will also cover some models and monitoring methods that could be adopted in a hydrological study. Ultimately this information will provide a basis of understanding of PF in soil which will help to accurately study and model flow paths in soil.

1.2.1.1. Models used in groundwater flow investigations

Table 1.1 serves as a summary of various models used in hydrological studies, including their input parameters and realistic time scales required. Figures 1.1 and 1.2, in the next section dealing with types of preferential flow paths, correlate with Table 1.1 as they show the PF patterns relative to the scale on which they can be investigated; but more on this later. This section will however aim to elaborate on selected equations that are often used in hydrological estimation models.

Table 1.1: Scales, conceptual models, critical parameters, and measurements relevant to flow in the vadose zone (Hendrickx & Flurry, 2001).

Spatial Scale	Domain	Conceptual Model	Physical Model	Critical Parameters	Smallest Temporal Measurement	Scale
Pore	Macropore, Fractures	Fluid Continuum	Hagen-Poisseuille	Fracture Width	Thin Sections, NMR	Minutes Days
Darcian	Laboratory, Soil Profiles	Representative Volume	Darcy-Buckingham	Hydraulic Properties	TDR, Neutron Attenuation, Tensiometers	Hours Months
Areal	Field, Local Depressions, Landscape Element	Mass Balance	Mass Balance	Weather, Soil water	Meteorological Stations, TDR, Neutron Attenuation, Remote Sensing, Groundwater Level	Days Years

The most accurate results in recharge investigations are obtained when using various monitoring methods in the same test site to compensate for limitations inherent to the individual methods (Uhlenbrook *et al*., 2005). As in the case where Delin *et al.* (2000) used well hydrograph analysis, tracer dye and unsaturated zone water balance methods to investigate a single site.

The established approaches to modelling water flow in a porous medium are Darcy's flow equation, Richards' flow equation and van Genuchten's analytical function. These three methods are supported by the continuum concept in which a representative elementary volume (REV) of porous medium is investigated in terms of the characteristic properties of the porous medium and the kinematic properties of the fluid (Feyen *et al*., 1998).

Darcy's law describes the flow of a fluid through a medium as the sum of the various micropore-flows, so doing, ignoring the intricate flow patterns in the medium. Thus by treating the soil as a uniform medium, the flux can be described as a macroscopic flow velocity vector through the REV (Hillel, 1980). Darcy's law (Eq. 1.1) states that the rate of flow of a liquid (q) through a porous medium is in the direction of and proportional to the hydraulic gradient ($\Delta H/L$). The flow is also proportional to the medium's ability to transmit a specific liquid; a parameter known as the hydraulic conductivity (K). These and other equation variables are summarized in Table 1.2.

Equation 1.1:

$$q = \frac{K\Delta H}{L} = Q/A = V/At$$

Table 1.2: Key terms used in equations.

q	Flux [L/T]	**θ**	Volumetric water content [L^3/L^3]
K	Hydraulic conductivity [L/T]	**ψ**	Pressure head [L]
H	Hydraulic head [L]	**z**	Depth [L]
L	Length of column [L]	**S_e**	Effective saturation
Q	Flux [L^3/T]	**n**	van Genuchten shape parameter
A	Area [L^2]	**m**	van Genuchten shape parameter
t	Time [T]	**x**	van Genuchten shape parameter
K_r	Relative hydraulic conductivity	**τ**	Tortuosity
C_1	Van Genuchten K parameter	**C_2**	van Genuchten sorptivity parameter
∇q	Three dimensional flux [L^3/T]	**V**	Volume (cm^3)
ρ_b	Bulk density (g/cm^3)	**ρ_w**	Bulk density of water (g/cm^3)
P_w	Gravimetric water content (g/g)	**ΔH/L**	Hydraulic gradient
ΔW	Soil Water Storage	**ET**	Evapotranspiration
R	Runoff	**P**	Rainfall

K is the proportionality constant linking the hydraulic gradient to the flux density (Feyen *et al*., 1998). This variable can be used to compare the conductivity of water in different soils and is thus a sought property in soil studies. There are variations on Darcy's Law that can be used to calculate K; for instance Equation 1.2 which is a derivation of Darcy's Law for flow in a vertical column (Hillel, 1980).

Equation 1.2:

$$q = \frac{K\Delta H}{L} + K$$

In order to use Darcy's equation, the volume of water infiltrating the soil over a specific area in a given timeframe must be known. Alternatively, the change in hydraulic head and length of the soil column can be measured. These parameters can be measured from field or laboratory infiltration experiments such as falling head or constant head infiltration.

A limitation of using Darcy's equation is that the presence of micro-heterogeneity can severely affect the infiltration rate and redistribution patterns of water in the soil (Feyen *et al*., 1998). This model also requires familiarity of soil-water retention curves or unsaturated hydraulic conductivity curves (de Vries & Simmers, 2002) which can be derived via indirect methods (van Genuchten, 1980; Saxton & Rawls, 2006).

Stoertz & Bradbury (1989) successfully used Darcy's law to model groundwater flow as part of the USGS Modular Groundwater Flow Model, to predict the flux of groundwater in a Wisconsin aquifer. They used borehole well data to calculate flux between adjacent wells, which when computed with aquifer thickness and hydraulic head was used to calculate K.

Richards combined Darcy's law with the continuity equation (Eq. 1.3) to generate the combined flow equation, also known as Richards' equation (Eq. 1.4). The Richards' equation is used to describe flow in unsaturated soils as it accounts for the contribution of the matrix potential to the conductivity and not only gravitational potential as in Darcy's law (Hillel, 1980). Here, θ(ψ) and K(ψ) are soil layer dependent hydraulic properties. These characteristics can be derived from direct measurements of θ and ψ, or K and ψ. Inverse optimization can also be applied to derive θ(ψ) and K(ψ) from the Richards' equation if the flux, pressure head and volumetric water content are known (Feyen *et al*., 1998).

Equation 1.3:

$$\frac{\Delta\theta}{\Delta t} = -\nabla q$$

Equation 1.4:

$$\frac{\theta(\psi)}{t} = K(\psi).(\psi + z)$$

An example of Richards' equation being used in a hydrological model is seen in the work by Xevi *et al*. (1997) who evaluated the sensitivity of the MIKE-SHE hydrological model in the Neuenkirchen catchment, Germany. Pressure head variation and soil water retention curves were used to numerically calculate the soil water content using the one-dimensional Richards' equation.

Another model is that of van Genuchten (1980). He advanced the model proposed by Maulem (1976) to generate Equation 1.5, called van Genuchten's equation. Here, *n, m* and *α* are the van Genuchten parameters for a specific soil type. These parameters are shown in Table 1.3, an excerpt showing the parameters for three different texture grades.

Equation 1.5:

$$K(\psi) = \frac{(1-(\alpha\psi)^{n-1}(1+(\alpha\psi)^{n})^{m})^{2}}{(1+(\alpha\psi)^{n})^{m\tau}}$$

Zhang (1997) then proposed the use of van Genucten's equation to calculate K in unsaturated soils using a mini disc infiltrometer. The infiltrometer allows the researcher to measure infiltration at varying suction pressures. (A more detailed discussion on the mini disc infiltrometer follows in Chapter 3). Zhang fitted cumulative mini disc infiltration and the square root of elapsed time to the function in Equation 1.6:

Equation 1.6:

$$\mathrm{I} = \mathrm{C_1 t} + \mathrm{C_2 t} - 0.5$$

C_1 and C_2 are van Genuchten's parameters relating to K and soil sorptivity respectively. K is calculated according to Equation 1.7.

Equation 1.7:

$$\mathrm{K} = \frac{\mathrm{C_1}}{\mathrm{A_G}}$$

Here A_G is the variable which relates the suction rate and radius of the infiltrometer disc to the van Genuchten parameters, found in Table 1.3.

The van Genuchten equation was applied by Boswell & Olyphant (2007) to link the unsaturated and saturated zones in a wetland marked for restoration in Northwest Indiana, USA. They successfully identified saturated and seasonally saturated areas that would sustain hydric-vegetation or required remediation respectively.

Table 1.3: van Genuchten's soil parameters (Decagon Devices Incorporated, 2007).

			h_0						
			-0.5	-1	-2	-3	-4	-5	-6
Texture	α	n	A_G						
Sand	0.145	2.68	2.84	2.40	1.73	1.24	0.89	0.64	0.46

A very useful model, consisting of a series of formulae, is proposed by Saxton & Rawls (2006) in which soil hydraulic properties can be inferred from textural data. The input parameters for the model are laboratory determined coarse gravel (> 2 mm), sand, silt and clay fractions as a mass percentage and organic matter (OM) content as percentage organic carbon. Saxton included OM as a dependent variable as OM has the ability to increase water holding capacity and conductivity. OM effects are however not well observed at low water contents and may be masked in soils with high clay contents. Gravel content is also included in the model as increasing the gravel content of a soil decreases the volume of soil available for water storage or conductivity. Using this type of model reduces the monetary costs of extensive hydrological monitoring but does require field sampling and extensive laboratory analysis.

Timlin *et al*. (1996) used the equations proposed by Rawls *et al*. (1991) to predict soil hydraulic properties as input parameters for the GLYCIM soybean growth and development model. They found the equations to be effective when using long term locally obtained databases as opposed to large regional databases. The latter datasets often provide overestimated yields due to overestimated water holding capacity. It should however be mentioned that Saxton & Rawls have since revised their equations to include organic matter, salinity, density (compaction) and coarse fraction as input parameters (Saxton & Rawls, 2006).

The equations were derived from a USDA dataset of approximately 8700 A-, B- and C horizon samples. The revised model was found to be more accurate yet it was still recommended to calibrate texture based hydrological property predictions using local knowledge and data (Saxton & Rawls, 2006).

There are thus numerous sets of equations that can be used to predict groundwater flow and estimate hydraulic properties. These equations however do not have to be used separately as efforts have been made to combine such equations into elaborate

hydrological models: Reference is made to Miller & Richard (1998). Some of these models have attempted to compensate for the effects of PF.

Ritsema & Dekker (2000) commented that not incorporating the hysteresis effects when modelling flow in unsaturated coarse textured or hydrophobic soils could yield very misleading estimations. Kung (1990) recommended viewing soils, not as a homogenous media as assumed by Darcy's law, but as a "columnsol", allowing for distinction to be made between vertical columns of soil with different hydraulic properties. This would allow for making more accurate flow estimates. A subsequent approach was to make further distinction; not only to take spatial differences into account but temporal changes as well. Hosang (1993) used a two-phase model to predict groundwater flow based on Richards' equation. The first phase was during periods of low infiltration and high redistribution rates during which no PF resulted, whereas the second phase dealt with heavy infiltration which formed PF paths.

Another effort to model PF was made by Swanson *et al*. (2006) who adapted their hydrological model to compensate for the presence of extensive lateral high permeability zones. They found that the Tunnel City Group of sandstone found in central and southern Wisconsin had large areas of PF. Calibration lead to more accurate predictions relative to the uncalibrated model.

These are but a handful of approaches that researches have taken to incorporate PF into prediction models. A common outcome from all of the above examples is that PF calibration should be done on a local scale and that a universal PF correction is unlikely. Site specific research to advance such calibrations would thus be justified.

1.2.1.2. Types and causes of preferential flow in soils

Macropore, unstable and funnel flow are three different flow patterns that have been identified in the field. Macropore flow is the PF of water or solutes through plant root channels, fissures, shrinking cracks or earthworm burrows. Macropore flow often occurs in structured, fine texture soils where such channels are present (Hendrickx & Flurry, 2001). Weiler & Naef (2002) reported that the variation of flow in macropores is dependent on the density of macropores and surface topography. Delin *et al.* (2000) further adds, that a topographical variation as small as 1 to 3 cm is enough to initiate PF.

Unstable flow occurs in coarse textured soils due to soil layering, water repellency, air entrapment or continuous, non-ponding infiltration. Funnelling however, takes place when impeding boundary layers cause the lateral redirection of infiltrated water or solutes to an area offering less resistance to percolation. These three different forms of PF may occur simultaneously, resulting in very complex flow systems (Hendrickx & Flurry, 2001). These intricate flow paths are thus influenced considerably by variability in both the pore configuration and spatial variability of soil properties, respectively known as micro- and macro-heterogeneity (Delin *et al*., 2000; Feyen *et al*., 1998).

PF can be investigated on different scales depending on the level of heterogeneity the researcher wants to focus on (Hendrickx & Flurry, 2001). These scales are summarized in Table 1.1 and are listed from smallest to largest: The Hagen-Poiseuille equation can be used to investigate PF on a pore scale (example of use: Lamparter *et al*., 2006). Darcy's equation (Eq. 1.1 & 1.2) can be used to investigate PF in a representative volume of porous medium on a "Darcian" scale (example of use: Hendrickx *et al.,* 1988). Finally, aerial mass balance (Eq. 1.8) or soil moisture budgeting models can be used on an aerial scale (example of use: Boers, 1994). The different PF patterns that are observed at these scales are illustrated in Figures 1.1 and 1.2.

Equation 1.8:

$$q_r = P + R - ET - \Delta W$$

Unstable wetting fronts are most often visible as finger-like flow patterns known as fingering. Fingering is known to facilitate groundwater recharge as flow rates are often higher than anticipated when fingering occurs (Hendrickx & Flurry, 2001). Evidence of recharge occurring due to fingering is given by Silillo & Tellman (2000): Groundwater recharge occurring much faster than predicted straight after a rainfall event; recharge occurring during high evapotranspiration rates; distinct lateral heterogeneity in soil water content in the unsaturated vadose zone and evident differences between predicted recharge values and field measurements.

Fingering will be favoured in initially dry, coarse textured, layered soils which display a large degree of spatial variability. Decreases in particle size from coarse to fine textured, will cause the finger diameter to increase and the distance between the fingers to decrease. An increase in flux will however decrease the distance between the fingers (Silillo & Tellman, 2000).

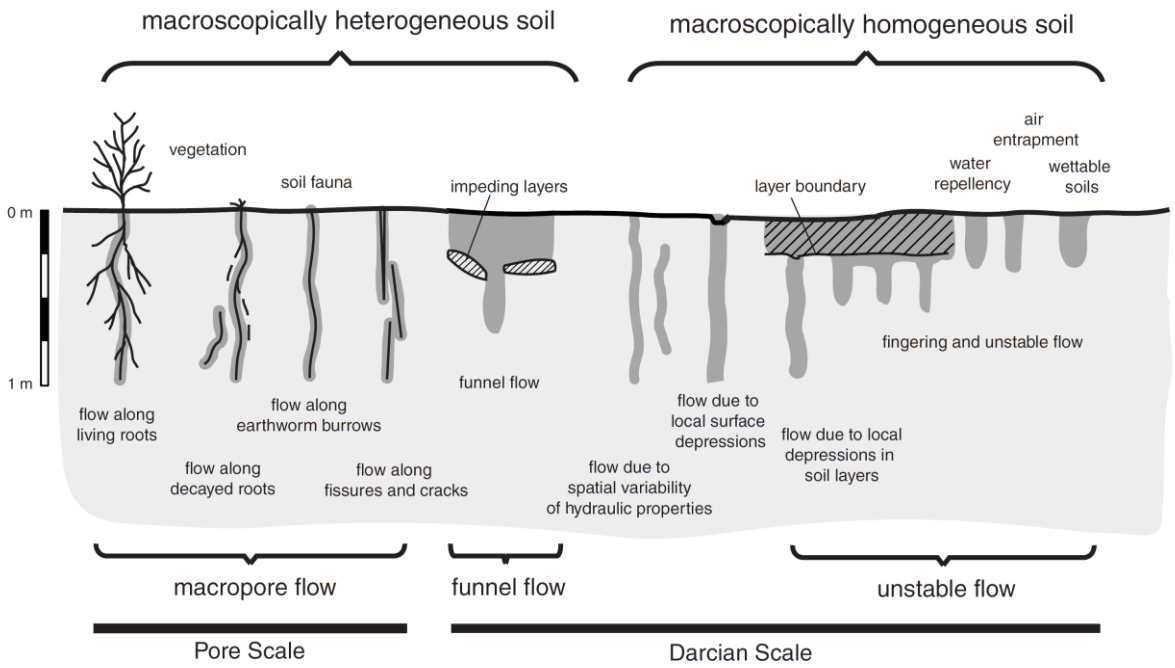

Figure 1.1: Schematic showing different preferential flow mechanisms observed at pore and Darcian scales (Hendrickx & Flurry, 2001).

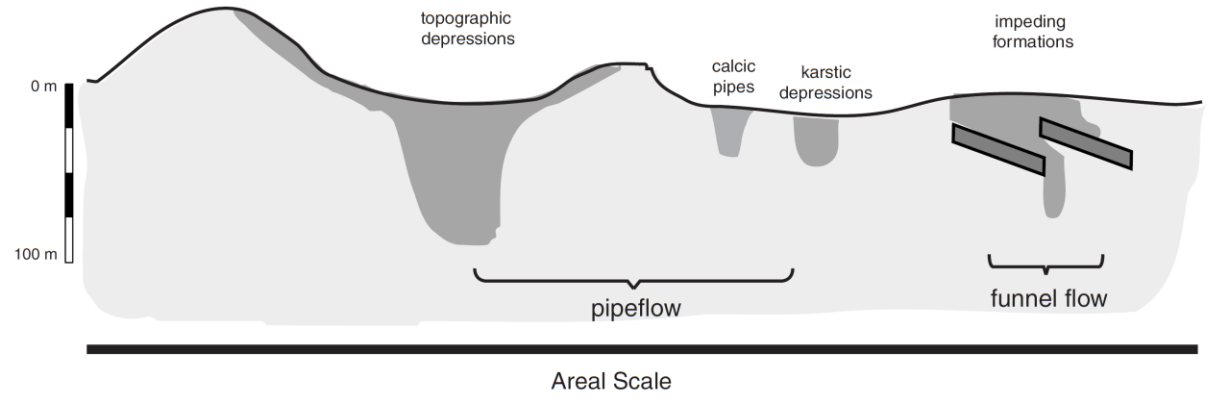

Figure 1.2: Schematic showing different preferential flow mechanisms observed at an aerial scale (Hendrickx & Flurry, 2001).

Unstable flow may be caused by various factors. Entrapment of air bubbles may cause stable flow to break off into fingers (Wang *et al*., 1998). The presence of displacement vaults in sandy soils of tectonically active regions may provide PF paths for unstable flow (Sigda, 1997). Non-ponding infiltration has been found to percolate as fingers in the absence of macropores and cracks (Hendrickx & Dekker, 1991). The latter may be due to spatial variability in hydraulic properties (Roth, 1995), possibly due to antecedent soil water in the PF paths (Hendrickx & Flurry, 2001). Layered soil profiles provide discontinuities which may concentrate the flow of water into small depressions at the horizon interface (Starr *et al*., 1978).

Funnel flow may cause unstable flow as water or solutes flow through the paths of least resistance in fine textured or structured soils (Kung 1990). The terminology in the latter case should be addressed as funnel flow is referred to as a separate type of PF by Hendrickx & Flurry (2001) yet here it is referred to as a possible cause of unstable flow. A possible differentiation could be made based on the scale of the flow pattern. Where funnel flow on a small scale may be defined as a cause of unstable flow, but where funnel flow occurs on a larger scale it may be classified as a separate type of PF. If such differentiation is made it should be clearly noted.

Hydrophobicity as a cause of PF is very common in topsoils in areas where veldfires occur regularly due to the amount and type of organic C that occurs (Lamparter *et al*., 2006; Ellerbrock *et al.,* 2005). The degree of hydrophobicity can be calculated from measurements using a mini-disc infiltrometer filled with an ethanol solution (Decagon Devices Incorporated, 2007), as done by Hallett *et al* (2004) who found a greater spatial variability in surface hydrophobicity than for geometric pore structure. Hydrophobicity has been found to alter the water retention capacity of soils which in turn changes the water content dependent hydraulic conductivity (Lamparter *et al*., 2006). Up to 80% of the infiltrated water has been found to enter the soil *via* PF in hydrophobic soils (Ritsema & Dekker, 1994). However, there is usually a divergence layer below the layer where PF occurs, in which lateral redistribution occurs (Van Dam *et al*., 1990). The hydrophobicity is also found to be dependent on volumetric water content and can be overcome at high moisture contents (Lamparter *et al*., 2006). On the other hand, PF can only occur after a minimum amount of water is supplied to the soil system at a high enough rate (Hendrickx & Flurry, 2001).

It is understandable why researchers recommend calibrating models based on local soil data when considering the various PF patterns mentioned above. Different PF mechanisms are inherent to specific soil patterns; this relationship is however not fully understood, thus justifying further catchment or even soil pattern specific PF modelling.

1.2.2. Soil pattern analysis and aquifer recharge estimation

Modelling groundwater recharge demands time and monetary expenses and a fair degree of know-how due to the inescapable time and spatial heterogeneity found in nature. This heterogeneity is manifested in soil pattern and surface conditions, climate, land use and vegetation differences which exist from the large geological scale to the macropore scale (Sivapalan, 2003).

In depth hydrological research is warranted as simplistic hydrological approaches have been proven inadequate due to the heterogeneity. One such approach is the assumption that all excess infiltration that does not evaporate or form soil water contributes to recharge. This approach is deficient as the net recharge was found to be less than the total downward flow to the water table (de Vries & Simmers, 2002).

In the study of groundwater; “where, when and how” water passes through the soil needs to be known and, where possible, related to the soil pattern or soil forming processes occurring in the area of interest. If this relationship can be effectively modelled, point observations (bulk density, soil colour, organic matter and porosity) can be linked to hillslope water dynamics and ultimately to large scale catchments (Lin *et al*., 2006). The interdisciplinary approach which investigates the relationship between soil pattern and hydrological responses is known as hydropedology.

Hydropedology is based on the principle that spatial distribution of soil features indicates the dominant water regime in the landscape. The soil system will change in relation to the soil forming processes, water being the dominant driving force, until equilibrium is reached between the soil and the environment (Fritsch & Fitzpatrick, 1994). Thus, soil features can either be in sync with the environment or out of phase. When equilibrium is reached the soil features will indicate current hydrological conditions. In contrast, an out of phase soil system may suggest a hydrological regime that is either wetter or drier than the actual regime. Identifying whether a soil system is in or near equilibrium is therfore important when inferring a water regime from soil features (Fritsch & Fitzpatrick, 1994).

This section of the literature review will investigate the water flow paths from the soil surface through to the subsoil. The aim is to justify using soil pattern as a focal point in groundwater recharge estimation. It will also discuss how soil survey information can be used to predict dominant water flow paths and ultimately improve groundwater recharge estimation.

1.2.2.1. Soil pattern dominated flow paths

Catchment response to a rainfall event is dictated by various factors including climate, topography, vegetation, geology and soil pattern (McDonnell *et al*., 1990; Sandström, 1996). Soil pattern refers to the spatial distribution of soils with respect to variation in soil properties in the horizontal and vertical plane.

Due to its position in the watershed, soil has a dominating effect on catchment dynamics as it is responsible for dividing rainfall into infiltration and surface runoff as illustrated in Figure 1.3. The infiltrated water is then divided into water liable to evapotranspiration and deep percolating water. The groundwater may recharge the underlying aquifer, redistribute laterally or be taken up by plants and transpire back into the atmosphere. It is thus practical that soil is viewed as a control point in water dynamics and that the implications of this are well understood (Pionke *et al.*, 1996).

Figure 1.4 illustrates the different possible flow paths along a slope as well as the respective diagnostic horizons that could form. The soil gets deeper and horizon development becomes more complex at the footslope where colluvium accumulates as the suspended soil particles in the surface runoff settle due to the slope decline. Water saturated conditions are also more likely to occur at the footslope.

The diagram also shows flow in the bedrock. This diagram is not universal, but serves as a useful example of a dissected hillside and the profile formation therein, known as a catena.

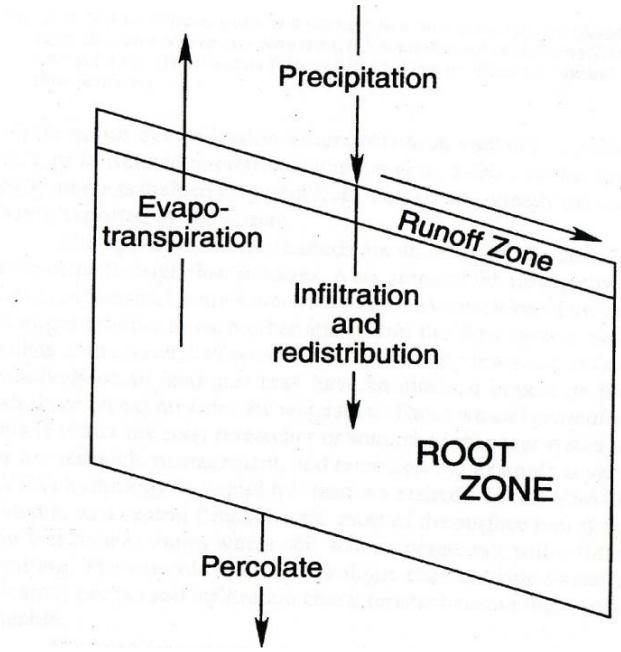

Figure 1.3: Showing possible fates of precipitation (Pionke, *et al.*, 1996).

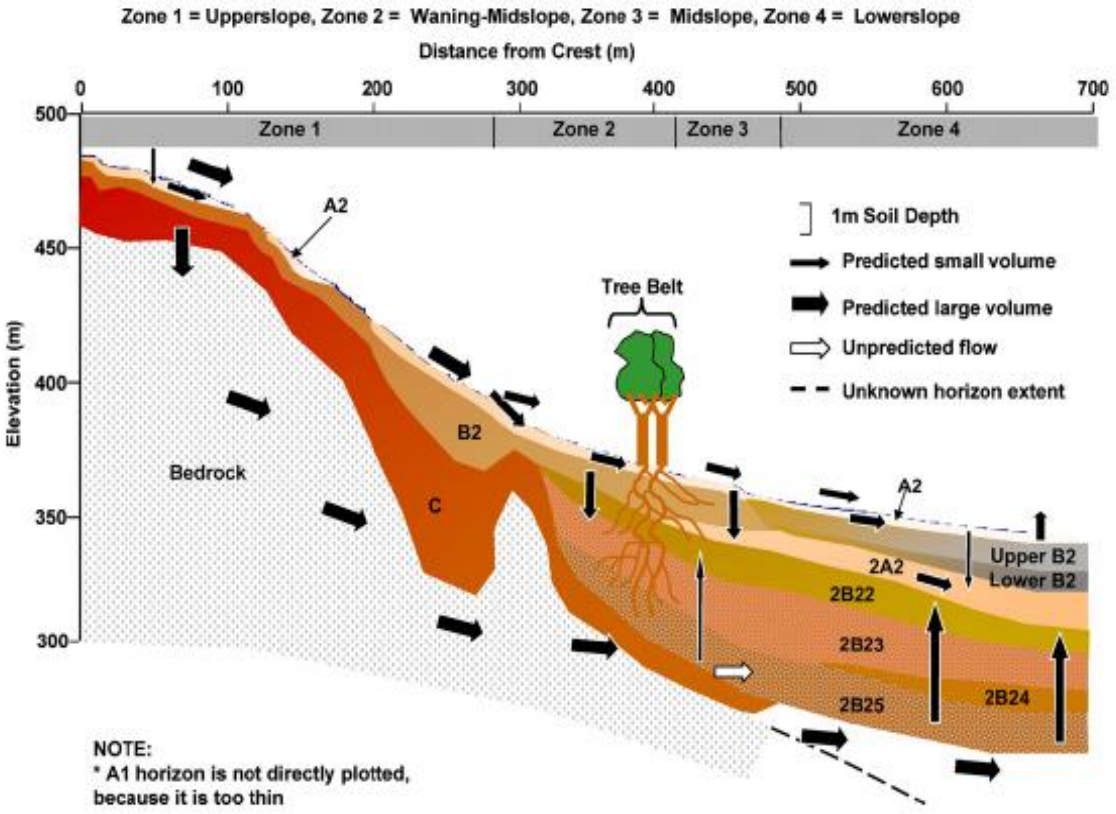

Figure 1.4. An illustration of a catena from the work of Ticehurst *et al*. (2007) to illustrate the soil depth and hillside flowpaths.

Lin *et al.* (2006) accurately described the four main flow paths in the soil. Close to the surface water will flow as subsurface seepage through macropore networks made by soil borne animals and roots. Variation in soil bulk density, structure and hydraulic properties between the A and B horizons will cause lateral redistribution. Similarly, water may flow laterally at the interface between the soil and bedrock. Investigating this type of flow is difficult due to observation restrictions. Finally, return flow of groundwater as surface water at the footslope may occur during the wet season.

Lin omits to mention the movement of water in fractures in the bedrock which according to Asano *et al*. (2002) and Ticehurst *et al.* (2007) is a large contributor to groundwater recharge. Vertical flow of groundwater is considered to be dependent on both the aperture and spacing of bedrock fractures and the thickness and hydraulic conductivity of the soil cover (Gleeson *et al.*, 2009). The contribution of bedrock as a PFP depends on the permeability of the rock (which is often too low to support flow) and the presence of fractures.

The presence of such bedrock fractures always increases the complexity of the modelling process as the hydraulic properties and geometry of the fractures need to be quantified or specified individually (Oxtobee & Novakowski, 2003). Groundwater recharge through these continuous fractures from surface water is often limited to areas where the fracture network is continuous. Deep percolation is often limited in mountainous terrain as much of the water may seep out in the form of interflow discharge due to impeding soil horizons that reduce vertical flow (Sophocleous, 2002) or limited permeability at depth (Colvin, 2008). These discharge zones can be seen as seeps on the soil surface.

Bedrock fractures are almost always filled to some extent with soil and vegetation. Infiltration may occur in these fractures but if the rate of rainfall is greater than the rate of infiltration, surface runoff, and possibly soil erosion, may occur. The effect of the soil and vegetation in the fractures is to reduce the volume of the fracture that is available for water flow. Infiltration into these soil filled fractures is often very high but the aperture of the fracture closes with depth and thus the infiltrated water may be transported laterally as interflow instead of deep drainage. The size of the fracture opening at the surface controls the degree of infiltration but the degree of recharge is governed by the size of the fracture at depth, thus large open fractures will favour rainfall infiltration and preferential recharge (Xu *et al.*, 2007).

The variable permeability of the aquifer is thus dependent on both the bedrock and soil cover hydraulic conductivities. The permeability will determine whether an aquifer section is a recharge area where addition of water to the system occurs, a flow area where water is laterally distributed or a discharge area where water is removed from the system (Xu *et al.*, 2007). Permeability of aquifers can be either primary, if inherited from the parent material, or secondary if formed as the parent material weathers.

The type of permeability will differ between rock types due to the type of weathering and differences in the physical and chemical nature of the rock. Figures 1.5 and 1.6 illustrate two possible secondary permeabilities. These two types of permeability will give rise to different groundwater discharge patterns: A flat, sandy unconsolidated aquifer (Fig. 1.5) may sustain terrestrial vegetation with a widespread shallow water table whilst a fractured meta-sediment system (Fig. 1.6) will discharge via faults and fractures which are seen on the surface as linear seeps or wetlands (Colvin *et al*., 2007).

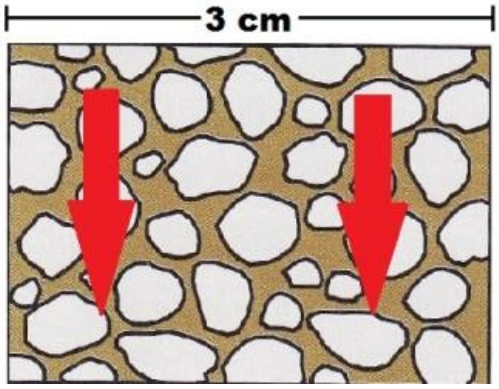

Figure 1.5: Flat, sandy, unconsolidated aquifer system (Colvin *et al*., 2007). Arrows indicate the general flow paths of infiltrating water.

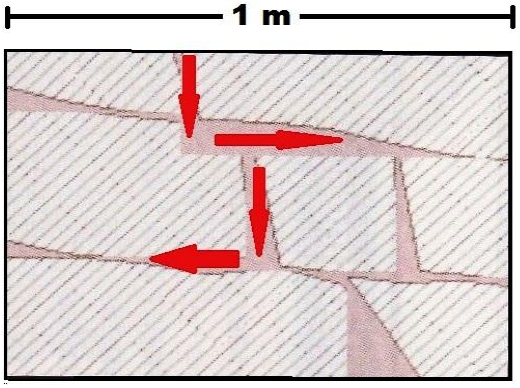

Figure 1.6: Fractured meta-sediment aquifer system (Colvin *et al*., 2007). Arrows indicate the general flow paths of infiltrating water.

Together with the permeability of the aquifer system, the slope of a hillside is a dominant factor regarding infiltration and recharge. A gentle slope will favour groundwater recharge whereas a steep slope will favour surface runoff (Xu *et al.*, 2007). Horizontal movement of water in a flat terrain only occurs under saturated conditions as gravity does not allow for transient flow (Karvonen *et al*., 1999). The bedrock contact dip angle, relative to the slope of the sediment is also important as this will determine the depth to which water can infiltrate (Fig. 1.7). If the bedrock is dipping away from the surface and the dip angle is greater than the slope angle, recharge will be favoured.

Based on the groundwater's location and hydraulic behaviour, it can be divided into one of two types; Transient Groundwater (TGW) and Perennial Groundwater (PGW). TGW moves through the soil relatively quickly, whereas PGW has a longer residence time in the profile. PGW can be found lower down in the landscape, whereas TGW is found higher up in the landscape. TGW moving laterally in the soil profile is affected by stratification, topography and soil layering (Asano *et al.*, 2002).

TGW and PGW have also been referred to as dynamic and static groundwater respectively (Jovanovic, 2009). These two forms are illustrated in Figure 1.8. The figure does not represent a specific aquifer system but merely serves to illustrate the two storage zones. The most important parameter in determining the rate at which a groundwater source is replenished is the recharge of the dynamic storage zone which is often in contact with, or well within, the soil cover.

Understanding the residence times of groundwater is important as the chemical reactions between soil and water are time dependent. Thus predicting water chemistry and temporal changes thereof requires residence times. PGW residence times were found to be positively correlated with the soil depth as well as upslope contributing area due to the large fraction of PGW which originates from the deep bedrock. The TGW was however found to be better correlated with the vertical infiltration depth. Even so, it is possible for these two flow paths to merge shortly before discharging at a footslope or lithological discontinuity as a spring or seep (Asano *et al.*, 2002)

1.2.2.2. Key soil parameters for hydropedology

Ticehurst *et al.* (2007) reported that the use of soil morphological factors to study hillslope hydrology is attractive as it depends on point observations taken at one place and time, but reflect the dominant hydrological processes at work. Point observations are low cost compared to hillslope monitoring and can thus be replicated at many locations at different times. Connecting watersheds to the above mentioned point observations can effectively be done with the use of a soil map (Lin *et al*., 2006).

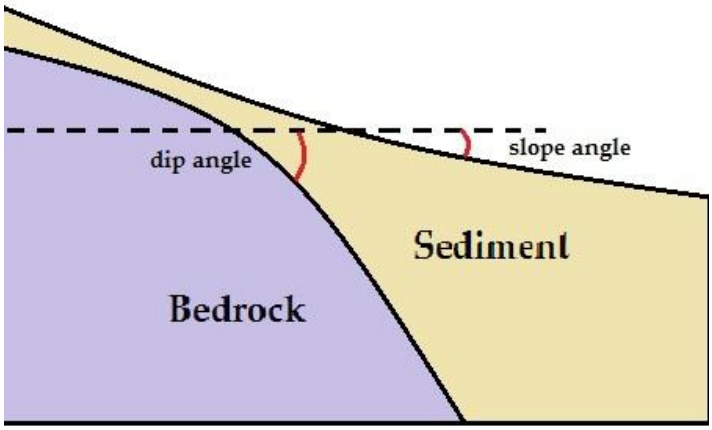

Figure 1.7: Illustration to show the contact dip angle relative to the slope gradient (Xu *et al.*, 2007).

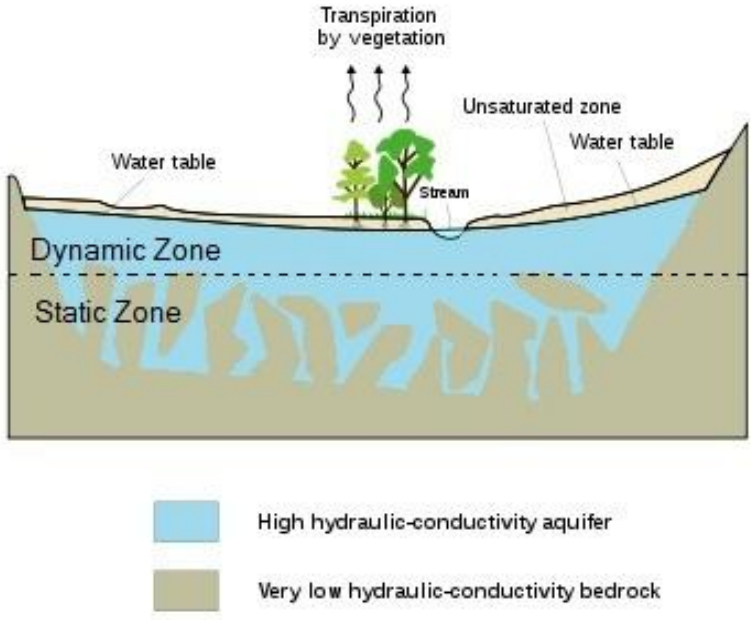

Figure 1.8: A simplified figure showing the static and dynamic groundwater storage zones (Adapted from Jovanovic, 2009).

Lin *et al.* (2006) caution that the distribution of soils and the understanding of the occurring processes are poorly understood as the actual sampling, sample point distribution and the modelling of the data are often poorly correlated. He recommends that the point observation at pedon scale and the landscape modelling based on aerial distribution should be linked through the effective use of soil maps. This entails the mapping of pedon observations and relating landscape features, such as vegetation, topography and geology, to the soil distribution. Features that could be observed at a pedon scale are discussed below. Not all these features will always be present but accurate description of these features is crucial if the data is to be effectively used in a hydrological study.

Mottling

To understand the existence of soil mottling one must grasp the fundamentals of soil redox potential as soil morphological development can largely be attributed to the change thereof. Anaerobic conditions during water saturated periods provide reducing conditions in the soil which will allow reduction of ferric iron (Fe^{3+}), a stable form of iron in the soil, to the more mobile ferrous iron (Fe^{2+}). The mobile form can be transported in the soil, either locally or removed from the profile all together, depending on the soil water regime (le Roux & du Preez, 2008). Fe^{2+} will oxidize to form Fe^{3+} when exposed to air as is the case when water saturated conditions cease (le Roux & du Preez, 2008; Veneman *et al.*, 1976). Other factors such as OM and biological activity also have an effect on redox potential.

Veneman *et al.* (1976) defined three broad soil water regimes that could be identified by the types of mottles present. The grouping is based on the relative presence of Fe and Mn manifested as the chroma of the ped interior. Short periods of saturation will only cause a decrease in Mn content, whereas longer periods of saturation will result in increasing Fe and Mn losses until all the Mn and Fe is removed from the system. This process is accompanied by a decrease in the chroma of the ped interior.

Mottles can be described by noting the colour contrast, size and abundance of mottles in the horizon (Soil Classification Working Group, 1991). A sharp transition between a mottle and the surrounding soil environment is the effect of bioturbation where a discrete oxygen gradient existed. A gradual transition between a mottle and the surrounding soil is a result of a chemical gradient, plinthite formation and/or Fe-Mn redistribution in the soil. Bioturbation is more prevalent closer to the soil surface whereas the number of diffuse mottles increases with depth (le Roux & du Preez, 2008).

The presence of mottles is the most important diagnostic criterion when classifying a soft plinthic B horizon (Soil Classification Working Group, 1991). However, the use of soft plinthic B horizons to predict the soil water regime in arid climates is questionable as the mottles found in arid regions could be relict from a wetter past regime (Loxton *et al.*, 1991) as South African soils have been subject to both wet and dry bioclimates (Tyson, 1986).

Cogger & Kennedy (1992) and McKeague (1965) found that reduction in the subsurface horizons of seasonally saturated soils is related to the saturation of the surface horizon. It is hypothesized that movement of O_2 to the subsoil is limited if the surface horizon is periodically saturated.

Water tables have been found higher up in the profile than what signs of wetness would suggest due to periods of saturation without reduction. This occurs when the soil is too cold to allow effective microbial activity to completely deplete the O_2 supply in the soil (Cogger & Kennedy, 1992). This however is not likely to occur in South Africa due to a more temperate climate.

Soil Colour

Soil colour can effectively be used to predict soil water regime (Cogger & Kennedy, 1992; Ticehurst *et al.*, 2007). Soil colour is mostly determined by the Fe-compounds present. The most common minerals that exist are; hematite, which has a dominant red colour and goethite, lepidocrocite and ferrihydrite, which are yellow (van Huyssteen, 1995). Gleyed soils contain grey colours when all Fe-compounds have been removed from the soil or blue and green colours when ferrous compounds are present (Soil Classification Working Group, 1991). The green rust and blue colours of gleyed soil will fade in the presence of oxygen and colour description must occur quickly upon exposing the profile to air (Richardson & Daniels, 1993).

The sequence of colours; red, brown, yellow and grey, corresponds to an increased degree of saturation (Ticehurst *et al*., 2007). This sequence corresponds to the hydrology as follows: the well drained soils on the upper-slope will be red, due to a low degree of saturation and thus negligible removal of Fe and Mn compounds. Further down-slope, the soils will progressively increase in depth and degree of saturation, accompanied by a decrease in red colours and an increase in grey colours. This catena development is shown by van Huyssteen (1995) in Figure 1.9.

Attention is focussed on the red apedal B horizon on the upper-slope, which grades into the yellow-brown apedal B, then a yellow E and G and then finally the grey E and G at the footslope. The presence of a soft plinthic B horizon also indicates a periodic water table as discussed in the section on mottling above.

The red edge effect, illustrated in figure 1.10, is a phenomenon where red soils occur closer to a valley backslope, while soils affected by more severe redoximorphic conditions, having paler colours, occur towards the level interior away from the slope. The sequence of soil colour formation seems to be somewhat common as it has been found in till, lacustrine, loess, fluvial and marine deposits (Richardson & Daniels, 1993).

Soil colour is described by using a Munsell colour chart (Munsell, 1912). A pedofeature is given a verbal description, e.g. yellow or brown, and the description is followed by a Munsell notation e.g. 10YR5/4 (Soil Classification Working Group, 1991). It has been found that the Munsell colour notation parameters can effectively be used as part of various indices to predict the percentage time that the specific soil is saturated in a year (van Huyssteen, 1995).

Van Huyssteen further commented that the Soil Classification Working Group is accurate in their differentiating between different wetness classes when classifying red apedal B, yellow-brown apedal B and E horizons.

Texture

When using textural analysis to determine hydrological properties, researchers refer to the relative mass percentages of sand, silt and clay. More fractional size classes are often used when studies are done in more detail (Rawls *et al.*, 1991). When compared to soil bulk density and OM content, soil texture showed the strongest correlation with water retention variations in soils (Vereecken *et al*., 1989). Fine textured soils have a greater potential to retain water relative to coarse textured soils. In soils with an intermediate texture, the water retention was found to have a strong correlation to grading; as a well graded soil has a higher water retention than a poorly graded soil at a given suction (Pachepsky *et al.*, 2006).

Fine soil particles may be transported and deposited on lowerslopes by slopewash, resulting in a relative accumulation of coarse textured soils upslope and fine textured soils at the footslope. The higher clay content would reduce the drainage in these soils and increase the probability of saturated conditions at the footslope (Ticehurst *et al*., 2007).

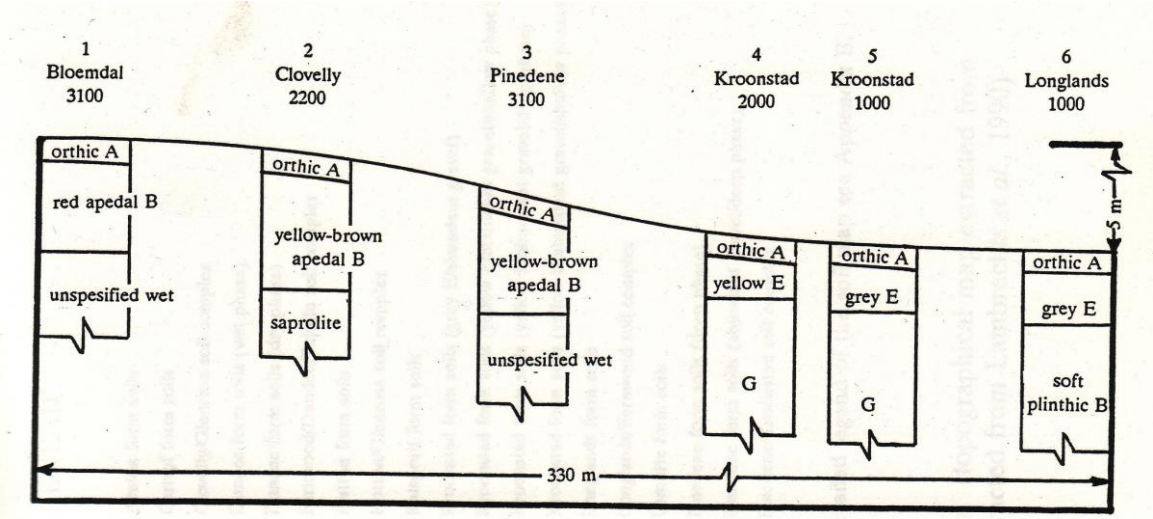

Figure 1.9: A schematic representation of a catena (van Huyssteen, 1995).

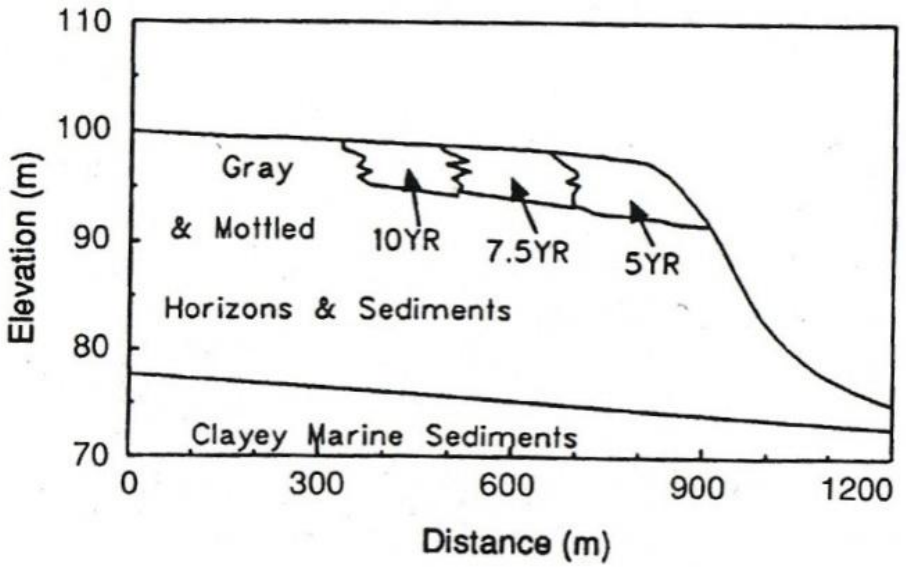

Figure 1.10: The red edge effect (Richardson and Daniels, 1993).

An abrupt textural discontinuity between adjacent soils is a characteristic of duplex soils. Acidification of topsoils may result in the formation of duplex soils as Fe-oxides and clay become unstable and leach from the topsoil into the subsoil causing an increase in structure formation. When this type of clay movement occurs, a perched water table may form as the water will not infiltrate the poorly permeable, clay rich subsoil horizon. Also characteristic of duplex soils is the relative accumulation of gravel and sand in the topsoil due to the concentrating effect of clay elluviation (Fritsch & Fitzpatrick, 1994).

Clay mineralogy becomes important when a soil contains more than 10% clay. For instance montmorillionite (2:1 swelling clay) will have more of an impact on water retention than kaolinite (1:1 non-swelling clay) (Rawls *et al.*, 1991). Broad clay classes were found to be an accurate input parameter for pedotransfer functions (Pachepsky *et al.*, 2006).

Structure, bulk density and organic material

Soil texture plays a crucial role in hydraulic functioning of soil water at a micropore level, however soil structure (pedality and porosity) becomes more important at a macropore level (Lin *et al.*, 1999). Soil structure is defined as the presence of "*repetitive soil bodies that are commonly bounded at planes or zones of weakness that are not an apparent consequence of composition differences*" (Soil Science Staff, 1997). The structural grade of these units can be described by referring to the relative strength of the units. The grade classes are: structureless, weak, moderate and strong (Pachepsky *et al.*, 2006). These structural characteristics are rarely incorporated into PTFs due to the difficulty in quantifying soil structure (Lin *et al*., 1999).

Soil structure has a large influence on soil water dynamics in that a fine textured soil with low porosity and strongly developed horizontal structure formation would promote lateral flow of water. On the other hand, vertical soil structure formation would reduce lateral flow, making vertical infiltration the dominant form (Ticehurst *et al*., 2007).

Soil OM content and bulk density both have an effect on soil structure. An increase in OM is usually accompanied by an increase in water retention capacity and a decrease in bulk density. At field capacity, bulk density commonly has a greater effect on water retention, as an increase in bulk density results in a decrease in water holding capacity (Rawls *et al.*, 1991).

Salinity and sodicity

Weathering of saprolite in downslope positions during saturated conditions will release salts into the fresh water. The water will rise to the surface via preferential flow paths or as a shallow water table at which point free salts may precipitate and concentrate at the evaporation front as water is removed from the soil system. This precipitate is usually in the form of halite or gypsum and can often be seen in saline or eroded patches (Fritsch & Fitzpatrick, 1994).

The salt precipitate on the surface may wash into deeper soil and cause clay dispersion after the next rainfall or irrigation event with fresh water (Seelig & Richardson, 1994). Saline soils can also result when the water level is changed as is the case when saline groundwater is diluted by fresh water to favour weathering of the saline soil which may lead to structure loss or severe soil swelling and hardsetting (Fritsch & Fitzpatrick, 1994).

Observing salinity may be obvious in the form of a white precipitate or less obvious as subsoil mottling (Brouwer & Fitzpatrick, 2002). Vegetation can also indicate salinity as certain species are better adapted to grow in severe saline conditions, for example *Distichlis spicata*, more commonly known as Saltgrass (Seelig & Richardson, 1994).

Erosion

Soil erosion by water is one of the most obvious indicators of water behaviour. Erosion exists due to successive cutting and deposition phases. The severity of water erosion will correlate with the volume and intensity of water that flows in the specific location. Sheet and rill erosion are less severe forms of water erosion but are none the less precursors to the more severe donga and gully erosion. Sheet and rill erosion is favoured in seepage areas where soil structure and cohesion is poor and stunted halophytic vegetation is found. These rills eventually converge to form shallow, and eventually deep, gullies closer to the streambed (Fritsch & Fitzpatrick, 1994).

To effectively correlate soil point observations to watershed dynamics, one requires understanding of both soil science (pedology, physics, ecology and chemistry) and hydrology.

1.2.2.3. Connecting soil survey data to hydrology using pedotransfer functions

Physical soil survey data can be used quantitatively by transforming the data using pedotransfer functions (PTFs). PTFs utilize regression, empirical or functional relationships

to translate physical soil survey information into complicated simulation input parameters (Pachepsky *et al.*, 2006). PTFs are most effective when used on a regional scale compared to a site-specific study (Lin *et al*., 1999).

Two types of PTFs exist: Continuous-PTFs with parameters such as clay, silt and sand fractions, organic carbon, dry bulk density, porosity and initial water content. These PTFs are derived from continuous variables. The other type, class-PTFs, has parameters: texture, pedality and ped size and shape, macroporosity, root density and root size. Class PTFs depend on specific class variables (Lin *et al*., 1999).

However, the use of PTFs is not without defect as the application of PTFs remains limited even when the number of relevant parameters is increased. The PTFs from one region could not be extrapolated to another region. Quantifying and qualifying morphological features is also difficult as is the case with soil structure which is usually described qualitatively with very broad classes, making it difficult to relate physical data to a hydrological function (Pachepsky *et al.*, 2006).

When choosing a model to use as a PTF, one must remember that the model must be able to incorporate land use as well as spatial heterogeneity of the catchment hydrology (Karvonen *et al*., 1999). To add to this, Karvonen *et al.* (1999) proposed that instead of working with a fully distributed catchment, the area can be divided into “hydrologically similar units” (HSUs). HSUs are areas in the catchment that have similar hydrological characteristics with reference to soil, land use, slope and vegetation. This is particularly useful when working with a very large area. HSUs make up the hillslopes, which are the fundamental landscape units which in turn make up sub-watersheds and ultimately watersheds (Ticehurst *et al.*, 2007).

Examples of such PTFs can be seen in the literature review section on flow paths.

1.2.2.4. Mapping of survey information

As recommended by Lin *et al.* (2006), soil point observations can be linked to the watershed by studying their relative distribution on a map. A soil map can be used to indicate reference groups which will display similar characteristics, as in the case where Voltz *et al.* (1997) used soil type and depth to the water table to outline such reference groups. They however commented that soil maps have subjective character depending on the experience of the surveyor. The assumption that variation of soil properties only exist between reference groups is also misleading. This assumption can only be made if the soil

map was accurately compiled on a scale between 1:10 000 or 1:25 000 (Voltz *et al.*, 1997). To further complicate the use of soil maps for hydrological purposes, Jaynes & Hunsaker (1989) found that temporal variations also exist during infield infiltration. It is in this light that Browning & Duniway (2011) recommend that updated maps with greater accuracy and resolution be compiled, not only of high potential agricultural lands but of drylands as well. They suggest that "digital, raster-based maps of soil properties" are ideal to assist in improving understanding of plant community patterns and dynamics.

De Vos *et al.* (2005) reported that reference groups may be taken as more or less homogenous strata when estimating soil water properties. With this said, the accuracy of the resulting map and the respective estimations is dependent on the degree of homogeneity of the classes and the precision with which data was collected. Nonetheless, using maps to display soil property distributions is done regularly with great effect as in the case where Vidacek *et al.* (2008) used ESRI GIS software to produce a hydropedological map of the Republic of Croatia.

The next challenge in compiling a soil map is to accurately interpolate or extrapolate values from monitored sites to unsampled areas. This is done as observation points are often limited in soil surveys, especially when conducted on small scale. Numerous methods have been developed to allocate values to the unsampled "space" between observations. For detailed comparative studies on the different methods refer to Motaghian & Mohammadi (2011), Voltz *et al.* (1997), Voltz & Goulard (1994), Comenga & Basile (1994), and Voltz & Webster (1990).

Voltz & Webster (1990) and Voltz & Goulard (1994) used an effective interpolation method where they combined kriging and soil classification. A common limitation to using kriging in soil surveys is that it requires many observations to generate accurate interpolations. Thus, by using soil classification as an additional input for interpolation, one can cope using fewer observations. A comparative study between using kriging, kriging-soil classification and nearest neighbour reported that combining kriging and soil classification method produced more accurate estimations relative to measured data (Voltz & Webster, 1990). This method works well when the within class variation is less than the universal variation of a specific property (Voltz & Goulard, 1994).

Hansen *et al.* (2009) used a binary decision tree (BDT) to compile a large scale map of a 2214 km^2 area in central Uganda. The decision tree was compiled by experts but the application thereof is fairly simple. BDT's can also be automated on GIS software. This

method of allocating information is attractive as it is unbiased and can be customized for a specific location.

1.3. Conclusion

Threats from growing populations, industry and agriculture and global warming is pressuring researchers to improve hydrological estimation models to better manage precious water resources, especially in water scarce countries like South-Africa. The Western Cape Province has numerous potable groundwater sources and management thereof depends on understanding two main factors: The rate of water extraction and the rate of water recharge. A drive to improve the accuracy of process based groundwater recharge estimations is ongoing by the CSIR. This literature review covered two main themes pertaining to this study namely: 1. Flow modelling in soils and 2. Soil pattern analysis.

Section 1 dealt with the different causes of preferential flow, which was identified as an influential factor in groundwater recharge, and provided an overview of numerous methods used to model flow. These models, referred to as PTFs, make it possible to link soil physical properties, such as texture and OM content, to hydrological properties like hydraulic conductivity.

Section 2 discussed the different flow paths and the factors that affect water dynamics in soil. It also dealt with the potential of using a soil survey as a “hydrological toolkit” by correlating physical soil observations with hydrological regimes. This section identified temporal and spatial heterogeneities and the difficulty to quantify physical soil properties as the most limiting factors when modelling soil water dynamics or upscaling estimation models. The soil properties discussed in section 2 can be displayed on a soil map to study their position relative to the landscape and so too the water regimes. These soil properties can thus be correlated to hydrological regime if they can be accurately quantified.

Researchers can thus use PTFs to estimate soil hydraulic properties using soil physical properties from soil surveys as input parameters. These estimated hydraulic properties can then be correlated to specific soil types using a soil map. Once these relationships are established, hydrological estimation models can be upscaled more accurately using soil survey information. These hydropedological relationships should be calibrated using long term site specific data.

1.4. References

ASANO, Y., UCHIDA, T. & NOBUHITO, O., 2002. Residence times and flow paths of water in steep unchannelled catchments, Tanakami, Japan. *Journal of Hydrology* 261, 173-192.

BOERS, TH.M., 1994. Rainwater harvesting in arid and semi-arid zones. P.hD. Thesis, Wageningen University, International Land Reclamation and Improvement Institute.

BOSWELL, J.S. & OLYPHANT. G.A., 2007. Modelling the hydrologic response of groundwater dominated wetlands to transient boundary conditions: Implications for wetland restoration. *Journal of Hydrology* 332, 467-476.

BROUWER, J. & FITZPATRICK, R.W., 2002. Interpretation of morphological features in a salt-affected duplex soil toposequence with an altered soil water regime in Western Australia. *Aust. J. Soil Res.* 40, 903-926.

BROWNING, D. & DUNIWAY, M., 2011. Digital soil mapping in the absence of field training data: a case study using terrain attributes and semiautomated soil signature derivation to distinguish ecological potential. *Applied and Environmental Soil Science*, 1-12.

COGGER, C.G. & KENNEDY. P.E., 1992. Seasonally saturated soils in the Puget Lowland I. Saturation, reduction, and color patterns. *Soil Science* 153, 421-433.

COLVIN, C., 2008. Ecological and environmental impacts of large-scale groundwater development in the TMG aquifer system. *WRC Report* No. K5/1327. Stellenbosch.

COLVIN, C., LEMAITRE, D., SAAYMAN S. & HUGHES, I., 2007. An introduction to aquifer dependent ecosystems in South Africa. *WRC Report* No. TT 301/07, Stellenbosch.

COMEGNA, V. & BASILE. A., 1994. Temporal stability of spatial patterns of soil water storage in a cultivated Vesuvian soil. *Geoderma* 62, 299-310.

DE VOS, B., VAN MEIRVENNE, M., QUATAERT, P., DECKERS, J. & MUYS, B., 2005. Predictive quality of pedotransfer functions for estimating bulk density of forest soils. *Soil Sci. Soc. of Am. Journal* 69, 500-510.

DE VRIES, J.J. & SIMMERS, I., 2002. Groundwater recharge: an overview of processes and challenges. *Hydrogeology Journal* 10, 5-17.

DECAGON DEVICES INCORPORATED, 2007. Mini Disc Infiltrometer User's Guide, Vol. 8. Decagon Devices Incorporated, Pullman.

DELIN, G.N., HEALY, R.W., LANDON, M.K. & BOHLKE, J.K., 2000. Effect of topography and soil properties on recharge at two sites in an agricultural field. *Journal of the American Water Resources Association* 36, 1401-1416.

ELLERBROCK, R.H., GERKE, H.H., GOEBEL, J. & BACHMANN, M.-O., 2005. Composition of organic matter fractions for explaining wettability of three forest soils. *Soil Sci. Soc. Am. J.* 69, 57-66.

FEYEN, J., JACQUES, D., TIMMERMEN, A. & VANDERBORGHT, J., 1998. Modelling water flow and solute transport in heterogenous soils: A review of recent approaches. *J. agric. Eng Res.* 70. 231-256.

FRITSCH, E. & FITZPATRICK, R.W., 1994. Interpretation of soil features produced by ancient and modern processes in degraded landscapes. I. A new method for constructing conceptual soil-water-landscape models. *Aust. J. Soil Res.* 32, 889-907.

GLEESON, T., NOVAKOWSKI, K. & KYSER, K., 2009. Extremely rapid and localized recharge to a fractured rock aquifer. *Journal of Hydrology* 376, 496-509.

HALLETT, P.D., NUNAN, N., DOUGLAS, J.T. & YOUNG, I.M., 2004. Millimeter-scale spatial variability in soil water sorptivity: scale, surface elevation, and subcritical repellency effects. *Soil Sci. Soc. Am. J.* 68, 352-358.

HANSEN, M.K., BROWN, D.J., DENNISON, P.E., GRAVES, S.A. & BRICKLEMYER, R.S., 2009. Inductively mapping expert-derived soil-landscape units within dambo wetland catenae using multispectral and topographic data. *Geoderma* 150, 72-84.

HENDRICKX, J.M.H. & FLURRY, M., 2001. Uniform and preferential flow mechanisms in the vadose zone. p. 149-187. *In*: Conceptual Models of Flow and Transport in the Fractured Vadose Zone, NATIONAL ACADEMY PRESS, Washington, D.C.

HENDRICKX, J.M.H. & DEKKER, L.W., 1991. Experimental evidence of unstable wetting fronts in non-layered soils. p. 22-31. *Proc. Natl. Symp. on Preferential Flow.* Chicago.

HENDRICKX, J.M.H., DEKKER, L.W., BANNINK, M.H. & VAN OMMEN, H.C., 1988. Significance of soil surey for agrohydrological studies. *Agricultural Water Management* 14, 195-208.

HILLEL, D., 1980. Fundementals of soil physics. Academic Press Inc., San Diego.

HOSANG, J., 1993. Modelling preferential flow of water in soils - a two-phase approach for field conditions. *Geoderma* 58, 149-163.

JAYNES, D.B. & HUNSAKER, D.J., 1989. Spatial and temporal variability of water content and infiltration on a flood irrigated field. *Trans. Am. Soc. Agric. Eng.* 32, 1229-1238.

JOEL, A. & MESSING, I., 2001. Infiltration rate and hydraulic conductivity measured with rain simulator and disc permeameter on sloping arid land. *Arid Land Research and Management* 15, 371-384.

JOVANOVIC, N., 2009. Reducing uncertainties of evapotranspiration and preferential flow in the estimation of groundwater recharge. *CSIR Research Proposal* No. 1001619, Stellenbosch, Western Cape.

KARVONEN, T., KOIVUSALO, H., JAUHIAINEN, M., PALKO, J. & WEPPLING, K., 1999. A hydrological model for predicting runoff from different land use areas. *Journal of Hydrology* 217, 253-265.

KUNG, K.-J.S., 1990. Preferential flow in a sandy vadose zone. 1. Field observation. *Geoderma* 46, 51-58.

LAMPARTER, A., DEURER, M., BACHMANN, J. & DUIJNISVELD, W.H.M., 2006. Effects of subcritical hydrophobicity in a sandy soil on water infiltration and mobile water content. *J. Plant Nutr. Soil Sci.* 169, 38-46.

LE ROUX, P.A.L. & DU PREEZ, C.C., 2008. Micromorphological evidence of redox activity in the soft plinthic B horizon of a soil of the Bainsvlei form in an arid bioclimate. *S. Afr. J. Plant Soil* 25, 84-91.

LIN, H.S., MCINNES, K.J., WILDING, L.P. & HALLMARK, C.T., 1999. Effects of soil morphology on hydraulic properties: II. Hydraulic Pedotransfer Functions. *Soil Sci. Soc. Am. J.* 63, 955-961.

LIN, H.S., KOGELMANN, W., WALKER, C. & BRUNS, M.A., 2006. Soil moisture patterns in a forested catchment: A hydropedological perspective. *Geoderma* 131, 345-368.

LOXTON, R.F., LAMBRECHTS, J.J.N. & ELLIS, F., 1991. Simonstown ferricrete sequence: a benchmark in quarternary landscape evolution. *The 17th Congress of the Soil Science Society of South Africa.* Pretoria, 1991.

MAULEM, Y., 1976. A new model for predicting the hydraulic conductivity of unsaturated porous media.*Water Resources Research* 12, 513-522.

MCDONNELL, J.J., BONELL, M., STEWART, M.K. & PEARCE, A.J., 1990. Deuterium variations in storm rainfall: Implications for stream hydrograph separation. *Water Resoures Research* 26, 455-458.

MCKEAGUE, J.A., 1965. Properties and genesis of three members of the Uplands catena. *Can. J. Soil Sci.* 46, 63-77.

MILLER, D.S. & RICHARD, A.W., 1998. A conterminous United States multilayer soil characteristics dataset for regional climate and hydrology modeling. *Earth Interactions* 2, 1-26.

MOTAGHIAN, H.R. & MOHAMMADI, J., 2011. Spatial estimation of saturated hydraulic conductivity from terrain attributes using regression, kriging, and artificial neural networks. *Pedosphere* 21, 170-177.

MUNSELL, A.H., 1912. A Pigment Color System and Notation. The American Journal of Psychology 23, 236-244.

OXTOBEE, J.P.A. & NOVAKOWSKI, K.S., 2003. Groundwater/surface water interaction in a fractured rock aquifer. *Ground Water* 41, 667-681.

PACHEPSKY, Y.A., RAWLS, W.J. & Lin, H.S., 2006. Hydropedology and pedotransfer functions. *Geoderma* 131, 308-316.

PIONKE, H.B., SCNABEL, R.R., & SHAFFER, J.A., 1996. The role of soil science in watershed research. p. 67-73. *In:* The role of soil science in interdisciplinary research, SSSA, Madison.

RAWLS, W.J., GISH, T.J. & BRAKENSIEK, D.L., 1991. Estimating soil water retention from soil physical properties and characteristics. *Advances in Soil Science* 16, 213-234.

RICHARDSON, J.L. & DANIELS, R.B., 1993. Stratigraphic and hydraulic influences on soil color development. p. 109-125. *In:* Soil Colour, SSSA, Madison.

RITSEMA, C.J. & DEKKER, L.W., 1994. How water moves in a water repellent sandy soil. 2. Dynamics of fingered flow. *Water Resour. Res.* 30, 2519-2531.

RITSEMA, C.J. & DEKKER, L.W., 2000. Preferential flow in water repellent sandy soils: principles and modeling implications. *Journal of Hydrology* 231-232, 308-319.

ROTH, K., 1995. Steady state flow in an unsaturated, two-dimensional, macroscopically homogeneous soils. *Water Resource Research* 31, 2127-2140.

SANDSTRÖM, K. 1996. Hydrochemical deciphering of streamflow generation in semi-arid east Africa. *Hydrological Processes* 10, 703-720.

SAXTON, K.E., & RAWLS, W.J., 2006. Soil water characteristic estimates by texture and organic matter for hydrologic solutions. *Soil Sci. Soc. Am. J.* 70, 1569-1578.

SEELIG, B.D. & RICHARDSON, J.L., 1994. Sodic soil toposequence related to focused water flow. *Soil Sci. Soc. Am. J.* 58, 156-163.

SIGDA, J.M., 1997. Effects of small-displacement faults on the permeability distribution of poorly consolidated Santa Fe Group sands, Rio Grande Rift New Mexico. M.Sc. Thesis, New Mexico Tech, Socorro.

SILILO, O.T.N. & TELLMAN, J.H., 2000. Fingering in unsaturated zone flow: a qualitative review with laboratory experiments on heterogenous systems. *ProQuest Agricultural Journals* 38.

SIVAPALAN, M., 2003. Prediction in ungauged basins: a grand challenge for theoretical hydrology. *Hydrological Processes* 17, 3163-3170.

SOIL CLASSIFICATION WORKING GROUP, 1991. Soil Classification - A Taxonomic System for South Africa. Memoirs on the agricultural natural resources of South Africa No. 15. Department of Agricultural Development. Pretoria, South Africa.

SOIL SCIENCE STAFF, 1997. National Soil Survey Characteritzation Data. U.S. Department of Agriculture-Natural Resource Conservation Service, Lincoln, NE., USA.

SOPHOCLEOUS, M., 2002. Interaction between groundwater and surface water: the state of the science. *Hydrogeology Journal* 10, 52-67.

STARR, J.L., DEROO, H.C., FRINK, C.R. & PARLANGE, J.-Y. 1978. Leaching characteristics of a layered field soil. *Soil Sci. Soc. Am. J.* 42, 386-391.

STOERTZ, M.W. & BRADBURY, K.R., 1989. Mapping recharge areas using a groundwater flow model - A case study. *Ground Water* 27, 220-228.

SWANSON, S.K., BAHR, J.M., KENNETH, R.B. & ANDERSON, K.M., 2006. Evidence for preferential flow through sandstone aquifers in Southern Wisconsin. *Sedimentary Geology* 184, 331-342.

TICEHURST, J.E., CRESSWELL, H.P., MCKENZIE, N.J. & GILOVER, M.R., 2007. Interpreting soil and topographic properties to conceptualise hillslope hydrology. *Geoderma* 137, 279-292.

TIMLIN, D.J., PACHEPSKY, B., ACOCK, B. & WHISLER, F., 1996. Indirect estimation of soil hydraulic properties to predict soybean yield using GLYCIM. *Agricultural Systems* 52, 331-353.

TYSON, P.D., 1986. Climate change and variability in Southern Africa. Oxford University Press, Cape Town.

UHLENBROOK, S., WENNINGER, J. & LORENTZ, S.A., 2005. What happens after the catchment caught the storm? Hydrological processes at the small, semi-arid Weatherley catchment, South-Africa. *Advances in Geosciences* 2, 237-241.

VAN DAM, J.C., HENDRICKX, J.M.H., VAN OMMEN, H.C., BANNINK, M.H., VAN GENUCHTEN, M.TH. & DEKKER, L.W., 1990. Simulation of water and solute transport through a water-repellent sand soil. *J. Hydrol* 120, 139-159.

VAN GENUCHTEN, M.TH., 1980. A closed-form equation for predicting the hydraulic conductivity of unsaturated soils. *Soil Sci. Soc. Am. J.* 44, 892-897.

VAN HUYSSTEEN, C.W., 1995. The relationship between subsoil colour and degree of wetness in a suite of soils in the Grabouw district, Western Cape. M.Sc. Thesis, Stellenbosch University, Stellenbosch.

VENEMAN, P.L.M., VEPRASKAS, M.J. & BOUMA, J., 1976. The physical significance of soil mottling in a Wisconsin toposequence. *Geoderma* 15, 103-118.

VEREECKEN, H., MAES, J., FEYEN, J. & DARIUS, P., 1989. Estimating the soil moisture retention characteristic from texture, bulk density, and carbon content. *Soil science* 148, 389-403.

VIDAČEK, Z., BOGUNOVIĆ, M., HUSNJAK, S., SRAKA, M. & BENSA, A., 2008. Hydropedological map of the Republic of Croatia. *Agriculturae Conspectus Scientificus* 73, 67-74.

VOLTZ, M. & GOULARD, M., 1994. Spatial interpolation of soil moisture retention. *Geoderma* 62, 109-123.

VOLTZ, M. & WEBSTER, R., 1990. A comparison of kriging, cubic splines and classification for predicting soil properties from sample information. *Journal of Soil Science* 41, 473-490.

VOLTZ, M., LAGACHERIE, P. & LOUCHART, X., 1997. Predicting soil properties over a region using sample information from a mapped reference area. *European Journal of Soil Science* 48, 19-30.

WANG, Z., FEYEN, J., VAN GENUCHTEN, M.TH. & NIELSEN, D.R., 1998. Air entrapment effects on infiltration rate and flow instability. *Water Resources Research* 34, 213-222.

WEILER, M. & NAEF, F., 2002. Simulating surface and subsurface initiation of macropore flow. *Journal of Hydrology* 273, 139-154.

XEVI, E., CHRISTIAENS, K., ESPINO, A., SEWNANDAN, W., MALLANTS, D., SORENSEN, H. & FEYEN, J., 1997. *Water Resources Management* 11, 219-242.

XU, Y., WU, Y. & DUAH, A., 2007. Grounwater recharge estimation of Table Mountaing Group aquifer systems with case studies. *WRC Report* No.1329/1/07. Gezina, South Africa.

ZHANG, R., 1997. Determination of soil sorptivity and hydraulic conductivity from the disk infiltrometer. *Soil Science Society of America Journal* 61, 1024-1030.

CHAPTER TWO

2. Groundwater Recharge Estimation using Soil Pattern Analysis

2.1. Introduction

"Using a Soil Survey as a Hydrological Toolkit"

Lin *et al.* (1999) and Sivapalan (2003a) suggests that the time consuming, expensive and complex nature of infield soil hydrological observation is encouraging the use of readily available soil survey information to indirectly predict soil hydrological properties. Such information includes particle-size distribution, bulk density and organic matter (OM) content.

Such observations can be made using invasive methods, such as augering, trench digging or well drilling, and can be combined with non-invasive methods, such as tracer studies (Sivapalan, 2003b). Soil survey data is increasingly being used to assist in modelling catchments. Albeit easier to use survey data than catchment monitoring, a survey is not without extensive fieldwork. Fritsch & Fitzpatrick (1994) discussed The Structural Analysis survey method:

> *"Using large scale geographic and climatic maps, select a smaller catchment that effectively represents the larger area of interest. Conduct a survey using aerial photography, soil auguring and pits to determine the dominant soil forms in the catchment. Describe soil morphological features such as texture, structure and colour found in the soil profiles. Create an inventory of the data and graphically delineate areas in the catchment that contain similar features. Select one toposequence that contains all the features of interest for further monitoring. Group soil features into soil systems based on concordant relationships and graphically display the toposequence in cross section, clearly illustrating the soil systems and their specific features."*

This method may seem laborious, but is more simplistic than assembling a full hydrological survey as seen in the study of Ticehurst *et al.* (2007). The factors used in grouping soils into systems, or larger compilations of systems called domains, are interchangeable depending on the aim of the research. Parent material or hydrological regimes are usually the most important (Brouwer & Fitzpatrick, 2002). This ideology leaves space to further investigate the grouping process of similar systems.

Gleeson *et al.* (2009) did soil characterisation and mapping by combining aerial photograph analysis, hand augering and soil depth determination by using a penetrometer and seismic refraction. He concluded in this study that mapping soil depth could serve useful in grouping hydrologically similar units in a recharge site. Other soil properties have also been used to characterise hydrology as discussed in the literature review.

The presence of bedrock fractures is not a soil pattern characteristic but may serve useful in a hydrological study. Fractures need to be accurately described if the data is to be used in an estimation model of sorts. The visible fractures can be described in terms of orientation and length and visual observations like surface roughness, mineral coating and the occurrence of soil infilling (Praamsma *et al*., 2009).

The use of soil morphology to study groundwater regimes should be done with care as some features, like relict concretions, may be from a previous water regime (Ticehurst *et al.*, 2007). Similarly, actual redoximorphic conditions may not always reflect the true water regime due to the effect that OM has on redox active soil constituents.

Quantifying physical properties is no simple task. Power functions, instead of exponential, cosine or error functions, are most often used to compute physical properties. The most common power functions used are those from Brooks & Corey (1964), Campbell (1974) and van Genuchten (1980). Many such studies have been done, correlating soil physical data to hydraulic properties. These studies aim to use as large a dataset as possible to ensure the validity of their results (Rawls *et al.*, 1991). Some of these models are discussed in more detail in the literature review section on pedotransfer functions (PTFs).

Soil survey data can also serve as input parameters for mass balance equations in which soil, vegetation and climate data are incorporated in a holistic manner. The volume of recharge can be calculated as the difference between rainfall and actual evapotranspiration, taking into account the soil characteristics that would affect deep percolation. This method is however not always practical, especially in semi arid or arid areas like South Africa, where the difference in rainfall and evapotranspiration is too small for accurate estimation. This method is also restricted as land-use changes would further complicate the calculations if the timescale in question is too broad (de Vries & Simmers, 2002).

The above discussion introduces the approach of using soil survey information as a lucrative alternative to strictly using monitoring equipment in a hydrological study. Survey

information that can be used includes infield observations such as soil depth (Asano *et al.*, 2002; Gleeson *et al.*, 2009), soil diagnostic horizon (Van Huyssteen *et al.*, 2005) and colour (van Huyssteen, 1995) and laboratory determinations such as texture, OM content (Lin *et al.*, 1999) and bulk density (Pachepsky *et al.*, 2006). Soil maps have also been used in hydrological studies but the purity of mapping units and the subjective nature of soil maps have been brought under question (Voltz *et al.*, 1990). McBratney *et al.* (2003) however insist that mapping of soil properties or discrete soil classes is possible and recommends a framework for digital soil mapping based on Jenny's five soil forming factors (Jenny, 1941) and spatial position.

This research will address the validity of using soil survey information in hydrological models. Two contrasting aquifer systems, one a fractured bedrock and the other a cover sand aquifer, will be surveyed during which soils will be classified according to South African Soil Classification system (Soil Classification Working Group, 1991) and samples will be taken at representative observation points. Hydrological properties will then be estimated from texture and OM content, determined from the soil samples of the various representative soil forms. The estimated hydrological data will then be statistically compared in order see whether there are significant hydrological differences between the different soil forms.

The two sites used in the study, the Kogelberg- and the Riverlands-Nature Reserves, have two very different landscapes. This affords the opportunity to also experiment with different soil surveying methods including a grid, transect and reference group based approach. A binary decision tree will also be defined as a set of rules to interpolate hydrological data.

The results from this research will expectantly amend our understanding of groundwater recharge and in doing so, improve scientist's ability to estimate groundwater recharge and upscale such models based on existing soil survey information.

2.2. Objectives

This chapter of the research will aim to address the general goals regarding the advancement of existing hydrological and soil mapping techniques as well as investigate the relationship between soil hydrology and soil pattern. The research objectives are thus:

- Select appropriate mapping approaches that will effectively balance inputs (time, money and expertise) with outputs (soil classifications and map accuracy and usability) for the different catchments.
- Estimate hydrological properties (hydraulic conductivity and plant available water) from field survey information (texture and organic matter content) using pedotransfer functions.
- Investigate the potential for using soil pattern distribution (soil classification) and terrain morphology as grounds for grouping hydrological similar units.
- Identify hydrologically similar units based on soil pattern distribution on a catchment scale soil map.
- Define a binary decision tree that can be used to interpolate hydrological data to unsampled plots within a catchment.

2.3. Site Description

Site selection was done based on hydrogeological and ecological criteria. The following criteria were also taken into consideration: (a) The site must have evidence of natural groundwater recharge into the aquifer with little groundwater use in the catchment and no plans of bulk water abstraction in future. (b) Existing monitoring infrastructure (weather stations and bore holes) and historical data (groundwater levels and meteorological data) will be helpful in creating a set of norms for the catchment. (c) The catchment must be ecologically undisturbed with respect to the soil, vegetation and water flow paths. (d) Infrastructure that will allow access by motor vehicle and by foot is required (Colvin, 2008).

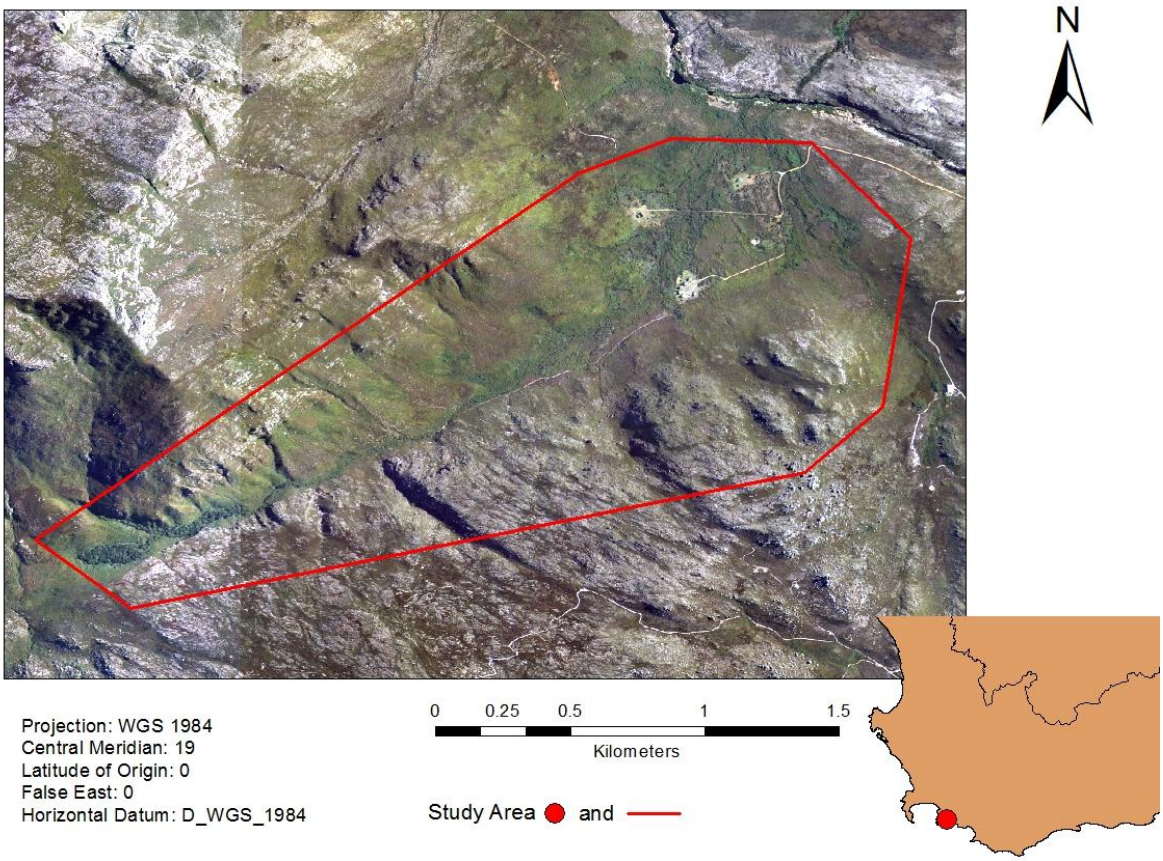

Figure 2.1: Location and boundary of Oudebos River catchment in the Kogelberg Reserve, Kleinmond.

The Oudebos catchment (Figure 2.1) in the Kogelberg Nature Reserve, near Kleinmond, South Africa, satisfies most of the above criteria and serves as a model fractured bedrock aquifer system. Kogelberg is situated 40 km south-east of Cape Town and stretches from Gordon's Bay in the west to Hawston in the east. The area experiences a Mediterranean climate (Boucher, 1978).

Rainfall occurs in the winter months from May to September which is associated with the prevailing north or north-westerly blowing winds. The summer months are generally hot and dry but at higher altitudes, the prevailing summer south-easterly wind can provide substantial amounts of moisture as cloud and mist condensation. The maximum average temperature of the warmest month (January) is 32.8^{o}C and the minimum average temperature in the coldest month (July) is 2.4^{o}C. This data was recorded at the Steenbras dam weather station inside Kogelberg at an altitude of 338 m. The same weather station reported a mean annual precipitation of 874 mm (Boucher, 1978).

Kogelberg predominantly has a mountainous landscape, with the Oudebos catchment being a great example of deep valleys and high peaks. The geology of the catchment is dominated by Table Mountain Group (TMG) sandstones, quartzites and shales. Rocky outcrops are commonly visible on the surface of higher lying areas. Rocky outcrop exposure is further favoured by steep slopes. The sediment is deposited at the footslopes by colluviation. Thus, in areas with steep slope and high rainfall, soils are poorly developed whereas lower lying, more level areas of slope wash accumulation show deeper soil development (Boucher, 1978).

Numerous fynbos communities can be identified on the rocky, shallow, sandy soils. The most common mountain fynbos vegetation is ericoid and restioid forms and the taller proteoid shrublands. In areas where the riverine vegetation is sheltered from fire, forest elements exist, but their extent is limited. The riparian vegetation consists of a mixture of these forest elements and fynbos (Boucher, 1978).

The Riverlands Nature Reserve (Figure 2.2) complies with the desired criteria and will serve as a model cover sand aquifer. The reserve is situated about 10 km south of Malmesbury, Western Cape. Riverlands falls in a catchment of the Groen River, which serves as a tributary of the Diep River. The sandy soil plains in the reserve are of aeolian and marine origin and are coarse textured, generally acidic, deep and well leached.

The vegetation found in Riverlands is characteristic of the deep sandy soil types. The dominant vegetation type has been termed Atlantis Sand Plain Fynbos (Rebelo *et al.*, 2006) which is common on the southern and western coast of the Western Cape Province. This vegetation type occurs as a series of islands in renosterveld and is confined to areas with deep sandy soils (Jovanovic *et al.*, 2008).

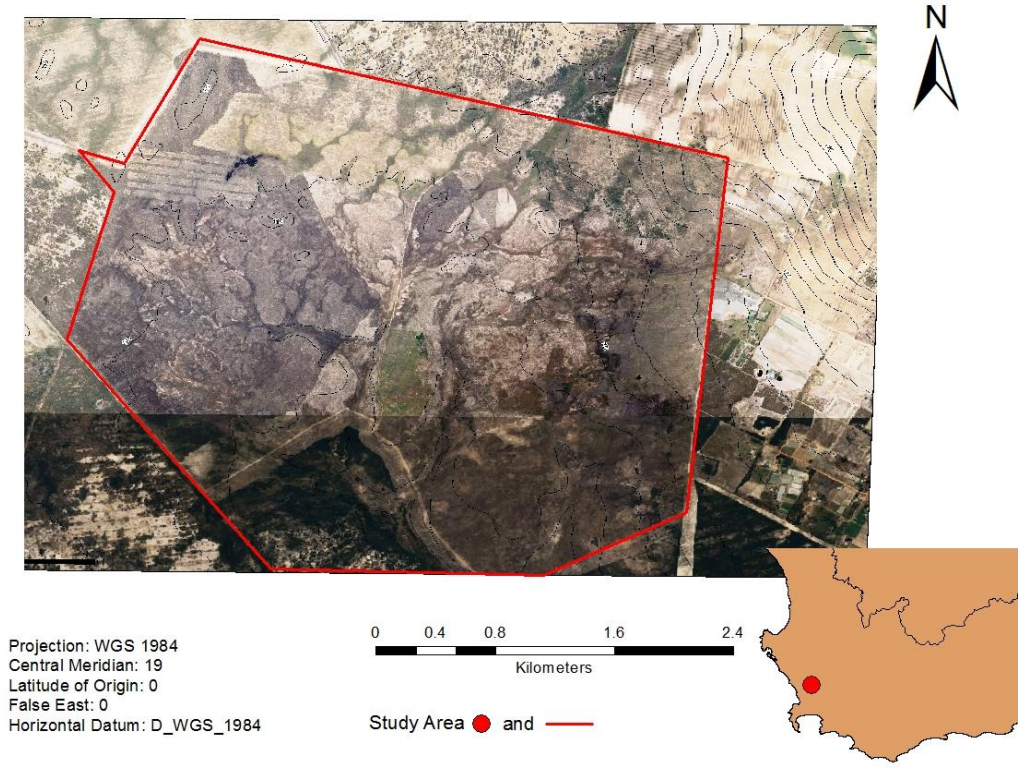

Figure 2.2: Location and boundary of Riverlands Nature Reserve site, Malmesbury.

The mean annual rainfall for this vegetation type is 444 mm with a mean annual coefficient of variation of 28% (Rebelo *et al.*, 2006) with the majority of the precipitation occurring from May to August. The mean annual evaporation is around 2150 mm, with daily means exceeding rainfall daily for approximately 70% of the year. The minimum and maximum monthly mean temperatures are 7.0^{o}C in July and 27.9^{o}C in February respectively (Jovanovic *et al.*, 2008).

2.4. Methodology

The methodology is divided into four phases:

i. A desk-top study
ii. Field work
iii. Laboratory analysis
iv. Data analysis

2.4.1. Desk-Top Study

A desk-top study was done to plan the field and laboratory work. A literature review was compiled which broadly addressed the subject of hydropedology after which followed a more in-depth discussion of the most critical factors for this investigation. Useful parameters from survey point observations were identified from the literature. These are: soil form and family, soil depth, particle size distribution (texture), organic matter content (OM), electrical conductivity (EC) and pH in water and KCl. Soil form and family, and soil depth can be determined in the field whereas soil samples are taken at representative observation sites for laboratory analyses to determine texture, OM content, pH and EC. Soil samples are to be taken of each diagnostic horizon at each representative profile and placed in labelled sample bags.

Areas of variation, and so too representative sampling sites, were identified using an innovative approach. Conducting a detailed grid soil survey in a catchment with limited accessibility, as is the case in Kogelberg, would be very time and labour intensive. A simplified, less field intensive approach was thus required for the Kogelberg survey. Favrot (1981) recommends grouping areas on an aerial photo that present similar geological and topographical patterns into reference groups (RGs). These RGs would indicate areas of variation which need to be studied during the soil survey as these sites most likely present different soil types. This method limits the number of observation sites to areas of predicted variation. This method is supported by Leenhardt *et al.* (1994) who said that representative profiles can be better estimates of class means than random samples. Such remote sensing (RS) techniques were found to be effective in soil surface feature characterization in drylands with sparse vegetative cover (Boettinger *et al.*, 2008).

As the terrain soil map would be used for hydropedological purposes, the RGs were classed based on expected wetness as this would indicate areas of variation requiring investigation.

The RGs were identified after two site visits and thorough aerial photo examination. ArcGIS software was used to delineate RGs from aerial photographs according to four factors; topography, aspect, surface vegetation/rock cover and expected wetness. The factors were classed 1 to 4 or 1 to 5 with regards to the expected wetness of the RG; with the higher numbers corresponding to a higher degree of expected wetness and *vice versa*. The values for each RG were summed to create a single expected moisture value (EMV) for each RG. This approach is similar to that of Storie (1976) who developed an index to rate agricultural soil for tax purpose, and Conacher & Dalrymple (1977) who used a number index to describe landscape morphology. Refer to Table A.1 of Appendix A for the index values of each RG.

The survey of Riverlands was less complicated as there are few limitations in terms of vegetation and terrain. The greatest limitation was the imposed restriction on digging profile pits. Due to this limitation, only a small detailed survey was allowed in two areas of the reserve (Figure 2.6) whereas a reconnaissance survey was done in the remainder of the reserve to look for deviation from the findings of the detailed survey. The detailed survey was conducted as:

I. A grid survey on the western boundary of the reserve where groundwater monitoring points are situated. This would allow the understanding of the short-distance variation of soil properties.
II. A transect survey along the northern boundary of the reserve. This transect encompassed most of the expected long-distance variation in the reserve from the laterite rich heights in the north-eastern corner to the deep sandy low lying areas further west.

2.4.2. Field Work

Soil surveys were conducted in Kogelberg and Riverlands to determine soil form and family according to South African Soil Classification system (Soil Classification Working Group, 1991). The areas of variation outlined in Figure 2.4 were used to choose

observation sites in Kogelberg instead of using a conventional grid or transect method as described for the survey of Riverlands. Some RGs could not be surveyed due to dense vegetation or steep slope. One such area is shown in Figure 2.3.

Figure 2.3: Photo showing an area with limited accessibility due to steep slope and dense vegetation in the Oudebos catchment.

Observation of a clear soil profile is preferred when classifying soil as the entire depth is visible and undisturbed. The use of a mechanical digger is prohibited in both sites, thus where a profile was not already exposed, holes had to be dug by hand. Exposed soil profiles were infrequently observed on the sides of dongas and on the fringes of an old rock quarry in Kogelberg. The very stony nature of the soils in Kogelberg made hand augering impractical and a “koevoet” hoe and pick had to be used. The deep sandy soils in the Riverlands site posed no such limitations and both auger and spade could be used.

The high rainfall and fynbos vegetation in both area are indicators that podzolic soils may be common (Fey, 2010). The “phenolphthalein soaked litmus paper test” proposed by Brydon & Day (1970) was used to improve the accuracy of in-field soil classification. The test works on the principle that NaF applied to a podzolic soil will increase the pH of the surrounding solution due to the displacement of hydroxide groups from the soil matrix. The increase in pH of the solution will cause the phenolphthalein indictor in the litmus paper to change colour to bright pink. If a soil sample causes a colour change, it does not mean the soil is podzolic for definite, but it does warrant further laboratory investigation of that

sample. The soil samples that caused a colour change on the litmus paper were collected for further laboratory analysis.

Point observations that were made in the field are soil form and family, depth (where digging stopped), position in the landscape, and colour according to a Munsell colour chart (Munsell, 1912) (only done in Riverlands survey). Digital photographs were taken of each soil observation point. Soil samples were taken from each diagnostic horizon at all observations in Riverlands but only at representative profiles in Kogelberg. A *Garmin* GPS was used to determine the exact position of each observation point, accurate to ±5 m.

2.4.3. Laboratory Work

The laboratory analyses were conducted according to the procedures outlined in *Methods of Soil Analysis*, *Parts* 1 (1986) and 3 (1996). Analyses that were performed include determination of pH(KCl) and pH(H_2O), electrical conductivity (EC), particle size distribution and identification of podzolic character (pH(NaF)).

Soil preparation was done by drying the soil samples in a forced draught drying room after which the soil was sieved through a 2 mm mesh diameter stainless steel sieve. The mass fraction remaining on the sieve represents the coarse fraction *(>2 mm)*.

Determination of pH in 1 M KCl solution was done in a 1:2.5 soil to solution ratio as proposed by Thomas (1996). Soil pH in distilled water was also determined in a 1:2.5 soil to water suspension on a mass basis. These results are reported as pH(KCl) and pH(H_2O) respectively. A *Metrohm, Swissmade, 827 pH lab* electronic pH meter was used for the determination.

Electrical conductivity (EC) indicates the total dissolved salt concentration in the soil. The EC was measured using a calibrated Microprocessor Capacitance Meter, *RE 387 Tx, Series 3,* instead of the laborious saturated paste extract method (Rhoades, 1996). EC is determined in a 1:5 soil to water suspension on a mass basis and reported as EC (µS/cm).

A simple laboratory method to determine podzolic character in soils is to measure the pH of a 1:2.5 soil to 1M NaF solution (Brydon & Day, 1970). This procedure was performed on those samples identified in the field as having podzolic character. A pH in 1 M NaF solution above 10.5 indicates convincingly that the soil has podzolic character. The results are reported as pH(NaF).

Particle size distribution was done on an 80 g subsample of dried soil which had the coarse fraction removed already. The soil particle classes to be determined are shown in Table 2.1 which is adapted from *Methods of Soil Analysis – Physical and Mineralogical Methods* (1986). The following procedures were done according to Gee & Bauder (1986).

Table 2.1: Soil particle size classes (Gee & Bauder, 1986).

Class	Particle diameter (mm)	Method of separation
Gravel	> 2,0	Sieve
Coarse sand	2.0 – 0.5	Sieve
Medium sand	0.5 – 0.25	Sieve
Fine sand	0.25 – 0.106	Sieve
Very fine sand	0.106 – 0.05	Sieve
Coarse silt	0.05 – 0.02	Sedimentation
Fine silt	0.02 – 0.002	Sedimentation
Clay	< 0.002	Sedimentation

The sample was chemically pre-treated by firstly removing the OM using 35 % by volume H_2O_2 solution. Secondly the iron oxyhydroxides were removed from the sample using the CBD method. Any loss of mass after OM removal is recorded as OM(g) whereas the change in mass after oxyhyroxide removal is added to the clay fraction.

Next, clay dispersal was done by adding 10 cm^3 Calgon solution to the sample and mechanically stirring the mixture for 5 minutes. Thereafter the clay and silt fractions were washed through a 0.053 mm mesh sieve into a 1 dm^3 sedimentation cylinder.

The remaining sand fraction is separated by sieving the dried sample through a series of stainless steel sieves with mesh diameters of 0.5, 0.25, 0.106 and 0.053 mm. The various fractions are weighed and reported as a percentage of the pre-treated soil fraction. The silt and clay fractions were determined last using the sedimentation technique and a Lowey pipette.

2.4.4. Data Analysis

The data was entered into Microsoft Excel 2007. The texture, OM and coarse fraction content were used to estimate plant available water (PAW) and saturated hydraulic conductivity (K_{sat}) using the model of Saxton & Rawls (2006), a revised version of Rawls *et al.* (1982) model. This model was found to be effective in estimating hydraulic properties in sandy soils by Bonsu (1992) in his study of Alfisols in Ghana. The calculations were done on SPAW software version 6.02.74. Further detail on this method can be found in the Methodology section of Chapter 3 on preferential flowpath assessment.

A one-way ANOVA without replication was done to investigate whether a significant difference exists between hydrological properties of different soil forms. The investigation was performed on PAW and soil form, and K_{sat} and soil form. A normal probability plot was constructed using the raw residuals to investigate the distribution. The "F-", "p-" and Kruskal-Wallis p-tests were interpreted as indicating significant difference between the groups if the $F_{calculated} > F_{critical}$ and if $p < 0.05$. Bonferroni's test was then performed to identify which groups differed significantly.

The point observations from both surveys were projected on ArcMAP as vector data with accompanying metadata. A terrain-soil map was compiled based on the RGs discussed above and the soil forms identified during the survey. The terrain-soil map is comprised of polygons that have a specific terrain unit and an association of soil forms. These polygons are termed "hydrological similar units" (HSUs). HSUs are defined by Flügel (1996) as "*distributed modelling entities that are used to preserve the spatial, three-dimensional heterogeneity within regional hydrological models".* This HSU-map is shown in Figure 2.4.

Interpolation of hydrological properties between observation points by kriging or the "nearest neighbour" method was not possible due to the limited number and spacious distribution of observations. An alternative method of allocating these properties was thus developed. The interpolation by soil classification method of Voltz & Goulard (1994) and the binary decision tree (BDT) approach of Hansen *et al.* (2009) were combined to develop a BDT for interpolating hydrological properties.

A BDT uses a series of "yes / no" questions to assign a value to an observation that lacks data. It is non-parametric and simple to train and interpret. The interpolation by soil classification was used by Voltz & Goulard (1994) as an alternative method when sample data is sparse. The method works well when the in class variation is less than the global variation. The BDT for interpolating K_{sat} in Kogelberg is shown in Figure 2.11. Tables 2.10 and 2.11 accompanying the BDT show the correlating hydrological response units and hydrological similar soil classes respectively.

The correlating hydrological response units in Table 2.10 are HSUs that have similar terrain characteristics but vary in their aspect or vegetative cover. The hydrologically similar soil classes are soil forms that were shown to have similar infiltration patterns during recharge. The separate grouping of deep and shallow soils is hydrologically sound as Royappen *et al.* (2002) found that shallow and deep soils will exhibit different

subsurface flow and baseflow discharge patterns. The coarse fraction content of the soil and the position in the landscape were however also taken into account when dividing the soils into groups as these factors were found to influence flow (Saxton & Rawls, 2006; Ticehurst, *et al.*, 2007).

The soil map of the two surveyed areas in Riverlands (Figure 2.6), combined with the observations made in the reconnaissance survey, was used to draw an interpolated terrain-soil map of Riverlands. Such mapping by interpolation techniques have been proven useful in local studies by Hensley *et al.* (2007) and Lorentz (2007). The observed soil forms were interpolated, along with their hydraulic properties, to other areas in the reserve that displayed similar terrain, hydrological and surface cover properties; factors that were shown dominant when Browning & Duniway (2011) compiled a soil map based on limited data. The Riverlands interpolated soil map can be seen in Figure 2.9 of the results.

2.5. Results

Table 2.2 shows the four factors used to derive the EMV's described on page 46 above. Each RG was rated for each of the four factors, and these index values were summated to derive the EMV for each RG. The RGs with their respective EMV's are shown in Figure 2.4; where brown colour units indicate expected dry RGs and blue units indicate wetter RGs as shown in the legend.

Table 2.2: Self defined index used to derive estimated moisture values (EMV) for reference groups in Kogelberg.

Slope	**Steep or Flat-high lying**	**1**
	Moderate / Steep	**2**
	Moderate	**3**
	Moderate / Flat	**4**
	Flat-low lying	**5**
Aspect	**North or Level-high lying**	**1**
	East or West	**2**
	South	**3**
	Level-low lying	**4**
Surface Cover	**Predominantly exposed rock**	**1**
	Soil and rock exposed with limited vegetative cover	**2**
	Exposed soil with sparse vegetative cover	**3**
	Predominant vegetative cover with sparse exposed soil	**4**
	Dense vegetative cover	**5**
Predicted Moisture	**Expected to only be moist during rainfall events**	**1**
	Expected to be moist during rainfall season	**2**
	Expected to be moist during, and shortly after, rainfall season	**3**
	Expected to be dry only during prolonged periods of drought	**4**
	Expected to be moist throughout the year	**5**

RG number 55 is used as an example of how the EMV is derived: Slope is very steep (1), with a southern aspect (3), with both soil and exposed rock but little dense vegetation (2) and the RG is expected to only be moist during rainfall periods due to the steep slope and position in the landscape (1). Thus RG number 55 has an EMV of 7 (1 + 3 + 2 + 1 = 7).

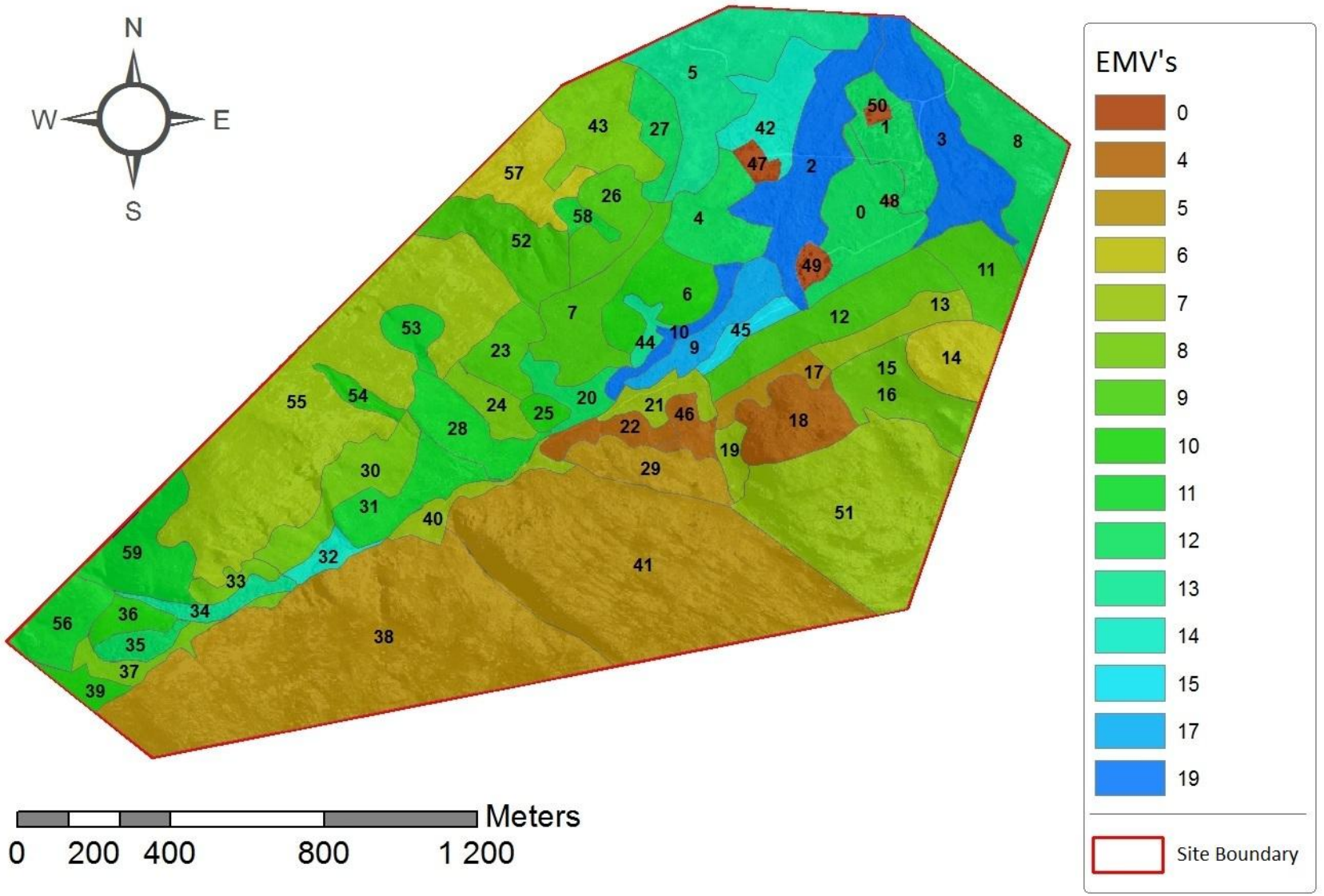

Figure 2.4: Reference groups (RGs), with RG identification numbers used to plan a soil survey in the Oudebos River catchment in Kogelberg. The RGs are colour coded according to their respective expected moisture values (EMV's).

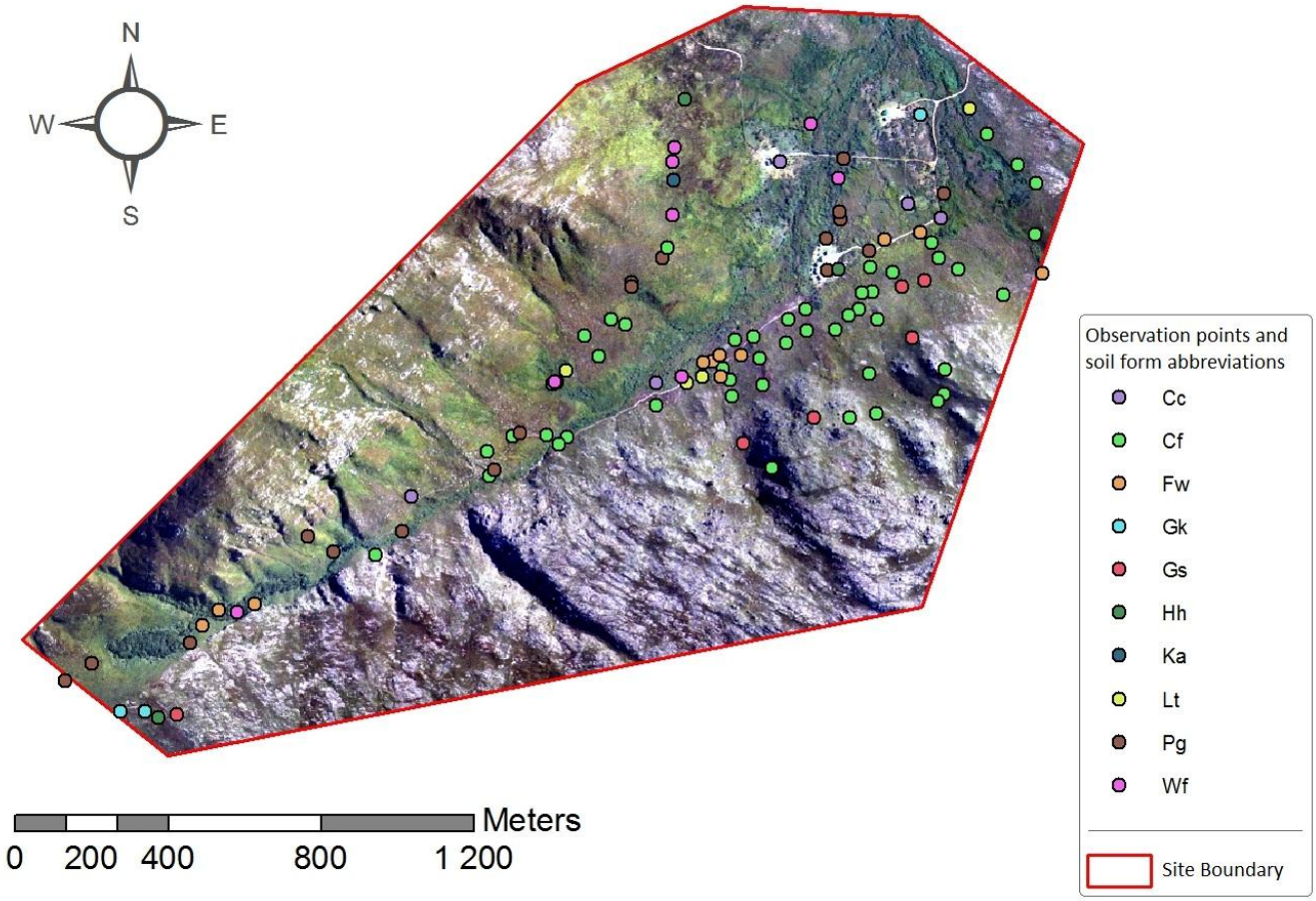

Figure 2.5: Soil observation points in the Oudebos River catchment, Kogelberg.

The soil survey of Kogelberg was done in two rounds, the first round was completed in February 2010 and the second in May 2010. A total of 108 observations were made during this time. The RG-map in Figure 2.4 was used to select areas for soil observation. These observation points are shown in Figure 2.5. The 10 different soil forms that were identified during the survey are shown in Table 2.3 below.

All the soils classified during the survey are reported in Table A.2 of Appendix A. From the 108 observations, 12 representative observation sites were selected where sampling from each diagnostic horizon was done for laboratory analysis. The laboratory analysis results are shown in Table A.3 of Appendix A.

Table 2.3: Soil forms observed during a survey of the Oudebos River catchment, Kogelberg.

Soil Form (Abbreviation)	Number of Observations	Average Maximum Observed Depth (mm)
Cartref (Cf)	47	426
Pinegrove (Pg)	18	548
Fernwood (Fw)	11	700
Witfontein (Wf)	9	761
Glenrosa (Gs)	6	210
Concordia (Cc)	5	762
Groenkop (Gk)	4	715
Lamotte (Lt)	4	787
Houwhoek (Hh)	3	650
Katspruit (Ka)	1	550

The soil survey of Riverlands was conducted on 9 and 10 November 2010. The survey focussed on two areas of the reserve shown in Figure 2.6. The 5 observation points from the transect survey, the 9 from the grid survey and numerous from the reconnaissance survey identified four different soil forms in total which are shown in Table 2.4.

Table 2.4: Soil forms observed during a survey of the Riverlands Nature Reserve.

Soil Form (Abbreviation)	Number of Observations	Average Maximum Observed Depth (mm)
Lamotte (Lt)	9	1153
Witfontein (Wf)	3	1454
Concordia (Cc)	2	1700
Fernwood (Fw)	Observed during reconnaissance survey without detailed notation	

The soils classified during the survey of Riverlands are shown in Table A.5 of Appendix A. Samples were collected for each diagnostic horizon at all 14 sites for laboratory analysis. The laboratory analysis data is shown in Table A.6 of Appendix A.

Figure 2.6: Soil observation points in Riverlands Nature Reserve.

PAW and K_{sat} were estimated for each diagnostic horizon sample from the percentage sand, silt, clay, OM and coarse fraction by mass using the model of Saxton & Rawls (2006). These results are reported in Tables A.4 and A.7 of Appendix A for Kogelberg and Riverlands respectively. The two hydraulic properties were compared against soil form separately, to investigate whether a statistical significant difference existed between the PAW and/or K_{sat} of the soil forms. The analysis was done separately for each reserve and then by grouping the data from both. For the purpose of this section, the results from the two reserves will be displayed separately.

Where necessary the statistical results are shown below, however the full statistical analysis is shown in Appendix C.

Table 2.5 summarizes the statistical analysis of PAW against soil form for each site separately. There is no significant difference between the PAW of the soil forms in Riverlands ($F_{cal} < F_{crit}$ and $p > 0.05$). The Kruskall-Wallis p-test however found a slight significant difference between the PAW of the soil forms in Kogelberg.

Table 2.5. Summary of statistical analysis of PAW and soil form.

Site	Independent Variable	Dependent Variable	F	p	Kruskal-Wallis (p)
Riverlands	Soil Form	PAW	0.1111	0.90	0.92
Kogelberg	Soil Form	PAW	1.8570	0.13	0.04

The boxplot in Figure 2.7 shows that the PAW of the Cartref and Pinegrove soil forms differ significantly. The “whiskers” of the boxplot also illustrates the variation of PAW in Kogelberg. These results are supported by a 2-tailed multiple comparisons p-test and a multiple comparisons z-test shown in Section 2 of Appendix C (Statistical analysis of PAW against soil form).

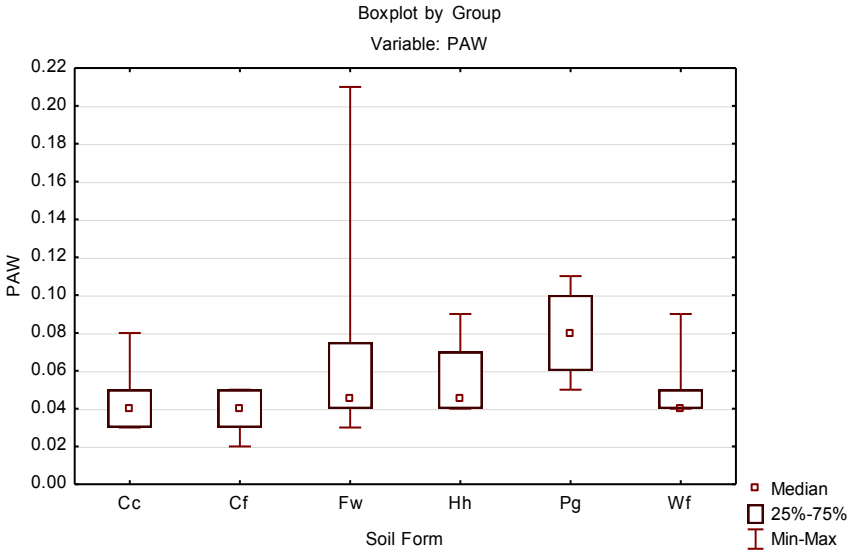

Figure 2.7. Boxplot of PAW against soil form in Kogelberg.

Table 2.6 summarizes the statistical analysis of K_{sat} against soil form for each site separately. It shows that there is no significant difference between the K_{sat} of the soil forms in Riverlands ($F_{cal} < F_{crit}$ and $p > 0.05$). The K_{sat} however differed significantly between the soil forms in Kogelberg ($p < 0.05$ and $F_{cal} > F_{crit}$).

Table 2.6: Summary of statistical analysis of K_{sat} and soil form.

Site	Independent Variable	Dependent Variable	F	p	Kruskal-Wallis (p)
Riverlands	Soil Form	K_{sat}	1.6902	0.20	0.42
Kogelberg	Soil Form	K_{sat}	2.7284	0.03	0.04

Bonferroni's test in Table 2.7 could however not identify which soil forms differed significantly and a LSD test (Table 2.8) was thus performed as this method is more sensitive to significant differences. Table 2.8 shows that the K_{sat} of the Cartref soil form differed most significantly from that of the Witfontein form ($p = 0.00839$), then the Fernwood form ($p = 0.00919$) and finally the Pinegrove form ($p = 0.01756$).

Table 2.7: Bonferroni test for significant difference of K_{sat} between soil forms in Kogelberg.

	Bonferroni's test; variable Ksat (Kogelberg) Probabilities for Post Hoc Tests Error: Between MS = 923.55, df = 35.000						
Cell No.	**Soil Form**	**{1} 117.93**	**{2} 100.78**	**{3} 141.50**	**{4} 113.9**	**{5} 140.70**	**{6} 148.14**
1	**Cc**		1.000	1.000	1.000	1.000	1.000
2	**Cf**	1.000		0.138	1.000	0.264	0.126
3	**Fw**	1.000	0.138		1.000	1.000	1.000
4	**Hh**	1.000	1.000	1.000		1.000	1.000
5	**Pg**	1.000	0.264	1.000	1.000		1.000
6	**Wf**	1.000	0.126	1.000	1.000	1.000	

Table 2.8: LSD test for significant difference of K_{sat} between the soil forms for Kogelberg.

	LSD test; variable Ksat (Kogelberg) Probabilities for Post Hoc Tests Error: Between MS = 923.55, df = 35.000						
Cell No.	**Soil Form**	**{1} 117.93**	**{2} 100.78**	**{3} 141.50**	**{4} 113.9**	**{5} 140.70**	**{6} 148.14**
1	**Cc**		0.239	0.119	0.805	0.164	0.083
2	**Cf**	0.239		0.009	0.495	0.018	0.008
3	**Fw**	0.119	0.009		0.140	0.961	0.704
4	**Hh**	0.805	0.495	0.140		0.173	0.097
5	**Pg**	0.164	0.018	0.961	0.173		0.689
6	**Wf**	0.083	0.008	0.704	0.097	0.689	

A terrain-soil map (Fig. 2.8) could be drawn for Kogelberg by merging RGs that contained soil forms with similar characteristics. Hydrological response units in Kogelberg were delineated based on a unit's position in the landscape and the soil forms present therein.

The soil distribution in Riverlands was less complex. The soil map of the surveyed areas is shown in Figure 2.9. The soil types were interpolated with reference to the observations made in the reconnaissance survey as well as the observed soil forms in Figure 2.9 to produce an interpolated soil map of the entire reserve (Fig 2.10). The observed soil types were compared according to their position in the landscape, lithology, slope, position relative to the tributaries and surface soil colour during interpolation.

Table 2.9. Description of HSUs in Figure 2.8.

HSU	Soil Forms	Terrain Description
Ba	Pg	Shale band
Bb	Cc	Shale band
Bc	Cf	Shale band
Bd	Pg; Cf	Shale band
Be	Wf	Shale band
Fn	Cf; Gs	Steep rock face; Northern Aspect
Fs	Cf; Gs	Steep rock face; Southern Aspect
La	Cf; Gs	High lying; Level Aspect
Lb	Pg	High lying; Level Aspect
Lc	Gk	High lying; Level Aspect
Mn	Cf; Gs	Moderate slope; Northern Aspect
Mw	Hh	Moderate slope; Western Aspect
R1a	Wf; Pg	Primary river
R1b	Cf; Wf	Primary river
R1c	Wf; Lt	Primary river
R1d	Cf; Pg	Primary river
R1e	Fw; Wf	Primary river
R2	Fw	Secondary river
T1	Cc	River terrace; Most Western Terrace
T2a	Pg; Cc; Fw; Hh; Gk	River terrace; Central Terrace
T2b	Cf	River terrace; Central Terrace
T3a	Cf	River terrace; Most Eastern Terrace
T3b	Lt	River terrace; Most Eastern Terrace

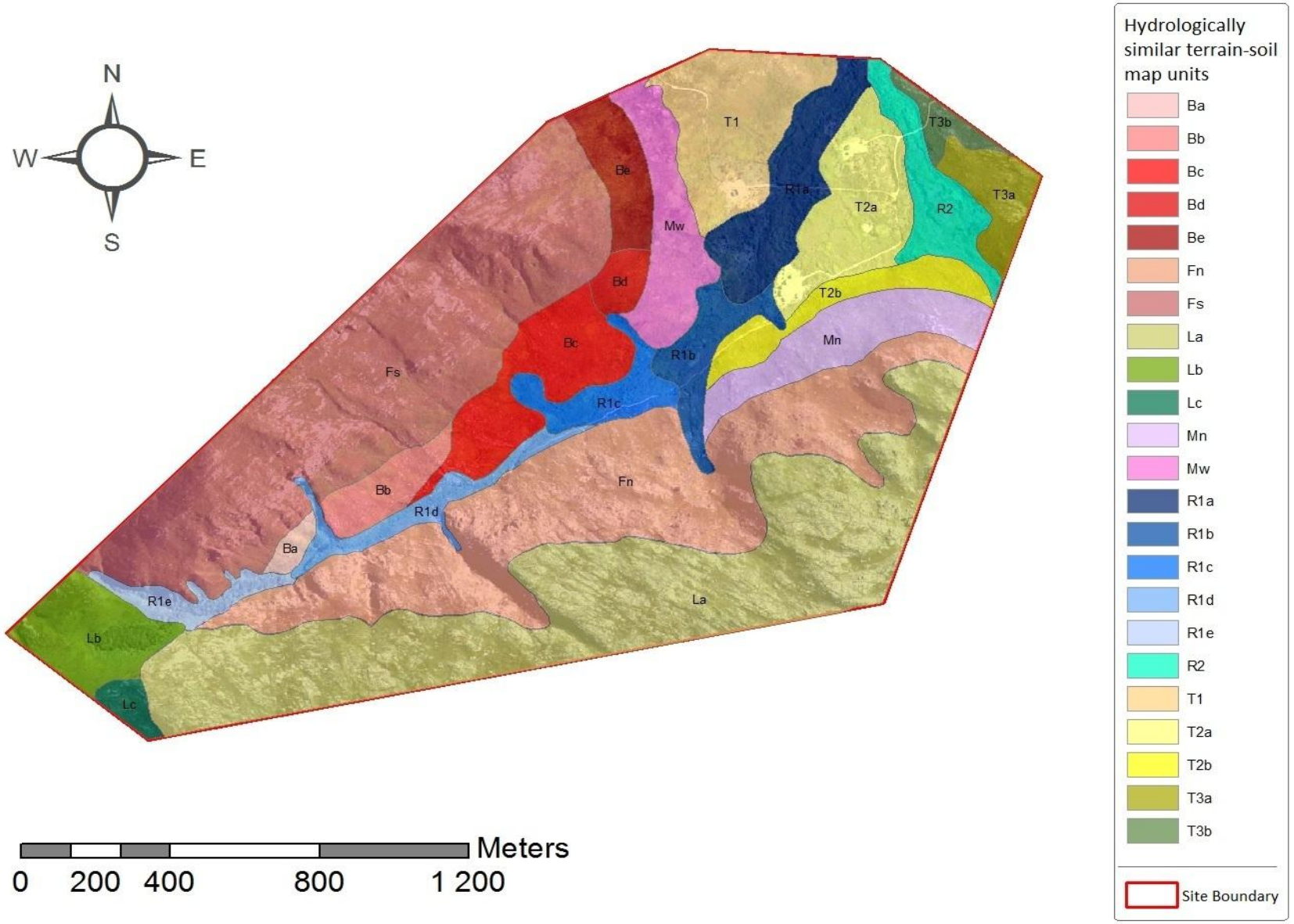

Figure 2.8: Hydrological Response Units, based on terrain units and hydrologically similar soil classes, in Kogelberg Nature Reserve.

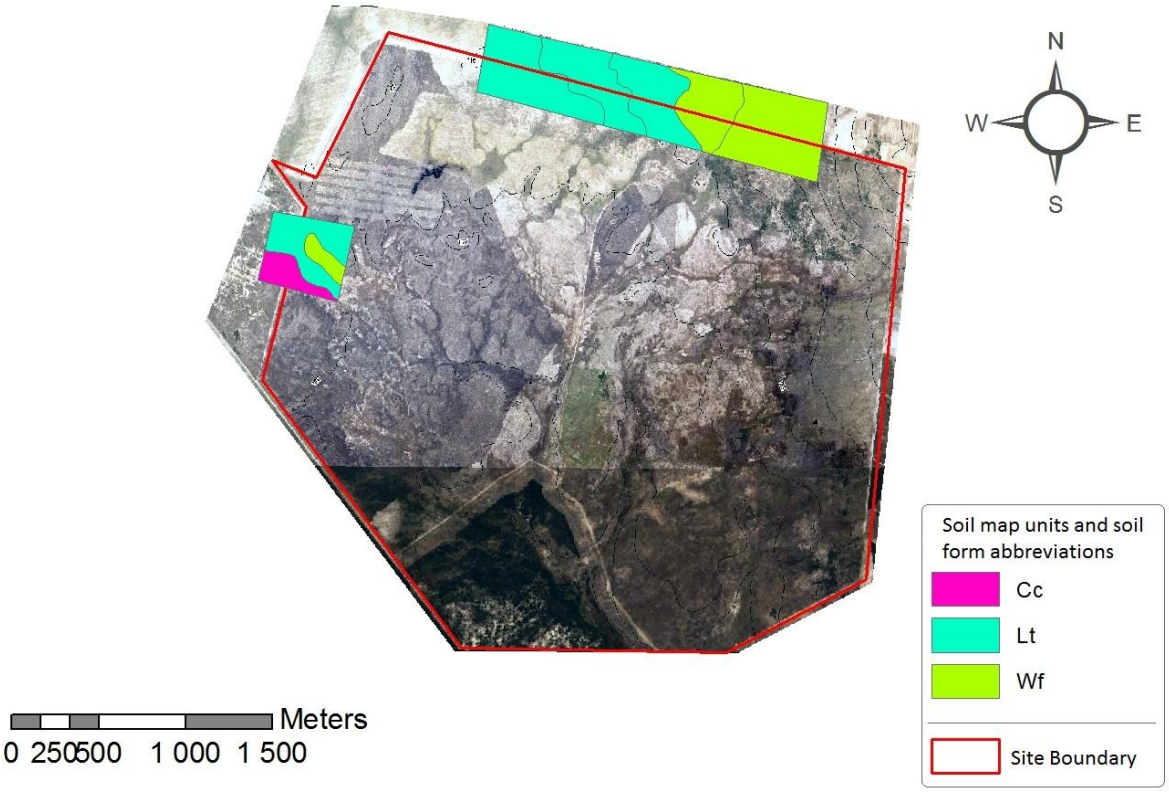

Figure 2.9: Soil map of surveyed areas in Riverlands Nature Reserve.

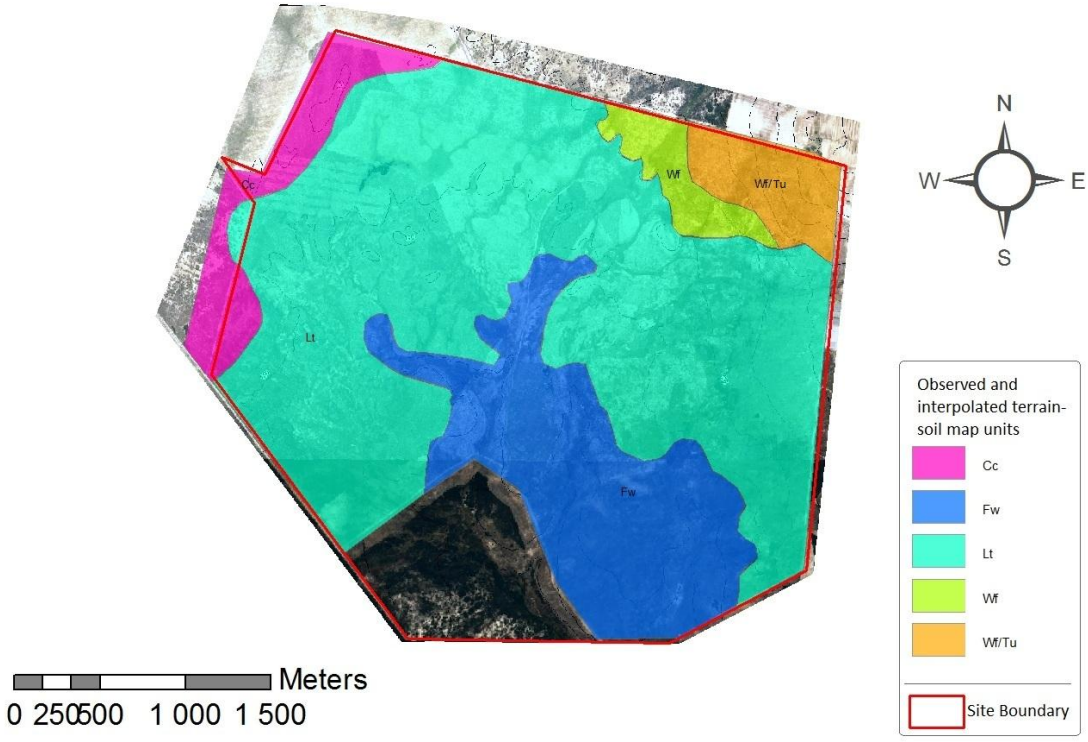

Figure 2.10: Interpolated terrain-soil map of Riverlands Nature Reserve.

The BDT that was compiled for interpolation in Kogelberg is shown in Figure 2.11. Tables 2.10 and 2.11 accompanying the BDT show the correlating HSUs and hydrologically similar soil classes respectively. Table 2.10 shows the HSUs that correlate and will be used on level 3 and 5 of the BDT. These classes are described in more detail in Table 2.9. Table 2.11 shows the soil forms that will have similar infiltration patterns based on position in landscape and soil form and will be used in level 4 and 5 in the BDT.

Table 2.10: Correlating hydrological similar units.

R1 + R2
Mw + Mn
T1 + T2 + T3
Ba + Bb + Bc + Bd + Be
Fs + Fn + La
Lb + Lc

Table 2.11: Hydrologically similar soil classes.

Description	Abbreviated Soil Forms
Deep sandy soils / Located on level or moderately sloping terrain / Accurately predictable	Fw, Cc, Ka, Lt, Pg, Wf
Shallow soil with a high coarse fraction / Grades to bedrock / Commonly occurring on high-lying or sloping terrain / Accurate prediction unlikely	Cf, Gk, Gs, Hh

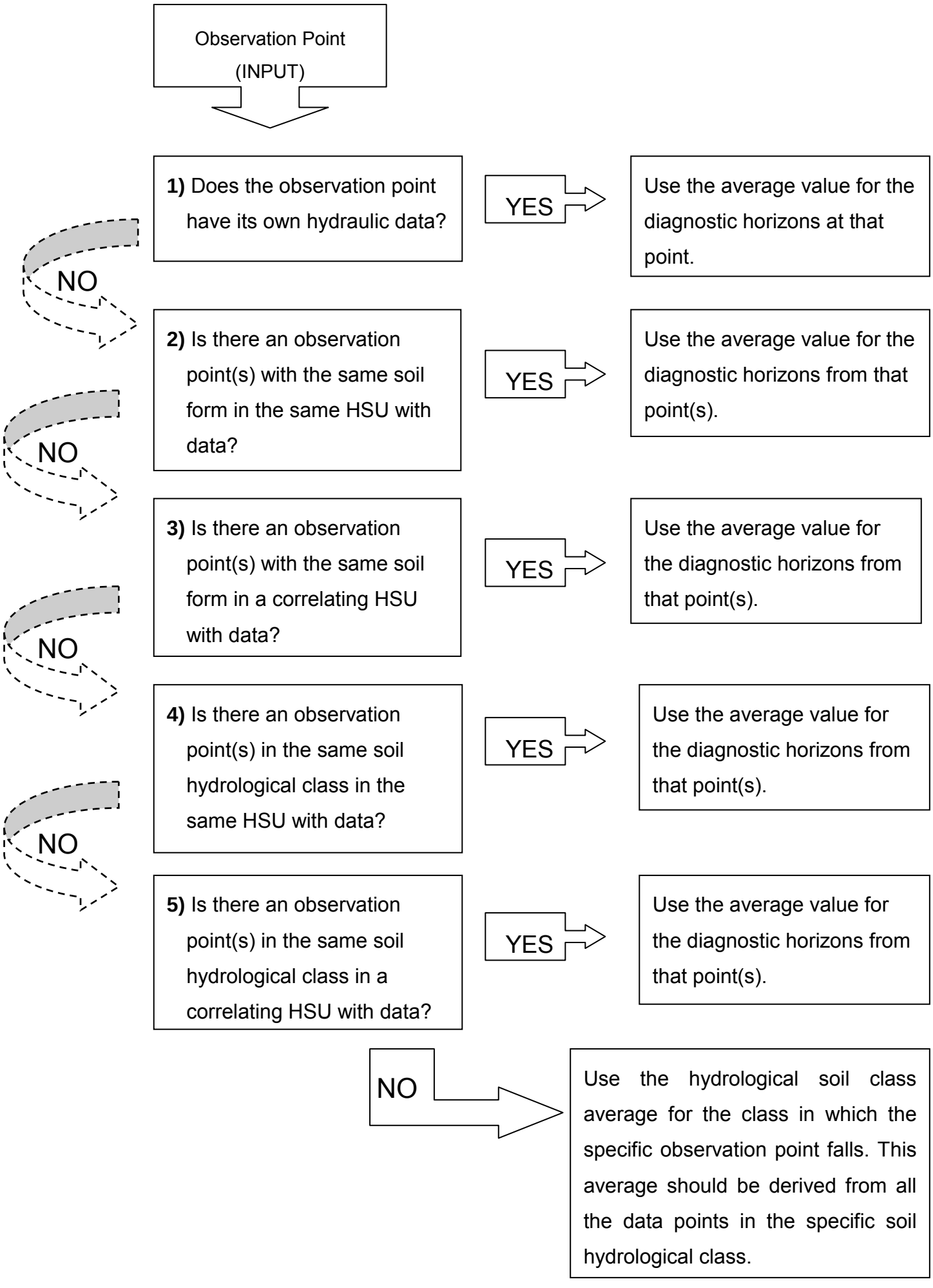

Figure 2.11: Binary Decision Tree for interpolating hydrological properties to unsampled observation points.

2.6. Discussion

2.6.1. Survey methods and soil complexity

The survey method used in Kogelberg, as proposed by Favrot (1981), was very effective for planning the survey. The RGs outlined in Figure 2.4 were very useful in identifying areas of variation in the reserve which lead to the identification of 10 different soil forms in Kogelberg and thus a broad degree of soil variation. The method of Favrot (1981) aims to reduce the number of soil survey observations required for accurate mapping. RGs did not have to be delineated in Riverlands prior to surveying as only limited areas could be surveyed due to park regulations.

Only two areas were chosen for detailed soil classification in Riverlands: A grid approach was effectively used to identify short-distance soil variation in an area where borehole monitoring is being done. A transect approach was used along the northern boundary of the reserve to investigate the catenary distribution and long-distance soil variation. The difference between short and long distance variation was inconsequential as only three different soil forms were identified. The reconnaissance survey of the remainder of the reserve showed little deviation from the observations made in the detailed survey areas as only one additional soil form was identified (Fw).

Thus the steep slopes and level valley floors on top of folded fractured bedrock in Kogelberg has lead to the development of a far more complex soil distribution than the level sandy terrain of Riverlands. This variation in soil pattern is caused by variations in slope inclination which contributes to catena complexity (Ticehurst *et al.*, 2007).

Mapping soil pattern was very helpful in linking the soil pattern to watershed dynamics. Lin *et al.* (2006) made a similar remark when using this approach in a study on soil moisture patterns in a forested catchment. The detailed observations made in the grid and transect survey were combined with rough reconnaissance observations, landscape position and surface properties during interpolation. Similar methods were successfully used by Favrot (1989), Lagacherie *et al.* (1995) and Browning & Duniway (2011).

The soils in Riverlands have formed from aeolian material (Jovanovic *et al.*, 2008) but there is an area in the north-eastern corner of the reserve where relict laterite is abundant. The soils in the reserve are however macroscopically homogenous and uniformly deep. The survey identified that the texture becomes finer closer to the confluence of the flow paths into the stream, a pattern which is common in landscapes (Ticehurst *et al.*, 2007). Humic acids leached from fynbos vegetation usually form organo-metal compounds in the soil, the accumulation of which gives rise to podzolic character (Midgley & Schafer, 1992). The soils in the laterite rich terrain were classified as Witfontein and Lamotte, with the possibility of being a Tukulu or Vilafontes forms respectively. The soils outside the laterite zone were classified as Lamotte, Witfontein, Concordia and Fernwood.

The soils in Kogelberg however, can roughly be grouped into one of two classes which were used as “hydrological similar soil classes”:

1. Deep, macroscopically homogenous, sandy textured soils, with a low coarse fraction content, predominantly occuring on moderately sloping or level terrain on foothills and valley floors. Examples of such deep sandy soil forms are Fernwood, Witfontein, Pinegrove, Lamotte, Katspruit and Concordia.
2. Shallower soils with a very high coarse fraction content, that gradually grade into bedrock. These soils are dominant on high-lying level terrain and steep slopes. Shallow rocky soil forms (and exposed bedrock) include Cartref, Glenrosa, Houwhoek and Groenkop.

2.6.2. Statistical analysis of hydrological properties and soil pattern

The statistical analysis revealed that the soils in Riverlands were fairly uniform regarding their PAW and K_{sat} as no significant differences were observed ($p > 0.05$; $F_{cal} < F_{crit}$). These soils would thus be regarded as having a similar hydrological response. This is in line with the low degree of expressed soil form variation relative to that of Kogelberg.

However, the same statistical analysis of the Kogelberg data showed that hydrological properties did differ between soil forms ($p < 0.05$; $F_{cal} > F_{crit}$). The PAW only differs between the Pinegrove and Cartref soil forms. The K_{sat} differed significantly between the Cartref and the Witfontein, Fernwood and Pinegrove soil

forms. Thus the general trend is that shallow rocky soils will behave hydrologically different to the deep sandy soils. See the “hydrological similar soil classes” in Table 2.10 above for a generalized grouping of these two soil classes.

The data thus showed that there are grounds for grouping soil forms based on their hydrological properties. This grouping could assist in the upscaling of hydrological models if sufficient soil survey information is available. The exact causes of the different infiltration patterns between the two mentioned hydrological similar soil classes is however not clear, thus the specific flow patterns for each group were investigated and reported on in Chapter 3.

The observation that the hydrological properties did differ significantly between contrasting soil forms is a development in hydropedology as it ties in with the findings of Van Huyssteen *et al.* (2005) who argue that the annual duration of saturation differs between diagnostic horizons according to South African Soil Classfication. These conclusions can aid in the upscaling of hydrological maps by providing grounds for grouping HSUs.

2.6.3. Soil mapping and hydrological property interpolation

The Riverlands catchment, as previously stated, was fairly homogenous in terms of relief, soil forms and soil depth. The observed soil forms and their relative position in the landscape could thus be used to predict a soil distribution map of the entire reserve, a method previously used by Browning & Duniway (2011) in New Mexico, USA. A reconnaissance survey was done to observe the soils outside the grid and transect boundaries in order to identify anomalies in the remainder of the reserve. These observations are not reported but were used in the interpolation process. The interpolation process took into account the expected degree of wetness, the abundance of vegetation, the relief and the lithology. Thus by incorporating the results of grid and transect surveys one can use ArcGIS software to interpolate the soil distribution if the correct input data is available (Hensley *et al.*, 2007; Lorentz, 2007). The available data includes soil point observations, an accurate georeferenced orthophoto and contour lines. Information that can further improve the accuracy of the interpolated map is a digital elevation model, which can be used to predict the water flow in the catchment.

The complexity of the Kogelberg catchment provided the opportunity to experiment with different methods of mapping and interpolation of hydrological properties. The terrain-soil map (Fig. 2.8) shows an ensemble of different hydrological similar units (HSUs), each with a unique combination of soil forms and terrain units. The conventional interpolation of hydrological properties was however not possible due to the limited number of observations and the large degree of variation. The combined approach of using the "soil classification" and "binary decision tree" methods was used to allocate the most accurate hydrological property to unsampled observation points using data from sampled observation points. Table D.1 in Appendix D shows the interpolated K_{sat} values for all 108 observation points in the Kogelberg site. The degree to which these outputs will improve recharge model estimations is however not yet clear but these data will be entered into the hydrological model of the catchment in the near future by researchers at the CSIR.

Helmschrot & Fügel (2002) used a RS approach to delineate HSUs but recommended that incorporating textural data would improve the accuracy of the analysis. The HSU-map shown in Figure 2.8, derived from combining RS, GIS and survey information, is thus expected to be more accurate and practical compared to using strictly RS techniques. The accuracy of using soil maps to interpolate hydrological data is however dependent on the degree of homogeneity of the mapping units and the accuracy of data collection. It is recommended that the resolution of the map used is less than 1:25 000 to minimize variation within map units (Voltz & Webster, 1990).

2.7. Conclusion

Two different aquifer systems were surveyed to investigate the effect of soil pattern on groundwater recharge. These findings were then graphically presented using different mapping techniques. The Oudebos catchment in the Kogelberg Nature Reserve served as a model fractured bedrock aquifer, whereas the Riverlands Nature Reserve served as a model cover sands aquifer. The concluding results are as follows:

- Use of GIS and RS techniques can help delineate reference groups in a sloping landscape, based on surface features and terrain morphology, to identify areas of expected variation which may aid to reduce the number of field observations required to conduct a comprehensive soil survey.
- PTFs can effectively be used to predict hydrological properties, K and PAW, from soil texture, gravel- and OM-content determined in a laboratory from soil samples.
- There is a statistical significant difference between the estimated K_{sat} of the deep sandy Fernwood, Witfontein and Pinegrove soil forms and shallow rocky Cartref soil forms in the Kogelberg Nature Reserve.
- There is a statistical significant difference between the estimated PAW of the deep Pinegrove soil form and shallow rocky Carterf soil form in the Kogelberg Nature Reserve.
- There is no statistical significant difference between either the K_{sat} or PAW of any of the soil forms sampled in the Riverlands Nature Reserve.
- GIS can be used to graphically delineate HSUs in a catchment based on terrain morphology and soil pattern distribution on grounds of the statistical difference mentioned above.
- A combination of the soil classification method and the rules defined by a binary decision tree can be used to interpolate hydrological properties in unsampled observation sites.

This research thus confirms that semi detail field soil survey information, such as a soil map showing soil form distribution and topography, can be used to assist in groundwater recharge estimation models by providing a basis for delineating HSUs. The research also shows that a combination of RS, GIS and survey techniques can

be used to compile terrain-soil maps, which can be used for hydrological model upscaling

2.8. References

ASANO, Y., UCHIDA, T. & NOBUHITO, O., 2002. Residence times and flow paths of water in steep unchannelled catchments, Tanakami, Japan. *Journal of Hydrology* 261, 173-192.

BOETTINGER, J., RAMSEY, R.D., BODILY, J.M., COLE, N.J., KIENAST-BROWN, S., NIELD, S.J., SAUNDERS, A.M. & STUM, A.K., 2008. Landsat spectral data for digital soil mapping. p. 193-202. *In:* A. Hartemink, A. McBratney, & M. Mendonca Santos (eds.). Digital soil mapping with limited data. Springer. Berlin, Germany.

BONSU, M., 1992. A study of a texture-based equation for estimating the hydraulic conductivity of an Alfisol in the sudan savannah ecological zone, Ghana. *Hydrological Sciences* 37, 599-606 .

BOUCHER, C., 1978. Cape Hangklip area: II. The vegetation. *Bothalia* 12, 455-497.

BROOKS, R., & COREY, A., 1964. Hydraulic properties of porous media. *Hydrology Papers, Colorado State University* 3.

BROUWER, J. & FITZPATRICK, R. 2002. Interpretation of morphological features in a salt-affected duplex soil toposequence with an altered soil water regime in Western Australia. *Aust. J. Soil Res.* 40, 903-926.

BROWNING, D. & DUNIWAY, M., 2011. Digital soil mapping in the absence of field training data: a case study using terrain attributes and semiautomated soil signature derivation to distinguish ecological potential. *Applied and Environmental Soil Science*, 1-12.

BRYDON, J. & DAY, J., 1970. Use of the Fieldes and Perrot sodium fluoride test to distinguish the B horizons of podzols in the field. *Can. J. Soil Sci.* 50, 35-41.

CAMPBELL, L. G., 1974. A simple method for determining unsaturated conductivity from moisture retention data. *Soil Sci.* 117, 311-314.

COLVIN, C., 2008. Ecological and environmental impacts of large-scale groundwater development in the TMG aquifer system. *WRC Report* No. K5/1327. Stellenbosch.

CONACHER, A. & DALRYMPLE, J., 1977. The nine unit landsurface model: an approach to pedogeomorphic research. *Geoderma* 18, 1 - 153.

DE VRIES, J. & SIMMERS, I., 2002. Groundwater recharge: an overview of processes and challenges. *Hydrogeology Journal* 10, 5-17.

FAVROT, J.-C., 1981. Pour une approche raisonnee du drainage agricole en France: La methode des secteurs de reference. *Comptes-Rendus des Seances de l'Academie d'Agriculture de France* 8, 716-723.

FAVROT, J.-C., 1989. Une stratégie d'inventaire cartographique à grande échelle: la méthode des secteurs de référence. *Science du Sot* 27, 351-368.

FEY, M., 2010. Soils of South Africa, 1st edn, Cambridge University Press, Cape Town.

FLÜGEL, W., 1996. Hydrologocal Response Units (HRUs) as modelling entities for hydrological river basin simultaion and their methodological potential for modelling complex environmental process systems. Results from the Sieg catchment. *Die Erde* 127, 43-62.

FRITSCH, E. & FITZPATRICK, R., 1994. Interpretation of soil features produced by ancient and modern processes in degraded landscapes. I. A new method for constructing conceptual soil-water-landscape models. *Aust. J. Soil Res.* 32, 889-907.

GEE, G. & BAUDER, J., 1986. Particle-size analysis. p. 383-411. *In:* M.A. Klute (ed.). Methods of soil analysis: Physical and mineralogical methods: Part 1 (2nd edn.). Soil Sci. Soc. Am.

GLEESON, T., NOVAKOWSKI, K. & KYSER, K., 2009. Extremely rapid and localized recharge to a fractured rock aquifer. *Journal of Hydrology* 376, 496-509.

HANSEN, M., BROWN, D., DENNISON, P., GRAVES, S. & BRICKLEMYER, R., 2009. Inductively mapping expert-derived soil-landscape units within dambo wetland catenae using multispectral and topographic data. *Geoderma* 150, 72-84.

HELMSCHROT, J. & FLUGEL, W.-A., 2002. Landuse characterisation and change detection analysis for hydrological model parameterisation of large scale afforested areas using remote sensing. *Physics and Chemistry of Earth* 27, 711-718.

HENSLEY, M., LE ROUX, P., GUTTER, J. & ZERIZGHY, M., 2007. A procedure for an improved soil survey technique for delineating land for rainwater harvesting. *WRC Report* No. TT311/07. Pretoria, South Africa.

JENNY, H., 1941. Factors of soil formation, A system of quantitative pedology. McGraw-Hill, New York.

JOVANOVIC, N., HON, A., ISRAEL, S., LE MAITRE, D., RUSINGA, F., SOLTAU, L., TREDOUX, G., FEY, M.V., ROZANOV, A. & VAN DER MERWE, N.D., 2008. Nitrate leaching from soils cleared of alien vegetation. *WRC Report* No. 1696/1/08. Cape Town, South Africa.

LAGACHERIE, P., LEGROS, J.-P. & BURROUGH, P., 1995. A soil survey procedure using the knowledge of soil pattern established on a previously mapped reference area. *Geoderma* 65, 283-301.

LE ROUX, P. & DU PREEZ, C., 2008. Micromorphological evidence of redox activity in the soft plinthic B horizon of a soil of the Bainsvlei form in an arid bioclimate. *S. Afr. J. Plant Soil* 25, 84-91.

LEENHARDT, D., VOLTZ, M., BORNAND, M. & WEBSTER, R., 1994. Evaluating soil maps for prediction of soil water properties. *European Journal of Soil Science* 45, 293-301.

LIN, H., KOGELMANN, W., WALKER, C. & BRUNS, M., 2006. Soil moisture patterns in a forested catchment: A hydropedological perspective. *Geoderma* 131, 345-368.

LIN, H., MCINNES, K., WILDING, L. & HALLMARK, C., 1999. Effects of soil morphology on hydraulic properties: II. Hydraulic Pedotransfer Functions. *Soil Sci. Soc. Am. J.* 63, 955-961.

LORENTZ, S.A., 2007. Interim annual report on data collection at local, field and catchment scale for each pollutant type, Wartburg research catchment. Report to Sigma Beta Consulting for WRC Project: K5/1467. Development of an intergrated modelling approach for the prediction of agricultural non-point source (NPS) pollution from field to catchment scales for selected agricultural NPS pollutants. University of Kwa-Zulu Natal. Pietermaritzburg, South Africa.

MCBRATNEY, A., MENDONCA SANTOS, M. & MINASNY, B., 2003. On digital soil mapping. *Geoderma* 117, 3-52.

MIDGLEY, J. & SCHAFER, G., 1992. Correlates of water colour in streams rising in Southern Cape catchments vegetated by fynbos and/or forest. *Water SA* 18, 93-100.

MUNSELL, A.H., 1912. A Pigment Color System and Notation. *The American Journal of Psychology* 23, 236-244.

PACHEPSKY, Y., RAWLS, W. & LIN, H., 2006. Hydropedology and pedotransfer functions. *Geoderma* 131, 308-316.

PRAAMSMA, T., NOVAKOWSKI, K., KYSER, K. & HALL, K., 2009. Using stable isotopes and hydraulic head data to investigate groundwater recharge and discharge in a fractured rock aquifer. *Journal of Hydrology* 366, 35-45.

RAWLS, W. J., BRAKENSIEK, R. L. & SAXTON, K. E., 1982. Estimation of soil water properties. *Trans. Am. Soc. Agric. Engrs.* 25, 1316-1320.

RAWLS, W., GISH, T. & BRAKENSIEK, D., 1991. Estimating soil water retention from soil physical properties and characteristics. *Advances in Soil Science* 16, 213-234.

REBELO, A., BOUCHER, C., HELME, N., MUCINA, L. & RUTHERFORD, M., 2006. Fynbos Biome. p. 53-219. *In*: L. Mucina & M. Rutherford (eds.). The vegetation of South Africa, Lesotho and Swaziland. Strelitzia, Pretoria.

RHOADES, J., 1996. Salinity: Electrical conductivity and total dissolved solids. p. 417-435. *In*: D.L. Sparks (ed.). Methods of soil analysis: Chemical methods: Part 3. Soil Sci. Soc. Am.

ROYAPPEN, M., DYE, P., SCHULZE, R. & GUSH, M., 2002. An analysis of catchment attributes and hydrological response characteristics in a range of small catchmnets. *WRC Report* No. 1193/1/02. Pretoria, South Africa.

SAXTON, K. & RAWLS, W., 2006. Soil water characteristic estimates by texture and organic matter for hydrologic solutions. *Soil Sci. Soc. Am. J.* 70, 1569-1578.

SIVAPALAN, M., 2003a. Process complexity at hillslope scale, process simplicity at the watershed scale: is there a connection? *Hydrological Processes* 17, 1037-1041.

SIVAPALAN, M., 2003b. Prediction in ungauged basins: a grand challenge for theoretical hydrology. *Hydrological Processes* 17, 3163-3170.

SOIL CLASSIFICATION WORKING GROUP, 1991. Soil Classification - A Taxonomic System for South Africa. Memoirs on the agricultural natural resources of South Africa No. 15. Department of Agricultural Development. Pretoria, South Africa.

KLUTE, M. (ed.). 1986. Methods of Soil Analysis Part 1 (2 ed.). Soil Sci. Soc. Am. Inc.

SPARKS, D.L. (ed.). 1996. Methods of Soil Analysis Part 3 (2 ed.). Soil Sci. Soc. Am. Inc.

STORIE, R., 1976. Storie index soil rating (revised). *Spec. Publ. Div. Agric. Sci. No. 3203* . Univ. of California. Berkley.

THOMAS, G., 1996. Soil pH and soil acidity. p. 475-490. *In*: D. Sparks (ed.). Methods of Soil Analysis: Chemical Methods. Part 3. Soil Sci. Soc. Am.

TICEHURST, J., CRESSWELL, H., MCKENZIE, N. & GILOVER, M., 2007. Interpreting soil and topographic properties to conceptualise hillslope hydrology. *Geoderma* 137, 279-292.

VAN GENUCHTEN, M., 1980. A closed-form equation for predicting the hydraulic conductivity of unsaturated soils. *Soil Sci. Soc. Am. J.* 44, 892-897.

VAN HUYSSTEEN, C., HENSLEY, M., LE ROUX, P., ZERE, T. & DU PREEZ, C., 2005. The relationship between soil water regime and soil profile morphology in the Weatherley catchment, an afforestation area in the north-eastern Eastern Cape. *WRC Report* No. K5/1317. Pretoria, South Africa.

VAN HUYSSTEEN, C.W., 1995.The relationship between subsoilcolour and degree of wetness in a suite of soils in the Grabouw district, Western Cape. M.Sc. Thesis, Stellenbosch: Stellenbosch University.

VOLTZ, M. & GOULARD, M., 1994. Spatial interpolation of soil moisture retention. *Geoderma* 62, 109-123.

VOLTZ, M. & WEBSTER, R., 1990. A comparison of kriging, cubic splines and classification for predicting soil properties from sample information. *Journal of Soil Science* 41, 473-490 .

VOLTZ, M., LAGACHERIE, P. & LOUCHART, X., 1990. Predicting soil properties over a region using sample information from a mapped reference area. *European Journal of Soil Science* 48, 19-30.

CHAPTER THREE

3. Preferential Flow Assessment in Soil on Fractured Bedrock and Cover Sand Aquifers.

3.1. Introduction

Water infiltration occurs in soil according to one of two flow patterns: uniform or non-uniform. Uniform flow occurs as a more or less horizontal wetting front, usually parallel to the soil surface. Non-uniform flow, referred to here as preferential flow (PF), occurs as an irregular wetting front in which water or solutes will move faster in certain areas of the vadose zone than in others (Hendrickx & Flurry, 2001).

Water and solute flow patterns in soil have been extensively researched. This has lead to the identification of three different types of non-uniform flow patterns: *macropore flow, unstable flow and funnel flow.* Many different causes have been suggested for the different types of PF; these causes are discussed in the literature review in Chapter 1. However, estimating whether PF will occur in soil cover and the degree to which the PF affects the rate of infiltration and recharge is not well understood. Thus research that aims to investigate which soil systems give rise to PF, and describe the effect of PF on recharge, can significantly reduce uncertainties in our groundwater recharge estimation models.

Traditional methods of investigating groundwater dynamics include the use of hydraulic head data, temperature profiles, stream flow, stable isotope and dye tracers, drip infiltrometers, double ring infiltrometers and mini-disc permeameters. Modelling flow in fractured bedrock aquifers face a unique challenge as using hydraulic information alone is not passable and temperature profiles are difficult to attain due to the rock content (Praasma *et al.*, 2009). Thus a selective combination of the following methods can be used in a flowpath modelling investigation.

Flow path tracers

Tracers are often used to study the flow paths of water or solutes by either monitoring the natural or applied tracers which move with the flux through the soil,

leaving evidence of the flowpath. The tracers can either be detected by lab analysis (Isotopes) or observed infield (Dyes). An advantage of using tracers is that a decrease in flux does not reduce the precision of the estimation (de Vries & Simmers, 2002).

Isotope studies, using ^{3}H and Cl^{-}, can distinguish between flow in topsoil and subsoil horizons on the meso-scale and have effectively been used in semi-arid / arid regions thus making it a particularly useful method (Rodgers *et al.,* 2005).The accuracy of this method is however threatened by the inaccurate estimation of atmospheric Cl^{-} additions and ^{3}H may be transported in vapour form if precipitation is less than 20 mm/year (de Vries & Simmers, 2002).

The changes in stable isotopes of oxygen (O^{18}/O^{16}) and hydrogen (H^{2}/H^{1}) in a specific catchment can be used to infer groundwater flow patterns and residence times (Rodgers *et al.,* 2005, Wenninger *et al.,* 2008) but cannot be used to quantify recharge (de Vries & Simmers, 2002). The isotope-tracer methods require the same level of field work as the dye-methods but accurate analysis requires the use of expensive, technical laboratory equipment.

Dyes are used to indicate flow patterns and give information about the pore fraction in soils as they mimic water, reactive or nonreactive solutes (Flury & Fluhler, 1995; Delin *et al.*, 2000). For a dye to be effective as a tracer it has to visibly contrast with the soil colour. It should be mobile in the soil yet be retained in the pore linings to a certain extent in order to make the flow paths visible. Another criterion for a good tracer-dye, which is only really applicable in field studies, is that the dye should be non-toxic to the environment (Flury & Fluhler, 1995).

Fluorescent dyes are very effective in showing flow paths in soils at very dilute concentrations (Flury & Fluhler, 1995). Reynolds (1966) compared the efficacy of 12 different fluorescent dyes in a rainwater percolation study. He found that Pyranine was the most suitable fluorescent dye when studying water flow paths. He however also commented that fluorescent dye performance is often lacking as observation is only possible under UV light and that the dye may become unstable and breakdown over time.

Delin *et al.* (2000) investigated flow paths in the unsaturated zone using the fluorescent tracer dye, Rhodamine WT. A downside of using such a tracer is that laboratory analysis of samples is required to determine dye fluorescence. Representative samples at recorded depths are thus required for analysis. However, these samples can then be used to determine bulk density, particle size distribution, organic carbon content and volumetric water content if desired.

Corey (1968) evaluated the use of dyes to study water flow in acid soils. The comparison between acid, basic and disperse dyes revealed that the number of anionic groups in the tracer was a good criterion when selecting an appropriate tracer. Acid dyes were found to be the most effective when visualizing water flow as they hydrolyze in water to form anions. He concluded that Azo Geranine 2G is the most suitable when tracing water flow in acid soils.

An effective method for studying flow paths in non-structured soils was presented by van Ommen *et al.* (1988). Their method relies on the colour change reaction between starch and iodine (I^-), facilitated by hydrogen peroxide. An I^- solution is applied on the soil surface and allowed to infiltrate. Consecutive cross sections of the soil are then thoroughly treated with a starch powder and a hydrogen peroxide spray to initiate the blue-violet colour formation. This method is limited to non-structured soils as the application of starch and peroxide must be uniform. This method has proven useful in further studies by Hangena *et al.* (2003) and Rozanov & De Clercq (2010). The concentration of the I^- solution can be between 7% (Rozanov & De Clercq, 2010) and 12% (Hangena *et al.,* 2003), depending on the colour of the soil as a higher I^- concentration would produce a darker blue colour.

Rozanov & De Clercq (2010) commented that this method is effective as it is inexpensive and can be used in the field *via* infiltrometer or irrigation application. They however criticized the technique as partial iodine retention occurred and iodine can also become volatilized and transported through air voids, possibly suggesting an overestimation of the flowpath density.

Relative to I^- and Br^- , Brilliant Blue FCF is a very effective in-field tracer in terms of its low toxicity and high visibility (Flury & Fluhler, 1995). The flow of the tracer is however retarded in soil, possibly due to the formation of ion pairs with Ca^{2+}, and the travel times of water can thus not be investigated using Brilliant Blue FCF.

Digital photographic manipulation has modernized the use of tracer dyes in flow path evaluation. A stained profile can be photographed in a "RAW format" (Rozanov & De Clercq, 2010), which is a file that has not yet been processed and thus stores a large volume of the available photographic data. This allows for extensive digital enhancement and colour contrasting, and statistical analysis on selective software such as Adobe Photoshop or ArcGIS respectively. Rozanov & De Clercq (2010) however recommend that calibration and interpretation studies be done to improve the accuracy and consistency of photographic evidence.

Rain simulator (Drip infiltrometer)

A rain simulator is a very realistic way of investigating rainfall infiltration in the field. It applies water to the soil with a certain energy which brings about the raindrop splash effect. This often decreases the infiltration capacity due a change in surface macropore structure (Joel & Messing, 2001). The simulator can be used to investigate flow paths by recording the rate of surface runoff at different rainfall intensities by collecting the surface runoff over a given time. The infiltration rate can be calculated by subtracting the runoff rate from the supply rate (Joel & Messing, 2001).

Joel & Messing (2001) further outlined some criteria for an effective rain simulator: The simulator should be able to supply water at different intensities; the splash effect should be mimicked; distribution should be uniform; the simulator should be easy and cheap to construct and it should be able to withstand harsh field conditions.

Mini disc infiltrometer (Disc permeameter or Tension infiltrometer)

Disc infiltrometers are regularly used to investigate the rate of infiltration and hydraulic conductivity (K) in the large pore system near saturation. This method does not disturb the pore structure as water is applied very gently to the surface under a predetermined negative hydraulic pressure (Joel and Messing, 2001). The infiltration rates at a given tension can be used in various models to determine the K of the soil as well as the contributing pore fraction. One such model, by Zhang (1997), is referred to in the literature review. It utilizes the van Genuchten parameters (van Genuchten, 1980) for a specific soil type to determine K from the infiltration rate at different tensions.

This method allows the pore system to remain intact as it avoids the splash effect. Infiltration is thus often overestimated compared to the rates determined during rain simulations or actual rainfall events. However, at higher tensions, the macropore contribution is reduced, at which point infiltration rates may reflect the same conditions as a rainfall event (Joel & Messing, 2001).

Solute transport can also be studied with a disc infiltrometer as solute transport in structured soils is strongly linked to K (Joel & Messing, 2001). The mini disc infiltrometer is very easy to use in the field as only the infiltrometer, water and a stopwatch is required to take measurements. The instruction manual for the instrument is also very user-friendly and easily attainable (Decagon Devices Incorporated, 2007). The infiltrometer may however be difficult to use in sloping terrain and uneven soil surfaces as contact between the disc and surface could be reduced.

Double ring infiltrometer

A double ring infiltrometer can be used to measure the infiltration rate for a specific soil and hydraulic conductivity can in turn be calculated from these measurements using Darcy's equation (Eq. 1.1). The double-ring infiltrometer consists of two concentric rings. The outer ring compensates for lateral flow of water so vertical infiltration can be measured more accurately. An advantage of this method is that it can be combined with other studies such as tracer dye investigations. A disadvantage is however the large volume of water required for a single measurement and performance is limited on steep sloping or uneven surfaces (Rozanov & De Clercq, 2010).

Extensive groundwater research has lead to the development of a large arsenal of recharge estimation models and methods as described in the literature review and above. Selecting a sound combination of models and methods is the key to accurate groundwater investigations which is vital if accurate recharge estimations are to be made.

Recalling the discussion on flow paths in the literature review, the soil cover has a dominant effect on distributing rainfall into runoff and infiltration. The use of existing soil survey information such as soil form is thus an attractive amendment to

estimation models as these data effectively account for a large degree of the natural variation observed in a catchment. The extent to which soil classification can be used to amend these models is however not yet fully understood as no formal correlations have been established between soil type and infiltration pattern. A comparison between two aquifer systems was thus done to improve our understanding by looking at the prevalence of PF in different soils and the effect thereof on recharge.

The Kogelberg Nature Reserve near Kleinmond represents a fractured bedrock aquifer whereas the Riverlands Nature Reserve near Malmesbury represents a cover sands aquifer system. The comparison was done on a quantitative and qualitative basis. The quantitative comparison was done using numeric data in the form of volumetric water measurements and hydraulic conductivity measurements, whereas the qualitative comparison was done based on photographic support of water flow paths using a staining dye and digital image classification.

3.2. Objectives

The aim of this investigation was to compare the water infiltration patterns of the dominant soil types found in a cover sands aquifer, in Riverlands Nature Reserve, and a fractured bedrock aquifer, in the Kogelberg Nature Reserve. The ultimate goal of gaining a better understanding of PF in these contrasting catchments was broken down into the following specific objectives:

- Model soil hydraulic parameters based on soil profile stratification and textural properties.
- Conduct a combination of infield experimental infiltration tests to validate the model results.
- Visualise specific flow paths to better understand soil hydrological behaviour observed in the dominant soil forms in the two study areas.
- Formulate an approach to reduce uncertainties regarding soil hydraulic properties in the study area.

This study will hopefully improve the understanding of preferential flow paths (PFPs) in the soil during water infiltration, which gives rise to interflow and groundwater recharge, and so doing improve the accuracy with which researchers can model catchment dynamics.

3.3. Methodology

3.3.1. Site description

The study areas are thoroughly described in Chapter 2, whereas the infiltration sites are described here. Two infiltration sites were selected at each study location. The aim was to do the infiltration experiments at contrasting soil observation points. The variation of soils in the study area can be broadly summarized into two groups; (1) Shallow soils with high coarse fraction, grading into bedrock, mostly found on sloping terrain (Site K1) or (2) Deep sandy soils, with low coarse fraction, predominantly on level valley floors (Sites K2, R1 and R2). Figures B.1 to B.4 in Appendix B summarize the site details and the basic soil properties at the points where infiltration tests were conducted. The sites are referred to as K1, K2, R1 and R2.

1a 1b 1c

2a 2b 2c

Figure 3.1: Kogelberg infiltration sites (1) K1 and (2) K2 showing (a) site location, (b) vegetation and (c) stained profile.

Kogelberg presented a large degree of soil variation as reported in the survey in Chapter 2. A shallow rocky Cartref (K1) and deep sandy Fernwood (K2) soil forms were selected for the infiltration tests as these represent the most divergent soil forms in terms of depth, coarse material content, expected moisture and position in the landscape. Both these sites were also easily accessible with all the required equipment. All the soils found in the reserve were slightly acidic with pH (H_2O) generally less than 6. Both sites had a coarse sand texture and low clay contents of no more than 2.75 and 3.95 % for K1 and K2 respectively. The coarse fraction however differed greatly as the K1 had up to 32 % and K2 having less than 1 %. The vegetation at K1 was disturbed by a fire the previous year (2010). However, the vegetation is generally knee to hip high grass with scattered fynbos. The lush riparian vegetation found at K2 is common for areas so close to the stream. The site locations, vegetation and profiles are shown in Figure 3.1.

1a 1b 1c

2a 2b 2c

Figure 3.2: Riverlands infiltration sites (1) R1 and (2) R2 showing (a) site location, (b) vegetation and (c) stained profile.

The soil survey of Riverlands revealed much less heterogeneity in terms of soil form and soil depth than in Kogelberg. The infiltration investigation was thus performed on two common soil forms found on different landscape positions. R1 is a Lamotte 1100 soil form with a medium sand texture and no coarse fragments found on a lowerlying concave slope. The vegetation is ankle high grass with scattered burnt remnants of fynbos. R2 is a Vilafontes 2110 (Transition to Lamotte) soil form with a medium sand texture on a high lying convex slope. The coarse fraction and clay content increase with depth where the texture eventually grades to loamy sand. The vegetation is similar to the grass found in R1 but with scattered restioid reeds. The soils in the reserve are generally acidic with regular readings of pH (H_2O) below 7. The site locations, vegetation and profiles are shown in Figure 3.2.

The textural analysis and pH determinations for all four the infiltration sites are shown in Table B.1 of Appendix B.

3.3.2. Experiments

The following experiments were done to investigate the presence and effect of PFPs on hydraulic conductivity at each of the four sites:

3.3.2.1. Double ring infiltration

Hydraulic conductivity was determined in the field using the constant head method in a large double ring infiltrometer. The rates of infiltration in both Riverlands and Kogelberg were very rapid which made it difficult to maintain a strictly constant water head using the available equipment.

The superficial vegetation in the selected sites was cleared using a spade, yet the root system was left intact, to allow good contact between the infiltrometer and the soil as to avoid any water leaks that would result in lateral surface flow. A KI solution was used instead of water to combine the infiltrometer and flowpath visualization experiments for convenience. The inner ring of the infiltrometer was gauged in 1 cm intervals. Both the inner and the outer ring were hastily filled with a KI solution to the top mark, at which point the time count was started at zero. The stop watch time was split every time the water level reached each consecutive 1 cm mark in the inner ring. The hydraulic conductivity could then be calculated using Darcy's law (Equation 1.1). The key for terms used in equations are summarized in Table 1.2.

Darcy's law states that the rate of flow of a liquid (q) through a porous medium is in the direction of and proportional to the hydraulic gradient (ΔH/t). The flow is also proportional to the conducting medium's ability to transmit the liquid, known as the conductivity (K) (Hillel 1980). The hydraulic conductivity (K) is the proportionality constant linking ΔH/t to q. This variable can be used to compare the conductivity of water in different soils. Flow in a vertical column is described by Equation 1.2. Here ΔH and L act in the same direction, resulting in the additional K term. A more in depth discussion on this can be seen in Hillel (1980).

Figure 3.3 shows the double ring infiltrometer setup in the field. Equation 1.2 was used to calculate K_{sat} using the data from the constant head infiltration experiment. ΔH is the change in height of the water head with the soil surface as reference level and L is calculated as the difference between the initial and final height of the water level in the specific time interval. L will be 1 cm in each case as time was taken as the dependent variable in this experiment. V is the volume of water infiltrating the soil in a given time; calculated using ΔH and the area of the inner ring.

Figure 3.3: Photo of double ring infiltrometer used during infiltration experiments.

Thus, K_{sat} was calculated using input variables A, t, L and ΔH as shown in Equation 3.1, a rearrangement of Equation 1.2. Table B.2 in Appendix B shows the full dataset used to calculate K_{sat}.

Equation 3.1

$$K = \frac{V.L}{\Delta H.A.t}$$

3.3.2.2. Visualization of water infiltration

The visualization of water flow paths experiment was conducted as proposed by Hangena *et al.* (2004) in their study to visualize flow paths in lignitic mine soils. The method is based on the colour change reaction between potassium-iodide (KI) and starch. Hangena *et. al.* (2004) used a 12% KI solution but a 7% solution is efficient to cause a colour change in the light coloured soils of the selected sites in this study. The KI solution was allowed to infiltrate the soil using the double ring infiltrometer as described above.

The infiltration site was then left undisturbed for 24hours, with the double ring infiltrometer left on the surface to reduce evaporation and drying of the top soil. After the waiting period a vertical soil section was carefully excavated through the zone where infiltration occurred. The exposed surface was thoroughly wetted with household starch spray from an aerosol canister. A 12% hydrogen-peroxide solution was then applied onto the surface using a spray bottle to facilitate the release of I_2 and favour the blue colour formation. A 10 minute waiting period was allowed for effective colour change to occur after which digital photographs were taken in "RAW format" for digital image processing. Adobe Photoshop Version 8.0 was used to convert the images from a RAW to a JPEG format as negative colour projections using a standardized filter. The negative colour images serves to contrast the blue dye with the surrounding unstained soil which can then be further analysed on ArcGIS software.

The photo was cropped to ensure that only the area of infiltration was analysed. The negative colour image was further contrasted by reducing all the pixels in the image to either blue, indicating flow paths, or red, indicating areas that were bypassed during infiltration. The classification of pixels was done using the maximum likelihood classification tool in the ARCToolbox window on ESRI GIS software version 9. The number of pixels in each class was then presented as a percentage relative to the total number of pixels in the image. These calculations can be seen in Table B.7 in Appendix B.

3.3.2.3. Water content, bulk and particle density determination

Samples were collected in 10 cm depth intervals from the area of infiltration. The samples were sealed in air tight plastic bags and weighed in the laboratory. These initial masses were noted as wet mass. The samples were then air dried in a force draft room and weighed again. This time the mass was noted as dry mass. The change in mass was used to calculate the gravimetric water content (GWC).

Particle density was calculated using the volumetric flask method as outlined by Blake & Hartge. (1986).

Bulk density was not determined in the field and a rapid assessment was thus done in the laboratory. A twenty gram sample was weighed off to three decimal places and placed into a measuring cylinder accurate to 1 cm^3. The cylinder was gently tapped on the worktable twenty times to allow partial consolidation to occur. The volume was recorded in cm^3 and is reported as measured bulk density.

An estimated bulk density was also calcualted in the SPAW software using texture and OM as input variables (Saxton & Rawls, 2006).

Both the measured and estimated bulk densities were used to calculate volumetric water content. The VWC calculated using measured and estimated BD are reported in the results as VWC_{meas} and VWC_{est} respectively.

Volumetric water content was calculated using Equation 3.2. The dataset used to calculate VWC can be found in Table 3.4 of the results.

Equation 3.2

$$\theta_w = \frac{P_w}{\rho_b} \times \frac{1000}{\rho_w}$$

3.3.2.4. Mini disc infiltration and contributing pore fraction determination

A mini disc infiltrometer was used to investigate the unsaturated hydraulic conductivity (K). Infiltration was investigated at four consecutive tensions (ψ) namely -0.5cm, -1cm, -2cm (-2.5cm at K2) and -5cm. This experiment could not be conducted at R2 due to extreme hydrophobicity of the topsoil.

The soil surface was cleared of vegetation and stones, and levelled to allow good disc-soil contact. Where contact was poor, a moist soil slurry was placed on the surface to improve contact. The infiltrometer was filled with water and the gauge in the bubble chamber set accordingly. The stop watch was started at time zero as contact was made with the soil surface. The time was split every time the water level dropped by 5 mL (a 2 mL interval was used where infiltration was very slow at tensions -2 cm or -5 cm).

The cumulative infiltration and the time elapsed was then used to calculate K according to the method by Zhang (1997). The cumulative infiltration and square root of time is fitted to Equation 3.3:

Equation 3.3

$$\mathrm{I} = \mathrm{C}_1\mathrm{t} + \mathrm{C}_2\mathrm{t}^{-0.5}$$

C_1 and C_2 are parameters relating to K and soil sorptivity respectively. K is calculated according to Equation 3.4.

Equation 3.4

$$\mathrm{K} = \frac{\mathrm{C}_1}{\mathrm{A}}$$

Here, A is the variable which relates the suction rate and radius of the infiltrometer disc to the van Genuchten parameters for the soil texture class. The four soils from both test sites were classified as sand, thus the same van Genuchten parameters were used for all test points (Table 3.1).

Table 3.1: Adapted table showing van Genuchten's parameters for sand (Decagon Devices Incorporated 2007).

			ho						
			-0.5	-1	-2	-3	-4	-5	-6
Pressure	α	n	A						
coefficient value	0.145	2.68	2.84	2.4	1.73	1.24	0.89	0.64	0.46

The contributing pore fraction diameter and hydrologically effective porosity (HEP) could be calculated using Equations 3.5 (Watson & Luxmoore, 1986) and 3.6 (Wilson & Luxmoore, 1988) respectively.

Equation 3.5

$$r = -\frac{0.15}{h}$$

Equation 3.6

$$\theta = \frac{(8\,\mu\,I_m)}{(g\rho r^2)}$$

Here *r* is the maximum pore radius (cm) of the contributing pore fraction and *h* is the tension (cm) in the infiltrometer. The HEP (θ) is the maximum volume of pores contributing to infiltration per volume of soil at a given suction. The input variables for HEP are viscosity of water (μ), density of water (ρ), acceleration due to gravity (g) and the minimum pore radius of the fraction. The macropore flow (I_m) is calculated as the difference between the infiltration rates at the given tensions at the upper and lower boundaries of the investigated pore fraction. The ranges for this study were two macropore fractions of 0 to -0.5 and - 0.5 to -1cm and two mesopore fractions of -1 to -2 and -2 to -5cm. Table 3.2 shows which pore fractions contribute to infiltration at a given suction. More in depth results are given in Tables B.4, B.5 and B.6 and Figures B.5, B.6 and B.7 in Appendix B.

Table 3.2: Contributing pore size fraction at different tensions.

Method	Double Ring	Mini Disc	Mini Disc	Mini Disc	Mini Disc	Estimated
Majour contributing pore fraction	Macro	Macro	Macro	Meso	Meso	Meso
Contributing pore radius fraction (cm)	All	<0.3	<0.15	<0.075	<0.03	<0.011
Tension (cm)	0	-0.5	-1	-2	-5	-14

3.3.2.5. Plant available water and hydraulic conductivity estimation

The texture, OM and coarse fraction content were used to estimate plant available water (PAW) and saturated hydraulic conductivity (K_{sat}) using the model of Saxton & Rawls (2006). These calculations were done on SPAW software version 6.02.74. The bulk density compensated plant available water (PAW_B) was calculated using Equation 3.7.

Equation 3.7

$$PAW_B = PAW(1 - R_V)$$

The PAW_B is given in mm of water available per m depth of soil. The PAW and R_V variables in Equation 3.7 are derived as follows in Equations 3.8 and 3.9 respectfully.

Equation 3.8

$$PAW = \theta_{33} - \theta_{1500}$$

Equation 3.9

$$R_V = \frac{(\alpha . R_w)}{[1 - R_w(1-\alpha)]}$$

Equation 3.10

$$\alpha = \frac{\rho}{2.65}$$

Here Θ_{33} and Θ_{1500} represent the soil water content at field capacity (-33 kPa) and permanent wilting point (-1500 kPa) respectively. R_V is the mass fraction of gravel in the soil (g/cm^3). R_W is the weight fraction of gravel (g/g). The matric soil density (ρ) divided by the gravel density (2.65 g/cm^3) is represented by *α* in Equation 3.10.

The Θ_{33} and Θ_{1500} are calculated from Equations 3.11, 3.12, 3.13 and 3.14.

Equation 3.11

$$\Theta_{1500} = \Theta_{1500t} + (0.14 \times \Theta_{1500t} - 0.02)$$

Equation 3.12

$$\theta_{1500t} = -0.024S + 0.487C + 0.006OM + 0.005(S \times OM) - 0.013(C \times OM) + 0.068(S \times C) + 0.031$$

Equation 3.13

$$\theta_{33} = \theta_{33t} + [1.283(\theta_{33t}) - 0.0015]$$

Equation 3.14

$$\theta_{33t} = -0.251S + 0.195C + 0.011OM + 0.006(S \times OM) - 0.027(C \times OM) + 0.452(S \times C) + 0.299$$

Multi-variable linear analysis often does not provide satisfactory predictive equations as some of the variables may not correlate linearly with the dependent variables. A second correlation (shown in Equations 3.12 and 3.14) is thus done to compensate for the poor linearity. Θ_{33t} and Θ_{15oot} represent the second correlations in Equations 3.11, 3.12, 3.13 and 3.14. The other variables are: S (Sand %weight), C (Clay %weight) and OM (Organic Carbon (OC) %weight).

Unsaturated hydraulic conductivity (K_Θ) can be calculated with Equation 3.15 using Saturated hydraulic conductivity (K_S).

Equation 3.15

$$K_\theta = K_S\left(\frac{\theta}{\theta_S}\right)^{[3+\left(\frac{2}{\lambda}\right)]}$$

K_S was calculated according to Equation 3.16 which originates from the work of Rawls *et al.* (1991) and Campbell (1974). Here Θ_s is the saturated moisture content as % volume and λ, in Equation 3.17, represents the inverse of the exponential tension-moisture curve, B in Equation 3.18.

Equation 3.16

$$K_S = 1930(\theta_S - \theta_{33})^{(3-\lambda)}$$

Equation 3.17

$$\lambda = \frac{1}{B}$$

Equation 3.18

$$B = \frac{[\ln(1500) - \ln(33)]}{[\ln(\theta_{33}) - \ln(\theta_{1500})]}$$

Θ_s is defined in equation 3.19.

Equation 3.19

$$\theta_S = \theta_{33} + \theta_{(S-33)} - 0.097S + 0.043$$

$\Theta_{(s-33)}$ is defined in Equations 3.20 and 3.21.

Equation 3.20

$$\theta_{(s-33)} = \theta_{(S-33)t} + (0.636\theta_{(s-33)t} - 0.017)$$

Equation 3.21

$$\theta_{(S-33)t} = 0.278S + 0.034C + 0.022OM - 0.018(S \times OM) - 0.027(C \times OM) - 0.854(S \times C) + 0.078$$

Saxton & Rawls (2006) included OM as a dependent variable as it has the capacity to increase water holding capacity and conductivity. These equations are only effective up to 8% OM. OM effects are not well observed at low water contents and only become prominent in moister conditions. High clay content in soils may mask the effect of OM as they respond similarly to an increase in moisture content. Gravel content, on a weight or volume basis, is also included in the model as increasing the gravel content of a soil decreases the volume of soil available for water storage or conductivity.

3.3.2.6. Recharge estimation accuracy

ArcMAP GIS software was used to compile a map to indicate areas of differing recharge estimation accuracy. The HSU map in Figure 2.7 was used to group areas where “accurate estimation is possible”, “moderately accurate estimation is possible, and “accurate estimation is unlikely”. These groupings were done based on the position of a HSU in the landscape, the soil forms present in the HSU, and thus the degree of expected PF. This map is shown in Figure 3.21. A similar grouping of hydropedological units was done by Vidacek *et al*. (2008) when they used broad soil classes and hydraulic conductivity to compile a hydropedological map of Croatia on GIS software.

3.4. Results and Discussion

3.4.1. Constant Hydraulic Head and using PTFs

A single factor ANOVA without replication was performed to ensure that K_{meas} was not dependent on the hydraulic head in the range of variation occurring in the infiltrometer. For the purpose of combining all the sites into one dataset the K_{sat} data (Appendix B, Table B2) for each profile was standardized to the mean of 0 and standard deviation of 1. This test was done for all the sites combined into one dataset.This would indicate whether the data could be analysed as being derived from constant head infiltration, even if the head varied within the given range. The combined scatterplot in Figure 3.4 shows that most variation occurs within +/-1 standard deviation interval with smaller percentage of observations falling within the range of +/-2 standard deviations. The two outliers from different profiles fall withing +3.5 standard devidiations and may represent a mistake of reading or recording in the field. The accompanying ANOVA (Table C.2 in Appendix C) shows a p value << 0.05 (7.62989E-40), F >> F_{crit} and the linear equation yields a r^2 value close to zero (4E-5), thus strongly indicating that there is no dependency or correlation between K_{sat} and hydraulic head.

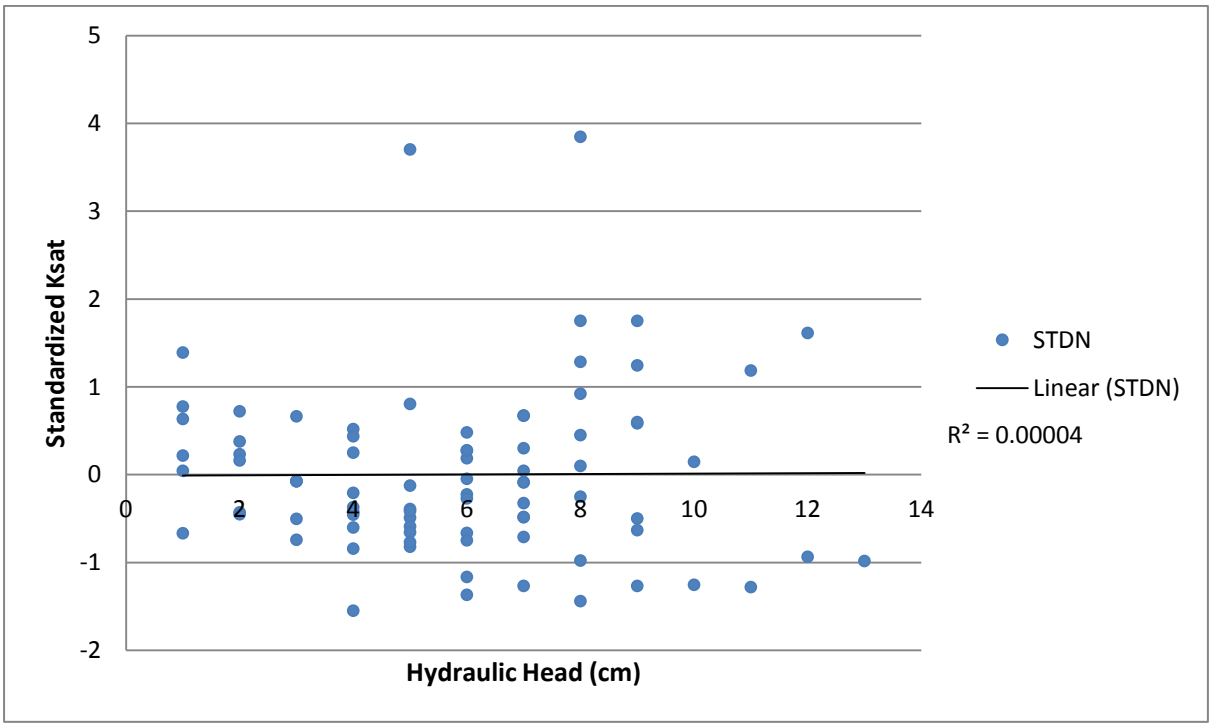

Figure 3.4: Combined scatterplot of Standardized K_{sat} vs. hydraulic head for all sites.

From these analyses it can be concluded that in the range of 1 to 15 cm, the hydraulic head does not affect the K_{sat}. The head could thus vary within this range and still be treated as a constant head. This result is supported by Rodgers & Mulqueen (2006) who reported a constant K_{sat} with varying hydraulic head within a wider range of hydraulic head.

The resulting constant head infiltration measurements were used to calculate K_{sat} (mm/hr) reported as K_{meas}. Bulk density (g/cm^3), particle density (g/cm^3), gravimetric water content (g/g) and subsequently volumetric water content were measured additionally. The PTFs used was that of Saxton & Rawls (2006) which uses inputs sand (%wt), clay (%wt), coarse fraction (%wt) and organic material (OC %wt) to generate estimated bulk density (g/cm^3), saturation (%), wilting point (%), field capacity (%), plant available water (%) and saturated hydraulic conductivity (mm/hr) reported as K_{est}. (These properties are all shown later in Table 3.4 of the result). The measured and estimated values were compared to firstly asses the efficacy of the PTF and then to investigate the infiltration patterns of four soil profiles.

Table 3.3 shows an ANOVA which compares the bulk densities as estimated by the PTF (BD_{est}) and measured in the laboratory (BD_{meas}). The reported p value (0.001509) and F value (11.52631) both indicate that there is a significant difference between BD_{est} and BD_{meas} [$p < 0.05$; $F > F_{crit}$]. This shows that there are dissimilarities between the estimation model and the “measuring cylinder method” used to measure BD.

Table 3.3: ANOVA comparing the estimated and measured bulk densities for all four observation sites.

ANOVA

Source of Variation	*SS*	*df*	*MS*	*F*	*P-value*	*F crit*
Between Groups	0.214218	1	0.214218	11.52631	0.001509	4.072654
Within Groups	0.780576	42	0.018585			
Total	0.994794	43				

Figure 3.5 shows that due to incomplete consolidation and perhaps material sorting, the "measuring cylinder method" produced expectedly low results but shows a general trend of increasing BD_{meas} with increasing depth. It is suspected that the humus content in the sample caused an underestimation of BD in K2, R1 and R2. The trend of the BD_{est} is much more consistent ranging from 1.3 to 1.6 g/cm^3.

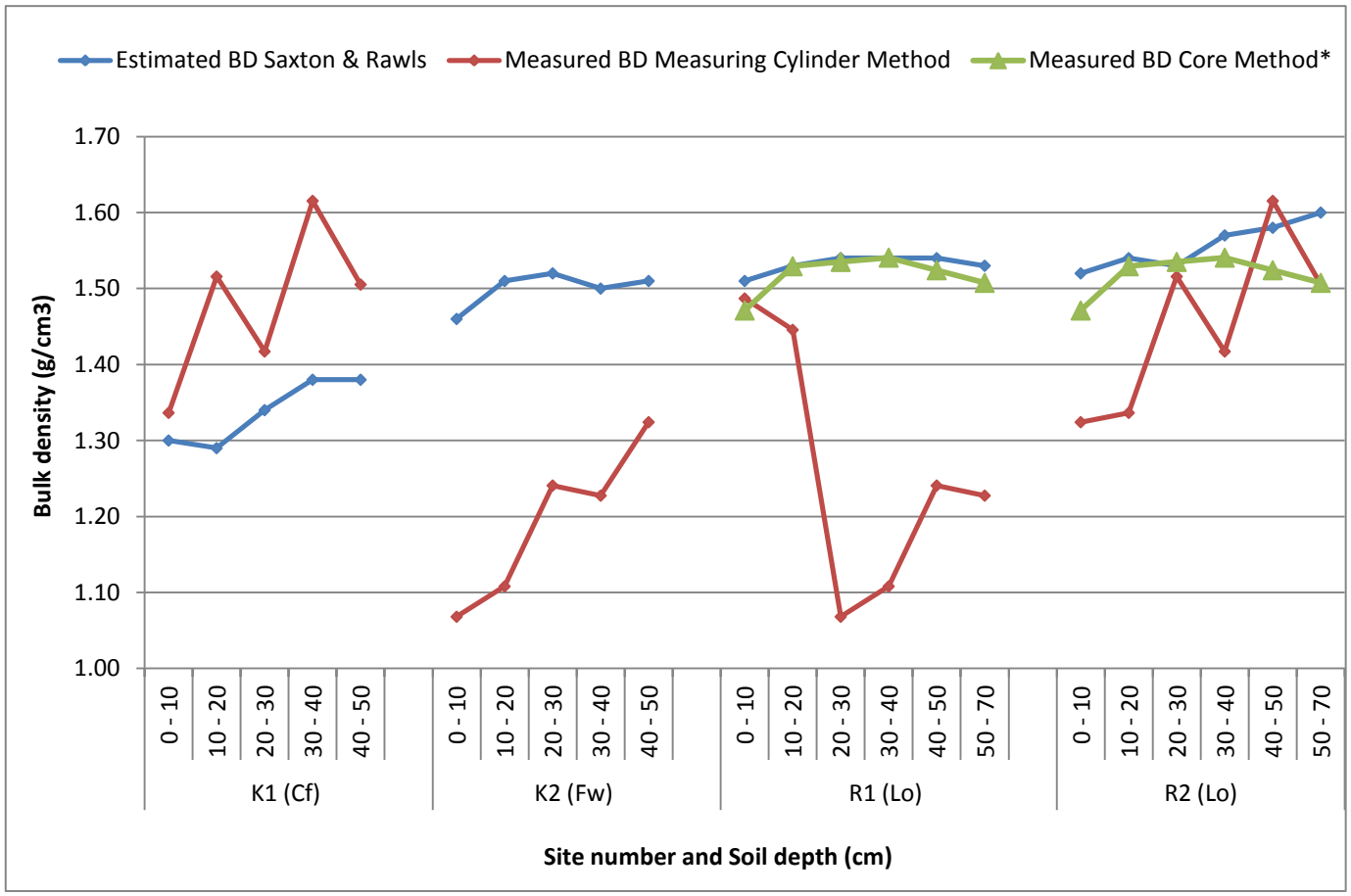

Figure 3.5: Graph to compare BDest and BDmeas for all four observation sites. * BD measured using the core method as done by Jovanovic *et al.* (2008) in Riverlands. The BD values are the average values found at three different sites in Riverlands.

The PTF seemed to have underestimated the effect of the coarse fraction in the K1 sample and this resulted in low BD estimations. Previous research by Jovanovic *et al.* (2008) in Riverlands reported BD measurements derived using the core method. These values, displayed in Figure 3.5, are the average BD values from three different sites in close proximity and correspond closely to the BD_{est} values.

These findings suggest that the “measuring cylinder method” produces inconsistent and underestimated bulk density measurements. These values would thus be inaccurate for use in modelling. The Saxton & Rawls (2006) model seems to produce more consistent values which are assumed to be more accurate. The third dataset, measured using the core method, shows that the BD_{est} values are fairly accurate in the homogenous sandy soils. Such data could not be collected in Kogelberg where the core method is not applicable due to rocky nature of soil and the effect of the high coarse fraction content on the PTFs estimations. These findings support the opinion of Hutson (1983) who said that models need to be calibrated with a local dataset to improve the quality of estimations.

It should also be mentioned that the format of the input parameters should be correct as using OM (%wt) instead of OM (OC %wt), for instance, will significantly affect all the estimated properties.

A shortcoming of the Saxton & Rawls (2006) model that leaves room for improvement is that the model assumes a partical density (PD) of 2.65 g/cm^3 for all samples. It was found that the PD varied between 2.17 and 2.65 g/cm^3 across the four sampled infiltration sites. Thus using measured PD values instead of assuming a value of 2.65 g/cm^3 would improve site specific estimations of porosity and saturation point.

The total porosity and saturation point in the K1 profile could not be correctly estimated by the Saxton & Rawls model due model insensitivity to organic matter content in particle density calculation. High concentration of particulate and humified organic material throughout the profile (Fig 3.6) leads to a substantial decrease in particle density (Table 3.4) compared to fixed value of 2.65 assigned by the model to sandy textures.

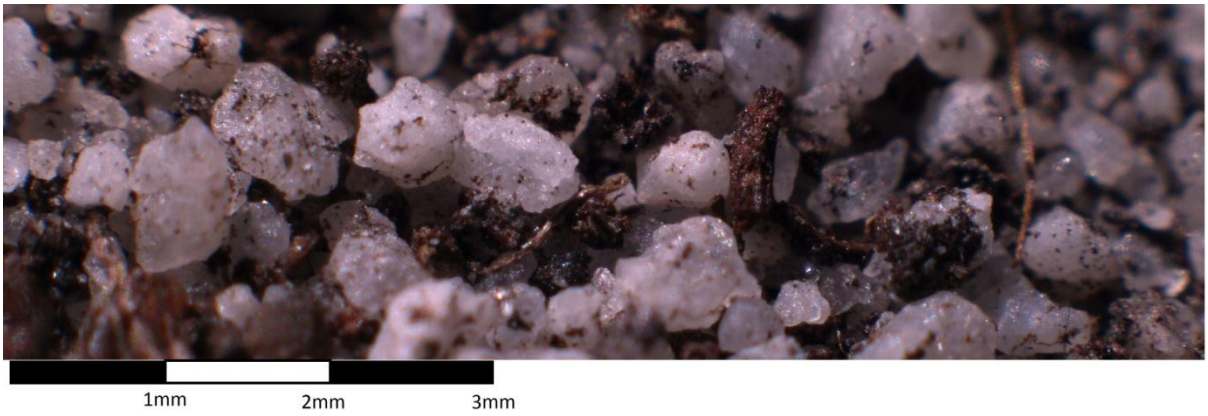

Figure 3.6: Image showing soil particles and partially decayed OM in the K1 profile. The OM is mostly present as particulate matter and not as OM coatings on mineral particles and would thus significanty lower particle density.

Another source of error is introduced as the Saxton & Rawls (2006) model assumes FC to be at -33 kPa suction. This is an arbitrary value and most conservative value, since the pressure at which FC occurs may vary depending on the texture, gravel content and OM content between -5 and -33 kPa (Hillel, 1980). Thus the FC_{est} as reported in the tables and figures below is estimated at -33 kPa, yet it is taken that actual FC is represented by the VWC as calculated from measured GWC. This assumption is made as the profiles were left for 24 hours after infiltration, after which free drainage had occured and the soil would be a FC. The pressure at which VWC_{est} was measured, as given by the model of Saxton & Rawls (2006), is also reported in Table 3.4.

Both the BD_{est} and BD_{meas} values were used to calculate VWC (%) from the measured GWC (%). These values are shown as VWC_{est} and VWC_{meas} respectively.

Table 3.4: Measured and estimated soil physical and hydraulic properties for the four infiltration sites in Kogelberg and Riverlands.

SITE	SAMPLE	Diagnistic Horizon	Estimated BD (g/cm3)	Measured* BD (g/cm3)	Particle Density (g/cm3)	Calculated Porosity** (%)	Estimated Saturation (%)	Estimated Wilting Point (%)	Estimated Field Capacity (%)
K1 (Cf 1200)	0 - 10	Orthic A	1.30	1.34	2.17	38.5	51.0	5.8	11.7
	10 - 20	Orthic A / E1	1.29	1.52	2.20	30.9	51.3	5.9	11.8
	20 - 30	E1	1.34	1.42	2.30	38.3	49.6	5.1	10.9
	30 - 40	Lithocutanic B1	1.38	1.62	2.39	32.5	47.8	3.5	8.8
	40 - 50	Lithocutanic B1	1.38	1.51	2.44	38.3	47.9	3.5	8.4
K2 (Fw 1110)	0 - 10	Orthic A	1.46	1.07	2.50	57.3	44.7	1.8	6.3
	10 - 20	Orthic A / E1	1.51	1.11	2.56	56.7	42.8	1.6	5.9
	20 - 30	E2	1.52	1.24	2.57	51.7	42.8	3.4	8.1
	30 - 40	E2	1.50	1.23	2.58	52.4	43.5	2.1	6.9
	40 - 50	E3	1.51	1.32	2.61	49.3	42.8	1.6	5.9
R1 (Lt 1100)	0 - 10	Orthic A	1.51	1.49	2.54	41.5	43.0	1.0	5.6
	10 - 20	E1	1.53	1.45	2.61	44.6	42.4	0.7	5.2
	20 - 30	E1	1.54	1.07	2.65	59.7	41.9	0.4	4.9
	30 - 40	E2	1.54	1.11	2.64	58.1	41.9	0.4	4.9
	40 - 50	E3 / Podzol	1.54	1.24	2.63	52.9	41.9	0.4	4.9
	50 - 70	E3 / Podzol	1.53	1.23	2.63	53.4	42.2	0.6	5.0
R2 (Vf 2110)	0 - 10	Orthic A	1.52	1.32	2.54	47.9	42.5	1.1	4.5
	10 - 20	E1	1.54	1.34	2.55	47.7	41.8	2.6	6.7
	20 - 30	E1	1.53	1.52	2.60	41.7	42.1	2.0	6.1
	30 - 40	Neocutanic B1	1.57	1.42	2.58	45.1	40.9	3.1	7.3
	40 - 50	Neocutanic B1	1.58	1.62	2.60	37.8	40.5	3.6	7.8
	50 - 70	Neocutanic B2	1.60	1.51	2.55	40.9	39.7	5.5	9.9

* BD excluding stone fraction (>2mm)

** Porosity = (PD – BDmeas) / PD

Table 3.4 continues: Measured and estimated soil physical and hydraulic properties for the four infiltration sites in Kogelberg and Riverlands

SITE	SAMPLE	Diagnistic Horizon	Estimated PAW (%)	kPa @ VWCest	VWC using est BD (%)	VWC using meas BD (%)	Estimated K_{sat} (mm/hr)	Measured K_{sat} (mm/hr)
K1 (Cf 1200)	0 - 10	Orthic A	6.00		0.00	0.00	139.9	492.3
	10 - 20	Orthic A / E1	5.00	28.00	17.63	20.72	122.2	492.3
	20 - 30	E1	5.00	27.00	18.00	19.04	99.4	492.3
	30 - 40	Lithocutanic B1	5.00	26.00	16.98	19.88	118.2	492.3
	40 - 50	Lithocutanic B1	4.00	28.00	13.40	14.61	121.3	492.3
K2 (Fw 1110)	0 - 10	Orthic A	4.00	26.00	14.73	10.78	148.1	117.7
	10 - 20	Orthic A / E1	4.00	25.00	15.15	11.12	135.3	117.7
	20 - 30	E2	5.00	23.00	19.29	15.75	102.3	117.7
	30 - 40	E2	5.00	21.00	20.86	17.07	128.6	117.7
	40 - 50	E3	4.00	24.00	16.22	14.22	135.3	117.7
R1 (Lt 1100)	0 - 10	Orthic A	5.00	32.00	7.10	6.99	157.3	182.6
	10 - 20	E1	4.00	32.00	6.52	6.16	168.9	182.6
	20 - 30	E1	4.00	33.00	5.56	3.86	184.1	182.6
	30 - 40	E2	4.00	33.00	5.50	3.96	184.1	182.6
	40 - 50	E3 / Podzol	4.00	32.00	5.69	4.59	184.1	182.6
	50 - 70	E3 / Podzol	4.00	32.00	6.22	4.99	175.3	182.6
R2 (Vf 2110)	0 - 10	Orthic A	3.00	32.00	6.62	5.77	152.6	148.2
	10 - 20	E1	4.00	32.00	7.67	6.65	102.4	148.2
	20 - 30	E1	4.00	30.00	9.29	9.21	112.7	148.2
	30 - 40	Neocutanic B1	4.00	30.00	10.73	9.68	88.0	148.2
	40 - 50	Neocutanic B1	4.00	30.00	11.52	11.78	77.9	148.2
	50 - 70	Neocutanic B2	4.00	30.00	12.63	11.89	54.8	148.2

.

3.4.2. Kogelberg Site 1 (K1), Cartref Soil Form

Table 3.5 shows that the VWC_{est} and VWC_{meas} are not statistically different [$p > 0.05$; $F < F_{crit}$]. Table 3.6 shows that the FC_{est} and VWC differ significantly [$p < 0.05$; $F > F_{crti}$] and FC is thus underestimated as actual FC is observed at higher water pressure than estimated in Figure 3.7. The actual FC is rather between -26 and -28 kPa as shown in Table 3.4. The reason for the higher measured VWC relative to the FC_{est} is that the coarse sandstone fraction in Kogelberg was found to be porous and is able to store water. This is discussed in more detail further in this chapter.

Table 3.5: ANOVA to investigate the correlation between VWCest and VWCmeas for K1.

ANOVA						
Source of Variation	SS	df	MS	F	P-value	F crit
Between Groups	8.480554	1	8.480554	1.42863	0.277083	5.987378
Within Groups	35.61686	6	5.936143			
Total	44.09741	7				

Table 3.6: ANOVA to investigate the correlation between VWC and estimated FC for K1.

ANOVA						
Source of Variation	SS	df	MS	F	P-value	F crit
Between Groups	114.2325	1	114.2325	27.44014	0.001941507	5.987378
Within Groups	24.97783	6	4.162972			
Total	139.2104	7				

Figure 3.7 also indicates that the VWC and FC_{est} did not show a consistent trend with depth but varied erratically. The rock fraction, estimated at around 20 to 30 %, is expected to increase with depth as the lithocutanic B horizon, starting at 30 cm, is expected to grade into bedrock according to the definition by the Soil Classification Working Group (1991). The inconsistent variation in VWC is thought to be due to the channelling of water into paths of least resistance between the coarse fractions.

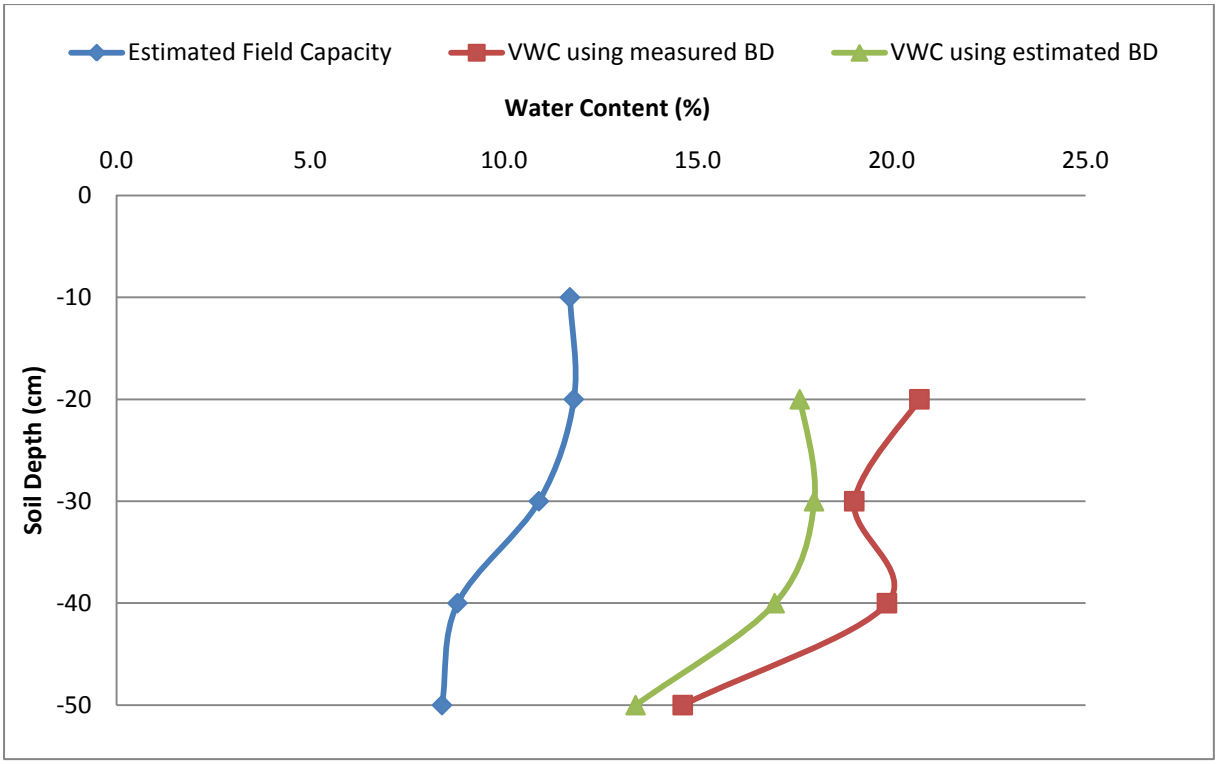

Figure 3.7: VWCest, VWCmeas and FCest with depth for K1.

Figure 3.7 emphasizes the effect that the increased coarse fraction and water channelling has on VWC, and presumably PAW, as the volume of soil bypassed during PF does not contribute to the total VWC and thus PAW. Thus PF is seen to accelerate recharge as less water is retained in the profile (Petersen, *et al.* 2001). The VWC also shows a decline with depth, indicating that the profile is more stoney.

Figure 3.8 shows that K_{est} is fairly uniform throughout the profile, ranging from a minimum of 99.4 to a maximum of 139.4 mm/hr. The K_{meas} of 492.3 mm/hr is however found to be much greater than the K_{est} for all five depth intervals. The vast difference between the values may be explained by the presence of PFPs in this profile as water is funnelled between the coarse fragments into channels of least resistance. This type of flow, known as funnel flow, occurs on a Darcian scale in macroscopically heterogeneous soils as discussed by Kung (1990) and Hendrickx & Flurry (2001). Figure 3.9 (left) shows the route of PF where the water converges into channels of least resistance between the coarse fragments. This PF pattern is not limited to one depth interval only; instead this trend is continuous throughout the profile.

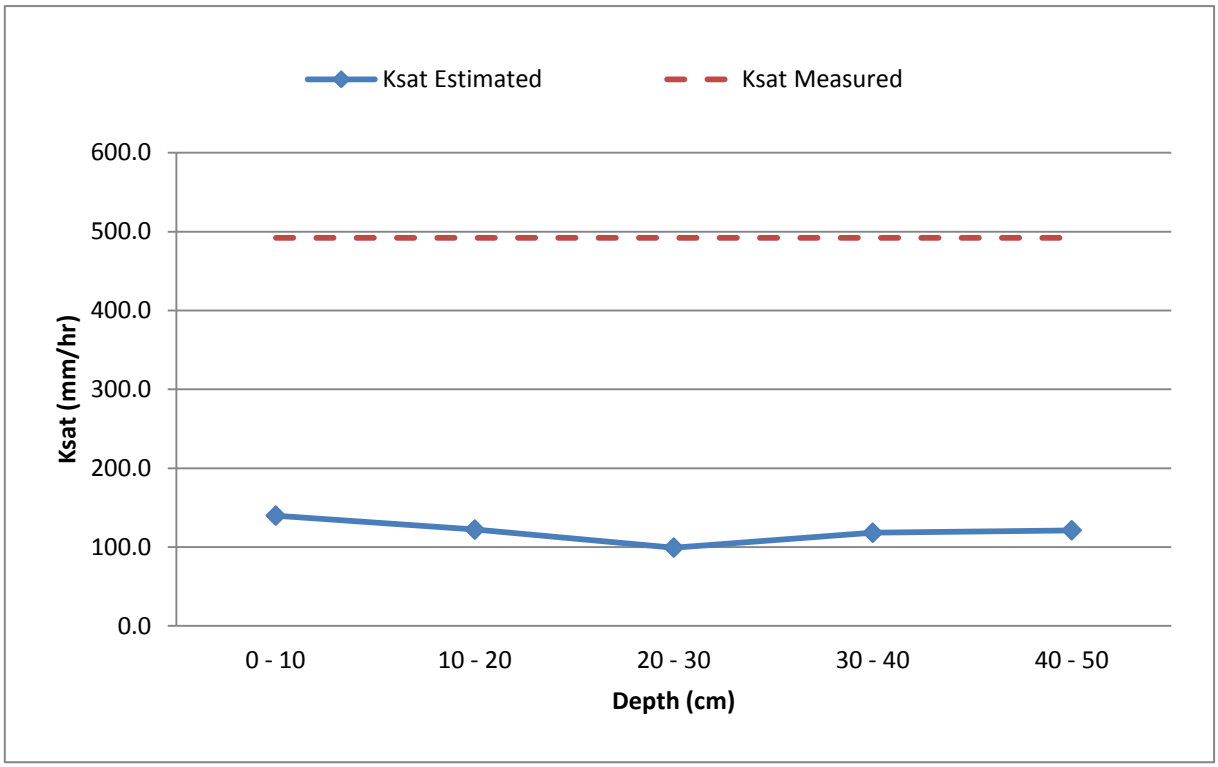

Figure 3.8: Comparison of measured and estimated K_{sat} for K1.

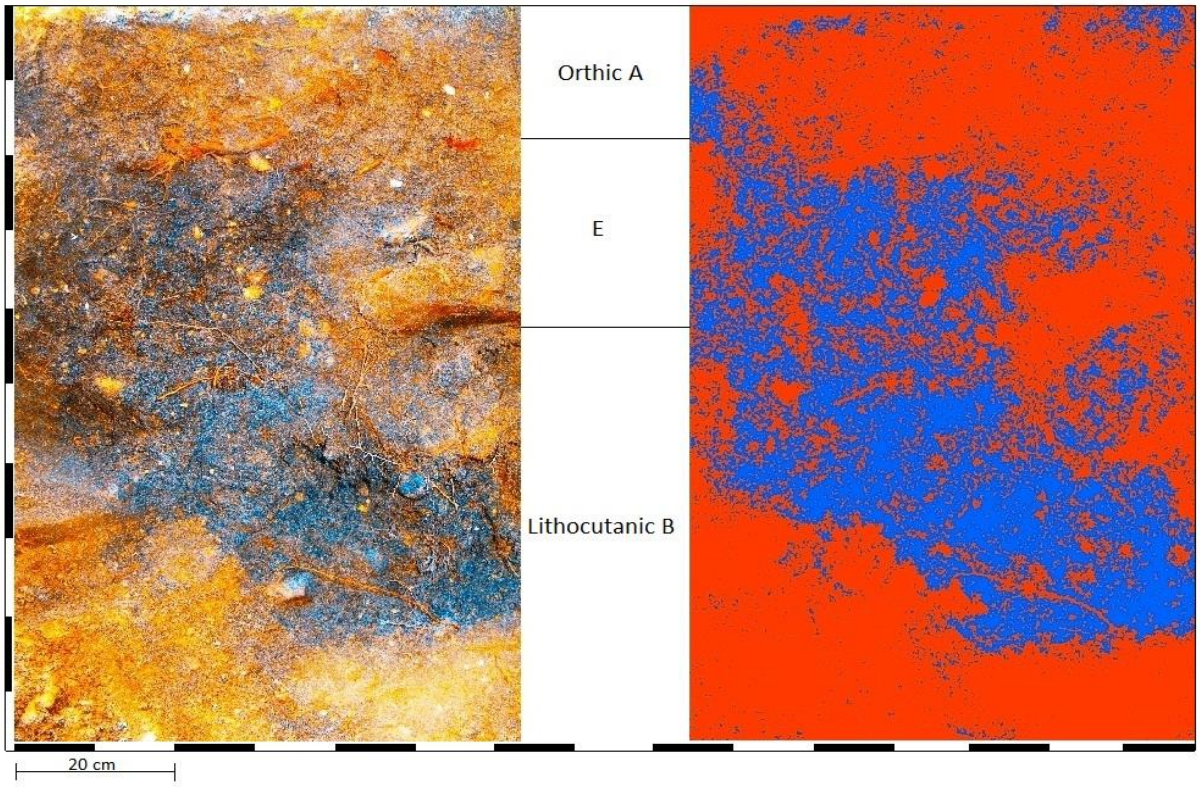

Figure 3.9: Left: Negative colour image of flowpath visualization for K1. Right: ArcGIS maximum likelihood colour analysis for K1 (Blue = Flowpath / Red = Bypassed).

Image analysis on ArcGIS software (Fig 3.9 right), revealed that the water flow paths only covered 32 % of the image, thus 68 % of the profile was bypassed during infiltration. Not all the soil between the coarse fractions indicated the presence of flow paths, thus emphasizing the importance of understanding the connectivity of the permeable fraction, as supported by Dahan *et al.* (1998).

As mentioned, the stones that limit infiltration (Table Mountain Sandstone origin) have the capacity to absorb water. The GWC was calculated for four stone samples; two natural and two after KI solution infiltration. The cumulative GWC (%) for the stones subjected to KI infiltration was 22% higher than that of the stone samples containing only antecedent moisture. Only the stone samples subjected to KI infiltration presented the blue colour formation after starch and peroxide treatment, thus confirming that the water was not antecedent but rather infiltrated overnight (Fig 3.10). See Table B.3 in Appendix B for calculations.

The Kogelberg site would thus possibly benefit from using a double continuum estimation model as proposed by Barenblatt & Zheltov (1960). The double continuum model takes the bedrock into account as a separate porous volume from the more porous fracture system. If a double continuum model is adopted, it should be determined whether the bedrock only stores groundwater or actually forms part of the transport system (Berkowitz, 2002).

Figure 3.10: Table mountain sandstone removed from profile K1: Left: No blue colour formation indicating antecedent moisture only. Right: Blue colour formation indicating infiltration of KI solution overnight.

3.4.3. Kogelberg Site 2 (K2) - Fernwood Soil Form

The ANOVA in Table 3.7 indicates that VWC_{est} and VWC_{meas} do not differ significantly [$p > 0.05$; $F < F_{crti}$]. Table 3.8 shows a significant difference between VWC and FC_{est} [$p < 0.05$; $F > F_{crit}$] and FC is thus not at – 33 kPa but rather between -21 and -26 kPa as seen in Table 3.4.

Table 3.7: ANOVA to investigate the correlation between VWCest and VWCmeas for K2.

ANOVA						
Source of Variation	SS	df	MS	F	P-value	F crit
Between Groups	29.98988	1	29.98988	3.994263	0.080695	5.317655
Within Groups	60.06592	8	7.50824			
Total	90.0558	9				

Table 3.8: ANOVA to investigate the correlation between VWC and FCest for K2.

ANOVA						
Source of Variation	SS	df	MS	F	P-value	F crit
Between Groups	197.9738	1	197.9738	48.38424	0.000117722	5.317655
Within Groups	32.73361	8	4.091701			
Total	230.7074	9				

Figure 3.11 shows an initial increase and then a gradual decline in VWC and FC_{est} with depth. The horizon where higher VWC was observed corrospond with the horizons that had minimal PF in the PVF. The WT observed during the survey is affected by the seasonal rainfall and expected to be closer to the surface during and shortly after rainfall season and the trend of decreasing VWC below 40 cm is expected to be inversed during high rainfall periods.

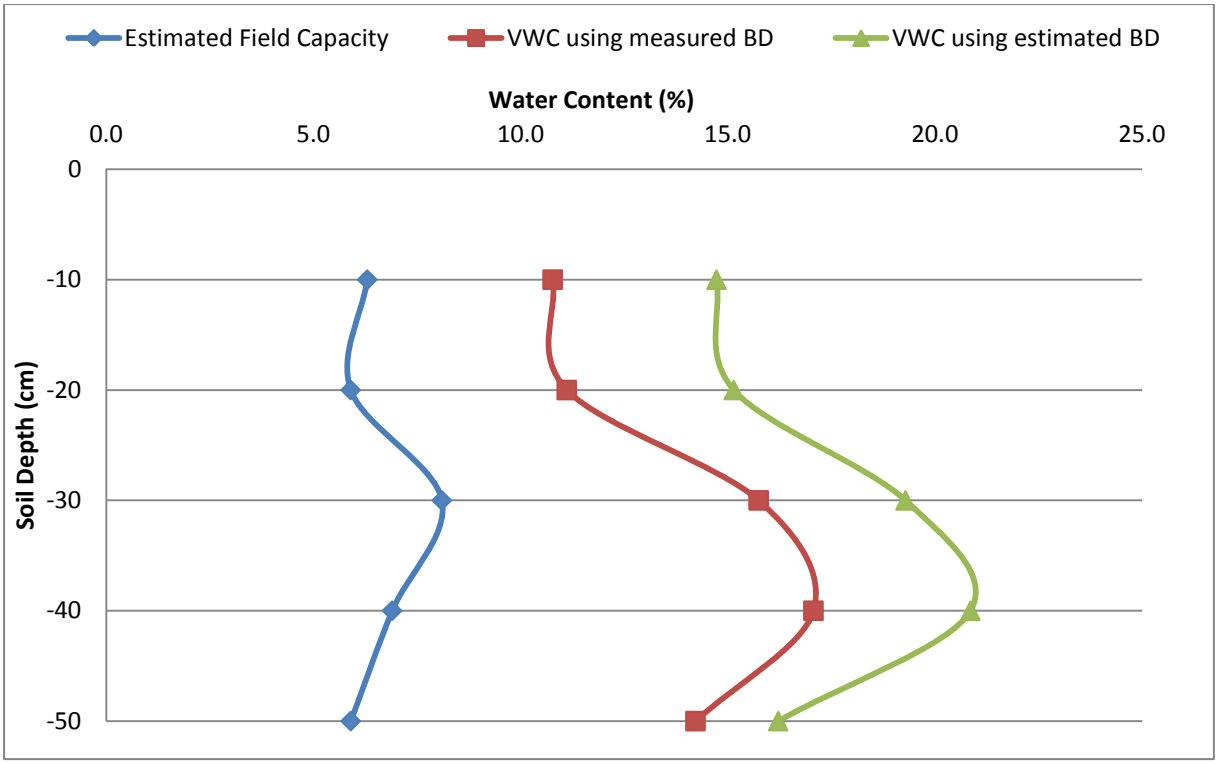

Figure 3.11: VWCest, VWCmeas and FCest with depth for K2.

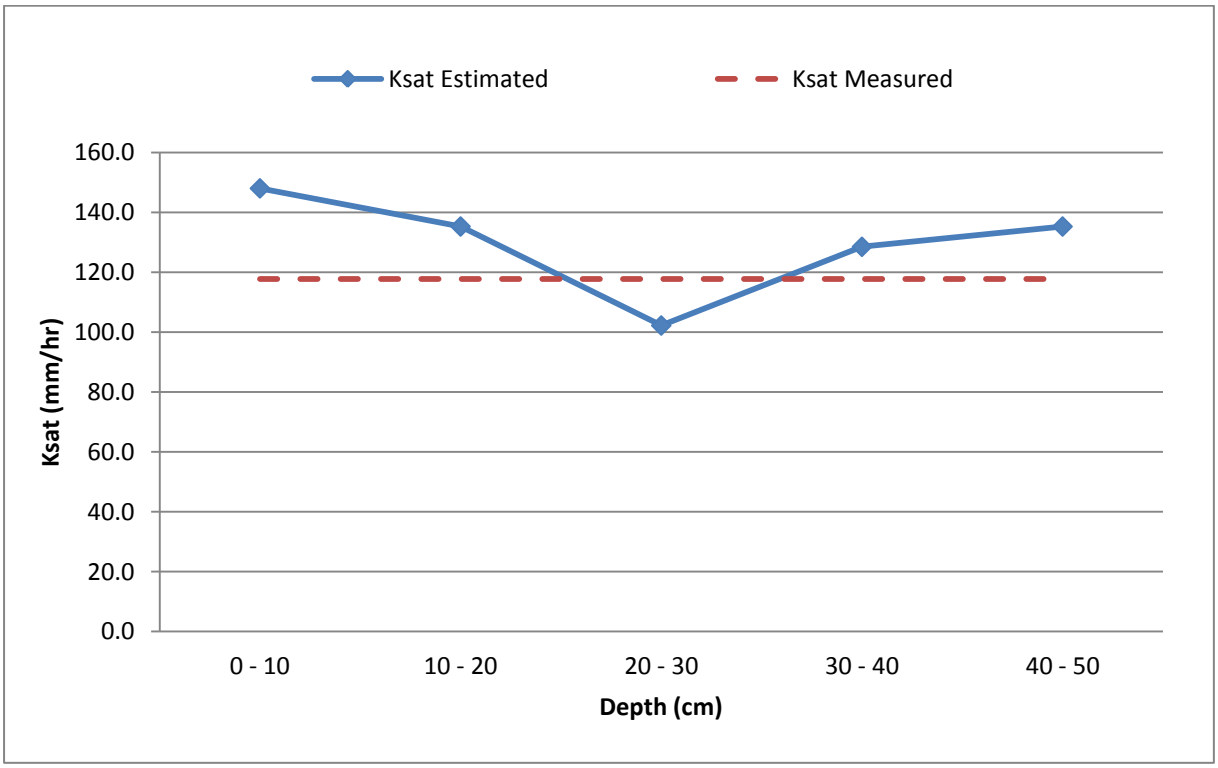

Figure 3.12: Comparison of measured and estimated K_{sat} for K2.

The K_{est} values were fairly consistent, ranging from 102.3 to 148.1 mm/hr, and did not differ greatly from the K_{meas} of 117.7 mm/hr as seen in Figure 3.12. It would thus seem that the estimates were fairly accurate in predicting K_{sat} at K2. The K_{meas} corresponded closely to the K_{est} of the infiltration rate limiting layers at depths of 20-30 cm and 30-40 cm.

The PFV in Figure 3.13 (left) indicates a uniform wetting front. This is supported by the image analysis (right), which shows that flow paths covered 82 % of the total area. The 18 % which was bypassed can be a result of dissimilarities in hydraulic properties and particle size distribution. This is a minor case of unstable flow which has limited impact of flow as the PF is not continuous, a feature commonly found in macroscopically homogenous soils (Kung, 1990; Hendrickx & Flurry, 2001). These PFPs were thus not as dominant as in K1 and the K_{sat} could thus effectively be estimated in this deep sandy soil profile in Kogelberg.

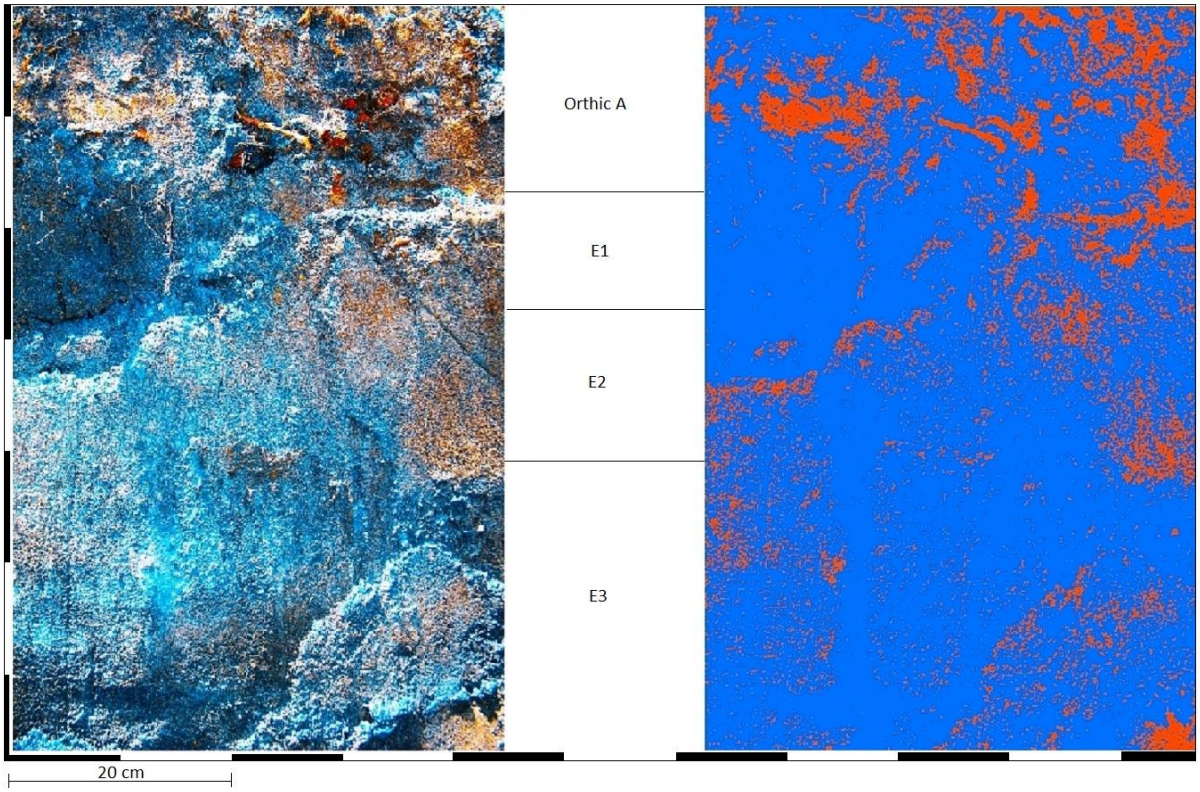

Figure 3.13: Left: Negative colour image of flowpath visualization for K2. Right: ArcGIS maximum likelihood colour analysis for K2 (Blue = Flowpath / Red = Bypassed).

3.4.4. Riverlands Site 1 (R1) – Lamotte Soil Form

Table 3.9 shows no significant difference between the VWC calculated from BD_{est} and BD_{meas} [$p > 0.05$; $F < F_{crit}$]. Table 3.10 also shows that the VWC and FC_{est} did not differ significantly. This is supported by Table 3.4 which reports that VWC_{est} occurs between -32 and -33 kPa. Figure 3.14 visually displays the VWC_{est} and VWC_{meas} against FC_{est} and the three curves show similar trends with depth. The VWC_{est} and VWC_{meas} however differ from a depth of 20 cm onwards, although not statistically. These differences are attributed to different BD_{est} and BD_{meas}.

Table 3.9: ANOVA to investigate the correlation between VWCest and VWCmeas for R1.

ANOVA						
Source of Variation	SS	df	MS	F	P-value	F crit
Between Groups	3.050813	1	3.050813	3.100885	0.108739	4.964603
Within Groups	9.838526	10	0.983853			
Total	12.88934	11				

Table 3.10: ANOVA to investigate the correlation between VWC and FCest for R1.

ANOVA						
Source of Variation	SS	df	MS	F	P-value	F crit
Between Groups	0.784629	1	0.784629	1.637116	0.229610334	4.964603
Within Groups	4.792748	10	0.479275			
Total	5.577377	11				

The VWC declines from the surface to the 20 to 30 cm layer but steadily increases again from 30 to 70 cm according to Figure 3.14. The initial decrease will be explained in due course. The latter increase in VWC would most likely continue until the water table is reached at depth.

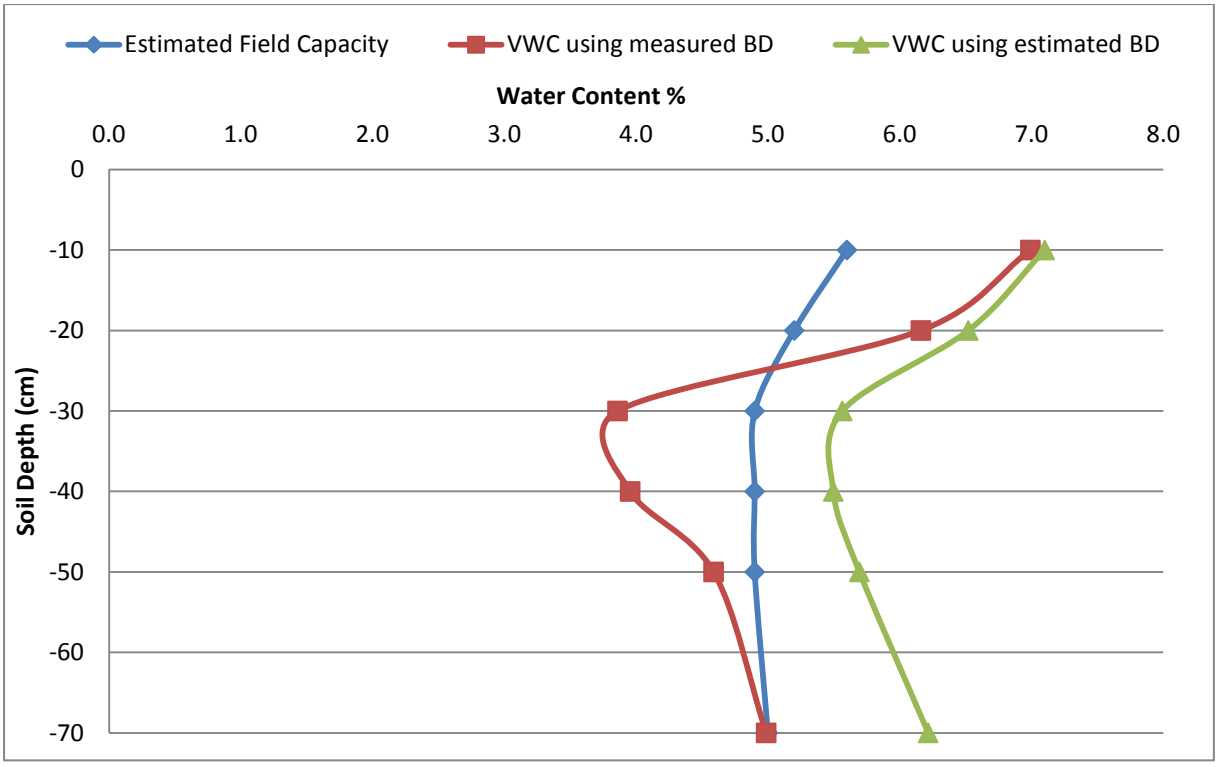

Figure 3.14: VWCest, VWCmeas and FCest with depth for R1.

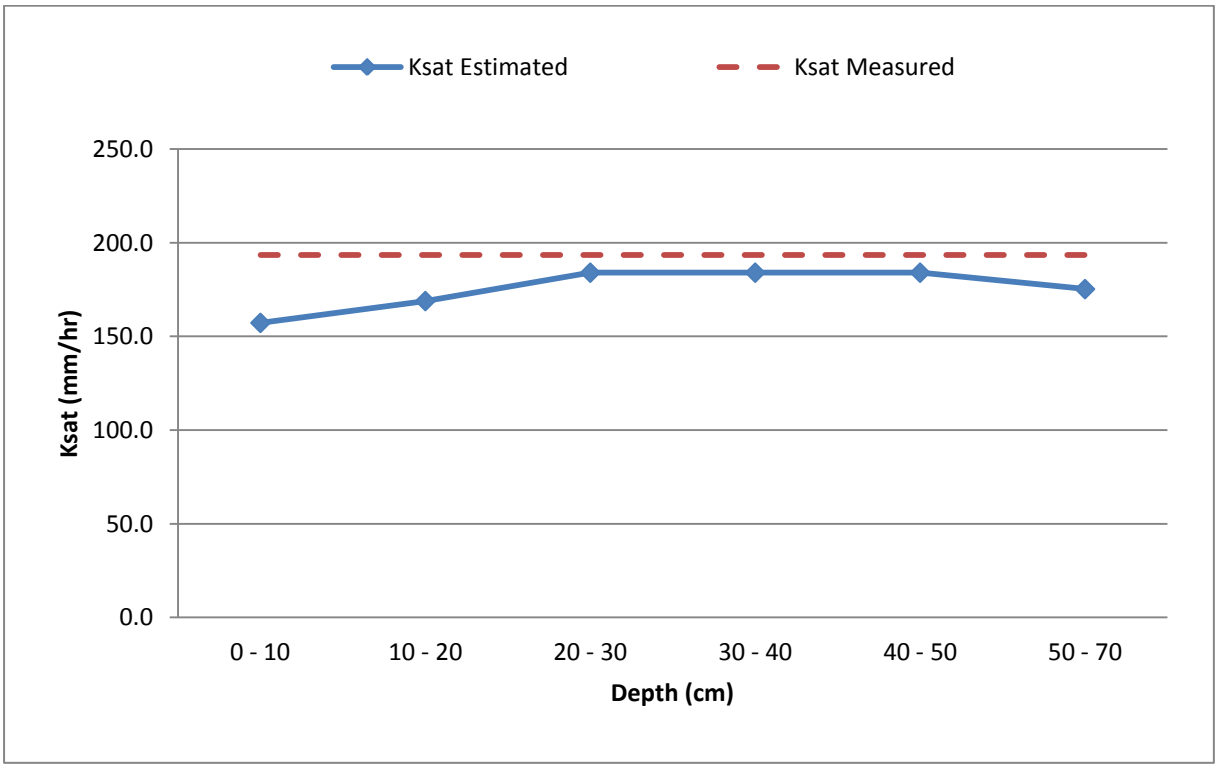

Figure 3.15: Comparison of measured and estimated K_{sat} for R1.

K_{est} is fairly consistent throughout the profile, ranging from 157.3 to 184.1 mm/hr (Fig 3.15). The K_{meas} of 182.6 mm/hr correlates closely to the maximum K_{est} value, opposite to the case in K2.

Figure 3.16 shows continuous zones of PF in the top 20 cm of the profile. This could explain why the K_{meas} is higher than the K_{est} for this layer. Flow through the layers from 20 to 40 cm was limited to PF as seen by three isolated flow paths through the layer. The VWC supports the PFV data as the decline in VWC_{est} and FC_{est} at depths 20 – 40 cm corresponds with the layers where only PF occurred.

The coarse sand fraction increases from 9.5 % in the 10 - 20 cm layer to 11.6 % in the 20 - 30 cm layer. The coarse sand fraction of the 30 to 40 cm layer is similar to that of the 20 - 30 cm layer at 12.1 %. This was the only striking textural discontinuity and may explain the formation and continuity of the PFPs in the 20 - 40 cm layers. Joel & Messing (2001), Feyen et. al. (1998) and Weiler & Naef (2002) have reported that a change in macropore density and configuration may cause PF. The importance of pore structure will be addressed again at a later stage.

A divergence layer is present at 40 - 50 cm. This could be due to the lower coarse sand fraction of 8.8 % and thus another change in macropore density and configuration. This trend of PF redistributing into uniform flow was also reported by Hendrickx & Flurry (2001). From this depth on the water is evenly distributed on the horizontal and infiltration occurs more or less uniformly. The image analysis reported that 62 % of the image consisted of flow paths. The PF in the 20 - 40 cm layer comprised the majority of the bypassed 38 %.

The K_{meas} values were up to 20 % higher than K_{est} which indicates that recharge estimations should be done with care in this soil type in Riverlands as textural discontinuities in the vertical plane may affect the predictability of recharge estimation.

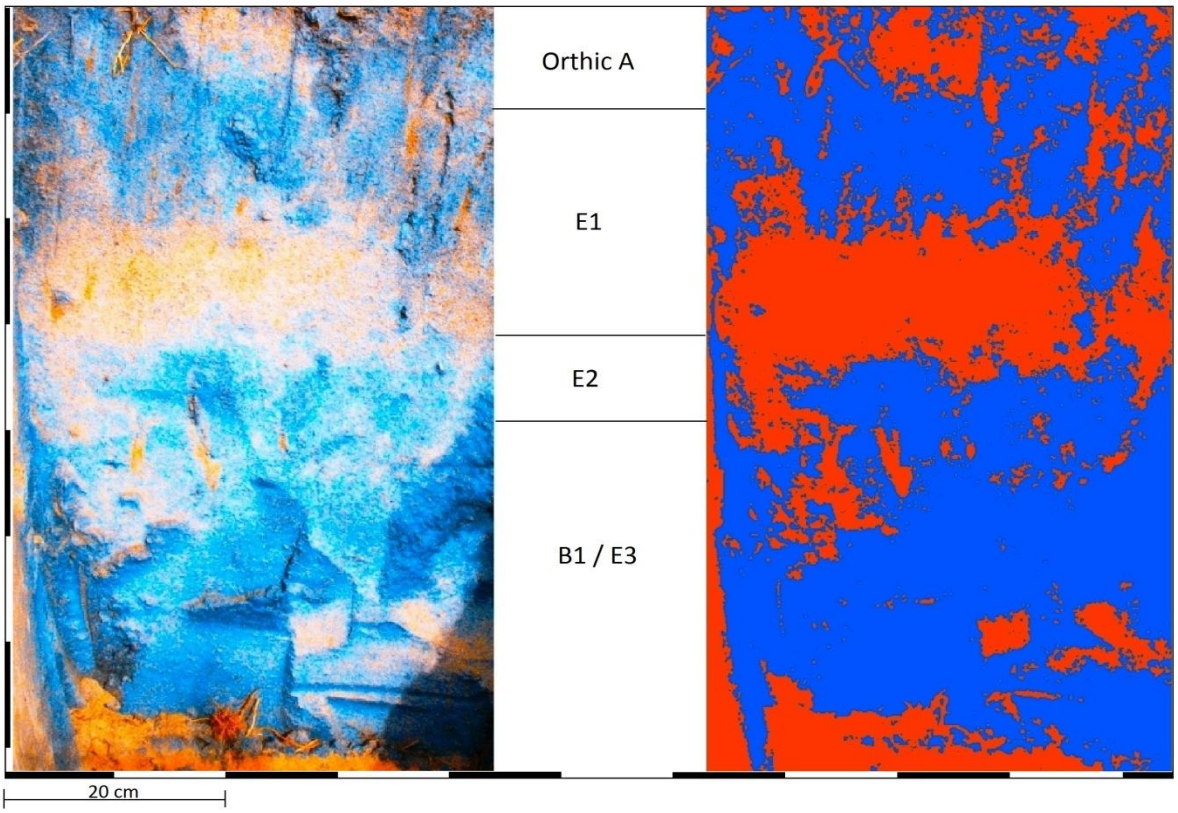

Figure 3.16: Left: Negative colour image of flowpath visualization for R1. Right: ArcGIS maximum likelihood colour analysis for R1 (Blue = Flowpath / Red = Bypassed).

3.4.5. Riverlands Site 2 (R2) – Vilafontes (Transition Lamotte) Soil Form

Table 3.11 shows that there is no significant difference between VWC_{est} and VWC_{meas} [$p > 0.05$; $F < F_{crit}$]. Table 3.12 shows that there is also no significant difference between VWC and FC_{est} [$p > 0.05$; $F < F_{crit}$] and the model is thus accurate in estimating FC at -33 kPa.

The VWC and FC_{est} increase gradually with depth which corresponds to the increase in clay content from 5.3 – 9.9 %. The coarse fraction also increases with depth from 5.7 – 12.3 %. The ability of clay to increase water holding capacity outweighs the effect of coarse material to decrease the volume of soil. Figure 3.17 also shows no erratic changes in VWC with depth; instead the increase in VWC is gradual compared to that of K1.

Table 3.11: ANOVA to investigate the correlation between VWCest and VWCmeas for R2.

ANOVA						
Source of Variation	SS	df	MS	F	P-value	F crit
Between Groups	1.012586	1	1.012586	0.171164	0.687813	4.964603
Within Groups	59.15889	10	5.915889			
Total	60.17148	11				

Table3.12: ANOVA to investigate the correlation between VWC and FCest for R2.

ANOVA						
Source of Variation	SS	df	MS	F	P-value	F crit
Between Groups	17.31711	1	17.31711	3.806666	0.07960723	4.964603
Within Groups	45.49154	10	4.549154			
Total	62.80865	11				

The trend of declining K_{est} in Figure 3.18 corresponds with the increase in coarse fraction and clay content. The K_{meas}, of 148.7 mm/hr, did not correspond to the limiting K_{est} value of 54.8 mm/hr in the 50 - 70 cm layer but rather corresponded to the highest K_{est} value of 152.6 mm/hr observed in the 0 - 10 cm layer. The flow paths comprised 72 % of the image shown in Figure 3.19, indicating predominant uniform flow. This assertion holds for the upper 40 cm after which the flow pattern changed. The converging of the wetting front occurred at 40 cm when the K_{est} dropped below 80 mm/hr.

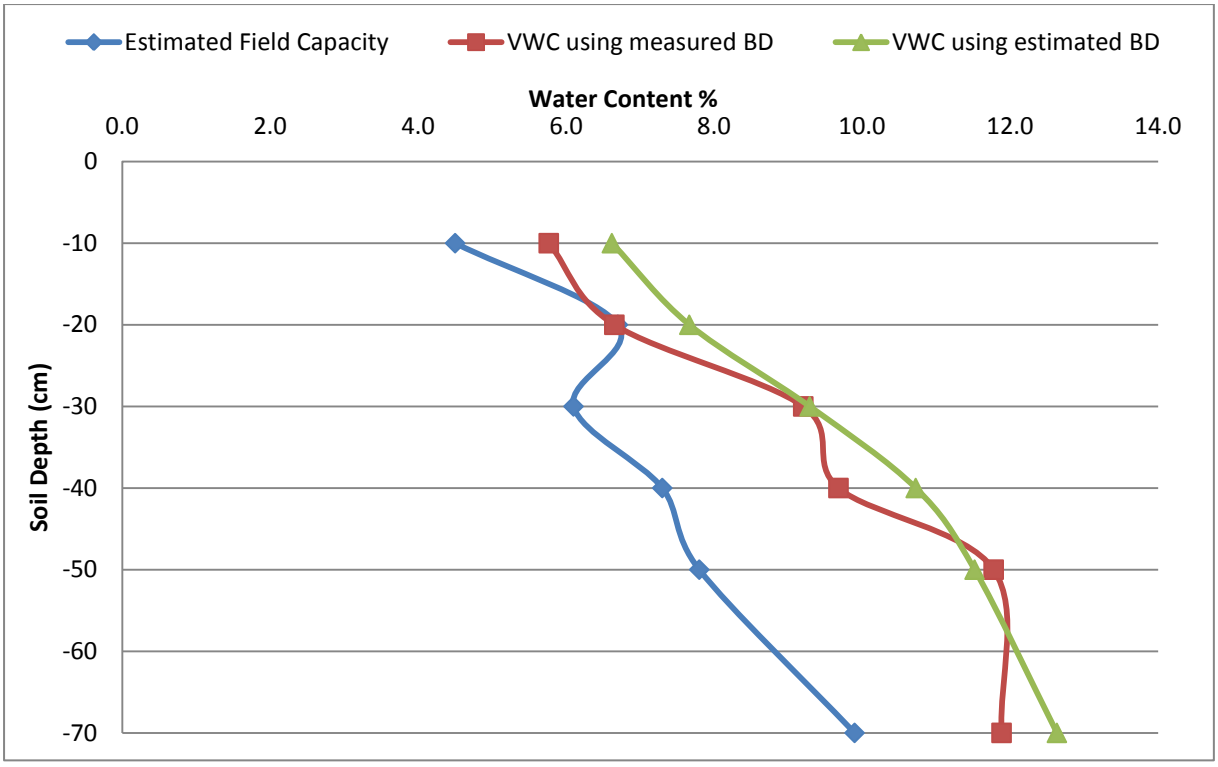

Figure 3.17: VWC with depth for R2.

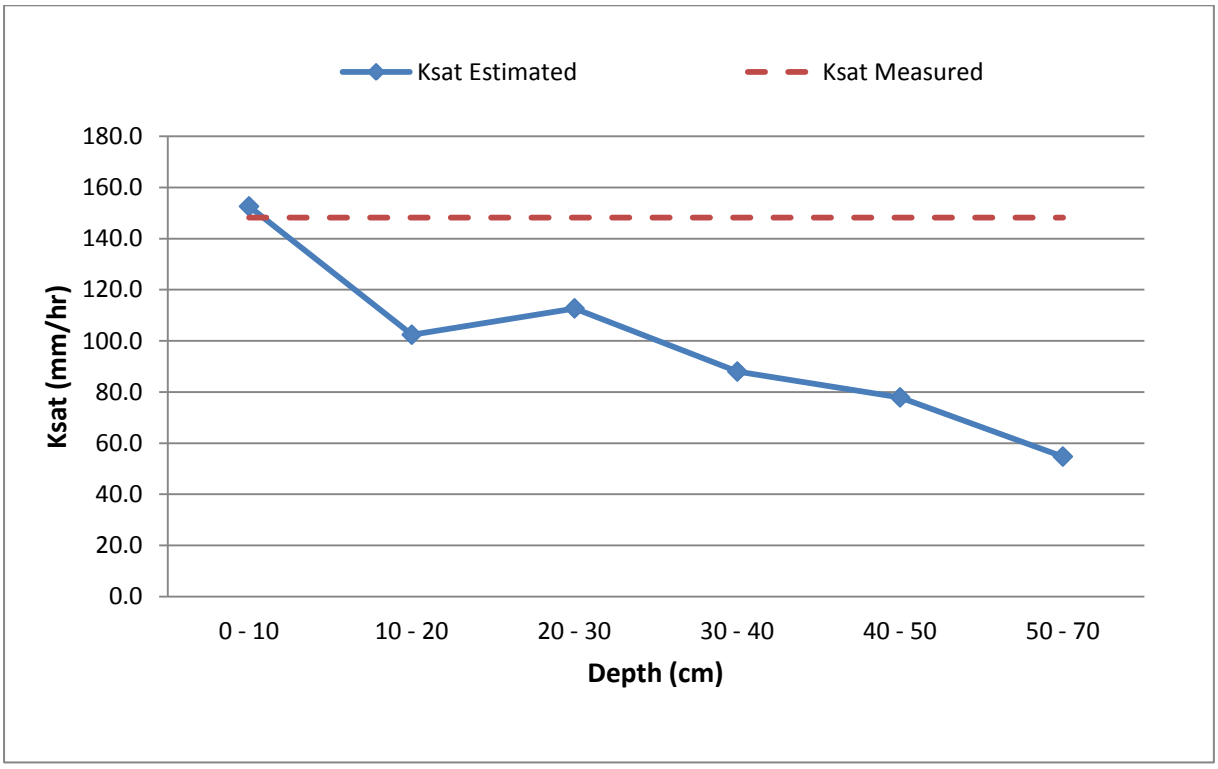

Figure 3.18: Comparing measured and estimated K_{sat} for R2.

The high K_{meas} value may be explained by one of two theories, or a combination of both. The presence of an E horizon above the Neocutanic B horizon (Figure 3.19) indicates that the subsoil presents a limitation to infiltration to some extent. Water may either dam up, forming a perched water table or flow laterally when it reaches this point (Lin *et al.,* 2006; Asano *et al.*, 2002). The continual lateral redistribution would allow surface water to infiltrate at a higher rate than the limiting horizon(s) allows at depth. Another theory is that PF in the subsoil, below 40 cm, is rapid enough to sustain the high K_{meas} in the topsoil. This theory may be supported by Glass *et al.* (2002) who found that the degree of PFPs increased with depth up to 5 m; it should however be noted that their work was done in an unsaturated fracture network. Everson *et al.* (1998) also reported that the flux between the B horizon and the groundwater zone is poorly understood and that models (like ACRU) do not effectively deal with this interface.

Figure 3.17 shows that VWC increases with depth, even though Figure 3.19 might imply otherwise. This may be explained by the increased clay content from 4.3 to 9.9% from the topsoil to 70 cm depth respectively as the water holding capacity will increase accordingly.

There is a small isolated area in Figure 3.19 at 10 cm depth which was bypassed during infiltration. This is lens of textural discontinuity possibly resulting from mole activity which is very common in the top 50 cm of the soils in the reserve. This emphasizes the effect that bioturbation has on creating variation in the soil and so too on infiltration (Weiler & Naef, 2002).

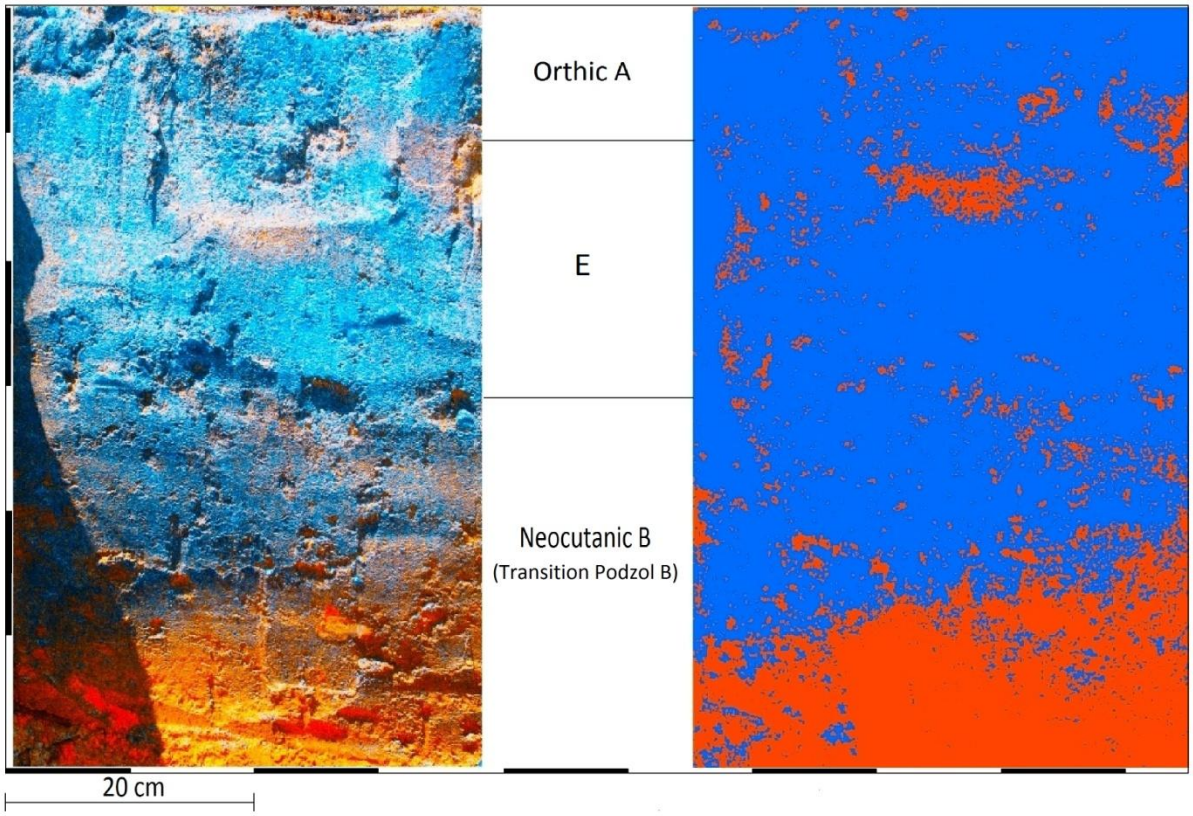

Figure 3.19: Left: Negative colour image of flowpath visualization for R2. Right: ArcGIS maximum likelihood colour analysis for R2 (Blue = Flowpath / Red = Bypassed).

3.4.6. K vs. Pore size distribution

Mini disc infiltrometer data is very useful in determining the proportional contribution of the different pore fractions to conductivity. The different pore fractions and their corresponding mini disc suction values are given in Table B.5 of Appendix B.

The K and Hydrologically Effective Porosity (m^3/m^3) were calculated to investigate two macro pore fractions, >0.3 mm and 0.3 - 0.15 mm, and two mesopore fractions, 0.15 - 0.075 mm and 0.075 - 0.03 mm. The average K trend was graphically compared to the HEP for the respective pore fractions shown in Figure 3.20. This graph illustrates that the macropores only make up a small portion of the total porosity by volume but contribute the vast majority of the conductivity. Kutilek (2004) confirms this finding as he stresses the importance of porosity as an indicator of the effect of structure on soil hydrology.

From this, the number and volume of macropores can be the dominant factors to consider when investigating the correlation between structure, porosity and infiltration. The importance of pore size distribution affirms that the textural discontinuity in R1 and R2 may be the cause of PF.

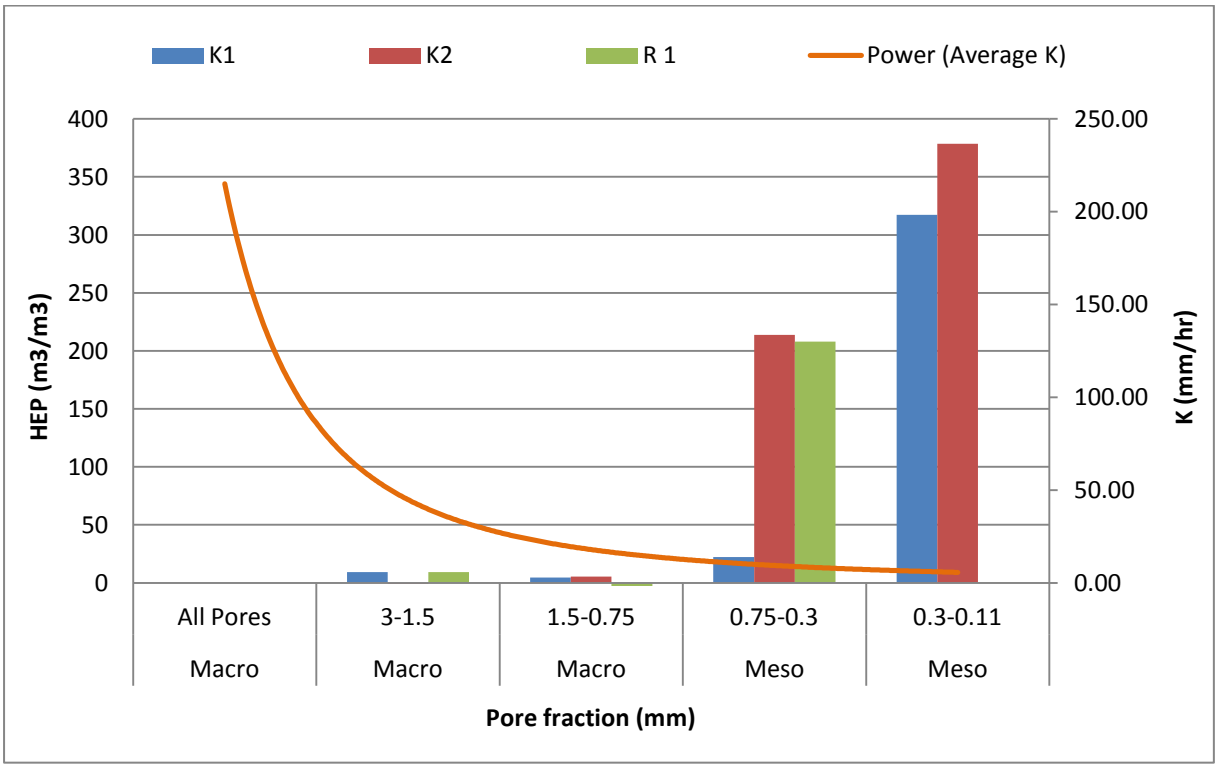

Figure3.20: Comparison of Hydrological Effective Pores (HEP m^3/m^3) and K (as a "power trend line" of average K (mm/hr)) for different pore size fractions

3.4.7. Accuracy of Recharge Estimation

Figure 3.21 shows the areas where recharge estimation accuracy is expected to vary. No such map was compiled for Riverlands as there was no expected variation in recharge estimation accuracy due to the observed soil homogeneity. Figure 3.21 illustrates that poor estimates would be made for the majority of the Oudebos catchment if soil pattern and position in landscape is not incorporated into the estimation model. The results also emphasize the importance of not only relying on estimations but to calibrate models using measured hydraulic parameters as well (Hutson, 1983).

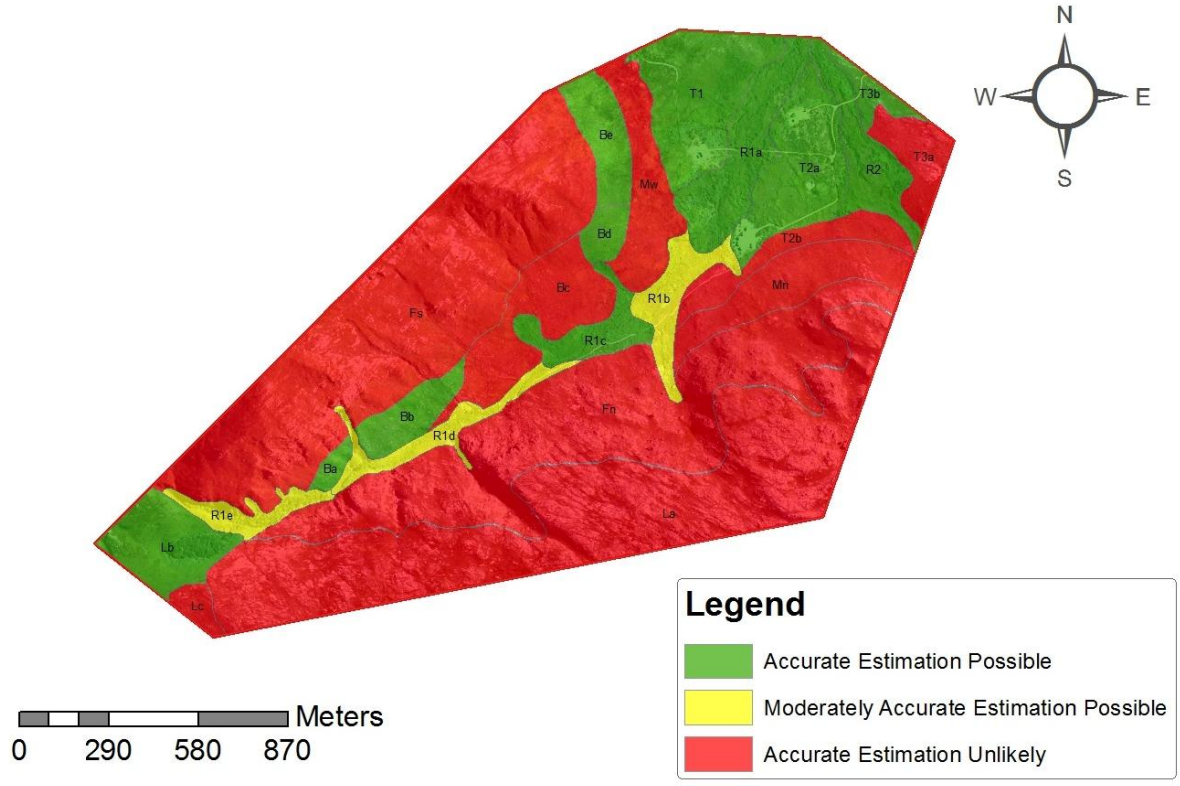

Figure 3.21: Map of the Oudebos River catchment in Kogelberg showing the predicted accuracy of recharge estimations, based on soil types and position in landscape.

Table 1.D in Appendix D shows the interpolated K_{sat} values for unsampled observation points. These interpolations were made using the estimated K_{sat} values from sampled points and the BDT in Figure 2.11. The HSU K_{sat} values are however not calibrated to compensate for PF, but the results do still give a fair estimate of the expected K in the areas where accurate estimation is possible and moderately possible.

3.5. Conclusion

Groundwater recharge estimation in unguaged catchments is commonly done based on parameters such as soil texture, coarse fraction and organic matter content. Pedotransfer functions (PTFs), such as the models by Saxton & Rawl (2006) and Zhang (1997), can be used to derive hydrological properties such as hydraulic conductivity (K) from these soil survey observations. This hydropedological approach was taken to investigate the effect of preferential flow paths on the accuracy of recharge estimation and to establish a relationship between soil pattern and infiltration pattern.

The study was designed to compare the recharge estimates of two contrasting aquifer systems: the Kogelberg Nature Reserve as a fractured bedrock aquifer and the Riverlands Nature Reserve as a cover sands aquifer. Surveys were conducted in both reserves to identify the dominant soil forms as well as their spatial distribution. Two sites were then chosen at each location where the infiltration experiments would be conducted. These experiments include volumetric water content (VWC) determination, preferential flow visualization (PFV) using staining dye and image analysis on ArcGIS software, K determination using the constant head method in a double ring infiltrometer, K determination using a mini disc infiltrometer and K estimation using PTFs. The findings were as follows.

Kogelberg presents a large degree of variation in terms of soil form observations. The greatest contrast could be made between the shallow, rocky Cartref soil form at site K1 and a deep sandy Fernwood soil form at site K2.

This comparison showed that a well drained, shallow rocky soil type that grades into bedrock, as at K1, would contain a large degree of PFPs throughout the depth of the profile. The PFPs are well connected and form as the water flows between the large stones, through the channels of least resistance. The bypassed volume of the profile amounted to 38 % and consisted of both soil and coarse fraction. This is a substantial portion of the profile and the PAW is thus expected to decrease as the percolating water increase. This form of PF is commonly referred to as funnel flow and occurs in macroscopically heterogeneous soils. This effect serves to increase the rate of infiltration relative to expected K in Kogelberg, contrary to the expected decrease in K as predicted by the Saxton & Rawls (2006) model. The estimated FC

was also found to be underestimated in the Kogelberg soils as it is suspected that the porous nature of the stone fraction increase the water holding capacity of the soil. This does not account for the total difference between estimated and actual FC but should be considered while doing estimations in fractured rock landscapes.

Infiltration in the homogenous Fernwood soil form occurred in a very predictable manner as the K_{meas} corresponded closely to the infiltration limiting layer's K_{est}. This is thought to be due to the lack of continuous PFPs, with the bypassed sections amounting to < 20 % of the profile. The soil's position at the foot of the mountain, next to the stream, may suggest that the soil will be well sorted, thus reducing the expected heterogeneity and so increasing the accuracy of predicted hydraulic properties. The FC_{est} was underestimated as actual FC was much higher. This is not an unusual occurrence as FC is dependent on texture, gravel and OM content.

The soils in Riverlands were similar to that of K2 in that they were deep, sandy and had a low coarse fraction. The soils were however better graded due to the level landscape. The K_{est} values from both R1 and R2 were very similar to their respective K_{meas} values. There were signs of PF in both sites but this did not significantly affect the rate of infiltration as it did in K1.The Saxton & Rawls (2006) model was also accurate in predicting FC for both sites in Riverlands.

Even though the estimates were accurate in the deep sandy soils, there were some irregularities which warrant discussion. The K_{meas} correlated well with the limiting K_{est} in K2 when uniform flow was > 80 % of the profile. However, as uniform flow decreased to show signs of continuous sections of PF, the K_{meas} correlated better with the maximum K_{est} as seen in R1 and R2 with flow paths of 62 and 72 % respectively. These variations are not as obvious as in K1 where the source of heterogeneity is the large stone fraction. Instead the PFPs are caused by textural discontinuities resulting in variations in pore size, bulk density and configuration. This trend thus shows as PF increases in Kogelberg and Riverlands, the infiltration rate tends to increase as well.

Bioturbation, specifically by mole rat activity in Riverlands, may enhance the formation of PFPs. The PF occurring in the subsoil, especially between the B horizon and groundwater zones, should be incorporated into hydrological models to more

accurately describe the flow in the subsoil; even in soils with limited PF as found in Riverlands.

In conclusion, soil survey information such as texture, coarse fragment content and organic matter content can be used to model groundwater recharge in deep homogenous sandy soils. The model could however underestimate recharge if PF is not incorporated as soil forms that display a high degree of PF, such as the Cf soil form in Kogelberg, will have substantially higher rates of infiltration than estimated by textural data alone. The model can also underestimate the actual FC if not field calibrated against the real water pressure at which field capacity is reached.

It is thus recommended to incorporate soil pattern into recharge models by identifying areas with hydrologically similar soil behaviour on a soil map and then to calibrate the model accordingly. The calibration should be done using a locally measured dataset to ensure the accuracy of hydrological estimations.

Other variables that could be investigated and incorporated into hydrological models were observed during this study:

- Table mountain sandstone has the capacity to absorb water as found during the infiltration experiment at K1. The extent to which sandstone can hold and conduct water in the soil profile is unknown and could be researched.
- Bioturbation, predominantly by mole rats in Riverlands, has a lasting and marked affect in the upper 50 cm of the soil cover and the effect of this should be investigated if site specific calibration data is desired for hydrological models.
- The hydrophobic topsoils in some areas in Riverlands can reduce the degree of infiltrating rainfall at the beginning of the rain season. It can thus be investigated how infiltration varies seasonally due to the seasonal rainfall variation.
- Finally, the specific pore fractions and their contribution to infiltration can be further investigated as it was found that the pore size is a dominant factor in hydraulic conductivity and thus groundwater recharge.

3.6. References

ASANO, Y., UCHIDA, T. & NOBUHITO, O., 2002. Residence times and flow paths of water in steep unchannelled catchments, Tanakami, Japan. *Journal of Hydrology* 261, 173-192.

BARENBLATT, G.I. & ZHELTOV, I.P., 1960. Fundamental equations of filtration of homogeneous liquids in fissured rocks. *Sov. Dokl. Akad. Nauk.* 132, 545-548.

BERKOWITZ, B., 2002. Characterizing flow and transport in fractured geological media: A review. *Advances in Water Resources* 25, 861-884.

BLAKE, G.R. & HARTGE, K.H., 1986. Particle density. P. 377-382. *In*: *M.A. Klute (ed.)* Methods of soil analysis. Physical and mineralogical methods: Part 1 (2nd edn.). Soil Sci. Soc. Am.

CAMPBELL, L. G., 1974. A simple method for determining unsaturated conductivity from moisture retention data. *Soil Sci.* 117, 311-314.

COREY, J.C., 1968. Evaluation of dyes for tracing water movement in acid soils. *Soil Science* 106, 182-187.

DAHAN, O., NATIV, R., ADAR, E.M. & BERKOWITZ, B., 1998. A measurement system to determine water flux and solute transport through fractures in the unsaturated zone. *Ground Water* 36, 444-449.

DE VRIES, J.J. & SIMMERS, I., 2002. Groundwater recharge: an overview of processes and challenges. *Hydrogeology Journal* 10, 5-17.

DECAGON DEVICES INCORPORATED, 2007. Mini Disc Infiltrometer User's Guide, Vol. 8. Decagon Devices Incorporated, Pullman.

DELIN, G.N., HEALY, R.W., LANDON, M.K. & BOHLKE, J.K., 2000. Effect of topography and soil properties on recharge at two site in an agricultural field. *Journal of the American Water Resources Association* 36, 1401-1416.

EVERSON, C.S., MOLEFE, G.L. & EVERSON, T.M, 1998. Monitoring and modelling components of the water balance in a grassland catchment in the summer rainfall area of South Africa. *WRC Report* No.493/1/98, Pretoria.

FEYEN, J., JACQUES, D., TIMMERMEN, A. & VANDERBORGHT, J., 1998. Modelling water flow and solute transport in heterogenous soils: A review of recent approaches. *J. agric. Eng Res.* 70. 231-256.

FLURY, M. & FLUHLER, H., 1995. Tracer characteristics of Brilliant Blue FCF. *Soil Science Society of Ameirca Journal* 59, 22-27.

GLASS, R.J., NICHOLL, M.J., RAMIREZ, A.L. & DAILY, W.D., 2002. Liquid phase structure within an unsaturated fracture network beneath a surface infiltration event: field experiment. *Water Resour. Res.* 38, 1199-1135.

HANGENA, E., GERKE, H.H., SCHAAF, W. & HUTTL, R.F., 2003. Flow path visualization in a lignitic mine soil using iodine-starch staining. *Geoderma* 120, 142-151.

HENDRICKX, J.M.H. & FLURRY, M., 2001. Uniform and preferential flow mechanisms in the vadose zone. p. 149-187. *In*: Conceptual Models of Flow and Transport in the Fractured Vadose Zone,. Washington, D.C., National Academy Press.

HILLEL, D., 1980. Fundementals of soil physics. Academic Press Inc., San Diego.

HUTSON, J.L., 1983. Estimation of hydrological properties of South African soils. Ph.D. Thesis. Pietermaritzburg.

JOEL, A. & MESSING, I., 2001. Infiltration rate and hydraulic conductivity measured with rain simulator and disc permeameter on sloping arid land. *Arid Land Research and Management* 15, 371-384.

KUNG, K.-J.S., 1990. Preferential flow in a sandy vadose zone. 1. Field observation. *Geoderma* 46, 51-58.

KUTILEK, M., 2004. Soil hydralic properties as related to soil structure. *Soil & Tillage Res.* 79, 175-184.

LIN, H.S., KOGELMANN, W., WALKER, C. & BRUNS, M.A., 2006. Soil moisture patterns in a forested catchment: A hydropedological perspective. *Geoderma* 131, 345-368.

PETERSEN, C.T., JENSENA, H.E., HANSENA, S. & BENDER KOCH, C., 2001. Susceptibility of a sandy loam soil to preferential flow as affected by tillage. *Soil & Tillage Research* 58, 81-89.

PRAASMA, T., NOVAKOWSKI, K. & KYSER, K., 2009. Using stable isotopes and hydraulic head data to investigate groundwater recharge and discharge in a fractured rock aquifer. *Journal of Hydrology* 366, 35-45.

RAWLS, W.J., GISH, T.J. & BRAKENSIEK, D.L., 1991. Estimating soil water retention from soil physical properties and characteristics. *Advances in Soil Science* 16, 213-234.

REYNOLDS, E.R.C., 1966. The percolation of rainwater through soil demonstrated by fluorescent dyes. *Journal of Soil Science* 17, 127-132.

RODGERS, M. & MULQUEEN, J., 2006. Field-saturated hydraulic conductivity of unsaturated soils from fallng-head well tests. *Agricultural Water Management* 79, 160-176.

RODGERS, P., SOULSBY, C. & WALDRON, S., 2005. Stable isotope tracers as diagnostic tools in upscaling flow path understanding and residence time estimates in a mountainous mesoscale catchment. *Hydrological Processes* 19, 2291-2307.

ROZANOV, A. & DE CLERCQ, W., 2010. In field visualisation of water infiltration and soluble salt transport. p. 56-59. Soil Solutions for a Changing World.*19th World Congress of Soil Science,* Brisbane. Published on DVD.

SAXTON, K.E. & RAWLS, W.J., 2006. Soil water characteristic estimates by texture and organic matter for hydrologic solutions. *Soil Sci. Soc. Am. J.* 70, 1569-1578.

SOIL CLASSIFICATION WORKING GROUP, 1991. Soil Classification - A Taxonomic System for South Africa. Memoirs on the agricultural natural resources of South Africa No. 15. Department of Agricultural Development. Pretoria, South Africa.

VAN GENUCHTEN, M., 1980. A closed-form equation for predicting the hydraulic conductivity of unsaturated soils. *Soil Sci. Soc. Am. J.* 44, 892-897.

VAN OMMEN, H.C., DEKKER, L.W., DIJKSMA, R., HULSHOF, J. & VAN DER MOLEN, W.H., 1988. A new technique for evaluating the presence of preferential

flow paths in nonstructured soils. *Soil Science Society of America Journal* 52, 1192-1193.

VIDAČEK, Z., BOGUNOVIĆ, M., HUSNJAK, S., SRAKA, M. & BENSA, A., 2008. Hydropedological map of the Republic of Croatia. *Agriculturae Conspectus Scientificus* 73, 67-74.

WATSON, K.W. & LUXMOORE, R.J., 1986. Estimating macroporosity in a forested watershed by use of a tension infiltrometer. *Soil Sci. Soc. Am. J.* 50, 578-582.

WEILER, M. & NAEF, F., 2002. Simulating surface and subsurface initiation of macropore flow. *Journal of Hydrology* 273, 139-154.

WENNINGER, J., UHLENBROOK, S., LORENTZ, S.A. & LEIBUNDGUT, C., 2008. Identification of runoff generation processes using combined hydrometric, tracer and geophysical methods in a headwater catchment in South Africa. *Hydrological Sciences* 53, 65-81.

WILSON, G.V. & LUXMOORE, R.J., 1988. Infiltration, macroporosity, and mesoporosity distributions on two forested watersheds. *Soil Sci. Soc. Am. J.* 52, 329-335.

ZHANG, R., 1997. Determination of soil sorptivity and hydraulic conductivity from the disk infiltrometer. *Soil Science Society of America Journal* 61, 1024-1030.

General Conclusions

A thorough literature review revealed that hydrologists most often struggle to accurately predict aquifer sustainability due to the spatial heterogeneity that is inherent to any and every catchment. This heterogeneity exists on a spatial and temporal scale and an increase in factors such as local relief and catchment size further complex such estimations.

Increased pressure on groundwater sources, due to increased population size and threats of climate change, is driving research to better understand the process of aquifer recharge and all the factors of concern. One such factor is the soil cover in a catchment which serves to partition rainwater into different flowpaths destined for surface runoff, evapotranspiration and deep percolation. Given the central position that soil cover has in the groundwater recharge process it would make sense to use the spatial soil distribution, or soil pattern, as a distinctive factor when modelling aquifer dynamics.

This ideology was used to formulate the main goal of this research which was to improve the catchment scale hydrological models of two aquifer systems: One a fractured bedrock system at the Kogelberg Nature Reserve, Kleinmond, and the other a cover sand system in Riverlands Nature Reserve, Malmesbury. The study focussed on strengthening the link between specific hydrological flow patterns and soil pattern, and formulating the results so that they may ultimately be used to calibrate the recharge prediction models for the respective catchments.

The research was done in two parts: The first phase was to conduct soil surveys in both reserves during which soils would be classified according to South African Soil Classification system. The surveys where done using a grid and transect approach in Riverlands and a reference group approach in Kogelberg. Samples were collected at representative observation points which provided textural data for use in pedotransfer functions (PTFs). These PTFs were used to estimate plant available water (PAW) and hydraulic conductivity (K_{est}) for the observed profiles. Infiltration experiments were subsequently done at four sites to compare the flow patterns of the two most contrasting soil forms from each reserve as part of the second phase.

The experiments included double ring infiltration, mini disc infiltration, volumetric water content determination and flow path visualisation using a staining dye.

The statistical comparison of the hydrological properties of different soil forms revealed that there is statistical significant difference between the estimated K_{sat} of the Cartref soil form and Fernwood, Pinegrove and Witfontein soil forms in Kogelberg. So too the PAW differed between the Pinegrove and Cartref soil forms in Kogelberg. The same analysis in Riverlands revealed no significant differences between soil forms. These comparisons may suggest that hydraulic properties differed between the deep sandy soil forms (Fernwood, Pinegrove and Witfontein in Kogelbreg and Witfontein, Concordia and Lamotte in Riverlands) and the shallow rocky soil forms (Cartref and Glenrosa in Kogelberg). Thus grouping of hydrological similar units (HSUs) can be done on the basis of the soil forms present within a given catchment.

The infiltration study revealed that soil pattern could also be used to predict the accuracy of recharge estimation. The study showed that shallow, rocky soils that grade into bedrock would have infiltration rates far greater than those estimated using PTFs. This is due to the prevalence of continuous preferential flow (PF) due to funnelling of water between coarse fragments in these profiles. Recharge estimates would thus be inaccurate in such soils and calibration using locally derived data is recommended. An example is the Cartref soil form which is dominant in Kogelberg.

On the contrary, PTFs produced accurate infiltration estimates relative to measured infiltration rates in deep sandy soils. The Fernwood, Lamotte and Vilafontes soil forms are examples of such soils. It should however be noted that an increase in PF in these soil forms produced measured K values slightly higher than estimated. Thus illustrating a much less severe case of the trend observed in the shallow rocky soil.

These results thus confirm that using soil survey information, in the form of a soil map showing soil forms, and calibrated hydrological properties, like measured and estimated K, one can delineate HSUs that encompass the full degree of heterogeneity in a given catchment. These HSUs would thus prove useful in upscaling recharge estimation models on a catchment scale.

Appendix A – Survey Information and Textural Analysis

Table A.1. Kogelberg reference groups and expected moisture values.

RG	Classes				RATING	RG	Classes				RATING
	Slope	Aspect	Surface Cover	Predicted Moisture			Slope	Aspect	Surface Cover	Predicted Moisture	
0	4	1	4	3	12	30	1	2	3	2	8
1	4	1	4	3	12	31	2	2	4	3	11
2	5	4	5	5	19	32	2	2	5	5	14
3	5	4	5	5	19	33	1	2	3	2	8
4	3	2	4	3	12	34	1	2	5	5	13
5	4	2	4	3	13	35	2	1	5	4	12
6	3	2	3	2	10	36	2	2	4	2	10
7	2	2	3	2	9	37	2	1	3	2	8
8	4	2	3	3	12	38	1	1	2	1	5
9	5	4	4	4	17	39	3	2	3	2	10
10	5	4	5	5	19	40	1	1	3	2	7
11	2	2	3	2	9	41	1	1	2	1	5
12	3	1	3	2	9	42	4	2	4	4	14
13	2	1	2	2	7	43	2	1	3	2	8
14	2	1	2	1	6	44	3	2	5	3	13
15	2	1	2	1	6	45	5	4	3	3	15
16	2	1	3	2	8	46	1	1	1	1	4
17	1	1	2	1	5	47	0	0	0	0	0
18	1	1	1	1	4	48	0	0	0	0	0
19	2	1	2	2	7	49	0	0	0	0	0
20	3	2	4	3	12	50	0	0	0	0	0
21	2	1	2	2	7	51	4	1	1	1	7
22	1	1	1	1	4	52	1	3	3	2	9
23	2	2	3	2	9	53	1	3	4	3	11
24	2	2	2	2	8	54	1	3	3	3	10
25	3	2	3	2	10	55	1	3	2	1	7
26	1	2	3	3	9	56	2	3	4	2	11
27	3	2	4	3	12	57	1	2	2	1	6
28	2	2	4	3	11	58	1	3	4	3	11
29	1	1	2	1	5	59	1	3	4	3	11

Table A.1: Kogelberg soil survey information.

Round	Profile	Longtitude	Latitude	Altitude (m)	Soil Form	Soil Family	Diagnostic Horizon	Transition Form	Transition Family	Transition Horizon	Horizon Depth (mm)	Profile Total Depth (mm)
1	1	-34.32493	18.96481	68	Pg	1000	Orthic A				0 - 50	550
1	1	-34.32493	18.96481	68	Pg	1000	Podzol B				50 - 500	550
1	1	-34.32493	18.96481	68	Pg	1000	Uncon No Wet				500 - 550	550
1	2	-34.32540	18.96439	72	Pg	1000	Orthic A				0 - 50	650
1	2	-34.32540	18.96439	72	Pg	1000	Podzol B				50 - 350	650
1	2	-34.32540	18.96439	72	Pg	1000	Uncon No Wet				350 - 650	650
1	3	-34.32614	18.96442	82	Pg	1000	Orthic A				0 - 50	600
1	3	-34.32614	18.96442	82	Pg	1000	Podzol B				50 - 200	600
1	3	-34.32614	18.96442	82	Pg	1000	Podzol B				200 - 500	600
1	3	-34.32614	18.96442	82	Pg	1000	Uncon No Wet				500 - 600	600
1	4	-34.32569	18.96563	79	Pg	1000	Orthic A				0 - 100	500
1	4	-34.32569	18.96563	79	Pg	1000	Podzol B				100 - 400	500
1	4	-34.32569	18.96563	79	Pg	1000	Uncon No Wet				400 - 500	500
1	5	-34.32541	18.96606	78	Fw	1100	Orthic A				0 - 100	500
1	5	-34.32541	18.96606	78	Fw	1100	E				100 - 400	500
1	5	-34.32541	18.96606	78	Fw	1100	E				400 - 500	500
1	6	-34.32612	18.96475	72	Hh	1200	Orthic A				0 - 100	1200
1	6	-34.32612	18.96475	72	Hh	1200	E				100 - 500	1200
1	6	-34.32612	18.96475	72	Hh	1200	Podzol B				500 - 800	1200
1	6	-34.32612	18.96475	72	Hh	1200	Saprolite				800 - 1200	1200
1	7	-34.32524	18.96708	77	Fw	1100	Orthic A				0 - 100	700
1	7	-34.32524	18.96708	77	Fw	1100	E				100 - 400	700

Table A.2: Continues

Round	Profile	Longtitude	Latitude	Altitude (m)	Soil Form	Soil Family	Diagnostic Horizon	Transition Form	Transition Family	Transition Horizon	Horizon Depth (mm)	Profile Total Depth (mm)
1	7	-34.32524	18.96708	77	Fw	1100	E				400 - 700	700
1	8	-34.32433	18.96774	73	Pg	1000	Orthic A				0 - 150	500
1	8	-34.32433	18.96774	73	Pg	1000	Podzol B				150 - 400	500
1	8	-34.32433	18.96774	73	Pg	1000	Uncon No Wet				400 - 500	500
1	9	-34.32248	18.96709	66	Gk	2100	Orthic A				0 - 50	760
1	9	-34.32248	18.96709	66	Gk	2100	Podzol B				50 - 400	760
1	9	-34.32248	18.96709	66	Gk	2100	Saprolite				400 - 760	760
1	11	-34.32269	18.96395	48	Wf	1100	Orthic A				0 - 200	800
1	11	-34.32269	18.96395	48	Wf	1100	Podzol B				200 - 600	800
1	11	-34.32269	18.96395	48	Wf	1100	Uncon With Wet				600 - 800	800
1	12	-34.32359	18.96308	60	Cc	2000	Orthic A / OB				0 - 200	1200
1	12	-34.32359	18.96308	60	Cc	2000	E				200 - 400	1200
1	12	-34.32359	18.96308	60	Cc	2000	Podzol B				400 - 800	1200
1	12	-34.32359	18.96308	60	Cc	2000	Podzol B				800 - 950	1200
1	12	-34.32359	18.96308	60	Cc	2000	Uncon No Wet				950 - 1200	1200
1	13	-34.32398	18.96476	54	Wf	1100	Orthic A				0 - 100	800
1	13	-34.32398	18.96476	54	Wf	1100	Podzol B				100 - 600	800
1	13	-34.32398	18.96476	54	Wf	1100	Uncon With Wet				600 - 800	800
1	14	-34.32233	18.96849	51	Lt	1100	Orthic A	Fw	1110	Orthic A	0 - 50	150
1	14	-34.32233	18.96849	51	Lt	1100	E	Fw	1110	E	50 - 100	150
1	14	-34.32233	18.96849	51	Lt	1100	Podzol B	Fw	1110	E	100 - 150	150
1	15	-34.32293	18.96897	59	Cf	1200	Orthic A	Hh	2100	Orthic A	0 - 50	200

Table A.3: Continues

Round	Profile	Longtitude	Latitude	Altitude (m)	Soil Form	Soil Family	Diagnostic Horizon	Transition Form	Transition Family	Transition Horizon	Horizon Depth (mm)	Profile Total Depth (mm)
1	15	-34.32293	18.96897	59	Cf	1200	E	Hh	2100	E	50 - 100	200
1	15	-34.32293	18.96897	59	Cf	1200	Litho B	Hh	2100	Podzol B	100 - 200	200
1	16	-34.32366	18.96985	66	Cf	1200	Orthic A	Hh	2100	Orthic A	0 -50	300
1	16	-34.32366	18.96985	66	Cf	1200	E	Hh	2100	E	50 - 100	300
1	16	-34.32366	18.96985	66	Cf	1200	Litho B	Hh	2100	Podzol B	100 - 300	300
1	17	-34.32409	18.97037	76	Cf	1200	Orthic A	Hh	2100	Orthic A	0 - 50	300
1	17	-34.32409	18.97037	76	Cf	1200	E	Hh	2100	E	50 - 200	300
1	17	-34.32409	18.97037	76	Cf	1200	Litho B	Hh	2100	Podzol B	200 - 300	300
1	18	-34.32531	18.97035	85	Cf	1200	Orthic A	Hh	2100	Orthic A	0 - 50	150
1	18	-34.32531	18.97035	85	Cf	1200	E	Hh	2100	E	50 - 100	150
1	18	-34.32531	18.97035	85	Cf	1200	Litho B	Hh	2100	Podzol B	100 - 150	150
1	19	-34.32623	18.97054	95	Fw	1110	Orthic A	Lt	1100	Orthic A	0 - 50	800
1	19	-34.32623	18.97054	95	Fw	1110	E	Lt	1100	E	50 - 400	800
1	19	-34.32623	18.97054	95	Fw	1110	E	Lt	1100	Podzol B	400 - 800	800
1	21	-34.32673	18.96945	101	Cf	1200	Orthic A	Hh	2100	Orthic A	0 - 50	300
1	21	-34.32673	18.96945	101	Cf	1200	E	Hh	2100	E	50 - 120	300
1	21	-34.32673	18.96945	101	Cf	1200	Litho B	Hh	2100	Podzol B	120 - 300	300
1	22	-34.32612	18.96815	96	Cf	1200	Orthic A	Hh	2100	Orthic A	0 - 50	200
1	22	-34.32612	18.96815	96	Cf	1200	E	Hh	2100	E	50 - 100	200
1	22	-34.32612	18.96815	96	Cf	1200	Litho B	Hh	2100	Podzol B	100 - 200	200
1	23	-34.32585	18.96760	89	Cf	1200	Orthic A	Hh	2100	Orthic A	0 - 50	200
1	23	-34.32585	18.96760	89	Cf	1200	E	Hh	2100	E	50 - 100	200
1	23	-34.32585	18.96760	89	Cf	1200	Litho B	Hh	2100	Podzol B	100 - 200	200
1	24	-34.32638	18.96718	95	Gs	2211	Orthic A	Gk	2100	Orthic A	0 - 50	400

Table A.4: Continues

Round	Profile	Longtitude	Latitude	Altitude (m)	Soil Form	Soil Family	Diagnostic Horizon	Transition Form	Transition Family	Transition Horizon	Horizon Depth (mm)	Profile Total Depth (mm)
1	24	-34.32638	18.96718	95	Gs	2211	Litho B	Gk	2100	Podzol B	50 - 200	400
1	24	-34.32638	18.96718	95	Gs	2211	Litho B	Gk	2100	Podzol B	200 - 400	400
1	25	-34.32653	18.96656	105	Gs	2211	Orthic A	Gk	2100	Orthic A	0 - 50	200
1	25	-34.32653	18.96656	105	Gs	2211	Litho B	Gk	2100	Podzol B	50 - 200	200
1	26	-34.32620	18.96630	103	Cf	1200	Orthic A	Hh	2100	Orthic A	0 - 50	200
1	26	-34.32620	18.96630	103	Cf	1200	E	Hh	2100	E	50 - 150	200
1	26	-34.32620	18.96630	103	Cf	1200	Litho B	Hh	2100	Podzol B	150 - 200	200
1	27	-34.32607	18.96564	89	Cf	1200	Orthic A	Hh	2100	Orthic A	0 - 100	400
1	27	-34.32607	18.96564	89	Cf	1200	E	Hh	2100	E	100 - 150	400
1	27	-34.32607	18.96564	89	Cf	1200	Litho B	Hh	2100	Podzol B	150 - 400	400
1	28	-34.32665	18.96571	106	Cf	1200	Orthic A	Hh	2100	Orthic A	0 - 50	500
1	28	-34.32665	18.96571	106	Cf	1200	E	Hh	2100	E	50 - 250	500
1	28	-34.32665	18.96571	106	Cf	1200	Litho B	Hh	2100	Podzol B	250 - 500	500
1	29	-34.32707	18.96533	98	Cf	1200	Orthic A	Hh	2100	Orthic A	0 - 50	600
1	29	-34.32707	18.96533	98	Cf	1200	E	Hh	2100	E	50 - 250	600
1	29	-34.32707	18.96533	98	Cf	1200	Litho B	Hh	2100	Podzol B	250 - 600	600
1	30	-34.32754	18.96467	115	Cf	1200	Orthic A	Hh	2100	Orthic A	0 - 50	800
1	30	-34.32754	18.96467	115	Cf	1200	E	Hh	2100	E	50 - 200	800
1	30	-34.32754	18.96467	115	Cf	1200	Litho B	Hh	2100	Podzol B	200 - 800	800
1	31	-34.32756	18.96384	80	Cf	1200	Orthic A	Hh	2100	Orthic A	0 - 50	600
1	31	-34.32756	18.96384	80	Cf	1200	E	Hh	2100	E	50 - 150	600
1	31	-34.32756	18.96384	80	Cf	1200	Litho B	Hh	2100	Podzol B	150 - 600	600
1	32	-34.32785	18.96325	101	Cf	1200	Orthic A	Hh	2100	Orthic A	0 - 40	800
1	32	-34.32785	18.96325	101	Cf	1200	E	Hh	2100	E	40 - 200	800

Table A.5: Continues

Round	Profile	Longtitude	Latitude	Altitude (m)	Soil Form	Soil Family	Diagnostic Horizon	Transition Form	Transition Family	Transition Horizon	Horizon Depth (mm)	Profile Total Depth (mm)
1	32	-34.32785	18.96325	101	Cf	1200	Litho B	Hh	2100	Podzol B	200 - 800	800
1	33	-34.32821	18.96251	106	Cf	1200	Orthic A	Hh	2100	Orthic A	0 - 40	500
1	33	-34.32821	18.96251	106	Cf	1200	E	Hh	2100	E	40 - 200	500
1	33	-34.32821	18.96251	106	Cf	1200	Litho B	Hh	2100	Podzol B	200 - 500	500
1	34	-34.32872	18.96167	97	Cf	1200	Orthic A	Hh	2100	Orthic A	0 - 40	320
1	34	-34.32872	18.96167	97	Cf	1200	E	Hh	2100	E	40 - 280	320
1	34	-34.32872	18.96167	97	Cf	1200	Litho B	Hh	2100	Podzol B	280 - 320	320
1	35	-34.32847	18.96147	89	Cf	1100	Orthic A	Hh	2100	Orthic A	0 - 100	1500
1	35	-34.32847	18.96147	89	Cf	1100	E	Hh	2100	E	100 - 1000	1500
1	35	-34.32847	18.96147	89	Cf	1100	Litho B	Hh	2100	Podzol B	1000 - 1500	1500
1	36	-34.32829	18.96117	89	Fw	1100	Orthic A	Lt	1100	Orthic A	0 - 50	450
1	36	-34.32829	18.96117	89	Fw	1100	E	Lt	1100	E	50 - 400	450
1	36	-34.32829	18.96117	89	Fw	1100	E	Lt	1100	Podzol B	400 - 450	450
1	37	-34.32815	18.96138	83	Fw	1100	Orthic A	Lt	1100	Orthic A	0 - 50	400
1	37	-34.32815	18.96138	83	Fw	1100	E	Lt	1100	E	50 - 400	400
1	38	-34.32816	18.96199	88	Fw	1100	Orthic A	Lt	1100	Orthic A	0 - 50	1000
1	38	-34.32816	18.96199	88	Fw	1100	E	Lt	1100	Podzol B	50 - 700	1000
1	38	-34.32816	18.96199	88	Fw	1100	E	Lt	1100	Podzol B	700 - 1000	1000
1	39	-34.32779	18.96182	79	Cf	1200	Orthic A	Hh	2100	Orthic A	0 - 50	600
1	39	-34.32779	18.96182	79	Cf	1200	E	Hh	2100	E	50 - 550	600
1	39	-34.32779	18.96182	79	Cf	1200	Litho B	Hh	2100	Podzol B	550 - 600	600
1	40	-34.32772	18.96234	85	Cf	1200	Orthic A	Hh	2100	Orthic A	0 - 80	300
1	40	-34.32772	18.96234	85	Cf	1200	E	Hh	2100	E	80 - 250	300
1	40	-34.32772	18.96234	85	Cf	1200	Litho B	Hh	2100	Podzol B	250 - 300	300

Table A.6: Continues

Round	Profile	Longtitude	Latitude	Altitude (m)	Soil Form	Soil Family	Diagnostic Horizon	Transition Form	Transition Family	Transition Horizon	Horizon Depth (mm)	Profile Total Depth (mm)
1	41	-34.32730	18.96333	82	Cf	1200	Orthic A	Hh	2100	Orthic A	0 -80	300
1	41	-34.32730	18.96333	82	Cf	1200	E	Hh	2100	E	80 - 250	300
1	41	-34.32730	18.96333	82	Cf	1200	Litho B	Hh	2100	Podzol B	250 - 300	300
1	42	-34.32707	18.96382	77	Cf	1200	Orthic A	Hh	2100	Orthic A	0 - 80	150
1	42	-34.32707	18.96382	77	Cf	1200	E	Hh	2100	E	80 - 120	150
1	42	-34.32707	18.96382	77	Cf	1200	Litho B	Hh	2100	Podzol B	120 - 150	150
1	43	-34.32491	18.96766	77	Cc	1000	Orthic A				0 - 50	650
1	43	-34.32491	18.96766	77	Cc	1000	E				50 - 550	700
1	43	-34.32491	18.96766	77	Cc	1000	Podzol B				550 - 650	700
1	43	-34.32491	18.96766	77	Cc	1000	Uncon No wet				650 - 700	700
1	44	-34.32457	18.96673	74	Cc	1000	Orthic A				0 - 50	450
1	44	-34.32457	18.96673	74	Cc	1000	E				50 - 250	450
1	44	-34.32457	18.96673	74	Cc	1000	Podzol B				250 - 400	450
1	44	-34.32457	18.96673	74	Cc	1000	Uncon No wet				400 - 450	450
1	45	-34.32667	18.96543	95	Cf	1120	Orthic A	Hh	2100	Orthic A	0 - 50	900
1	45	-34.32667	18.96543	95	Cf	1200	E	Hh	2100	E	50 - 200	900
1	45	-34.32667	18.96543	95	Cf	1200	E	Hh	2100	E	200 - 450	900
1	45	-34.32667	18.96543	95	Cf	1200	Litho B	Hh	2100	Podzol B	450 - 900	900
1	46	-34.32731	18.96584	119	Cf	1200	Orthic A	Hh	2100	Orthic A	0 - 50	700
1	46	-34.32731	18.96584	119	Cf	1200	E	Hh	2100	E	50 - 350	700
1	46	-34.32731	18.96584	119	Cf	1200	Litho B	Hh	2100	Podzol B	350 - 700	700
1	47	-34.32773	18.96683	143	Gs	2212	Orthic A	Gk	2100	Orthic A	0 - 100	350
1	47	-34.32773	18.96683	143	Gs	2212	Litho B	Gk	2100	Podzol B	100 - 350	350
1	48	-34.32848	18.96777	203	Cf	1200	Orthic A	Hh	2100	Orthic A	0 - 40	350

Table A.7: Continues

Round	Profile	Longtitude	Latitude	Altitude (m)	Soil Form	Soil Family	Diagnostic Horizon	Transition Form	Transition Family	Transition Horizon	Horizon Depth (mm)	Profile Total Depth (mm)
1	48	-34.32848	18.96777	203	Cf	1200	E	Hh	2100	E	40 - 120	350
1	48	-34.32848	18.96777	203	Cf	1200	Litho B	Hh	2100	Podzol B	120 - 350	350
1	49	-34.32906	18.96776	205	Cf	1200	Orthic A	Hh	2100	Orthic A	0 - 150	1200
1	49	-34.32906	18.96776	205	Cf	1200	E	Hh	2100	E	150 - 550	1200
1	49	-34.32906	18.96776	205	Cf	1200	E	Hh	2100	E	550 - 1100	1200
1	49	-34.32906	18.96776	205	Cf	1200	Litho B	Hh	2100	Podzol B	1100 - 1200	1200
1	50	-34.32924	18.96756	212	Cf	1200	Orthic A	Hh	2100	Orthic A	0 - 50	400
1	50	-34.32924	18.96756	212	Cf	1200	E	Hh	2100	E	50 - 150	400
1	50	-34.32924	18.96756	212	Cf	1200	Litho B	Hh	2100	Podzol B	150 - 400	400
1	51	-34.32963	18.96507	215	Cf	1200	Orthic A	Hh	2100	Orthic A	0 - 100	550
1	51	-34.32963	18.96507	215	Cf	1200	E	Hh	2100	E	100 - 450	550
1	51	-34.32963	18.96507	215	Cf	1200	Litho B	Hh	2100	Podzol B	450 - 550	550
1	52	-34.32963	18.96404	212	Gs	2212	Orthic A	Gk	2100	Orthic A	0 - 50	100
1	52	-34.32963	18.96404	212	Gs	2212	Litho B	Gk	2100	Podzol B	50 - 100	100
1	53	-34.32884	18.96259	112	Cf	1200	Orthic A	Hh	2100	Orthic A	0 - 50	400
1	53	-34.32884	18.96259	112	Cf	1200	E	Hh	2100	E	50 - 150	400
1	53	-34.32884	18.96259	112	Cf	1200	Litho B	Hh	2100	Podzol B	150 - 400	400
1	54	-34.32865	18.96086	87	Lt	1200	Orthic A				0 - 100	1200
1	54	-34.32865	18.96086	87	Lt	1200	E				100 - 500	1200
1	54	-34.32865	18.96086	87	Lt	1200	Podzol B				500 - 1000	1200
1	54	-34.32865	18.96086	87	Lt	1200	Uncon With Wet				1000 - 1200	1200
1	55	-34.32880	18.96044	99	Lt	1200	Orthic A				0 - 200	1200
1	55	-34.32880	18.96044	99	Lt	1200	E				200 - 800	1200

Table A.2: Continues

Round	Profile	Longtitude	Latitude	Altitude (m)	Soil Form	Soil Family	Diagnostic Horizon	Transition Form	Transition Family	Transition Horizon	Horizon Depth (mm)	Profile Total Depth (mm)
1	55	-34.32880	18.96044	99	Lt	1200	Podzol B				800 - 1000	1200
1	55	-34.32880	18.96044	99	Lt	1200	Uncon With Wet				1000 - 1200	1200
1	56	-34.32865	18.96028	98	Wf	1100	Orthic A				0 - 50	1000
1	56	-34.32865	18.96028	98	Wf	1100	Podzol B				50 - 800	1000
1	56	-34.32865	18.96028	98	Wf	1100	Uncon With Wet				800 - 1000	1000
1	57	-34.32933	18.95955	107	Cf	1200	Orthic A	Hh	2100	Orthic A	0 - 80	300
1	57	-34.32933	18.95955	107	Cf	1200	E	Hh	2100	E	100 - 250	300
1	57	-34.32933	18.95955	107	Cf	1200	Litho B	Hh	2100	Podzol B	250 - 300	300
1	58	-34.33009	18.95702	116	Cf	1200	Orthic A	Hh	2100	Orthic A	0 - 50	400
1	58	-34.33009	18.95702	116	Cf	1200	E	Hh	2100	E	50 - 350	400
1	58	-34.33009	18.95702	116	Cf	1200	Litho B	Hh	2100	Podzol B	350 - 400	400
1	59	-34.33025	18.95680	121	Cf	1200	Organic Litter	Hh	2100	Organic Litter	-50 - 0	300
1	59	-34.33025	18.95680	121	Cf	1200	Orthic A	Hh	2100	Orthic A	0 - 50	300
1	59	-34.33025	18.95680	121	Cf	1200	E	Hh	2100	E	50 - 250	300
1	59	-34.33025	18.95680	121	Cf	1200	Litho B	Hh	2100	Podzol B	250 - 300	300
1	60	-34.33002	18.95645	124	Cf	1200	Orthic A	Hh	2100	Orthic A	0- 50	450
1	60	-34.33002	18.95645	124	Cf	1200	E	Hh	2100	E	50 - 400	450
1	60	-34.33002	18.95645	124	Cf	1200	Litho B	Hh	2100	Podzol B	400 - 450	450
1	61	-34.33005	18.95549	137	Cf	1200	Orthic A	Hh	2100	Orthic A	0 - 50	250
1	61	-34.33005	18.95549	137	Cf	1200	E	Hh	2100	E	50 - 200	250
1	61	-34.33005	18.95549	137	Cf	1200	Litho B	Hh	2100	Podzol B	200 - 250	250
1	62	-34.33099	18.95481	146	Cf	1200	Orthic A	Hh	2100	Orthic A	0 - 50	300

Table A.2: Continues

Round	Profile	Longtitude	Latitude	Altitude (m)	Soil Form	Soil Family	Diagnostic Horizon	Transition Form	Transition Family	Transition Horizon	Horizon Depth (mm)	Profile Total Depth (mm)
1	62	-34.33099	18.95481	146	Cf	1200	E	Hh	2100	E	50 - 250	300
1	62	-34.33099	18.95481	146	Cf	1200	Litho B	Hh	2100	Podzol B	250 - 300	300
1	63	-34.33147	18.95259	170	Cc	1000	Orthic A				0 - 80	350
1	63	-34.33147	18.95259	170	Cc	1000	E				80 - 150	350
1	63	-34.33147	18.95259	170	Cc	1000	Podzol B				150 - 300	350
1	63	-34.33147	18.95259	170	Cc	1000	Uncon No wet				300 - 350	350
1	64	-34.33286	18.95159	175	Cf	1200	Orthic A	Hh	2100	Orthic A	0 - 50	600
1	64	-34.33286	18.95159	175	Cf	1200	E	Hh	2100	E	50 - 400	600
1	64	-34.33286	18.95159	175	Cf	1200	Litho B	Hh	2100	Podzol B	400 - 600	600
1	65	-34.33279	18.95039	213	Pg	1000	Orthic A				0 - 70	350
1	65	-34.33279	18.95039	213	Pg	1000	Podzol B				70 - 280	350
1	65	-34.33279	18.95039	213	Pg	1000	Podzol B				280 - 300	350
1	65	-34.33279	18.95039	213	Pg	1000	Uncon No wet				300 - 350	350
1	66	-34.33242	18.94967	240	Pg	2000	Orthic A				0 - 50	1250
1	66	-34.33242	18.94967	240	Pg	2000	Podzol B				50 - 400	1250
1	66	-34.33242	18.94967	240	Pg	2000	Podzol B				400 - 800	1250
1	66	-34.33242	18.94967	240	Pg	2000	Uncon No Wet				800 - 1200	1250
1	66	-34.33242	18.94967	240	Pg	2000	Bedrock				1200 - 1250	1250
1	67	-34.33041	18.95475	129	Cf	1200	Orthic A	Hh	2100	Orthic A	0 - 40	350
1	67	-34.33041	18.95475	129	Cf	1200	E	Hh	2100	E	40 - 200	350
1	67	-34.33041	18.95475	129	Cf	1200	Litho B	Hh	2100	Podzol B	200 - 350	350
1	68	-34.32882	18.95662	128	Gk	2100	Orthic A				0 - 50	800
1	68	-34.32882	18.95662	128	Gk	2100	Podzol B				50 - 600	800
1	68	-34.32882	18.95662	128	Gk	2100	Saprolite				600 - 800	800

Table A.8: Continues

Round	Profile	Longtitude	Latitude	Altitude (m)	Soil Form	Soil Family	Diagnostic Horizon	Transition Form	Transition Family	Transition Horizon	Horizon Depth (mm)	Profile Total Depth (mm)
1	69	-34.32851	18.95699	131	Lt	1100	Orthic A				0 - 50	600
1	69	-34.32851	18.95699	131	Lt	1100	E				50 - 150	600
1	69	-34.32851	18.95699	131	Lt	1100	Podzol B				150 - 500	600
1	69	-34.32851	18.95699	131	Lt	1100	Uncon With Wet				500 - 600	600
1	70	-34.32818	18.95792	123	Cf	1200	Orthic A	Hh	2100	Orthic A	0 - 50	300
1	70	-34.32818	18.95792	123	Cf	1200	E	Hh	2100	E	50 - 250	300
1	70	-34.32818	18.95792	123	Cf	1200	Litho B	Hh	2100	Podzol B	250 - 300	300
1	71	-34.32770	18.95752	134	Cf	1200	Orthic A	Hh	2100	Orthic A	0 - 50	300
1	71	-34.32770	18.95752	134	Cf	1200	E	Hh	2100	E	50 - 250	300
1	71	-34.32770	18.95752	134	Cf	1200	Litho B	Hh	2100	Podzol B	250 - 300	300
1	72	-34.32730	18.95829	132	Cf	1200	Orthic A	Hh	2100	Orthic A	0 - 50	500
1	72	-34.32730	18.95829	132	Cf	1200	E	Hh	2100	E	50 - 300	500
1	72	-34.32730	18.95829	132	Cf	1200	Litho B	Hh	2100	Podzol B	300 - 500	500
1	73	-34.32643	18.95887	130	Pg	1000	Orthic A				0 - 50	400
1	73	-34.32643	18.95887	130	Pg	1000	Podzol B				50 - 200	400
1	73	-34.32643	18.95887	130	Pg	1000	Uncon No Wet				200 - 400	400
1	74	-34.32586	18.95974	132	Pg	1000	Orthic A				0 - 50	400
1	74	-34.32586	18.95974	132	Pg	1000	Podzol B				50 - 150	400
1	74	-34.32586	18.95974	132	Pg	1000	Uncon No Wet				150 - 400	400
1	75	-34.32484	18.96004	121	Wf	1100	Orthic A				0 - 100	450
1	75	-34.32484	18.96004	121	Wf	1100	Podzol B				100 - 400	450
1	75	-34.32484	18.96004	121	Wf	1100	Uncon With Wet				400 - 450	450

Table A.9: Continues

Round	Profile	Longtitude	Latitude	Altitude (m)	Soil Form	Soil Family	Diagnostic Horizon	Transition Form	Transition Family	Transition Horizon	Horizon Depth (mm)	Profile Total Depth (mm)
1	76	-34.32401	18.96007	124	Ka	1000	Orthic A				0 - 50	550
1	76	-34.32401	18.96007	124	Ka	1000	G				50 - 400	550
1	76	-34.32401	18.96007	124	Ka	1000	G				400 - 550	550
1	77	-34.32325	18.96010	115	Wf	1100	Orthic A				0 - 50	750
1	77	-34.32325	18.96010	115	Wf	1100	Podzol B				50 - 300	750
1	77	-34.32325	18.96010	115	Wf	1100	Podzol B				300 - 700	750
1	77	-34.32325	18.96010	115	Wf	1100	Uncon With Wet				700 - 750	750
1	78	-34.32210	18.96039	101	Hh	2100	Orthic A				0 - 50	400
1	78	-34.32210	18.96039	101	Hh	2100	E				50 - 150	400
1	78	-34.32210	18.96039	101	Hh	2100	Podzol B				150 - 350	400
1	78	-34.32210	18.96039	101	Hh	2100	Saprolite				350 - 400	400
1	79	-34.20085	18.56284	260	Wf	1100	Orthic A				0 - 100	300
1	79	-34.20085	18.56284	260	Wf	1100	Podzol B				100 - 250	300
1	79	-34.20085	18.56284	260	Wf	1100	Uncon With Wet				250 - 300	300
1	80	-34.20108	18.56545	270	Fw	1210	Orthic A	Lt	1100	Orthic A	0 - 200	600
1	80	-34.20108	18.56545	270	Fw	1210	E	Lt	1100	E / Podzol B	200 - 600	600
1	81	-34.33452	18.94667	311	Fw	1100	Orthic A	Pg	1000	Orthic A	0 - 250	1000
1	81	-34.33452	18.94667	311	Fw	1100	E	Pg	1000	Podzol B	250 - 600	1000
1	81	-34.33452	18.94667	311	Fw	1100	E	Pg	1000	Podzol B	600 - 1000	1000
1	82	-34.33542	18.94352	352	Pg	1000	Orthic A				0 - 100	650
1	82	-34.33542	18.94352	352	Pg	1000	Podzol B				100 - 400	650
1	82	-34.33542	18.94352	352	Pg	1000	Podzol B				400 - 600	650

Table A.10: Continues

Round	Profile	Longtitude	Latitude	Altitude (m)	Soil Form	Soil Family	Diagnostic Horizon	Transition Form	Transition Family	Transition Horizon	Horizon Depth (mm)	Profile Total Depth (mm)
1	82	-34.33542	18.94352	352	Pg	1000	Uncon No Wet				600 - 650	650
1	83	-34.33654	18.94434	357	Gk	2100	Orthic A				0 - 300	1050
1	83	-34.33654	18.94434	357	Gk	2100	Podzol B				300 - 1000	1050
1	83	-34.33654	18.94434	357	Gk	2100	Saprolite				1000 - 1050	1050
1	84	-34.33654	18.94502	363	Gk	2100	Orthic A				0 - 100	250
1	84	-34.33654	18.94502	363	Gk	2100	Podzol B				100 - 200	250
1	84	-34.33654	18.94502	363	Gk	2100	Saprolite				200 - 250	250
2	1	-34.33663	18.94592	369	Gs	2211	Orthic A	Gk	2100	Orthic A	0 - 50	110
2	1	-34.33663	18.94592	369	Gs	2211	Litho B	Gk	2100	Podzol B	50 - 150	110
2	2	-34.33670	18.94542	364	Hh	1200	Orthic A				0 - 100	350
2	2	-34.33670	18.94542	364	Hh	1200	E				100 - 200	350
2	2	-34.33670	18.94542	364	Hh	1200	Podzol B				200 - 280	350
2	2	-34.33670	18.94542	364	Hh	1200	Podzol B				280 - 350	350
2	4	-34.33583	18.94276	355	Pg	2000	Orthic A				0 - 50	350
2	4	-34.33583	18.94276	355	Pg	2000	Podzol B				50 - 250	350
2	4	-34.33583	18.94276	355	Pg	2000	Uncon No Wet				250 - 350	350
2	5	-34.33493	18.94630	330	Pg	1000	Orthic A				0 - 100	350
2	5	-34.33493	18.94630	330	Pg	1000	Podzol B				100 - 250	350
2	5	-34.33493	18.94630	330	Pg	1000	Uncon No Wet				250 - 350	350
2	7	-34.33402	18.94814	277	Fw	1210	Orthic A	Lt	1100	Orthic A	0 - 50	350
2	7	-34.33402	18.94814	277	Fw	1210	E	Lt	1100	E / Podzol B	50 - 350	350
2	10	-34.33229	18.95235	175	Pg	1000	Orthic A				0 - 20	300
2	10	-34.33229	18.95235	175	Pg	1000	Podzol B				20 - 250	300
2	10	-34.33229	18.95235	175	Pg	1000	Podzol B				250 - 300	300

Table A.11: Continues

Round	Profile	Longtitude	Latitude	Altitude (m)	Soil Form	Soil Family	Diagnostic Horizon	Transition Form	Transition Family	Transition Horizon	Horizon Depth (mm)	Profile Total Depth (mm)
2	11	-34.33086	18.95496	162	Pg	1000	Orthic A				0 - 50	300
2	11	-34.33086	18.95496	162	Pg	1000	Podzol B				50 - 250	300
2	11	-34.33086	18.95496	162	Pg	1000	Uncon No Wet				250 - 300	300
2	12	-34.32999	18.95570	143	Pg	1000	Orthic A				0 - 20	120
2	12	-34.32999	18.95570	143	Pg	1000	Podzol B				20 - 100	120
2	12	-34.32999	18.95570	143	Pg	1000	Uncon No Wet				100 - 120	120
2	13	-34.32877	18.95674	123	Wf	1100	Orthic A				0 - 80	1100
2	13	-34.32877	18.95674	123	Wf	1100	Podzol B				80 - 350	1100
2	13	-34.32877	18.95674	123	Wf	1100	Podzol B				350 - 500	1100
2	13	-34.32877	18.95674	123	Wf	1100	Uncon With Wet				500 - 750	1100
2	13	-34.32877	18.95674	123	Wf	1100	Uncon With Wet				750 - 1100	1100
2	14	-34.32878	18.95669	122	Wf	1100	Orthic A				0 - 50	1100
2	14	-34.32878	18.95669	122	Wf	1100	Podzol B				50 - 400	1100
2	14	-34.32878	18.95669	122	Wf	1100	Podzol B				400 - 800	1100
2	14	-34.32878	18.95669	122	Wf	1100	Uncon With Wet				800 - 1100	1100
2	15	-34.32743	18.95870	120	Cf	1200	Orthic A	Hh	2100	Orthic A	0 - 100	350
2	15	-34.32743	18.95870	120	Cf	1200	E	Hh	2100	E	100 - 300	350
2	15	-34.32743	18.95870	120	Cf	1200	Litho B	Hh	2100	Podzol B	300 - 350	350
2	16	-34.32652	18.95888	126	Pg	1200	Orthic A				0 - 50	400
2	16	-34.32652	18.95888	126	Pg	1200	Podzol B				50 - 100	400
2	16	-34.32652	18.95888	126	Pg	1200	Podzol B				100 - 300	400
2	16	-34.32652	18.95888	126	Pg	1200	Uncon No Wet				300 - 400	400

Table A.12: Continues

Round	Profile	Longtitude	Latitude	Altitude (m)	Soil Form	Soil Family	Diagnostic Horizon	Transition Form	Transition Family	Transition Horizon	Horizon Depth (mm)	Profile Total Depth (mm)
2	17	-34.32561	18.95990	132	Cf	1200	Orthic A	Hh	2100	Orthic A	0 - 100	260
2	17	-34.32561	18.95990	132	Cf	1200	E	Hh	2100	E	100 - 250	260
2	17	-34.32561	18.95990	132	Cf	1200	Litho B	Hh	2100	Podzol B	250 - 260	260
2	19	-34.32359	18.96002	123	Wf	1000	Orthic A				0 - 50	550
2	19	-34.32359	18.96002	123	Wf	1000	Podzol B				50 - 500	550
2	19	-34.32359	18.96002	123	Wf	1000	Uncon With Wet				500 - 550	550
2	20	-34.32881	18.95955	72	Cc	1100	Orthic A				0 - 200	1110
2	20	-34.32881	18.95955	72	Cc	1100	E				200 - 400	1110
2	20	-34.32881	18.95955	72	Cc	1100	Podzol B				400 - 700	1110
2	20	-34.32881	18.95955	72	Cc	1100	Podzol B				700 - 1000	1110
2	20	-34.32881	18.95955	72	Cc	1100	Uncon No wet				1000 -1110	1110
2	21	-34.32865	18.96140	83	Fw	1100	Orthic A	Pg	1000	Orthic A	0 - 150	800
2	21	-34.32865	18.96140	83	Fw	1100	E	Pg	1000	Podzol B	150 - 450	800
2	21	-34.32865	18.96140	83	Fw	1100	E	Pg	1000	Podzol B	450 - 800	800
2	22	-34.32831	18.96091	80	Fw	1100	Orthic A				0 - 200	1100
2	22	-34.32831	18.96091	80	Fw	1100	E				200 - 600	1100
2	22	-34.32831	18.96091	80	Fw	1100	E				600 - 1100	1100
2	25	-34.32912	18.96171	117	Cf	1200	Orthic A	Hh	2100	Orthic A	0 - 50	300
2	25	-34.32912	18.96171	117	Cf	1200	E	Hh	2100	E	50 - 250	300
2	25	-34.32912	18.96171	117	Cf	1200	Litho B	Hh	2100	Podzol B	250 - 300	300
2	26	-34.33023	18.96205	170	Gs	2211	Orthic A				0 - 50	100
2	26	-34.33023	18.96205	170	Gs	2211	Litho B				50 - 100	100
2	27	-34.33080	18.96284	194	Cf	1200	Orthic A	Hh	2100	Orthic A	0 - 20	250

Table A.13: Continues

Round	Profile	Longtitude	Latitude	Altitude (m)	Soil Form	Soil Family	Diagnostic Horizon	Transition Form	Transition Family	Transition Horizon	Horizon Depth (mm)	Profile Total Depth (mm)
2	27	-34.33080	18.96284	194	Cf	1200	E	Hh	2100	E	20 - 200	250
2	27	-34.33080	18.96284	194	Cf	1200	Litho B	Hh	2100	Podzol B	200 - 250	250
2	29	-34.32952	18.96583	197	Cf	1200	Orthic A	Hh	2100	Orthic A	0 - 50	150
2	29	-34.32952	18.96583	197	Cf	1200	E	Hh	2100	E	50 - 100	150
2	29	-34.32952	18.96583	197	Cf	1200	Litho B	Hh	2100	Podzol B	100 - 150	150
2	30	-34.32859	18.96563	165	Cf	1200	Orthic A	Hh	2100	Orthic A	0 - 50	300
2	30	-34.32859	18.96563	165	Cf	1200	E	Hh	2100	E	50 - 120	300
2	30	-34.32859	18.96563	165	Cf	1200	E	Hh	2100	E	120 - 240	300
2	30	-34.32859	18.96563	165	Cf	1200	Litho B	Hh	2100	Podzol B	240 - 300	300
2	31	-34.32720	18.96505	127	Cf	1200	Orthic A	Hh	2100	Orthic A	0 - 20	250
2	31	-34.32720	18.96505	127	Cf	1200	E	Hh	2100	E	20 - 200	250
2	31	-34.32720	18.96505	127	Cf	1200	Litho B	Hh	2100	Podzol B	200 - 250	250
2	32	-34.32352	18.96489	62	Pg	1000	Orthic A				0 - 100	1100
2	32	-34.32352	18.96489	62	Pg	1000	Podzol B				150 - 200	1100
2	32	-34.32352	18.96489	62	Pg	1000	Podzol B				200 - 300	1100
2	32	-34.32352	18.96489	62	Pg	1000	Podzol B				300 - 400	1100
2	32	-34.32352	18.96489	62	Pg	1000	Podzol B				400 - 800	1100
2	32	-34.32352	18.96489	62	Pg	1000	Uncon No Wet				800 - 1100	1100
2	33	-34.32477	18.96478	58	Pg	1000	Orthic A				0 - 200	1100
2	33	-34.32477	18.96478	58	Pg	1000	Podzol B				200 - 400	1100
2	33	-34.32477	18.96478	58	Pg	1000	Podzol B				400 - 500	1100
2	33	-34.32477	18.96478	58	Pg	1000	Podzol B				500 - 800	1100
2	33	-34.32477	18.96478	58	Pg	1000	Uncon No Wet				800 - 1100	1100

Table A.14: Continues

Round	Profile	Longtitude	Latitude	Altitude (m)	Soil Form	Soil Family	Diagnostic Horizon	Transition Form	Transition Family	Transition Horizon	Horizon Depth (mm)	Profile Total Depth (mm)
2	34	-34.32549	18.96740	73	Cf	1200	Orthic A	Pg	1000	Orthic A	0 - 50	400
2	34	-34.32549	18.96740	73	Cf	1200	E	Pg	1000	Podzol B	50 - 250	400
2	34	-34.32549	18.96740	73	Cf	1200	E	Pg	1000	Podzol B	250 - 350	400
2	34	-34.32549	18.96740	73	Cf	1200	Litho B	Pg	1000	Podzol B	350 - 400	400

Table A.3: Kogelberg laboratory analyses results.

Round	Profile	Soil Form	Soil Series	Diagnostic Horizon	pH H20	pH KCl	EC (uS/cm)	pH NaF	SAND %	SILT %	CLAY %	OM %	Co Frac %	Sand Grade	Texture Class
1	12	Cc	2000	Orthic A	6.43	5.93	62.5		85.0	6.8	6.2	2.0	0.0	Fi Sand	LOAMY SAND
1	12	Cc	2000	E	6.6	5.95	31.4		89.0	6.6	2.9	1.4	0.0	Fi Sand	SAND
1	12	Cc	2000	Podzol	6.41	6.07	9.35	9.44	91.0	8.4	0.5	0.1	0.0	Fi Sand	SAND
1	12	Cc	2000	Podzol	6.33	4.84	29.4	12.31	81.0	10.2	4.5	4.3	0.0	Fi Sand	LOAMY SAND
1	12	Cc	2000	Unspec No Wet	6.41	5.14	14.09		84.6	10.2	4.8	0.3	0.0	Fi Sand	LOAMY SAND
1	26	Cf	1200	Orthic A	4.87	3.32	49.2		90.2	4.0	1.6	4.2	4.7	Med Sand	SAND
1	26	Cf	1200	E	5.31	3.39	23.4		94.1	3.7	1.0	1.3	72.3	Co Sand	SAND
1	26	Cf	1200	Litho B	5.55	3.54	18.38		94.3	4.3	0.4	1.1	64.6	Co Sand	SAND
1	36	Wf	1100	Orthic A	4.15	3.1	105.1		94.5	-5.9	2.6	8.8	0.0	Co Sand	SAND
1	36	Wf	1100	Podzol	4.48	3.03	57.3	7.37	94.9	-1.3	1.1	5.2	0.0	Co Sand	SAND
1	36	Wf	1100	Uncon	5.3	4.11	13.11		96.1	2.7	0.7	0.5	3.4	Co Sand	SAND
1	49	Cf	1200	Orthic A	4.9	3.56	50.5		86.8	4.5	1.6	7.1	70.9	Co Sand	SAND
1	49	Cf	1200	E	6.18	5.06	22.2		91.1	7.9	0.7	0.4	16.3	Co Sand	SAND
1	49	Cf	1200	E	5.73	4.28	11.18		92.5	6.0	1.2	0.3	3.0	Co Sand	SAND
2	2	Hh	1200	Orthic A	3.9	3.15	63.3		87.4	-3.4	3.6	12.5	0.0	Co Sand	SAND
2	2	Hh	1200	E	4.05	3.6	30.1		89.5	6.4	2.0	2.1	25.1	Co Sand	SAND
2	2	Hh	1200	Podzol	4.04	3.68	27.7	7.54	87.0	8.3	3.3	1.3	4.8	Co Sand	SAND
2	2	Hh	1200	Saprolite	4.18	3.71	33.2		87.6	7.4	2.8	2.2	25.3	Co Sand	SAND
2	4	Pg	2000	Orthic A	4.17	3.21	40.7		85.8	-2.0	3.0	13.1	0.0	Co Sand	LOAMY SAND

Table A.3: Continues

Round	Profile	Soil Form	Soil Series	Diagnostic Horizon	pH H20	pH KCl	EC (uS/cm)	pH NaF	SAND %	SILT %	CLAY %	OM %	Co Frac %	Sand Grade	Texture Class
2	4	Pg	2000	Podzol	4.17	3.07	22.4	6.97	88.0	4.1	1.5	6.4	1.3	Co Sand	SAND
2	4	Pg	2000	Uncon No Wet	4.26	3.28	17.23		89.2	6.8	2.1	1.9	8.1	Co Sand	SAND
2	7	Fw	1100	Orthic A	6.86	6.05	626		28.5	51.3	6.8	13.3	0.0	Fi Sand	SILTY LOAM
2	7	Fw	1100	E	6.03	5.06	83.5		76.2	13.7	5.8	4.3	18.2	Fi Sand	LOAMY SAND
2	11	Pg	1000	Orthic A	4.57	3.27	61.6		78.7	2.0	5.0	14.4	0.0	Fi Sand	LOAMY SAND
2	11	Pg	1000	Podzol	4.36	0.05	65.9	7.45	79.1	11.3	2.7	6.9	0.0	Fi Sand	LOAMY SAND
2	11	Pg	1000	Uncon No Wet	4.64	3.26	51		79.6	13.9	3.6	2.9	12.4	Fi Sand	LOAMY SAND
2	13	Wf	1100	Orthic A	4.84	3.58	81.1		83.7	2.9	4.8	8.6	0.0	Fi Sand	LOAMY SAND
2	13	Wf	1100	Podzol	5.29	3.88	28.4	8.51	91.5	5.4	2.0	1.0	0.0	Fi Sand	SAND
2	13	Wf	1100	Podzol	5.39	3.83	25.4	8.24	93.2	3.1	2.2	1.5	0.0	Fi Sand	SAND
2	13	Wf	1100	Uncon Wet	5.43	3.81	24.9		93.0	3.2	1.7	2.1	0.0	Fi Sand	SAND
2	13	Wf	1100	Uncon Wet	5.44	3.76	30.5		91.7	2.1	2.7	3.5	0.0	Fi Sand	SAND
2	15	Cf	1200	Orthic A	5.49	3.91	34.7		87.8	6.2	3.4	2.7	6.7	Fi Sand	SAND
2	15	Cf	1200	E	5.65	3.66	48.9		87.0	6.8	4.1	2.1	14.8	Fi Sand	SAND
2	15	Cf	1200	Litho B	5.76	3.88	30		86.6	7.9	3.9	1.6	37.1	Fi Sand	SAND
2	20	Cc	1000	Orthic A	5.43	3.65	21.1		93.8	4.6	0.4	1.2	5.2	Co Sand	SAND
2	20	Cc	1000	E	5.88	4.1	9.39		96.1	3.4	0.3	0.2	2.9	Co Sand	SAND
2	20	Cc	1000	Podzol	5.86	4.42	10.15	9.12	95.7	3.2	1.1	0.1	2.0	Co Sand	SAND
2	20	Cc	1000	Podzol	5.75	4.45	10.7	9.88	93.6	5.7	0.6	0.2	2.6	Co Sand	SAND

Table A.3: Continues

Round	Profile	Soil Form	Soil Series	Diagnostic Horizon	pH H20	pH KCl	EC (uS/cm)	pH NaF	SAND %	SILT %	CLAY %	OM %	Co Frac %	Sand Grade	Texture Class
2	22	Fw	1100	Orthic A	4.33	3.49	55.8		87.0	-4.4	2.2	15.2	0.0	Co Sand	SAND
2	22	Fw	1100	E	5.41	4.03	16.26		93.2	3.7	2.2	0.8	1.4	Co Sand	SAND
2	22	Fw	1100	E	5.98	3.69	14.94		92.7	5.9	0.7	0.7	3.0	Co Sand	SAND

Table A.4: Kogelberg hydraulic property estimations.

Round	Profile	Soil Form	Soil Series	Diagnostoc Horizon	FC %	Saturation %	PAW (cm/cm)	Ksat (mm/hr)	Matric Bulk Density (g/cm3)
1	12	Cc	2000	Orthic A	10.7	44.6	0.1	92.9	1.5
1	12	Cc	2000	E	7.4	44.4	0.1	128.9	1.5
1	12	Cc	2000	Podzol	5.2	41.8	0.0	144.4	1.5
1	12	Cc	2000	Podzol	14.6	50.6	0.1	109.8	1.3
1	12	Cc	2000	Unspec No Wet	7.8	41.0	0.1	97.0	1.6
1	26	Cf	1200	Orthic A	11.0	51.5	0.1	142.4	1.3
1	26	Cf	1200	E	5.7	45.0	0.0	62.4	1.5
1	26	Cf	1200	Litho B	5.4	44.6	0.0	63.3	1.5
1	36	Wf	1100	Orthic A	16.9	60.0	0.0	173.1	1.1
1	36	Wf	1100	Podzol	11.7	52.8	0.1	152.8	1.3
1	36	Wf	1100	Uncon	4.9	43.1	0.0	146.9	1.5
1	49	Cf	1200	Orthic A	16.4	59.0	0.0	69.2	1.1
1	49	Cf	1200	E	5.1	42.7	0.0	130.1	1.5
1	49	Cf	1200	E	4.6	42.8	0.0	171.7	1.5
2	2	Hh	1200	Orthic A	19.1	60.4	0.1	155.6	1.1
2	2	Hh	1200	E	7.7	46.5	0.0	96.7	1.4
2	2	Hh	1200	Podzol	7.7	44.0	0.1	115.8	1.5
2	2	Hh	1200	Saprolite	8.8	46.2	0.0	85.5	1.4
2	4	Pg	2000	Orthic A	18.9	61.2	0.1	168.4	1.0

Table A.4: Continues

Round	Profile	Soil Form	Soil Series	Diagnostoc Horizon	FC %	Saturation %	PAW (cm/cm)	Ksat (mm/hr)	Matric Bulk Density (g/cm3)
2	4	Pg	2000	Podzol	15.1	57.3	0.1	165.7	1.1
2	4	Pg	2000	Uncon No Wet	7.6	45.9	0.1	126.5	1.4
2	7	Fw	1100	Orthic A	34.0	68.7	0.2	98.1	0.8
2	7	Fw	1100	E	16.2	50.5	0.1	72.3	1.3
2	11	Pg	1000	Orthic A	21.6	61.0	0.1	140.2	1.0
2	11	Pg	1000	Podzol	18.7	59.2	0.1	153.3	1.1
2	11	Pg	1000	Uncon No Wet	12.3	47.6	0.1	90.2	1.4
2	13	Wf	1100	Orthic A	20.2	60.1	0.1	142.1	1.1
2	13	Wf	1100	Podzol	5.7	44.2	0.0	154.7	1.5
2	13	Wf	1100	Podzol	6.2	45.3	0.0	152.5	1.5
2	13	Wf	1100	Uncon Wet	7.1	46.7	0.0	151.0	1.1
2	13	Wf	1100	Uncon Wet	9.9	49.4	0.1	140.4	1.3
2	15	Cf	1200	Orthic A	9.5	47.4	0.1	116.9	1.4
2	15	Cf	1200	E	9.4	45.6	0.1	90.9	1.4
2	15	Cf	1200	Litho B	8.7	44.4	0.0	60.2	1.5
2	20	Cc	1000	Orthic A	6.6	44.0	0.0	116.3	1.5
2	20	Cc	1000	E	5.3	42.0	0.0	123.1	1.5
2	20	Cc	1000	Podzol	5.1	41.8	0.0	125.9	1.5
2	20	Cc	1000	Podzol	5.3	42.0	0.0	123.1	1.5
2	22	Fw	1100	Orthic A	18.2	61.8	0.1	175.0	1.0

Table A.4: Continues

Round	Profile	Soil Form	Soil Series	Diagnostoc Horizon	FC %	Saturation %	PAW (cm/cm)	Ksat (mm/hr)	Matric Bulk Density (g/cm3)
2	22	Fw	1100	E	5.2	43.8	0.0	158.2	1.5
2	22	Fw	1100	E	5.1	43.6	0.0	155.7	1.5

Table A.5: Riverlands soil survey information.

Profile	Longitude	Latitude	Altitude m	Soil Form	Soil Family	Diagnostic Horizon	Transition Horizon	Horizon Depth (mm)	Dry Colour	Moist Colo	Comment
1	-33.483540	18.603650	137	Wf	1100	Orthic A	Tu 2110	0 - 200	10YR 5/2	10YR5/2	Mole activity, Hard rock at 2
1	-33.483540	18.603650	137	Wf	1100	Podzol B	Tu 2110	200 - 500	10YR 6/3	10YR 7/3	Mole activity, Hard rock at 2
1	-33.483540	18.603650	137	Wf	1100	Podzol B	Tu 2110	500 - 1400	10YR 7/4	10YR 7/4	
1	-33.483540	18.603650	137	Wf	1100	Podzol B	Tu 2110	1400 - 1600	10YR 8/2	10YR 8/4	
1	-33.483540	18.603650	137	Wf	1100	Uncon With Wet	Tu 2110	1600 - 2000	10YR 8/1	10YR 7/2	Hard rock at 2 m
2	-33.480230	18.587810	127	Lt	1100	Orthic A		0 - 50	10YR 6/3	10YR 6/2	Mole activity, Fine roots.
2	-33.480230	18.587810	127	Lt	1100	E		50 - 500	10YR 7/3	10YR 6/2	Mole activity, Fine roots.
2	-33.480230	18.587810	127	Lt	1100	Podzol B		500 - 1250	10YR 7/4	10YR 6/4	Thicker roots
3	-33.481110	18.592070	126	Lt	1000	Orthic A		0 -50	10YR 7/3	10YR 6/3	Mole activity, Fine roots.
3	-33.481110	18.592070	126	Lt	1000	E		50 - 600	10YR 7/3	10YR 6/2	Mole activity, Fine roots.
3	-33.481110	18.592070	126	Lt	1000	Podzol B		600 - 1200	10YR 7/4	10YR 6/4	Thicker roots
4	-33.481850	18.595460	128	Lt	1100	Orthic A	Vf 2110	0 - 60	10YR 5/3	10YR 4/4	Restioid patch, little other vegetation.
4	-33.481850	18.595460	128	Lt	1100	E	Vf 2110	60 - 260	10YR 7/4	10YR 6/4	Mole activity.
4	-33.481850	18.595460	128	Lt	1100	Podzol B	Vf 2110	260 - 800	10YR 7/3	10YR 7/3	
4	-33.481850	18.595460	128	Lt	1100	Uncon With Wet	Vf 2110	800 - 1200	10YR 6/3	10YR 4/3	
5	-33.482230	18.597390	130	Wf	1100	Orthic A	Tu 2110	0 - 80	10YR 5/3	10YR 5/4	Laterite outcrop within 5 m, Restioid patches.
5	-33.482230	18.597390	130	Wf	1100	Podzol B	Tu 2110	80 - 900	10YR 7/4	10YR 6/6	
5	-33.482230	18.597390	130	Wf	1100	Podzol B	Tu 2110	900 - 1000	10YR 7/3	10YR 6/4	
6	-33.490200	18.572790	119	Cc	1000	Orthic A		0 - 50	10YR 7/2	10YR 5/3	Hydrophobic topsoil
6	-33.490200	18.572790	119	Cc	1000	E		50 - 650	10YR 7/2	10YR 6/3	
6	-33.490200	18.572790	119	Cc	1000	Podzol B		650 - 1200	10YR 7/3	10YR 7/6	
6	-33.490200	18.572790	119	Cc	1000	Podzol B		1200 - 1600	10YR 7/3	10YR 6/4	
6	-33.490200	18.572790	119	Cc	1000	Podzol B		1600 - 1800	10YR 7/3	10YR 6/4	Moist at 1800 mm

Table A.5: Continues

Profile	Longitude	Latitude	Altitude m	Soil Form	Soil Family	Diagnostic Horizon	Transition Horizon	Horizon Depth (mm)	Dry Colour	Moist Colo	Comment
6	-33.490200	18.572790	119	Cc	1000	Uncon No Wet		1800 - 2000	10YR 8/3	10YR 7/2	Laterite granules
7	-33.490390	18.573330	123	Cc	1000	Orthic A		0 - 50	10YR 7/1	10YR 5/2	Hydrophobic
7	-33.490390	18.573330	123	Cc	1000	E		50 - 800	10YR 7/2	10YR 7/3	
7	-33.490390	18.573330	123	Cc	1000	Podzol B		800 - 1000	10YR 7/3	10YR 6/4	
7	-33.490390	18.573330	123	Cc	1000	Uncon With Wet		1000 - 1250	10YR 7/3	10YR 7/3	
8	-33.490470	18.574140	120	Lt	1100	Orthic A		0 - 50	10YR 5/2	10YR 5/1	
8	-33.490470	18.574140	120	Lt	1100	E		50 - 450	10YR 6/2	10YR 5/2	
8	-33.490470	18.574140	120	Lt	1100	Podzol B		450 - 650	10YR 6/2	10YR 5/3	
8	-33.490470	18.574140	120	Lt	1100	Uncon With Wet		650 - 850	10YR 5/4	10YR 4/3	
8	-33.490470	18.574140	120	Lt	1100	Uncon With Wet		850 - 1000	10YR 7/4	10YR 4/4	High coarse fraction, Laterite granules
9	-33.489660	18.574450	119	Wf	1100	Orthic A		0 - 80	10YR 7/2	10YR 6/2	Near monitoring well, Restiod strip
9	-33.489660	18.574450	119	Wf	1100	Podzol B		80 - 800	10YR 6/4	10YR 6/3	
9	-33.489660	18.574450	119	Wf	1100	Uncon With Wet		800 - 1000	10YR 6/3	10YR 7/4	Water table at 1 m, High coarse fraction.
10	-33.489500	18.573540	123	Lt	1100	Orthic A		0 - 50	10YR 7/1	10YR 6/1	Soil moist
10	-33.489500	18.573540	123	Lt	1100	E		50 - 650	10YR 7/2	10YR 7/3	Soil moist
10	-33.489500	18.573540	123	Lt	1100	Podzol B		650 - 1200	10YR 7/3	10YR 6/3	Soil moist
11	-33.489360	18.572820	119	Lt	1100	Orthic A		0 - 50	10YR 7/2	10YR 5/2	Close to 2 monitorring holes
11	-33.489360	18.572820	119	Lt	1100	E		50 - 400	10YR 7/2	10YR 5/2	
11	-33.489360	18.572820	119	Lt	1100	Podzol B		400 - 1200	10YR 7/3	10YR 6/4	800+ mm soil is moist
12	-33.488050	18.572940	121	Lt	1100	Orthic A		0 - 50	10YR 7/2	10YR 5/2	
12	-33.488050	18.572940	121	Lt	1100	E		50 - 400	10YR 7/3	10YR 5/3	
12	-33.488050	18.572940	121	Lt	1100	Podzol B		400 - 1000	10YR 7/4	10YR 6/4	Moist at 800 mm
13	-33.488320	18.573850	125	Lt	1100	Orthic A		0 - 50	10YR 7/3	10YR 5/3	Very fine sand / Falls through auger, knee high

Table A.5: Continues

Profile	Longitude	Latitude	Altitude m	Soil Form	Soil Family	Diagnostic Horizon	Transition Horizon	Horizon Depth (mm)	Dry Colour	Moist Colo	Comment
13	-33.488320	18.573850	125	Lt	1100	E		50 - 550	10YR 7/2	10YR 5/3	
13	-33.488320	18.573850	125	Lt	1100	Podzol B		550 - 1200	10YR 7/4	10YR 5/3	
14	-33.488260	18.574450	120	Lt	1100	Orthic A		0 - 50	10YR 6/2	10YR 6/2	Soil moist from 50 mm.
14	-33.488260	18.574450	120	Lt	1100	E		50 - 400	10YR 6/3	10YR 5/3	
14	-33.488260	18.574450	120	Lt	1100	Podzol B		400 - 800	10YR 6/4	10YR 6/4	
14	-33.488260	18.574450	120	Lt	1100	Uncon With Wet		800 - 1200	10YR 5/6	10YR 6/6	

Table A.615: Riverlands laboratory analyses results.

Profile	Soil Form	Soil Famil	Diagnostic Horizon	pH (H2O)	pH (KC)	pH (NaF)	EC (uS/cm)	OM %	Co Frac %	Sand %	Silt %	Clay %	Sand Grade	Texture Class
1	Wf	1100	Orthic A	6.6	6.1	0.0	36.2	1.6	0.1	94.8	3.6	2.0	Med Sand	SAND
1	Wf	1100	Podzol B	6.4	5.7	10.2	20.6	0.6	0.1	94.0	-2.2	4.3	Med Sand	SAND
1	Wf	1100	Podzol B	6.6	5.5	11.2	11.0	0.3	0.1	94.2	2.4	2.8	Med Sand	SAND
1	Wf	1100	Podzol B	6.6	5.3	11.4	15.9	0.1	0.0	94.7	-0.4	2.7	Med Sand	SAND
1	Wf	1100	Uncon With Wet	6.5	5.3	11.8	14.6	0.1	0.5	94.3	-1.9	4.8	Med Sand	SAND
2	Lt	1100	Orthic A	5.6	4.6	0.0	11.6	0.9	0.2	95.8	-0.4	4.2	Med Sand	SAND
2	Lt	1100	E	5.0	4.0	8.8	13.3	0.7	0.6	97.0	0.3	1.9	Med Sand	SAND
2	Lt	1100	Podzol B	6.5	5.0	10.8	14.1	0.3	0.8	96.1	1.5	3.1	Med Sand	SAND
3	Lt	1000	Orthic A	5.7	4.4	0.0	7.6	0.4	0.2	96.7	-0.3	0.3	Med Sand	LOAMY SAND
3	Lt	1000	E	5.1	4.1	9.1	5.6	0.3	0.1	97.1	2.1	5.5	Med Sand	LOAMY SAND
3	Lt	1000	Podzol B	5.8	4.6	11.0	4.8	0.3	0.1	96.0	-0.3	2.0	Med Sand	SAND
4	Lt	1100	Orthic A	5.9	4.6	0.0	10.4	0.4	0.3	97.2	-2.5	5.3	Med Sand	SAND
4	Lt	1100	E	6.0	4.7	10.3	7.6	0.3	0.1	95.8	0.5	1.4	Med Sand	SAND
4	Lt	1100	Podzol B	6.4	5.2	10.5	11.4	0.1	0.2	96.5	4.9	-1.2	Med Sand	SAND
4	Lt	1100	Uncon With Wet	5.7	4.4	8.7	8.6	0.4	0.2	97.2	0.4	2.1	Med Sand	SAND
5	Wf	1100	Orthic A	6.1	4.7	0.0	24.8	1.1	1.0	94.8	2.9	2.0	Med Sand	SAND
5	Wf	1100	Podzol B	6.6	5.9	9.3	13.7	0.1	0.4	97.8	-2.5	4.1	Med Sand	SAND
5	Wf	1100	Podzol B	6.4	5.8	9.8	23.6	0.3	32.4	97.0	-0.1	4.8	Med Sand	SAND
6	Cc	1000	Orthic A	5.5	4.7	0.0	12.7	0.6	0.0	97.1	-0.7	2.9	Med Sand	LOAMY SAND
6	Cc	1000	E	5.5	4.4	8.9	7.9	0.4	0.0	97.3	-0.6	0.7	Med Sand	SAND
6	Cc	1000	Podzol B	5.4	4.6	9.5	6.2	0.3	0.0	96.9	-1.4	2.6	Med Sand	LOAMY SAND
6	Cc	1000	Podzol B	5.6	4.9	10.6	11.1	0.1	0.1	96.9	-0.1	1.0	Med Sand	SAND
6	Cc	1000	Podzol B	6.2	5.3	11.3	52.4	0.3	15.3	96.7	-0.3	2.9	Med Sand	SAND
6	Cc	1000	Uncon No Wet	6.8	5.6	11.5	116.4	0.5	2.2	89.1	-1.7	9.4	Med Sand	SANDY LOAM
7	Cc	1000	Orthic A	5.2	4.1	0.0	8.6	0.6	0.0	97.0	3.6	2.5	Med Sand	SAND
7	Cc	1000	E	5.2	4.2	8.7	6.3	0.3	0.0	96.6	-1.1	3.0	Med Sand	SAND

Table A.6: Continues

Profile	Soil Form	Soil Famil	Diagnostic Horizon	pH (H2O)	pH (KC)	pH (NaF)	EC (uS/cm)	OM %	Co Frac %	Sand %	Silt %	Clay %	Sand Grade	Texture Class
7	Cc	1000	Podzol B	5.6	4.6	10.5	13.0	0.3	7.5	96.6	-0.3	0.2	Med Sand	SAND
7	Cc	1000	Uncon With Wet	6.1	5.1	10.6	14.4	0.0	2.3	96.0	-1.3	3.1	Med Sand	SAND
8	Lt	1100	Orthic A	5.4	4.4	0.0	13.0	0.4	0.0	97.2	4.6	1.2	Fi Sand	LOAMY SAND
8	Lt	1100	E	5.3	4.4	8.7	7.9	0.4	0.0	97.6	1.4	2.1	Med Sand	SAND
8	Lt	1100	Podzol B	5.3	4.6	9.9	8.9	0.3	0.0	97.8	-1.6	4.8	Med Sand	SAND
8	Lt	1100	Uncon With Wet	5.7	4.6	11.6	19.6	0.5	0.0	96.9	-1.1	4.9	Med Sand	SAND
8	Lt	1100	Uncon With Wet	5.9	5.1	11.2	45.4	0.1	16.5	96.9	-3.4	6.6	Med Sand	SAND
9	Wf	1100	Orthic A	5.5	4.5	0.0	12.4	0.4	0.0	97.9	2.2	-0.1	Med Sand	LOAMY SAND
9	Wf	1100	Podzol B	5.1	4.6	11.0	16.9	0.4	0.0	97.4	0.6	3.6	Med Sand	LOAMY SAND
9	Wf	1100	Uncon With Wet	5.4	5.4	11.1	33.6	0.4	55.3	95.0	1.4	3.3	Med Sand	LOAMY SAND
10	Lt	1100	Orthic A	5.2	4.3	0.0	8.8	0.4	0.0	97.4	-1.0	1.5	Fi Sand	SAND
10	Lt	1100	E	5.9	4.7	9.2	5.6	0.0	0.0	97.4	0.4	-0.5	Med Sand	SAND
10	Lt	1100	Podzol B	6.2	4.8	10.3	5.6	0.1	0.0	96.7	6.9	-0.6	Med Sand	SAND
11	Lt	1100	Orthic A	5.8	4.7	0.0	11.3	0.6	0.0	96.8	5.1	0.1	Med Sand	SAND
11	Lt	1100	E	5.7	4.5	9.1	9.5	0.4	0.0	96.5	-0.9	1.3	Med Sand	LOAMY SAND
11	Lt	1100	Podzol B	5.7	4.6	11.9	8.4	0.4	0.0	94.7	-1.2	5.5	Med Sand	SAND
12	Lt	1100	Orthic A	5.8	4.6	0.0	9.8	0.6	0.0	97.1	2.8	-0.5	Med Sand	SAND
12	Lt	1100	E	5.5	4.5	9.9	8.2	0.3	0.0	96.9	-2.3	2.0	Med Sand	SAND
12	Lt	1100	Podzol B	5.8	4.7	11.6	5.6	0.3	0.0	96.3	-2.2	2.9	Med Sand	SAND
13	Lt	1100	Orthic A	5.8	4.7	0.0	7.6	0.4	0.0	98.2	0.3	0.6	Med Sand	LOAMY SAND
13	Lt	1100	E	5.8	4.8	9.4	7.0	0.3	0.0	97.9	0.4	2.8	Med Sand	LOAMY SAND
13	Lt	1100	Podzol B	5.9	4.7	10.2	5.7	0.1	0.0	97.7	0.4	1.2	Med Sand	LOAMY SAND
14	Lt	1100	Orthic A	5.3	4.4	0.0	8.8	0.4	0.0	96.9	2.7	-1.2	Fi Sand	SAND
14	Lt	1100	E	5.7	4.6	9.7	7.2	0.4	0.0	97.2	6.2	-0.3	Med Sand	SAND
14	Lt	1100	Podzol B	6.0	4.9	11.4	8.7	0.1	0.0	96.1	-1.3	5.2	Med Sand	SAND
14	Lt	1100	Uncon With Wet	6.0	4.6	11.8	7.8	0.4	0.0	94.9	0.8	3.3	Med Sand	SAND

Table A.16: Riverlands hydraulic property estimations.

Profile	Soil Form	Soil Famil	Diagnostic Horizon	FC %	Saturation %	PAW %	Ksat (mm/hr)	Matric BulK Density (g/cm3)
1	Wf	1100	Orthic A	7.70	47.60	4	151.36	1.39
1	Wf	1100	Podzol B	6.80	42.30	5	116.46	1.53
1	Wf	1100	Podzol B	5.70	42.10	4	137.84	1.54
1	Wf	1100	Podzol B	4.40	42.30	3	155.36	1.53
1	Wf	1100	Uncon With Wet	4.30	42.10	3	158.81	1.54
2	Lt	1100	Orthic A	6.70	42.40	5	125.44	1.53
2	Lt	1100	E	7.60	43.10	5	114.17	1.51
2	Lt	1100	Podzol B	4.70	42.70	3	148.09	1.52
3	Lt	1000	Orthic A	7.80	40.70	5	90.45	1.57
3	Lt	1000	E	8.00	41.20	5	90.74	1.56
3	Lt	1000	Podzol B	5.10	42.40	4	145.35	1.53
4	Lt	1100	Orthic A	5.50	42.20	4	140.35	1.53
4	Lt	1100	E	7.10	41.60	4	104.39	1.55
4	Lt	1100	Podzol B	5.30	42.60	5	164.08	1.52
4	Lt	1100	Uncon With Wet	3.90	42.60	4	210.10	1.52
5	Wf	1100	Orthic A	7.10	43.80	5	139.23	1.49
5	Wf	1100	Podzol B	5.30	41.70	4	127.52	1.55
5	Wf	1100	Podzol B	6.20	41.50	3	64.64	1.55
6	Cc	1000	Orthic A	7.50	41.40	6	117.22	1.55
6	Cc	1000	E	5.30	42.00	4	142.19	1.54
6	Cc	1000	Podzol B	7.80	41.90	6	116.00	1.54
6	Cc	1000	Podzol B	4.80	42.00	4	149.90	1.54
6	Cc	1000	Podzol B	5.30	42.30	3	112.95	1.53
6	Cc	1000	Uncon No Wet	12.80	39.80	5	45.18	1.59
7	Cc	1000	Orthic A	4.80	42.90	4	148.47	1.51

Table A.7: Continues

Profile	Soil Form	Soil Famil	Diagnostic Horizon	FC %	Saturation %	PAW %	Ksat (mm/hr)	Matric BulK Density (g/cm3)
7	Cc	1000	E	4.50	44.00	3	170.92	1.49
7	Cc	1000	Podzol B	3.80	42.90	3	200.79	1.51
7	Cc	1000	Uncon With Wet	3.70	42.70	3	216.11	1.52
8	Lt	1100	Orthic A	8.10	41.20	7	124.73	1.56
8	Lt	1100	E	3.80	42.90	3	200.79	1.51
8	Lt	1100	Podzol B	4.50	44.00	3	170.92	1.49
8	Lt	1100	Uncon With Wet	4.10	43.40	3	183.68	1.50
8	Lt	1100	Uncon With Wet	4.10	43.40	3	183.68	1.50
9	Wf	1100	Orthic A	8.80	40.90	8	116.41	1.57
9	Wf	1100	Podzol B	8.50	41.00	6	98.62	1.56
9	Wf	1100	Uncon With Wet	6.90	41.80	3	49.74	1.54
10	Lt	1100	Orthic A	4.50	42.50	3	152.59	1.52
10	Lt	1100	E	4.70	42.70	3	150.33	1.52
10	Lt	1100	Podzol B	4.50	42.50	3	152.59	1.52
11	Lt	1100	Orthic A	4.90	43.10	4	146.92	1.51
11	Lt	1100	E	8.40	41.70	7	109.33	1.55
11	Lt	1100	Podzol B	4.70	42.30	4	150.00	1.53
12	Lt	1100	Orthic A	6.30	43.60	4	125.58	1.49
12	Lt	1100	E	5.30	42.00	4	128.82	1.54
12	Lt	1100	Podzol B	6.30	43.60	4	125.58	1.49
13	Lt	1100	Orthic A	8.20	40.80	7	108.51	1.57
13	Lt	1100	E	7.60	41.40	5	106.72	1.55
13	Lt	1100	Podzol B	6.90	40.80	6	122.98	1.57
14	Lt	1100	Orthic A	4.80	42.90	4	148.47	1.51
14	Lt	1100	E	4.80	42.90	4	148.47	1.51
14	Lt	1100	Podzol B	4.10	43.40	3	183.68	1.50
14	Lt	1100	Uncon With Wet	5.60	42.40	4	138.82	1.53

Appendix B – Data Processing

K1: Cartref 1200

Coordinates (Decimal Degrees):
S34.322 / E18.969
Altitude (m.a.s.l.):
53
Position (Terrain):
Foot-slope position on a convex hill
Vegetation:
Scattered grass and fynbos (Fire affected)

Horizon	Diagnostic Horizon	Depth	pH (H_2O)	Clay %	Coarse Fraction %	Sand Grade	Texture Class
A1	Orthic A	0 – 15	4.89	2.75	13.3	Coarse Sand	Sand
E1	E	15 – 30	5.22	1.4	31.7	Coarse Sand	Sand
B1	Lithocutanic B	30 – 50	4.88	1.7	21.6	Coarse Sand	Sand

Figure B.8: K1 site description summary.

K2: Fernwood 1110

Coordinates (Decimal Degrees):
S34.323 / E18.965
Altitude (m.a.s.l.):
50
Position (Terrain):
Adjacent to the stream on river terrace
Vegetation:
Lush riparian vegetation

Horizon	Diagnostic Horizon	Depth (cm)	pH (H_2O)	Clay %	Coarse Fraction %	Sand Grade	Texture Class
A1	Orthic A	0 - 15	5.13	1.6	0.9	Coarse Sand	Sand
E1	E	15 – 25	4.89	2.7	0.5	Coarse Sand	Sand
E2	E	25 – 40	4.63	3.95	0.85	Coarse Sand	Sand
E3	E	40 - 50	4.86	2.9	0.6	Coarse Sand	Sand

Figure B.2: K2 site description summary.

R1: Lamotte 1100

Coordinates (Decimal Degrees):
S33.481 / E18.591
Altitude (m.a.s.l.):
119
Position (Terrain):
Concave slope in lower lying area of the reserve
Vegetation:
Ankle to knee high grass with scattered burnt remnants of fynbos

Horizon	Diagnostic Horizon	Depth	pH (H_2O)	Clay %	Coarse Fraction %	Sand Grade	Texture Class
A1	Orthic A	0 – 10	6.46	2.0	0.0	Med Sand	Sand
E1	E	10 –30	6.35	2.15	0.3	Med Sand	Sand
E2	E	30 – 40	6.36	1.7	0.1	Med Sand	Sand
E3	E	40 - 70	6.35	1.7	0.1	Med Sand	Sand
B	Podzol B	70+	Augered with no sample taken				

Figure B.9: R1 site description summary.

R2: Vilafontes 2110 (Transition to Lamotte 1100)

Coordinates (Decimal Degrees):
S33.485 / E18.603
Altitude (m.a.s.l.):
127
Position (Terrain):
Convex slope on high lying area of the reserve
Vegetation:
Knee high grass plains with common lush restioid reeds

Horizon	Diagnostic Horizon	Depth	pH (H_2O)	Clay %	Coarse Fraction %	Sand Grade	Texture Class
A1	Orthic A	0 – 10	6.63	4.3	0.2	Med Sand	Sand
E1	E	10 – 30	5.72	4.8	6.8	Med Sand	Sand
B1	Neocutanic B (Podzol)	30 - 50	5.69	6.2	7.9	Med Sand	Sand
B2	Neocutanic B (Podzol)	50 – 70	5.16	9.9	12.3	Med Sand	Loamy Sand

Figure B.4: R2 site description summary.

Table B.1: Preferential flow test sites; pH and textural analyses.

SITE	SAMPLE	Diagnistic Horizon	Soil Form & Family	pH (H20)	pH (KCl)	pH (NaF)	EC (uS/cm)	SAND %	SILT %	CLAY %	OM %	Co Frac %	Sand Grade	Texture Class
K1	0 - 10	Orthic A	Cf 1200	4.89	3.69		16.73	89.3	3.4	2.9	7.3	9.7	Co Sand	SAND
K1	10 - 20	Orthic A / E1	Cf 1200	5.22	3.47	6.89	58.10	88.6	3.9	2.6	7.5	16.9	Co Sand	SAND
K1	20 - 30	E1	Cf 1200					87.6	6.1	1.4	6.3	31.7	Co Sand	SAND
K1	30 - 40	Lithocutanic B1	Cf 1200	4.99	3.57	6.84	50.70	89.1	6.1	2.0	4.7	22.1	Co Sand	SAND
K1	40 - 50	Lithocutanic B1	Cf 1200	4.77	3.71	6.97	61.40	91.2	5.1	1.4	3.6	21.1	Co Sand	SAND
K2	0 - 10	Orthic A	Fw 1110	5.13	3.37		40.40	91.1	6.6	1.6	2.3	0.9	Co Sand	SAND
K2	10 - 20	Orthic A / E1	Fw 1110	4.89	3.40	7.51	53.90	91.0	7.9	2.7	1.1	0.5	Co Sand	SAND
K2	20 - 30	E2	Fw 1110	4.73	3.21	7.38	72.60	88.4	9.7	5.4	1.8	0.5	Co Sand	SAND
K2	30 - 40	E2	Fw 1110	4.53	3.11	7.33	74.00	89.2	8.8	2.5	2.0	1.2	Co Sand	SAND
K2	40 - 50	E3	Fw 1110	4.86	3.38	7.47	40.90	90.5	8.4	2.9	1.0	0.6	Co Sand	SAND
R 1	0 - 10	Orthic A	Lt 1100	6.46	4.62		42.00	96.6	2.4	2.0	1.0	0.0	Med Sand	SAND
R 1	10 - 20	E1	Lt 1100	6.24	6.52	8.83	37.70	96.9	2.6	1.8	0.5	0.4	Med Sand	SAND
R 1	20 - 30	E1	Lt 1100	6.41	4.84	9.00	27.90	97.5	2.2	2.5	0.2	0.2	Med Sand	SAND
R 1	30 - 40	E2	Lt 1100	6.36	5.05	9.49	24.60	98.1	1.7	1.7	0.2	0.1	Med Sand	SAND
R 1	40 - 50	E3 / Podzol	Lt 1100	6.50	5.33	10.02	21.10	97.7	2.1	1.8	0.1	0.1	Med Sand	SAND
R 1	50 - 70	E3 / Podzol	Lt 1100	6.20	5.11	10.34	22.10	98.2	1.5	1.6	0.3	0.1	Med Sand	SAND
R 2	0 - 10	Orthic A	Vf 2110	6.63	5.29		61.60	95.2	4.2	4.3	0.4	0.2	Med Sand	SAND

Table B.1: Continues

SITE	SAMPLE	Diagnistic Horizon	Soil Form & Family	pH (H20)	pH (KCl)	pH (NaF)	EC (uS/cm)	SAND %	SILT %	CLAY %	OM %	Co Frac %	Sand Grade	Texture Class
R 2	10 - 20	E1	Vf 2110	5.60	4.68	7.67	45.30	91.4	7.8	5.3	0.7	5.7	Med Sand	SAND
R 2	20 - 30	E1	Vf 2110	5.85	4.28	8.31	48.30	90.7	8.5	4.2	0.7	7.8	Med Sand	SAND
R 2	30 - 40	Neocutanic B1	Vf 2110	5.66	4.31	8.36	50.10	88.9	10.6	5.6	0.4	7.0	Med Sand	SAND
R 2	40 - 50	Neocutanic B1	Vf 2110	5.71	4.40	8.23	49.90	88.8	10.7	6.7	0.3	8.7	Med Sand	SAND
R 2	50 - 70	Neocutanic B2	Vf 2110	5.16	4.38	8.49	58.60	87.1	12.5	9.9	0.2	12.3	Med Sand	LOAMY SAND

Table B.2: Calculation of saturated hydraulic conductivity from double ring infiltrometer data in the four test sites. (* Outliers)

Site	Total Infiltrated water in inner ring (mm)	Infiltrated Water Interval (mm)	Running Time (s)	Time Interval (sec)	Volume (mm3)	Area (mm2)	Q (mm3/sec)	Hydraulic Head (mm)	L (mm)	Vertical Flow K (cm/s)	Vertical Flow K (mm/hr)	Average Ksat per site (mm/hr)
K1	10	10	7	7	1654.68	1654.68	236.38	120	10	0.155	557.14	
K1	20	10	11	4	1654.68	1654.68	413.67	110	10	0.273	*981.82	
K1	30	10	17	6	1654.68	1654.68	275.78	100	10	0.183	660.00	
K1	40	10	27	10	1654.68	1654.68	165.47	90	10	0.111	400.00	
K1	50	10	36	9	1654.68	1654.68	183.85	80	10	0.125	450.00	
K1	60	10	50	14	1654.68	1654.68	118.19	70	10	0.082	293.88	
K1	70	10	62	12	1654.68	1654.68	137.89	60	10	0.097	350.00	
K1	80	10	67	5	1654.68	1654.68	330.94	50	10	0.240	*864.00	
K1	90	10	86	19	1654.68	1654.68	87.09	40	10	0.066	236.84	
K1	10	10	8	8	1654.68	1654.68	206.84	80	10	0.141	506.25	
K1	20	10	24	16	1654.68	1654.68	103.42	70	10	0.071	257.14	
K1	30	10	35	11	1654.68	1654.68	150.43	60	10	0.106	381.82	
K1	40	10	50	15	1654.68	1654.68	110.31	50	10	0.080	288.00	
K1	50	10	62	12	1654.68	1654.68	137.89	40	10	0.104	375.00	
K1	10	10	8	8	1654.68	1654.68	206.84	90	10	0.139	500.00	
K1	20	10	15	7	1654.68	1654.68	236.38	80	10	0.161	578.57	

Table B.2: Continues

Site	Total Infiltrated water in inner ring (mm)	Infiltrated Water Interval (mm)	Running Time (s)	Time Interval (sec)	Volume (mm3)	Area (mm2)	Q (mm3/sec)	Hydraulic Head (mm)	L (mm)	Vertical Flow K (cm/s)	Vertical Flow K (mm/hr)	Average Ksat per site (mm/hr)
K1	30	10	25	10	1654.68	1654.68	165.47	70	10	0.114	411.43	
K1	40	10	39	14	1654.68	1654.68	118.19	60	10	0.083	300.00	
K1	50	10	59	20	1654.68	1654.68	82.73	50	10	0.060	216.00	
K1	60	10	72	13	1654.68	1654.68	127.28	40	10	0.096	346.15	
K1	10	10	2	2	1654.68	1654.68	827.34	80	10	0.563	*2025.00	
K1	20	10	12	10	1654.68	1654.68	165.47	70	10	0.114	411.43	
K1	30	10	18	6	1654.68	1654.68	275.78	60	10	0.194	700.00	
K1	40	10	39	21	1654.68	1654.68	78.79	50	10	0.057	205.71	
K1	50	10	57	18	1654.68	1654.68	91.93	40	10	0.069	250.00	438.383
K2	10	10	25	25	1654.68	1654.68	66.19	130	10	0.043	155.08	
K2	20	10	49	24	1654.68	1654.68	68.95	120	10	0.045	162.50	
K2	30	10	85	36	1654.68	1654.68	45.96	110	10	0.030	109.09	
K2	40	10	120	35	1654.68	1654.68	47.28	100	10	0.031	113.14	
K2	50	10	156	36	1654.68	1654.68	45.96	90	10	0.031	111.11	
K2	60	10	204	48	1654.68	1654.68	34.47	80	10	0.023	84.38	
K2	70	10	241	37	1654.68	1654.68	44.72	70	10	0.031	111.20	
K2	80	10	285	44	1654.68	1654.68	37.61	60	10	0.027	95.45	117.744

Table B.2: Continues

Site	Total Infiltrated water in inner ring (mm)	Infiltrated Water Interval (mm)	Running Time (s)	Time Interval (sec)	Volume (mm3)	Area (mm2)	Q (mm3/sec)	Hydraulic Head (mm)	L (mm)	Vertical Flow K (cm/s)	Vertical Flow K (mm/hr)	Average Ksat per site (mm/hr)
R 1	10	10	9.00	9	1654.68	1654.68	183.85	90	10	0.123	*444.44	
R 1	20	10	28.00	19	1654.68	1654.68	87.09	80	10	0.059	213.16	
R 1	30	10	48.00	20	1654.68	1654.68	82.73	70	10	0.057	205.71	
R 1	40	10	73.00	25	1654.68	1654.68	66.19	60	10	0.047	168.00	
R 1	50	10	97.00	24	1654.68	1654.68	68.95	50	10	0.050	180.00	
R 1	60	10	116.00	19	1654.68	1654.68	87.09	40	10	0.066	236.84	
R 1	70	10	139.00	23	1654.68	1654.68	71.94	30	10	0.058	208.70	
R 1	80	10	165.00	26	1654.68	1654.68	63.64	20	10	0.058	207.69	
R 1	10	10	26.00	26	1654.68	1654.68	63.64	100	10	0.042	152.31	
R 1	20	10	46.00	20	1654.68	1654.68	82.73	90	10	0.056	200.00	
R 1	30	10	71.00	25	1654.68	1654.68	66.19	80	10	0.045	162.00	
R 1	40	10	94.00	23	1654.68	1654.68	71.94	70	10	0.050	178.88	
R 1	50	10	124.00	30	1654.68	1654.68	55.16	60	10	0.039	140.00	
R 1	60	10	143.00	19	1654.68	1654.68	87.09	50	10	0.063	227.37	
R 1	70	10	171.00	28	1654.68	1654.68	59.10	40	10	0.045	160.71	
R 1	80	10	199.00	22	1654.68	1654.68	75.21	30	10	0.061	218.18	
R 1	90	10	235.00	36	1654.68	1654.68	45.96	20	10	0.042	150.00	

Table B.2: Continues

Site	Total Infiltrated water in inner ring (mm)	Infiltrated Water Interval (mm)	Running Time (s)	Time Interval (sec)	Volume (mm3)	Area (mm2)	Q (mm3/sec)	Hydraulic Head (mm)	L (mm)	Vertical Flow K (cm/s)	Vertical Flow K (mm/hr)	Average Ksat per site (mm/hr)
R 1	10	10	25.00	25	1654.68	1654.68	66.19	80	10	0.045	162.00	
R 1	20	10	60.00	35	1654.68	1654.68	47.28	70	10	0.033	117.55	
R 1	30	10	86.00	26	1654.68	1654.68	63.64	60	10	0.045	161.54	
R 1	40	10	114.00	28	1654.68	1654.68	59.10	50	10	0.043	154.29	
R 1	50	10	145.00	31	1654.68	1654.68	53.38	40	10	0.040	145.16	
R 1	60	10	174.00	29	1654.68	1654.68	57.06	30	10	0.046	165.52	
R 1	70	10	193.00	19	1654.68	1654.68	87.09	20	10	0.079	284.21	182.601
R 2	10	10	18.00	18	1654.68	1654.68	91.93	100	10	0.061	220.00	
R 2	20	10	42.00	24	1654.68	1654.68	68.95	90	10	0.046	166.67	
R 2	30	10	69.00	27	1654.68	1654.68	61.28	80	10	0.042	150.00	
R 2	40	10	99.00	30	1654.68	1654.68	55.16	70	10	0.038	137.14	
R 2	50	10	131.00	32	1654.68	1654.68	51.71	60	10	0.036	131.25	
R 2	60	10	169.00	38	1654.68	1654.68	43.54	50	10	0.032	113.68	
R 2	70	10	200.00	31	1654.68	1654.68	53.38	40	10	0.040	145.16	
R 2	80	10	237.00	37	1654.68	1654.68	44.72	30	10	0.036	129.73	
R 2	90	10	273.00	36	1654.68	1654.68	45.96	20	10	0.042	150.00	
R 2	10	10	31.00	31	1654.68	1654.68	53.38	100	10	0.035	127.74	

Table B.2: Continues

Site	Total Infiltrated water in inner ring (mm)	Infiltrated Water Interval (mm)	Running Time (s)	Time Interval (sec)	Volume (mm3)	Area (mm2)	Q (mm3/sec)	Hydraulic Head (mm)	L (mm)	Vertical Flow K (cm/s)	Vertical Flow K (mm/hr)	Average Ksat per site (mm/hr)
R 2	20	10	68.00	37	1654.68	1654.68	44.72	90	10	0.030	108.11	
R 2	30	10	96.00	28	1654.68	1654.68	59.10	80	10	0.040	144.64	
R 2	40	10	130.00	34	1654.68	1654.68	48.67	70	10	0.034	121.01	
R 2	50	10	144.00	14	1654.68	1654.68	118.19	60	10	0.083	*300.00	
R 2	60	10	195.00	51	1654.68	1654.68	32.44	50	10	0.024	*84.71	
R 2	70	10	226.00	31	1654.68	1654.68	53.38	40	10	0.040	145.16	
R 2	80	10	257.00	31	1654.68	1654.68	53.38	30	10	0.043	154.84	
R 2	90	10	288.00	31	1654.68	1654.68	53.38	20	10	0.048	174.19	
R 2	10	10	23.00	23	1654.68	1654.68	71.94	100	10	0.048	172.17	
R 2	20	10	52.00	29	1654.68	1654.68	57.06	90	10	0.038	137.93	
R 2	30	10	86.00	34	1654.68	1654.68	48.67	80	10	0.033	119.12	
R 2	40	10	121.00	35	1654.68	1654.68	47.28	70	10	0.033	117.55	
R 2	50	10	157.00	36	1654.68	1654.68	45.96	60	10	0.032	116.67	
R 2	60	10	190.00	33	1654.68	1654.68	50.14	50	10	0.036	130.91	
R 2	70	10	221.00	31	1654.68	1654.68	53.38	40	10	0.040	145.16	
R 2	80	10	248.00	27	1654.68	1654.68	61.28	30	10	0.049	177.78	
R 2	90	10	278.00	30	1654.68	1654.68	55.16	20	10	0.0500	180.00	144.665

Table B.3: GWC of Table Mountain sandstone samples from Kogelberg.

		Wet Mass	Dry Mass	GWC %
Sandstone Site2LithB	Stone Natural	363.788	354.268	2.69
Sandstone Site2LithB	Stone Infiltrated	225.621	216.571	4.18

TableB.4: Calculation of unsaturated hydraulic conductivity under tension according to the work of Zhang (1997).

			Van Genuchten's parameters					
Site	ho	C1	a	n	r0	A	K (cm/s)	K (mm/hr)
K1	-0.5	0.0294	0.124	2.28	2.25	2.9853	0.009848	35.45372
K1	-1	0.0079	0.124	2.28	2.25	2.786831	0.002835	10.20514
K1	-2.5	0.0045	0.124	2.28	2.25	2.267141	0.001985	7.145563
K1	-5	0.0021	0.124	2.28	2.25	1.60728	0.001307	4.703597
K2	-0.5	0.024	0.145	2.68	2.25	2.835701	0.008464	30.46866
K2	-1	0.022	0.145	2.68	2.25	2.40407	0.009151	32.94413
K2	-2	0.014	0.145	2.68	2.25	1.727908	0.008102	29.16823
K2	-5	0.001	0.145	2.68	2.25	0.641565	0.001559	5.611279
R1	-0.5	0.027	0.145	2.68	2.25	2.835701	0.009521	34.27724
R1	-1	0.006	0.145	2.68	2.25	2.40407	0.002496	8.984763
R1	-2	0.011	0.145	2.68	2.25	1.727908	0.006366	22.91789

Table B.5: Calculation of contributing pore fractions (Watson and Luxmoore, 1986).

Investigation method	Double ring infiltrometer	Mini disc infiltrometer	Mini disc infiltrometer	Mini disc infiltrometer	Mini disc infiltrometer	Estimated from curve
Majour contributing pore fraction	Macro	Macro	Macro	Meso	Meso	Meso
Contributing pore radius fraction (cm)	All	0.3>	0.15>	0.075>	0.03>	0.011>
Tension (cm)	0	-0.5	-1	-2	-5	-14
K1	394.34	35.45	10.21	7.15	4.70	1.377E-12
K2	117.74	30.47	32.94	29.17	5.61	5.200E-07
R 1	182.60	34.28	8.98	22.92	2.640E-06	3.817E-22
Average	267.84	33.40	17.38	19.74	3.45	1.73E-07

Table B.6: Hydrologically effect pores (Wilson and Luxmoore, 1988).

Majour contributing pore fraction		Macro	Macro	Meso	Meso
Pore radius range (cm)		0.3 to 0.15	0.15 to 0.075	0.075 to 0.03	0.03 to 0.011
Hydrologically Effective Pores (mm3/mm3)	K1	9.16	4.44	22.15	317.33
	K2	-0.90	5.48	213.67	378.56
	R1	9.18	-20.22	207.87	0.00

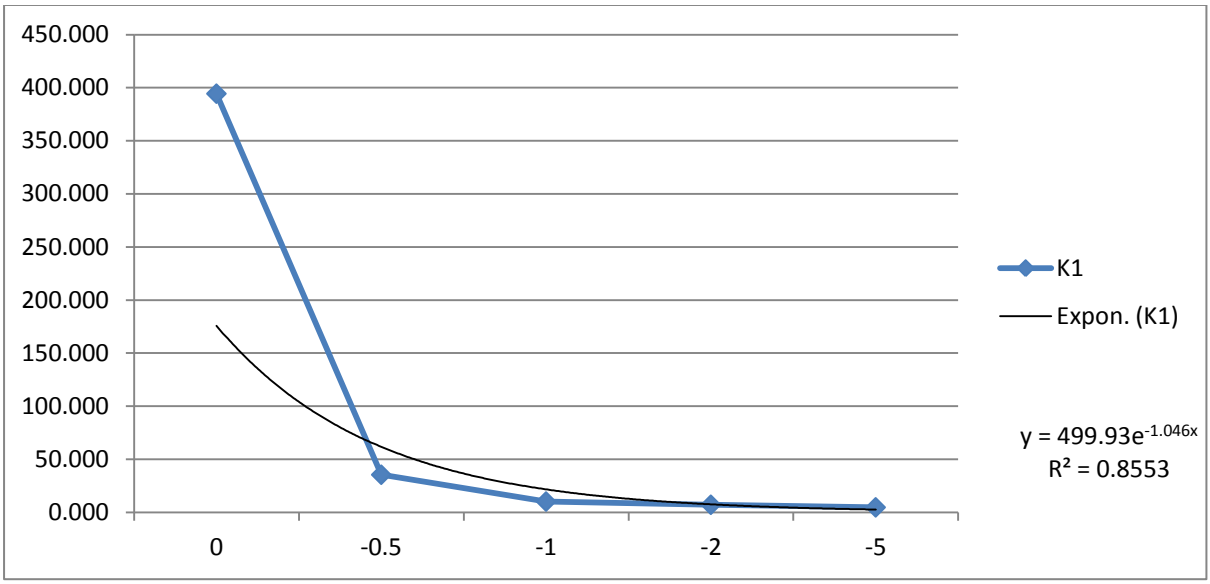

Figure B.5: Infiltration rate as a function of infiltration tension for K1.

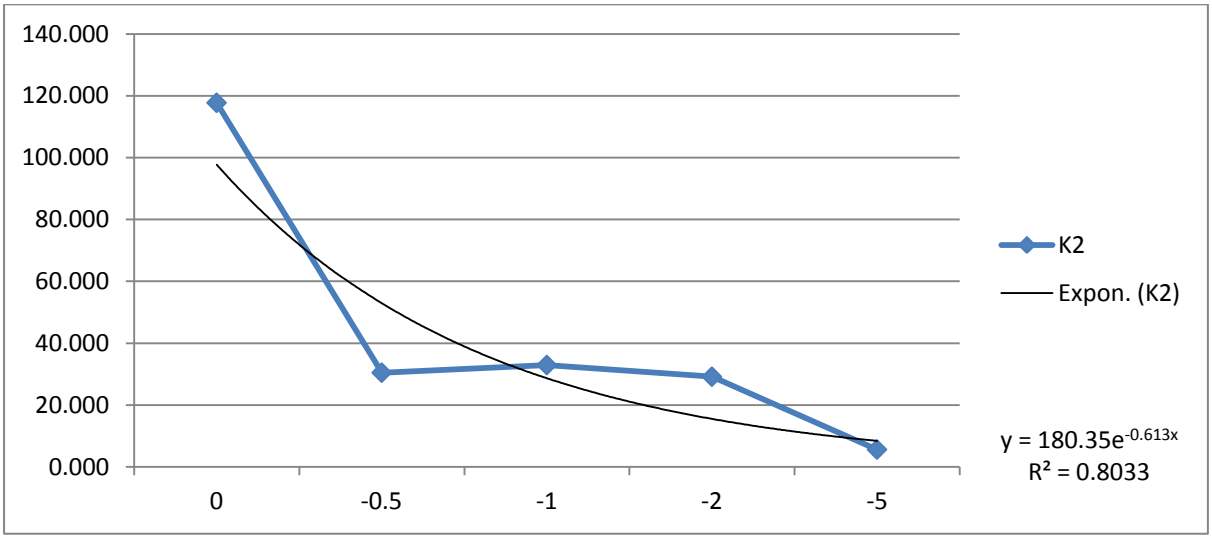

Figure B.6: Infiltration rate as a function of infiltration tension for K2.

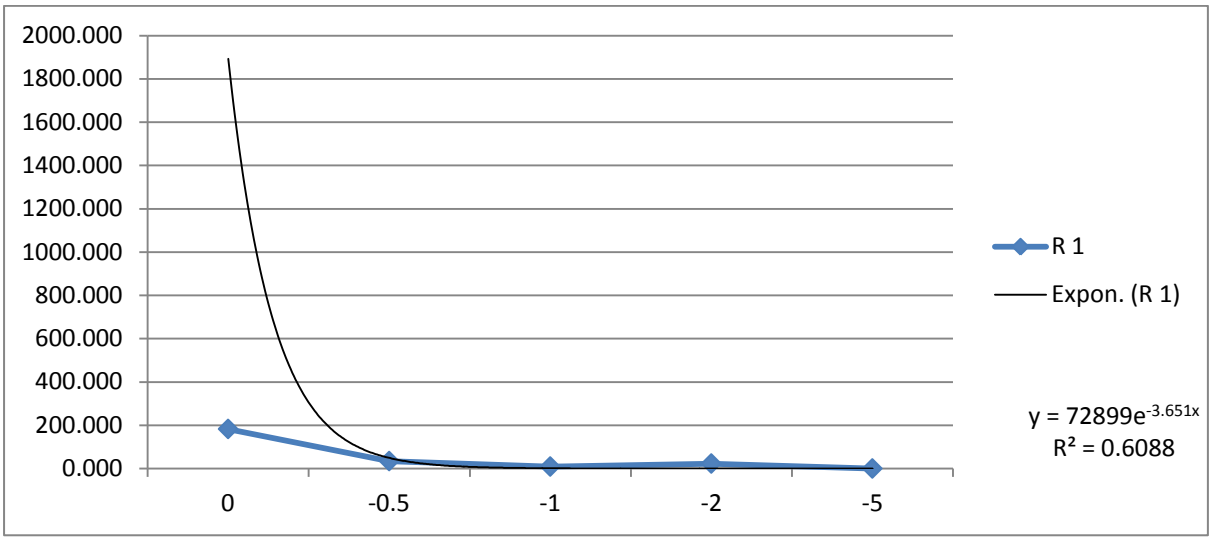

Figure B.7: Infiltration rate as a function of infiltration tension for R1

Table B.7: Semi-quantification of flow path visualization.

Site	Pixel Count		Total	FlowPath %	ByPassed %
	Wet (Blue)	Dry (Orange)			
K1	1140675	2414953	3555628	32	68
K2	3083005	678995	3762000	82	18
R1	786330	478118	1264448	62	38
R2	1984371	758677	2743048	72	28

Appendix C – Statistical Analysis

ANOVA of Ksat against Hydraulic Head

Statistical analysis of PAW against Soil Form.

Statistical analysis of Ksat against Soil Form.

ANOVA of Ksat against Hydraulic Head

Table C.1: Summary for single factor ANOVA in Table C.2.

Groups	*Count*	*Sum*	*Average*	*Variance*
Headcm	83	483	5.819277	8.052307
STDN	83	0.173268	0.002088	0.92876

Table C.2: ANOVA comparing hydraulic head and normalised Ksat [Normalisation = ((Ksat-Mean)/STDEV)]

Source of Variation	*SS*	*df*	*MS*	*F*	*P-value*	*F crit*
Between Groups	1404.347	1	1404.347	312.7351	7.62989E-40	3.898786645
Within Groups	736.4475	164	4.490534			
Total	2140.795	165				

Statistical analysis of PAW against Soil Form.

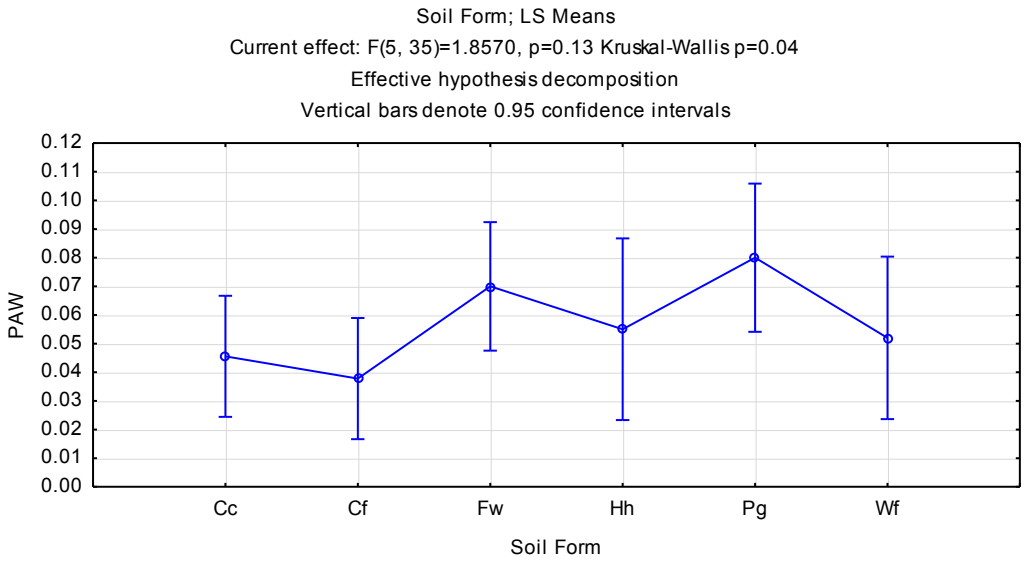

Figure C.1: Soil Form; LS Means plot of PAW for Kogelberg.

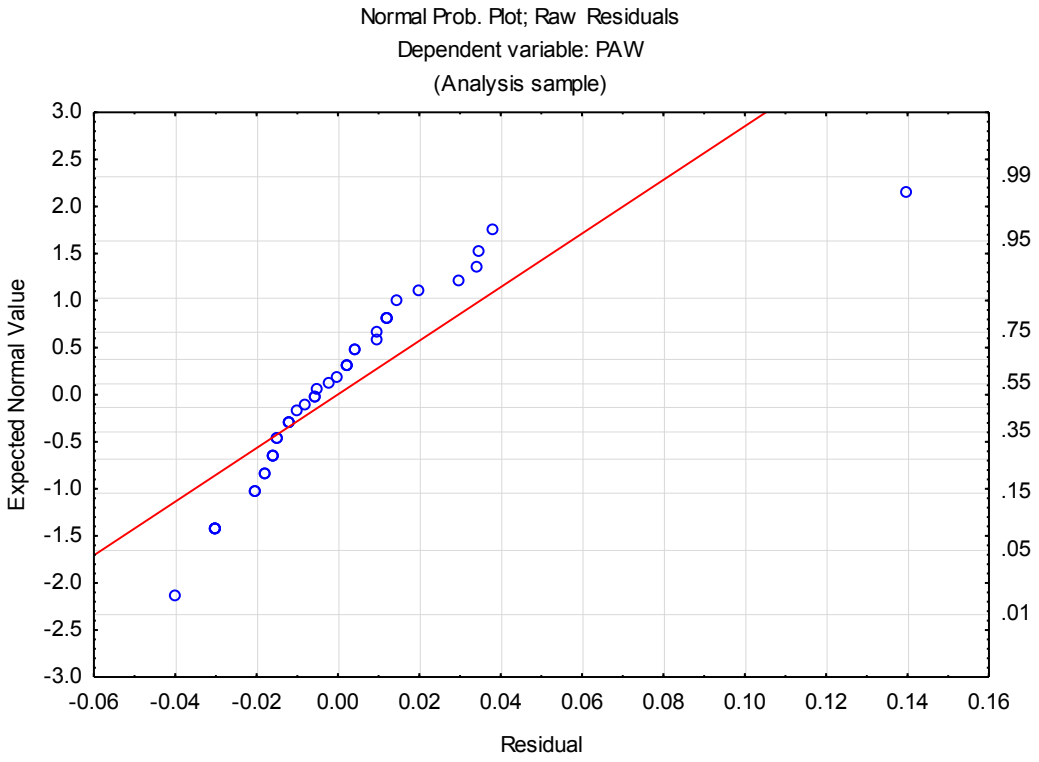

Figure C.2: Normal probability plot of raw residuals of PAW and Soil Form for Kogelberg.

Table C.3: Levene's test for homogeneity of variances for PAW and Soil Form for Kogelberg.

Levene's Test for Homogeneity of Variances (Kogel in DATA 20110
Effect: "Soil Form"
Degrees of freedom for all F's: 5, 35

	MS Effect	MS Error	F	p
PAW	0.00079	0.00045	1.75081	0.14886

Table C.4: Bonferroni's test for variable PAW between Soil Forms for Kogelberg.

	Bonferroni test; variable PAW (Kogel in DATA 20110510) Probabilities for Post Hoc Tests Error: Between MS = .00098, df = 35.000						
Cell No.	Soil Form	{1} .04556	{2} .03778	{3} .07000	{4} .05500	{5} .08000	{6} .05200
1	Cc		1.00000	1.00000	1.00000	0.65641	1.00000
2	Cf	1.00000		0.61392	1.00000	0.22177	1.00000
3	Fw	1.00000	0.61392		1.00000	1.00000	1.00000
4	Hh	1.00000	1.00000	1.00000		1.00000	1.00000
5	Pg	0.65641	0.22177	1.00000	1.00000		1.00000
6	Wf	1.00000	1.00000	1.00000	1.00000	1.00000	

TableC.5: Soil Form; LS Means of PAW for Kogelberg.

	Soil Form; LS Means (Kogel in DATA 20110510) Current effect: F(5, 35)=1.8570, p=.12722 Effective hypothesis decomposition					
Cell No.	Soil Form	PAW Mean	PAW Std.Err.	PAW -95.00%	PAW +95.00%	N
1	Cc	0.04555	0.01041	0.02441	0.06669	9
2	Cf	0.03777	0.01041	0.01663	0.05891	9
3	Fw	0.07000	0.01104	0.04757	0.09242	8
4	Hh	0.05500	0.01562	0.02329	0.08671	4
5	Pg	0.08000	0.01275	0.05410	0.10589	6
6	Wf	0.05200	0.01397	0.02363	0.08036	5

Table C.6: Descriptive Statistics of PAW and Soil Form for Kogelberg.

	Descriptive Statistics (Kogel in DATA 20110510)						
Effect	Level of Factor	N	PAW Mean	PAW Std.Dev.	PAW Std.Err	PAW -95.00%	PAW +95.00%
Total		41	0.05536	0.03287	0.00513	0.04499	0.06574
Soil Form	Cc	9	0.04555	0.01666	0.00555	0.03274	0.05836
Soil Form	Cf	9	0.03777	0.01201	0.00400	0.02854	0.04701
Soil Form	Fw	8	0.07000	0.05904	0.02087	0.02064	0.11935
Soil Form	Hh	4	0.05500	0.02380	0.01190	0.01712	0.09287
Soil Form	Pg	6	0.08000	0.02366	0.00966	0.05516	0.10483
Soil Form	Wf	5	0.05200	0.02167	0.00969	0.02508	0.07891

Nonparametric Kruskal-Wallis ANOVA and median test dialog following the non-normal distribution of PAW and Soil Form data for KNR.

Table C.7: Kruskal-Wallis ANOVA by Ranks; PAW

Kruskal-Wallis ANOVA by Ranks; PAW (Kogel in DATA 20110510
Independent (grouping) variable: Soil Form
Kruskal-Wallis test: H (5, N= 41) =11.69284 p =.0393

Depend.: PAW	Code	Valid N	Sum of Ranks	Mean Rank
Cc	101	9	158.000	17.5555
Cf	102	9	125.000	13.8888
Fw	103	8	180.000	22.5000
Hh	104	4	90.000	22.5000
Pg	105	6	204.000	34.0000
Wf	106	5	104.000	20.8000

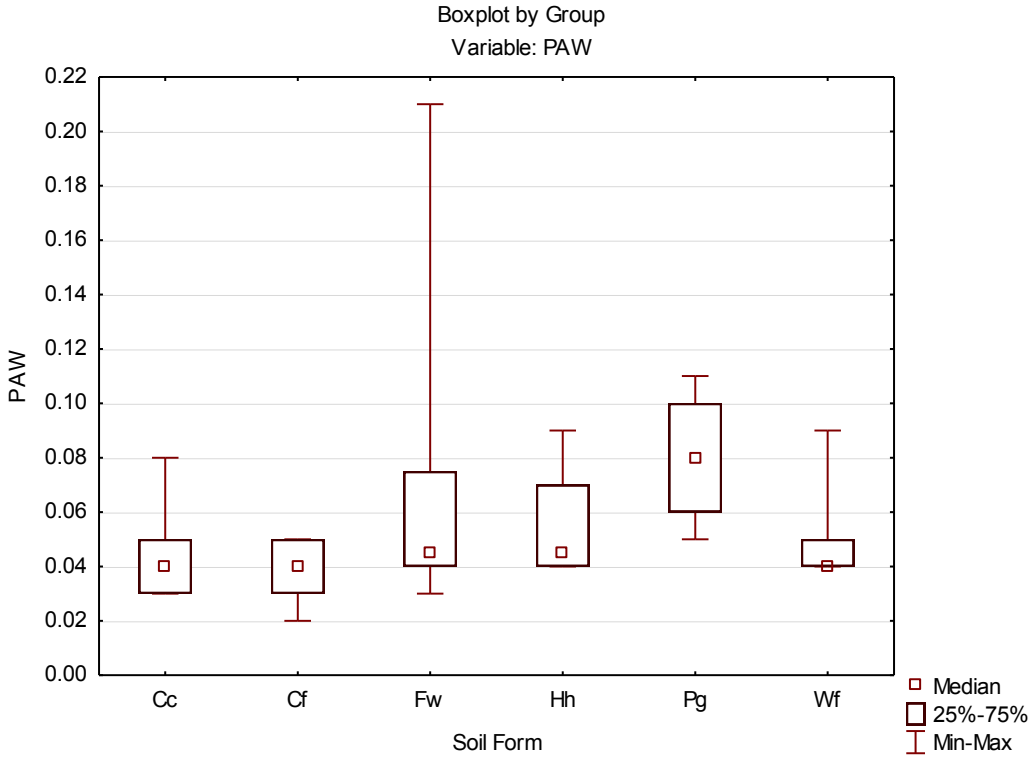

Figure C.3: Boxplot by group of PAW against Soil Form in the Kogelberg.

Table C.8: Multiple Comparisons z' values; PAW between Soil Forms in the Kogelberg.

	Multiple Comparisons z' values; PAW (Kogel in DATA 20110510) Independent (grouping) variable: Soil Form Kruskal-Wallis test: H (5, N= 41) =11.69284 p =.0393					
Depend.: PAW	Cc R:17.556	Cf R:13.889	Fw R:22.500	Hh R:22.500	Pg R:34.000	Wf R:20.800
Cc		0.64930	0.84944	0.68686	2.60462	0.48557
Cf	0.64930		1.47936	1.19622	3.18538	1.03434
Fw	0.84944	1.47936		0.00000	1.77757	0.24893
Hh	0.68686	1.19622	0.00000		1.48722	0.21155
Pg	2.60462	3.18538	1.77757	1.48722		1.81975
Wf	0.48557	1.03434	0.24893	0.21155	1.81975	

Table C.9: Multiple Comparisons p values (2-tailed); PAW between Soil Forms in the Kogelberg.

	Multiple Comparisons p values (2-tailed); PAW (Kogel in DATA 20110510 Independent (grouping) variable: Soil Form Kruskal-Wallis test: H (5, N= 41) =11.69284 p =.0393					
Depend.: PAW	Cc R:17.556	Cf R:13.889	Fw R:22.500	Hh R:22.500	Pg R:34.000	Wf R:20.800
Cc		1.00000	1.00000	1.00000	0.13796	1.00000
Cf	1.00000		1.00000	1.00000	0.02168	1.00000
Fw	1.00000	1.00000		1.00000	1.00000	1.00000
Hh	1.00000	1.00000	1.00000		1.00000	1.00000
Pg	0.13796	0.02168	1.00000	1.00000		1.00000
Wf	1.00000	1.00000	1.00000	1.00000	1.00000	

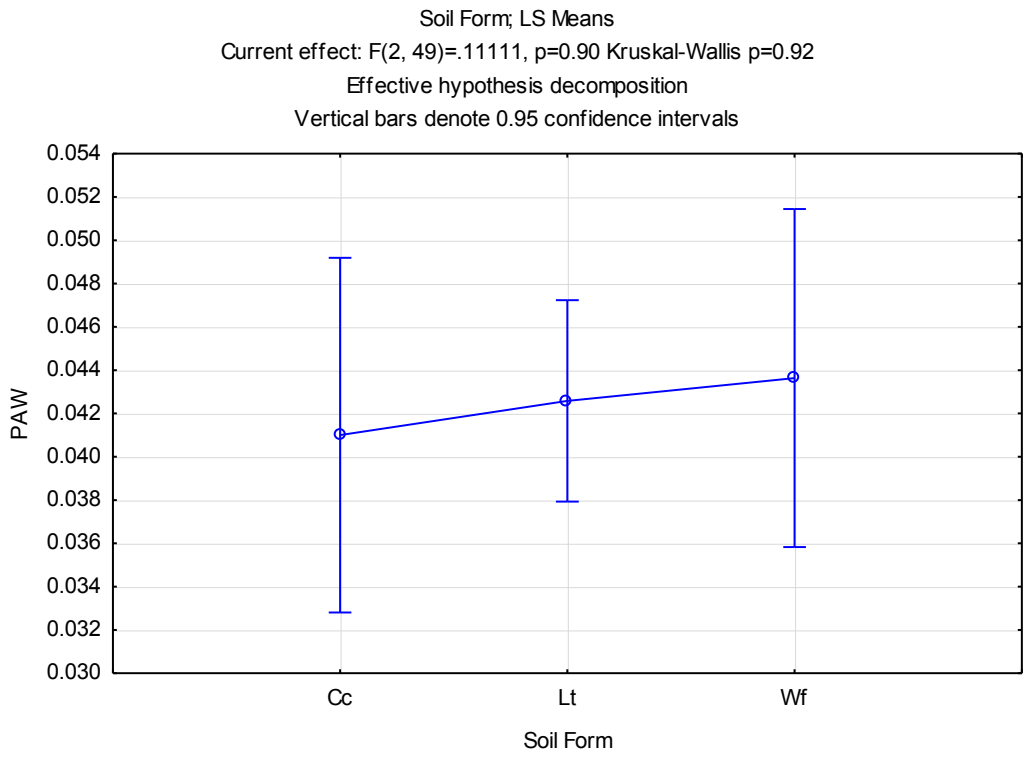

Figure C.4: Soil Form; LS Means plot of PAW for Riverlands.

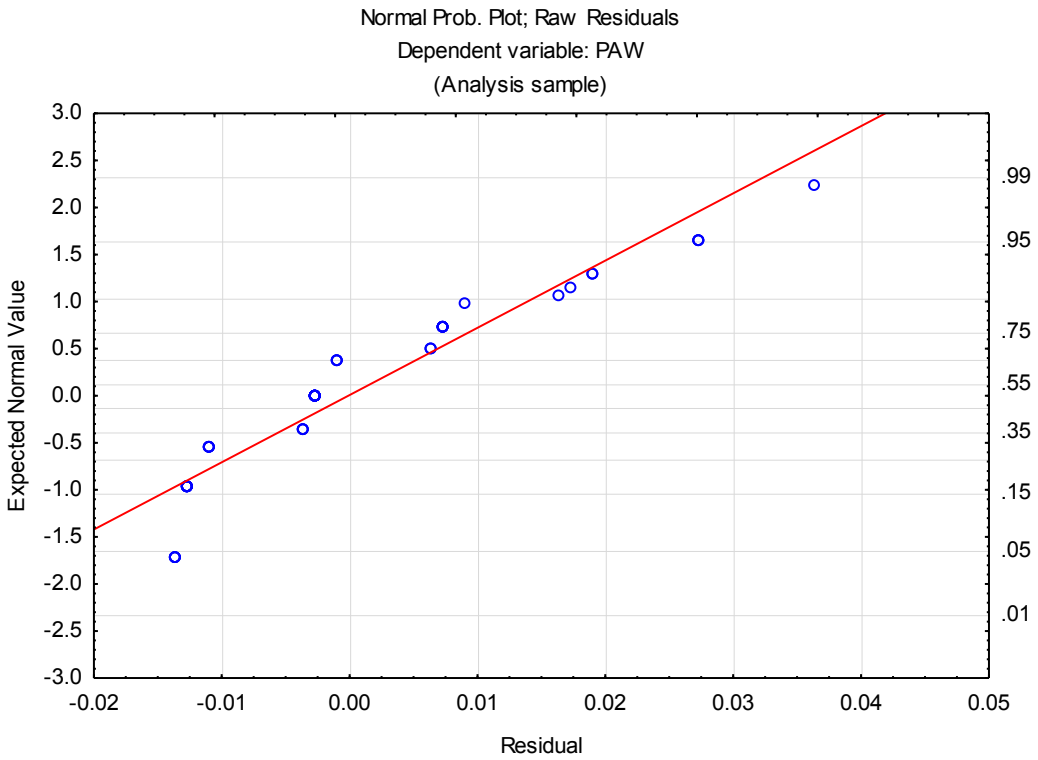

Figure C.5: Normal probability plot of raw residuals of PAW and Soil Form for Riverlands.

Table C.10: Levene's test for homogeneity of variances for PAW and Soil Form for Riverlands.

| | Levene's Test for Homogeneity of Variances (River in DATA 20110
Effect: "Soil Form"
Degrees of freedom for all F's: 2, 49 | | | |
|---|---|---|---|---|
| | MS Effect | MS Error | F | p |
| PAW | 0.00002 | 0.00006 | 0.46783 | 0.62912 |

Table C.11: Bonferroni's test for variable PAW between Soil Forms for Riverlands.

| | Bonferroni test; variable PAW (River in DATA 2011051
Probabilities for Post Hoc Tests
Error: Between MS = .00017, df = 49.000 | | | |
|---|---|---|---|---|
| Cell No. | Soil Form | {1} .04100 | {2} .04258 | {3} .04364 |
| 1 | Cc | | 1.00000 | 1.00000 |
| 2 | Lt | 1.00000 | | 1.00000 |
| 3 | Wf | 1.00000 | 1.00000 | |

Table C.12: Soil Form; LS Means for PAW and Soil Form for Riverlands.

| | Soil Form; LS Means (River in DATA 20110510)
Current effect: F(2, 49)=.11111, p=.89507
Effective hypothesis decomposition | | | | | |
|---|---|---|---|---|---|---|
| Cell No. | Soil Form | PAW Mean | PAW Std.Err. | PAW -95.00% | PAW +95.00% | N |
| 1 | Cc | 0.04100 | 0.00407 | 0.03281 | 0.04919 | 10 |
| 2 | Lt | 0.04258 | 0.00231 | 0.03792 | 0.04723 | 31 |
| 3 | Wf | 0.04363 | 0.00388 | 0.03582 | 0.05144 | 11 |

Table C.13: Descriptive Statistics of PAW and Soil Form for Riverlands.

	Descriptive Statistics (River in DATA 20110510)						
Effect	Level of Factor	N	PAW Mean	PAW Std.Dev.	PAW Std.Err	PAW -95.00%	PAW +95.00%
Total		52	0.04250	0.01266	0.00175	0.03897	0.04602
Soil Form	Cc	10	0.04100	0.01197	0.00378	0.03243	0.04956
Soil Form	Lt	31	0.04258	0.01210	0.00217	0.03814	0.04702
Soil Form	Wf	11	0.04363	0.01566	0.00472	0.03311	0.05416

Statistical analysis of Ksat against Soil Form.

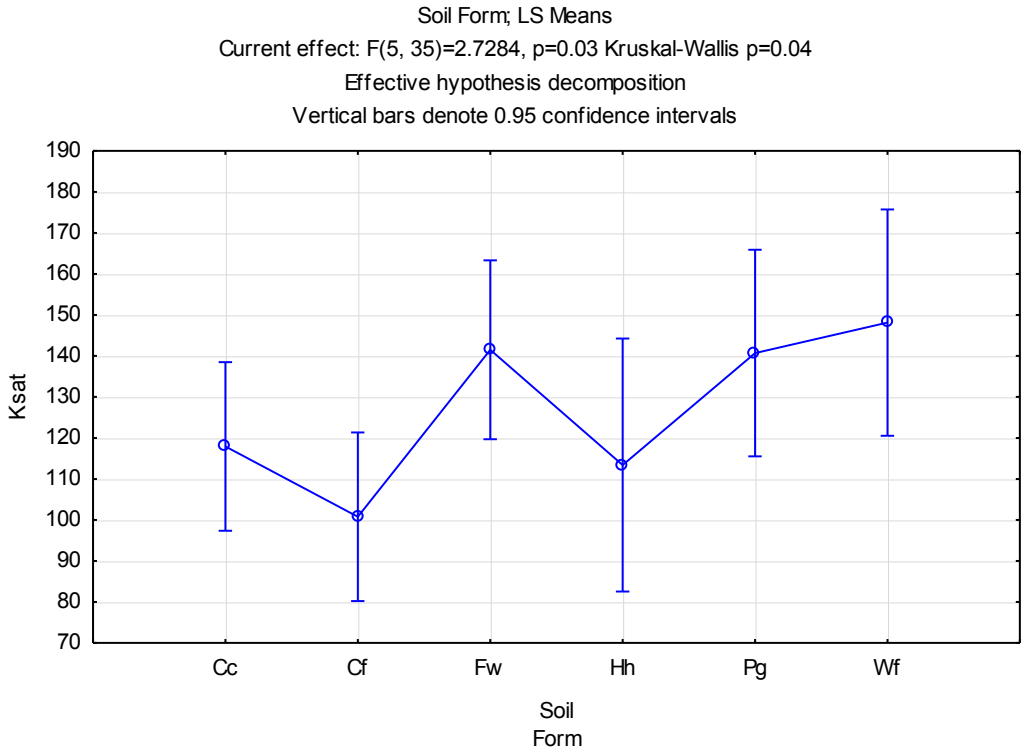

Figure C.6: Soil Form; LS Means for Ksat for Kogleberg.

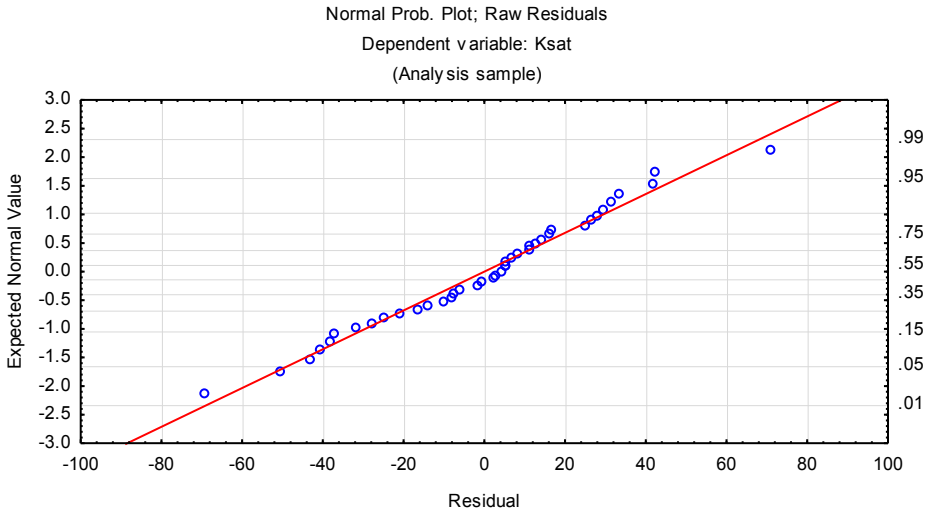

Figure C.7: Normal probability plot of raw residuals of Ksat and Soil form for Kogelberg.

Table C.14: Levene's test for homogeneity of variances between Ksat and Soil Form for Kogelberg.

| | Levene's Test for Homogeneity of Variances (Kogel in DATA 20110
Effect: "Soil Form"
Degrees of freedom for all F's: 5, 35 | | | |
|---|---|---|---|---|
| | MS Effect | MS Error | F | p |
| Ksat | 806.711 | 243.514 | 3.31278 | 0.01489 |

Table C.15: Bonferroni's test for variable Ksat between Soil Forms for Kogelberg.

| | Bonferroni test; variable Ksat (Kogel in DATA 20110510)
Probabilities for Post Hoc Tests
Error: Between MS = 923.55, df = 35.000 | | | | | | |
|---|---|---|---|---|---|---|---|
| Cell No. | Soil Form | {1} 117.93 | {2} 100.78 | {3} 141.50 | {4} 113.39 | {5} 140.70 | {6} 148.14 |
| 1 | Cc | | 1.00000 | 1.00000 | 1.00000 | 1.00000 | 1.00000 |
| 2 | Cf | 1.00000 | | 0.13786 | 1.00000 | 0.26352 | 0.12586 |
| 3 | Fw | 1.00000 | 0.13786 | | 1.00000 | 1.00000 | 1.00000 |
| 4 | Hh | 1.00000 | 1.00000 | 1.00000 | | 1.00000 | 1.00000 |
| 5 | Pg | 1.00000 | 0.26352 | 1.00000 | 1.00000 | | 1.00000 |
| 6 | Wf | 1.00000 | 0.12586 | 1.00000 | 1.00000 | 1.00000 | |

Table C.16: SoilForm; LS Means for Ksat for Kogelberg.

| | Soil Form; LS Means (Kogel in DATA 20110510)
Current effect: F(5, 35)=2.7284, p=.03489
Effective hypothesis decomposition | | | | | |
|---|---|---|---|---|---|---|
| Cell No. | Soil Form | Ksat Mean | Ksat Std.Err. | Ksat -95.00% | Ksat +95.00% | N |
| 1 | Cc | 117.925 | 10.1299 | 97.360 | 138.490 | 9 |
| 2 | Cf | 100.780 | 10.1299 | 80.215 | 121.344 | 9 |
| 3 | Fw | 141.501 | 10.7444 | 119.688 | 163.313 | 8 |
| 4 | Hh | 113.387 | 15.1949 | 82.540 | 144.234 | 4 |
| 5 | Pg | 140.701 | 12.4066 | 115.514 | 165.888 | 6 |
| 6 | Wf | 148.138 | 13.5907 | 120.547 | 175.728 | 5 |

Table C.17: Descriptive Statistics of Ksat and Soil Form for Kogelberg.

Effect	Descriptive Statistics (Kogel in DATA 20110510)						
	Level of Factor	N	Ksat Mean	Ksat Std.Dev.	Ksat Std.Err	Ksat -95.00%	Ksat +95.00%
Total		41	125.3368	33.5123	5.2337	114.759	135.914
Soil Form	Cc	9	117.925	16.1122	5.3707	105.540	130.310
Soil Form	Cf	9	100.780	41.0746	13.6915	69.2072	132.352
Soil Form	Fw	8	141.501	36.7133	12.9801	110.808	172.194
Soil Form	Hh	4	113.387	30.7898	15.3949	64.394	162.381
Soil Form	Pg	6	140.701	29.3375	11.9770	109.913	171.489
Soil Form	Wf	5	148.138	6.4745	2.8955	140.098	156.177

Table C.18: Univariate tests of significance for Ksat for Kogelberg.

Effect	Univariate Tests of Significance for Ksat (Kogel in DATA 201105 Sigma-restricted parameterization Effective hypothesis decomposition				
	SS	Degr. of Freedom	MS	F	p
Intercept	603083.	1	603083.	653.008	0.00000
Soil Form	12599.	5	2519.	2.728	0.03489
Error	32324.	35	923.		

Table C.19: LSD test for variable Ksat between the Soil Forms for Kogelberg.

Cell No.	LSD test; variable Ksat (Kogel in DATA 20110510) Probabilities for Post Hoc Tests Error: Between MS = 923.55, df = 35.000						
	Soil Form	{1} 117.93	{2} 100.78	{3} 141.50	{4} 113.39	{5} 140.70	{6} 148.14
1	Cc		0.23942	0.11936	0.80520	0.16387	0.08336
2	Cf	0.23942		0.00919	0.49451	0.01756	0.00839
3	Fw	0.11936	0.00919		0.13984	0.96142	0.70398
4	Hh	0.80520	0.49451	0.13984		0.17258	0.09713
5	Pg	0.16387	0.01756	0.96142	0.17258		0.68859
6	Wf	0.08336	0.00839	0.70398	0.09713	0.68859	

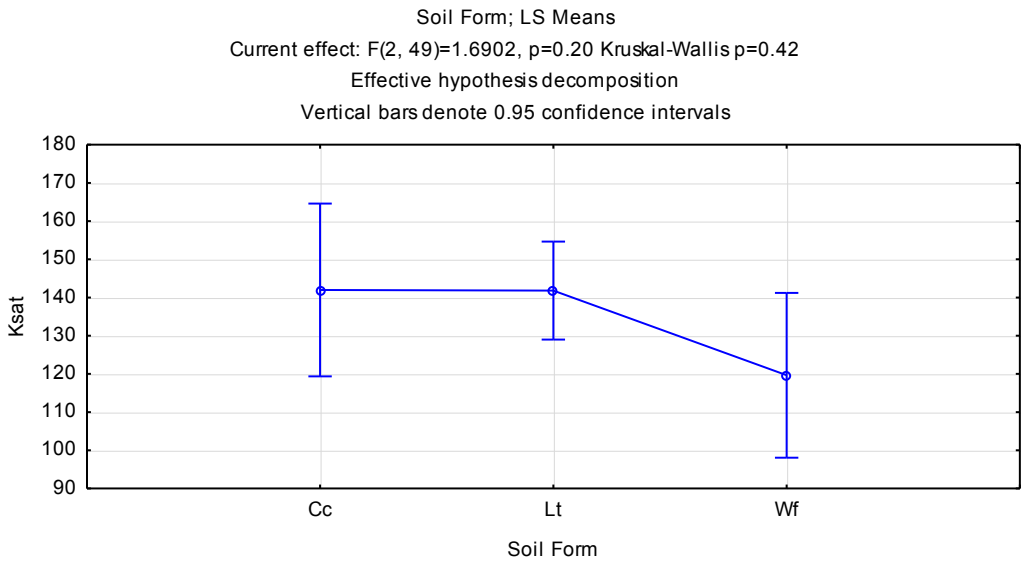

Figure C.8: Soil Form; LS Means of Ksat for Riverlands.

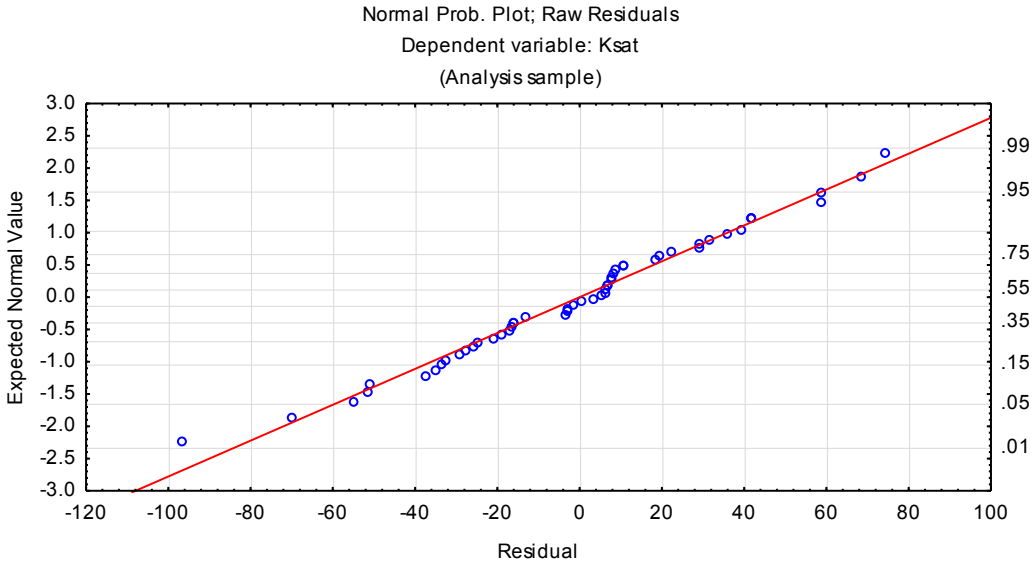

FigureC.9: Normal probability plot of raw residuals of Ksat and Soil Form for Riverlands.

TableC.20: Levene's test for homogeneity of variances between Ksat and Soil Form for Riverlands.

	Levene's Test for Homogeneity of Variances (River in DATA 20110 Effect: "Soil Form" Degrees of freedom for all F's: 2, 49			
	MS Effect	MS Error	F	p
Ksat	495.223	478.461	1.03503	0.36284

Table C.21: Bonferroni's test for variable Ksat between Soil Forms for Riverlands.

	Bonferroni test; variable Ksat (River in DATA 201105 Probabilities for Post Hoc Tests Error: Between MS = 1266.8, df = 49.000			
Cell No.	Soil Form	{1} 141.97	{2} 141.82	{3} 119.64
1	Cc		1.00000	0.47175
2	Lt	1.00000		0.24591
3	Wf	0.47175	0.24591	

Table C.22: Soil Form; LS Means of Ksat for Riverlands.

	Soil Form; LS Means (River in DATA 20110510) Current effect: F(2, 49)=1.6902, p=.19506 Effective hypothesis decomposition					
Cell No.	Soil Form	Ksat Mean	Ksat Std.Err.	Ksat -95.00%	Ksat +95.00%	N
1	Cc	141.973	11.2553	119.354	164.591	10
2	Lt	141.817	6.3925	128.971	154.664	31
3	Wf	119.635	10.7315	98.069	141.201	11

Table C.23: Descriptive Statistics of Ksat and Soil Form for Riverlands.

	Descriptive Statistics (River in DATA 20110510)						
Effect	Level of Factor	N	Ksat Mean	Ksat Std.Dev.	Ksat Std.Err	Ksat -95.00%	Ksat +95.00%
Total		52	137.155	36.0708	5.00213	127.113	147.197
Soil Form	Cc	10	141.973	48.7593	15.4190	107.092	176.853
Soil Form	Lt	31	141.817	30.3918	5.4585	130.669	152.965
Soil Form	Wf	11	119.635	36.0095	10.8572	95.443	143.827

APPENDIX D
Estimated K_{sat} for HSUs derived using the BDT.

Table D.1: Estimated K for HSUs derived using the BDT for interpolation.

Round	Profile	Soil Form	TS map unit	Ksat Interpolated	Level of BDT	Interpolation Source	Ksat HSU
1	19	Fw	R2	160.3	3	2.22, 1.36	160.3
1	19	Fw	R2	160.3	3	2.22, 1.37	160.3
1	19	Fw	R2	160.3	3	2.22, 1.38	160.3
1	66	Pg	Ba	134.9	6	Ave	134.9
1	66	Pg	Ba	134.9	6	Ave	134.9
1	66	Pg	Ba	134.9	6	Ave	134.9
1	66	Pg	Ba	134.9	6	Ave	134.9
1	66	Pg	Ba	134.9	6	Ave	134.9
1	63	Cc	Bb	134.9	6	Ave	134.9
1	63	Cc	Bb	134.9	6	Ave	134.9
1	63	Cc	Bb	134.9	6	Ave	134.9
1	63	Cc	Bb	134.9	6	Ave	134.9
2	15	Cf	Bc	89.3	1	Obs	95.0
2	15	Cf	Bc	89.3	1	Obs	95.0
2	15	Cf	Bc	89.3	1	Obs	95.0
1	60	Cf	Bc	89.3	2	2.15	95.0
1	60	Cf	Bc	89.3	2	2.15	95.0
1	60	Cf	Bc	89.3	2	2.15	95.0
1	61	Cf	Bc	89.3	2	2.15	95.0
1	61	Cf	Bc	89.3	2	2.15	95.0
1	61	Cf	Bc	89.3	2	2.15	95.0
1	67	Cf	Bc	89.3	2	2.15	95.0
1	67	Cf	Bc	89.3	2	2.15	95.0
1	67	Cf	Bc	89.3	2	2.15	95.0
1	70	Cf	Bc	89.3	2	2.15	95.0
1	70	Cf	Bc	89.3	2	2.15	95.0
1	70	Cf	Bc	89.3	2	2.15	95.0
1	71	Cf	Bc	89.3	2	2.15	95.0
1	71	Cf	Bc	89.3	2	2.15	95.0
1	71	Cf	Bc	89.3	2	2.15	95.0
1	72	Cf	Bc	89.3	2	2.15	95.0
1	72	Cf	Bc	89.3	2	2.15	95.0
1	72	Cf	Bc	89.3	2	2.15	95.0
2	12	Pg	Bc	134.9	6	Ave	95.0
2	12	Pg	Bc	134.9	6	Ave	95.0
2	12	Pg	Bc	134.9	6	Ave	95.0
2	17	Cf	Bd	89.3	3	2.15	124.4
2	17	Cf	Bd	89.3	3	2.15	124.4

Table D.1: Continues

Round	Profile	Soil Form	TS map unit	Ksat Interpolated	Level of BDT	Interpolation Source	Ksat HSU
2	17	Cf	Bd	89.3	3	2.15	124.4
2	16	Pg	Bd	134.9	6	Ave	124.4
2	16	Pg	Bd	134.9	6	Ave	124.4
2	16	Pg	Bd	134.9	6	Ave	124.4
2	16	Pg	Bd	134.9	6	Ave	124.4
1	73	Pg	Bd	134.9	6	Ave	124.4
1	73	Pg	Bd	134.9	6	Ave	124.4
1	73	Pg	Bd	134.9	6	Ave	124.4
1	74	Pg	Bd	134.9	6	Ave	124.4
1	74	Pg	Bd	134.9	6	Ave	124.4
1	74	Pg	Bd	134.9	6	Ave	124.4
1	76	Ka	Be	134.9	6	Ave	134.9
1	76	Ka	Be	134.9	6	Ave	134.9
1	76	Ka	Be	134.9	6	Ave	134.9
2	19	Wf	Be	134.9	6	Ave	134.9
2	19	Wf	Be	134.9	6	Ave	134.9
2	19	Wf	Be	134.9	6	Ave	134.9
1	75	Wf	Be	134.9	6	Ave	134.9
1	75	Wf	Be	134.9	6	Ave	134.9
1	75	Wf	Be	134.9	6	Ave	134.9
1	77	Wf	Be	134.9	6	Ave	134.9
1	77	Wf	Be	134.9	6	Ave	134.9
1	77	Wf	Be	134.9	6	Ave	134.9
1	77	Wf	Be	134.9	6	Ave	134.9
2	27	Cf	Fn	123.7	2	1.49	123.7
2	27	Cf	Fn	123.7	2	1.49	123.7
2	27	Cf	Fn	123.7	2	1.49	123.7
2	29	Cf	Fn	123.7	2	1.49	123.7
2	29	Cf	Fn	123.7	2	1.49	123.7
2	29	Cf	Fn	123.7	2	1.49	123.7
2	30	Cf	Fn	123.7	2	1.49	123.7
2	30	Cf	Fn	123.7	2	1.49	123.7
2	30	Cf	Fn	123.7	2	1.49	123.7
2	30	Cf	Fn	123.7	2	1.49	123.7
1	49	Cf	Fn	123.7	1	Obs	123.7
1	49	Cf	Fn	123.7	1	Obs	123.7
1	49	Cf	Fn	123.7	1	Obs	123.7
1	49	Cf	Fn	123.7	2	1.49	123.7
1	50	Cf	Fn	123.7	2	1.49	123.7
1	50	Cf	Fn	123.7	2	1.49	123.7
1	50	Cf	Fn	123.7	2	1.49	123.7
1	51	Cf	Fn	123.7	2	1.49	123.7
1	51	Cf	Fn	123.7	2	1.49	123.7
1	51	Cf	Fn	123.7	2	1.49	123.7

Table D.1: Continues

Round	Profile	Soil Form	TS map unit	Ksat Interpolated	Level of BDT	Interpolation Source	Ksat HSU
1	64	Cf	Fn	123.7	2	1.49	123.7
1	64	Cf	Fn	123.7	2	1.49	123.7
1	64	Cf	Fn	123.7	2	1.49	123.7
2	26	Gs	Fn	123.7	4	1.49	123.7
2	26	Gs	Fn	123.7	4	1.49	123.7
1	47	Gs	Fn	123.7	4	1.49	123.7
1	47	Gs	Fn	123.7	4	1.49	123.7
1	52	Gs	Fn	123.7	4	1.49	123.7
1	52	Gs	Fn	123.7	4	1.49	123.7
1	48	Cf	La	123.7	3	1.49	123.7
1	48	Cf	La	123.7	3	1.49	123.7
1	48	Cf	La	123.7	3	1.49	123.7
2	1	Gs	La	123.7	3	1.49	123.7
2	1	Gs	La	123.7	3	1.49	123.7
2	4	Pg	Lb	153.5	1	Obs	153.5
2	4	Pg	Lb	153.5	1	Obs	153.5
2	4	Pg	Lb	153.5	1	Obs	153.5
2	5	Pg	Lb	153.5	2	2.4	153.5
2	5	Pg	Lb	153.5	2	2.4	153.5
2	5	Pg	Lb	153.5	2	2.4	153.5
1	82	Pg	Lb	153.5	2	2.4	153.5
1	82	Pg	Lb	153.5	2	2.4	153.5
1	82	Pg	Lb	153.5	2	2.4	153.5
1	82	Pg	Lb	153.5	2	2.4	153.5
1	83	Gk	Lc	113.4	4	2.2	113.4
1	83	Gk	Lc	113.4	4	2.2	113.4
1	83	Gk	Lc	113.4	4	2.2	113.4
1	84	Gk	Lc	113.4	4	2.2	113.4
1	84	Gk	Lc	113.4	4	2.2	113.4
1	84	Gk	Lc	113.4	4	2.2	113.4
2	2	Hh	Lc	113.4	1	Obs	113.4
2	2	Hh	Lc	113.4	1	Obs	113.4
2	2	Hh	Lc	113.4	1	Obs	113.4
2	2	Hh	Lc	113.4	1	Obs	113.4
1	21	Cf	Mn	104.7	6	Ave	104.7
1	21	Cf	Mn	104.7	6	Ave	104.7
1	21	Cf	Mn	104.7	6	Ave	104.7
1	22	Cf	Mn	104.7	6	Ave	104.7
1	22	Cf	Mn	104.7	6	Ave	104.7
1	22	Cf	Mn	104.7	6	Ave	104.7
1	28	Cf	Mn	104.7	6	Ave	104.7
1	28	Cf	Mn	104.7	6	Ave	104.7
1	28	Cf	Mn	104.7	6	Ave	104.7
1	29	Cf	Mn	104.7	6	Ave	104.7

Table D.1: Continues

Round	Profile	Soil Form	TS map unit	Ksat Interpolated	Level of BDT	Interpolation Source	Ksat HSU
1	29	Cf	Mn	104.7	6	Ave	104.7
1	29	Cf	Mn	104.7	6	Ave	104.7
1	30	Cf	Mn	104.7	6	Ave	104.7
2	31	Cf	Mn	104.7	6	Ave	104.7
2	31	Cf	Mn	104.7	6	Ave	104.7
2	31	Cf	Mn	104.7	6	Ave	104.7
1	33	Cf	Mn	104.7	6	Ave	104.7
1	33	Cf	Mn	104.7	6	Ave	104.7
1	33	Cf	Mn	104.7	6	Ave	104.7
1	45	Cf	Mn	104.7	6	Ave	104.7
1	45	Cf	Mn	104.7	6	Ave	104.7
1	45	Cf	Mn	104.7	6	Ave	104.7
1	45	Cf	Mn	104.7	6	Ave	104.7
1	46	Cf	Mn	104.7	6	Ave	104.7
1	46	Cf	Mn	104.7	6	Ave	104.7
1	46	Cf	Mn	104.7	6	Ave	104.7
1	53	Cf	Mn	104.7	6	Ave	104.7
1	53	Cf	Mn	104.7	6	Ave	104.7
1	53	Cf	Mn	104.7	6	Ave	104.7
1	24	Gs	Mn	104.7	6	Ave	104.7
1	24	Gs	Mn	104.7	6	Ave	104.7
1	24	Gs	Mn	104.7	6	Ave	104.7
1	25	Gs	Mn	104.7	6	Ave	104.7
1	25	Gs	Mn	104.7	6	Ave	104.7
1	78	Hh	Mw	104.7	6	Ave	104.7
1	78	Hh	Mw	104.7	6	Ave	104.7
1	78	Hh	Mw	104.7	6	Ave	104.7
1	78	Hh	Mw	104.7	6	Ave	104.7
2	32	Pg	R1a	127.9	3	2.11	138.0
2	32	Pg	R1a	127.9	3	2.11	138.0
2	32	Pg	R1a	127.9	3	2.11	138.0
2	32	Pg	R1a	127.9	3	2.11	138.0
2	32	Pg	R1a	127.9	3	2.11	138.0
2	32	Pg	R1a	127.9	3	2.11	138.0
1	11	Wf	R1a	148.1	3	2.13	138.0
1	11	Wf	R1a	148.1	3	2.13	138.0
1	11	Wf	R1a	148.1	3	2.13	138.0
1	13	Wf	R1a	148.1	3	2.13	138.0
1	13	Wf	R1a	148.1	3	2.13	138.0
1	13	Wf	R1a	148.1	3	2.13	138.0
2	25	Cf	R1b	104.7	6	Ave	134.6
2	25	Cf	R1b	104.7	6	Ave	134.6
2	25	Cf	R1b	104.7	6	Ave	134.6
1	34	Cf	R1b	104.7	6	Ave	134.6

Table D.1: Continues

Round	Profile	Soil Form	TS map unit	Ksat Interpolated	Level of BDT	Interpolation Source	Ksat HSU
1	34	Cf	R1b	104.7	6	Ave	134.6
1	34	Cf	R1b	104.7	6	Ave	134.6
1	35	Cf	R1b	104.7	6	Ave	134.6
1	35	Cf	R1b	104.7	6	Ave	134.6
1	35	Cf	R1b	104.7	6	Ave	134.6
1	39	Cf	R1b	104.7	6	Ave	134.6
1	39	Cf	R1b	104.7	6	Ave	134.6
1	39	Cf	R1b	104.7	6	Ave	134.6
2	21	Fw	R1b	160.3	2	2.22	134.6
2	21	Fw	R1b	160.3	2	2.22	134.6
2	21	Fw	R1b	160.3	2	2.22	134.6
2	22	Fw	R1b	160.3	1	Obs	134.6
2	22	Fw	R1b	160.3	1	Obs	134.6
2	22	Fw	R1b	160.3	1	Obs	134.6
1	36	Fw	R1b	160.3	1	Obs	134.6
1	36	Fw	R1b	160.3	1	Obs	134.6
1	36	Fw	R1b	160.3	1	Obs	134.6
1	37	Fw	R1b	160.3	2	2.22	134.6
1	37	Fw	R1b	160.3	2	2.22	134.6
1	38	Fw	R1b	160.3	2	2.22	134.6
1	38	Fw	R1b	160.3	2	2.22	134.6
1	38	Fw	R1b	160.3	2	2.22	134.6
2	20	Cc	R1c	122.1	1	Obs	133.0
2	20	Cc	R1c	122.1	1	Obs	133.0
2	20	Cc	R1c	122.1	1	Obs	133.0
2	20	Cc	R1c	122.1	1	Obs	133.0
2	20	Cc	R1c	122.1	1	Obs	133.0
1	57	Cf	R1c	104.7	6	Ave	133.0
1	57	Cf	R1c	104.7	6	Ave	133.0
1	57	Cf	R1c	104.7	6	Ave	133.0
1	68	Gk	R1c	104.7	6	Ave	133.0
1	68	Gk	R1c	104.7	6	Ave	133.0
1	68	Gk	R1c	104.7	6	Ave	133.0
1	54	Lt	R1c	136.6	4	2.20, 2.13	133.0
1	54	Lt	R1c	136.6	4	2.20, 2.14	133.0
1	54	Lt	R1c	136.6	4	2.20, 2.15	133.0
1	54	Lt	R1c	136.6	4	2.20, 2.16	133.0
1	55	Lt	R1c	136.6	4	2.20, 2.17	133.0
1	55	Lt	R1c	136.6	4	2.20, 2.18	133.0
1	55	Lt	R1c	136.6	4	2.20, 2.19	133.0
1	55	Lt	R1c	136.6	4	2.20, 2.20	133.0
1	69	Lt	R1c	136.6	4	2.20, 2.21	133.0
1	69	Lt	R1c	136.6	4	2.20, 2.22	133.0
1	69	Lt	R1c	136.6	4	2.20, 2.23	133.0

Table D.1: Continues

Round	Profile	Soil Form	TS map unit	Ksat Interpolated	Level of BDT	Interpolation Source	Ksat HSU
1	69	Lt	R1c	136.6	4	2.20, 2.24	133.0
2	13	Wf	R1c	148.1	1	Obs	133.0
2	13	Wf	R1c	148.1	1	Obs	133.0
2	13	Wf	R1c	148.1	1	Obs	133.0
2	13	Wf	R1c	148.1	1	Obs	133.0
2	13	Wf	R1c	148.1	1	Obs	133.0
2	14	Wf	R1c	148.1	2	2.13	133.0
2	14	Wf	R1c	148.1	2	2.13	133.0
2	14	Wf	R1c	148.1	2	2.13	133.0
2	14	Wf	R1c	148.1	2	2.13	133.0
1	56	Wf	R1c	148.1	2	2.13	133.0
1	56	Wf	R1c	148.1	2	2.13	133.0
1	56	Wf	R1c	148.1	2	2.13	133.0
1	58	Cf	R1d	104.7	6	Ave	116.3
1	58	Cf	R1d	104.7	6	Ave	116.3
1	58	Cf	R1d	104.7	6	Ave	116.3
1	59	Cf	R1d	104.7	6	Ave	116.3
1	59	Cf	R1d	104.7	6	Ave	116.3
1	59	Cf	R1d	104.7	6	Ave	116.3
1	59	Cf	R1d	104.7	6	Ave	116.3
1	62	Cf	R1d	104.7	6	Ave	116.3
1	62	Cf	R1d	104.7	6	Ave	116.3
1	62	Cf	R1d	104.7	6	Ave	116.3
2	10	Pg	R1d	127.9	2	2.11	116.3
2	10	Pg	R1d	127.9	2	2.11	116.3
2	10	Pg	R1d	127.9	2	2.11	116.3
2	11	Pg	R1d	127.9	1	Obs	116.3
2	11	Pg	R1d	127.9	1	Obs	116.3
2	11	Pg	R1d	127.9	1	Obs	116.3
1	65	Pg	R1d	127.9	2	2.11	116.3
1	65	Pg	R1d	127.9	2	2.11	116.3
1	65	Pg	R1d	127.9	2	2.11	116.3
1	65	Pg	R1d	127.9	2	2.11	116.3
2	7	Fw	R1e	85.2	1	Obs	104.1
2	7	Fw	R1e	85.2	1	Obs	104.1
1	80	Fw	R1e	85.2	1	Obs	104.1
1	80	Fw	R1e	85.2	2	2.7	104.1
1	81	Fw	R1e	85.2	2	2.7	104.1
1	81	Fw	R1e	85.2	2	2.7	104.1
1	81	Fw	R1e	85.2	2	2.7	104.1
1	79	Wf	R1e	148.1	3	2.13	104.1
1	79	Wf	R1e	148.1	3	2.13	104.1
1	79	Wf	R1e	148.1	3	2.13	104.1
1	12	Cc	T1	114.6	1	Obs	114.6

Table D.1: Continues

Round	Profile	Soil Form	TS map unit	Ksat Interpolated	Level of BDT	Interpolation Source	Ksat HSU
1	12	Cc	T1	114.6	1	Obs	114.6
1	12	Cc	T1	114.6	1	Obs	114.6
1	12	Cc	T1	114.6	1	Obs	114.6
1	12	Cc	T1	114.6	1	Obs	114.6
1	43	Cc	T2a	114.6	3	1.12	110.4
1	43	Cc	T2a	114.6	3	1.12	110.4
1	43	Cc	T2a	114.6	3	1.12	110.4
1	43	Cc	T2a	114.6	3	1.12	110.4
1	44	Cc	T2a	114.6	3	1.12	110.4
1	44	Cc	T2a	114.6	3	1.12	110.4
1	44	Cc	T2a	114.6	3	1.12	110.4
1	44	Cc	T2a	114.6	3	1.12	110.4
1	5	Fw	T2a	114.6	5	1.12	110.4
1	5	Fw	T2a	114.6	5	1.12	110.4
1	5	Fw	T2a	114.6	5	1.12	110.4
1	7	Fw	T2a	114.6	5	1.12	110.4
1	7	Fw	T2a	114.6	5	1.12	110.4
1	7	Fw	T2a	114.6	5	1.12	110.4
1	9	Gk	T2a	89.4	5	1.26	110.4
1	9	Gk	T2a	89.4	5	1.26	110.4
1	9	Gk	T2a	89.4	5	1.26	110.4
1	6	Hh	T2a	89.4	5	1.26	110.4
1	6	Hh	T2a	89.4	5	1.26	110.4
1	6	Hh	T2a	89.4	5	1.26	110.4
1	6	Hh	T2a	89.4	5	1.26	110.4
1	1	Pg	T2a	114.6	5	1.12	110.4
1	1	Pg	T2a	114.6	5	1.12	110.4
1	1	Pg	T2a	114.6	5	1.12	110.4
1	2	Pg	T2a	114.6	5	1.12	110.4
1	2	Pg	T2a	114.6	5	1.12	110.4
1	2	Pg	T2a	114.6	5	1.12	110.4
1	3	Pg	T2a	114.6	5	1.12	110.4
1	3	Pg	T2a	114.6	5	1.12	110.4
1	3	Pg	T2a	114.6	5	1.12	110.4
1	3	Pg	T2a	114.6	5	1.12	110.4
1	4	Pg	T2a	114.6	5	1.12	110.4
1	4	Pg	T2a	114.6	5	1.12	110.4
1	4	Pg	T2a	114.6	5	1.12	110.4
1	8	Pg	T2a	114.6	5	1.12	110.4
1	8	Pg	T2a	114.6	5	1.12	110.4
1	8	Pg	T2a	114.6	5	1.12	110.4
2	33	Pg	T2a	114.6	5	1.12	110.4
2	33	Pg	T2a	114.6	5	1.12	110.4
2	33	Pg	T2a	114.6	5	1.12	110.4

Table D.1: Continues

Round	Profile	Soil Form	TS map unit	Ksat Interpolated	Level of BDT	Interpolation Source	Ksat HSU
2	33	Pg	T2a	114.6	5	1.12	110.4
2	33	Pg	T2a	114.6	5	1.12	110.4
1	23	Cf	T2b	89.4	2	1.26	89.4
1	23	Cf	T2b	89.4	2	1.26	89.4
1	23	Cf	T2b	89.4	2	1.26	89.4
1	26	Cf	T2b	89.4	1	Obs	89.4
1	26	Cf	T2b	89.4	1	Obs	89.4
1	26	Cf	T2b	89.4	1	Obs	89.4
1	27	Cf	T2b	89.4	2	1.26	89.4
1	27	Cf	T2b	89.4	2	1.26	89.4
1	27	Cf	T2b	89.4	2	1.26	89.4
1	30	Cf	T2b	89.4	2	1.26	89.4
1	30	Cf	T2b	89.4	2	1.26	89.4
1	31	Cf	T2b	89.4	2	1.26	89.4
1	31	Cf	T2b	89.4	2	1.26	89.4
1	31	Cf	T2b	89.4	2	1.26	89.4
1	32	Cf	T2b	89.4	2	1.26	89.4
1	32	Cf	T2b	89.4	2	1.26	89.4
1	32	Cf	T2b	89.4	2	1.26	89.4
2	34	Cf	T2b	89.4	2	1.26	89.4
2	34	Cf	T2b	89.4	2	1.26	89.4
2	34	Cf	T2b	89.4	2	1.26	89.4
2	34	Cf	T2b	89.4	2	1.26	89.4
1	40	Cf	T2b	89.4	2	1.26	89.4
1	40	Cf	T2b	89.4	2	1.26	89.4
1	40	Cf	T2b	89.4	2	1.26	89.4
1	41	Cf	T2b	89.4	2	1.26	89.4
1	41	Cf	T2b	89.4	2	1.26	89.4
1	41	Cf	T2b	89.4	2	1.26	89.4
1	42	Cf	T2b	89.4	2	1.26	89.4
1	42	Cf	T2b	89.4	2	1.26	89.4
1	42	Cf	T2b	89.4	2	1.26	89.4
1	15	Cf	T3a	89.4	3	1.26	89.4
1	15	Cf	T3a	89.4	3	1.26	89.4
1	15	Cf	T3a	89.4	3	1.26	89.4
1	16	Cf	T3a	89.4	3	1.26	89.4
1	16	Cf	T3a	89.4	3	1.26	89.4
1	16	Cf	T3a	89.4	3	1.26	89.4
1	17	Cf	T3a	89.4	3	1.26	89.4
1	17	Cf	T3a	89.4	3	1.26	89.4
1	17	Cf	T3a	89.4	3	1.26	89.4
1	18	Cf	T3a	89.4	3	1.26	89.4
1	18	Cf	T3a	89.4	3	1.26	89.4
1	18	Cf	T3a	89.4	3	1.26	89.4

Table D.1: Continues

Round	Profile	Soil Form	TS map unit	Ksat Interpolated	Level of BDT	Interpolation Source	Ksat HSU
1	14	Lt	T3b	114.6	5	1.12	114.6
1	14	Lt	T3b	114.6	5	1.12	114.6
1	14	Lt	T3b	114.6	5	1.12	114.6